Disclaimer

This Report, including the data and information contained in this Report, is provided to you on an "as is" and "as available" basis at the sole discretion of the Government of Alberta and subject to the terms and conditions of use below (the "Terms and Conditions"). The Government of Alberta has not verified this Report for accuracy and does not warrant the accuracy of, or make any other warranties or representations regarding, this Report. Furthermore, updates to this Report may not be made available. Your use of any of this Report is at your sole and absolute risk.

This Report is provided to the Government of Alberta, and the Government of Alberta has obtained a license or other authorization for use of the Reports, from:

> Shell Canada Energy, Chevron Canada Limited. and Marathon Oil Canada Corporation, for the Quest Project
>
> (collectively the "Project")

Each member of the Project expressly disclaims any representation or warranty, express or implied, as to the accuracy or completeness of the material and information contained herein, and none of them shall have any liability, regardless of any negligence or fault, for any statements contained in, or for any omissions from, this Report. Under no circumstances shall the Government of Alberta or the Project be liable for any damages, claims, causes of action, losses, legal fees or expenses, or any other cost whatsoever arising out of the use of this Report or any part thereof or the use of any other data or information on this website.

Terms and Conditions of Use

Except as indicated in these Terms and Conditions, this Report and any part thereof shall not be copied, reproduced, distributed, republished, downloaded, displayed, posted or transmitted in any form or by any means, without the prior written consent of the Government of Alberta and the Project.

The Government of Alberta's intent in posting this Report is to make them available to the public for personal and non-commercial (educational) use. You may not use this Report for any other purpose. You may reproduce data and information in this Report subject to the following conditions:

- any disclaimers that appear in this Report shall be retained in their original form and applied to the data and information reproduced from this Report
- the data and information shall not be modified from its original form
- the Project shall be identified as the original source of the data and information, while this website shall be identified as the reference source, and
- the reproduction shall not be represented as an official version of the materials reproduced, nor as having been made in affiliation with or with the endorsement of the Government of Alberta or the Project

By accessing and using this Report, you agree to indemnify and hold the Government of Alberta and the Project, and their respective employees and agents, harmless from and against any and all claims, demands, actions and costs (including legal costs on a solicitor-client basis) arising out of any breach by you of these Terms and Conditions or otherwise arising out of your use or reproduction of the data and information in this Report.

Your access to and use of this Report is subject exclusively to these Terms and Conditions and any terms and conditions contained within the Report itself, all of which you shall comply with. You will not use this Report for any purpose that is unlawful or prohibited by these Terms and Conditions. You agree that any other use of this Report means you agree to be bound by these Terms and Conditions. These Terms and Conditions are subject to modification, and you agree to review them periodically for changes. If you do not accept these Terms and Conditions you agree to immediately stop accessing this Report and destroy all copies in your possession or control.

These Terms and Conditions may change at any time, and your continued use and reproduction of this Report following any changes shall be deemed to be your acceptance of such change.

If any of these Terms and Conditions should be determined to be invalid, illegal or unenforceable for any reason by any court of competent jurisdiction then the applicable provision shall be severed and the remaining provisions of these Terms and Conditions shall survive and remain in full force and effect and continue to be binding and enforceable.

These Terms and Conditions shall: (i) be governed by and construed in accordance with the laws of the province of Alberta and you hereby submit to the exclusive jurisdiction of the Alberta courts, and (ii) ensure to the benefit of, and be binding upon, the Government of Alberta and your respective successors and assigns.

Heavy Oil

Controlled Document

Quest CCS Project

Generation-4 Integrated Reservoir Modeling Report

Project	Quest CCS Project
Document Title	Generation-4 Integrated Reservoir Modeling Report
Document Number	07-3-AA-5726-0001
Document Revision	02
Document Status	Final
Document Type	AA5726-Field Development Plan
Owner / Author	Mario Winkler
Issue Date	2011-10-03
Expiry Date	None
ECCN	EAR 99
Security Classification	
Disclosure	None

Revision History shown on next page

Revision History

REVISION STATUS			APPROVAL		
Rev.	Date	Description	Originator	Reviewer	Approver
01	2011-08-18	Draft for Review	Mario Winkler	Jan Sherman	Syrie Crouch
02	2011-10-03	Final Version	Mario Winkler	Jan Sherman	Syrie Crouch

- All signed originals will be retained by the UA Document Control Center and an electronic copy will be stored in Livelink

Signatures for this revision

Date	Role	Name	Signature or electronic reference (email)
	Originator	Mario Winkler	Actual signature
	Reviewer	Jan Sherman	Actual signature
	Approver	Syrie Crouch	Actual signature

Summary

The Generation-4 (or Gen-4) integrated modeling activities were framed to directly support decisions associated with the Quest Storage Development Plan (SDP), are related to confirm aspects of the regulatory submissions and provided detail input to the MMV plan while also defining and quantifying conformance criteria for the Quest project. This report summarizes the results of work performed between November, 2010 and August, 2011, documents the key findings that have been subsequently used in the Quest Storage Development Plan and in the Quest MMV plan while also informing the Quest regulatory submissions and updates.

Keywords

AOSP, Quest, CCS, CO2 Sequestration, Integrated Reservoir Modeling, Generation-4, FDP, SDP

DCAF Authorities

Date	Role	Name	Signature or electronic reference (email)
		Add name	Actual signature
		Add name	Actual signature
		Add name	Actual signature

Page intentionally left blank

1. EXECUTIVE SUMMARY

The outcomes as documented in this Generation-4 Integrated Reservoir Modeling Report are the result of work performed between November, 2010 and August, 2011.

This work, as part of an iterative integrated subsurface modeling strategy builds directly on the Generation-3 integrated models while maturing them further taking the availability of new data into account, such as the appraisal well data of the Radway 8-19 well and a completed and reprocessed Phase1 Quest seismic survey. The second aspect of the Quest iterative modeling strategy is to align the subsurface description and outputs with the decision needs of the project in this particular phase of the project maturation.

The Generation-4 (or Gen-4) integrated modeling activities were framed to directly support decisions associated with the Quest Storage Development Plan (SDP), are related to confirm aspects of the regulatory submissions and provided detail input to the MMV plan while also defining and quantifying conformance criteria for the Quest project.

The following paragraphs provide an executive summary of the key results of the Gen-4 integrated modeling activities.

The static model as used in the Gen-4 modeling has seen an additional calibration while incorporating the better than expected reservoir quality found in the Radway 8-19 appraisal well. Base on that, a 2D trend map was used to distribute porosity in addition to a simple 1D trend as was carried in Gen-3. The environment of deposition consisting of Tide-dominated Bay Margin, Proximal Bay and Distal Bay was confirmed. In addition, the contribution of High Energy Dunes (present in all 3 appraisal well cores) was increased from 5% to now 10% and was distributed more consistently at the base of the interval.

The dynamic simulator received an update of the relative permeability Corey model. The key difference, if compared to the Gen-3 version, is the use of imbibitions relative permeability experimental data to define the Corey exponents of the CO_2-brine primary drainage relative permeability curves, rather than using drainage relative permeability data. In contrast to the Gen-3 models, high and low case capillary pressure curves have been introduced in addition to a slightly updated base case.

Detailed CO_2 plume migration modeling of a 3 injector well scheme concluded a CO_2 plume radius of 4100m at the end of injection for the expectation case. If, for regulatory (D65) or public acceptance purposes, smaller CO_2 plumes are desired it was estimated that a CO_2 plume around a 5 well case would reach 3050m at the end of injection while an 8 well case would carry the expectation of an average plume sizes radius of only 2400m at the same time. Uncertainties around these values have been quantified while also identifying the key subsurface variables that drives the uncertainty in CO_2 plume size. It was found that, due to "sampling at different scales" and the change in drive mechanism the uncertainty drives

become time dependent. During injection the plume size uncertainty is mainly related to the uncertainty in reservoir baffle ratio, porosity/permeability and relative permeability. Contrarily, during shut-in key uncertainty drivers for plume size and migration are related to relative permeability effects and geological variations (variogram).

An aquifer flow study revealed average flow rates within the BCS of 1 cm/year with a low estimate of 0.3 cm/year and an high estimate of 39 cm/year, leading to the conclusion that such small flow velocities will have no impact on CO_2 plume migration, even at very long term dynamic simulations of 1000 years.

Thermal modeling of the injection of cold CO_2 into the BCS estimated a cooling zone of 320m after 25 years for a 3 injector development (190m for 5 injectors, 170m for 8 injectors). Geomechanical modeling and an analytical estimate of the fracture pressure reduction due to such formation cooling, however confirmed that the current range of Bottom Hole Pressure (BHP) constraints (low case = 26 MPa, base case = 28 MPa, high case = 32 MPa) still provides sufficient safety margin to avoid injection under fracture conditions.

Full field pressure modeling concluded that 3 to 8 vertical injectors provide sufficient injection capacity to mitigate the remaining range in subsurface uncertainty. The pore pressure at legacy wells was computed as well to inform the MMV plan and to quantify the risk of accidental leakage at those locations.

An estimate of leak rates a the closest legacy well (Imperial Darling-1, approx. 21 km away from the center of the Quest development) showed in a worst case scenario, such as an open borehole, very minor cross flow and leakage into overburden formations. Additional geochemical modeling was performed to quantify the hypothetical impact on the release of contaminants such as As, Pb or Fe while hypothetically leaking CO_2, acidic brine or native formation brine into Belly River Aquifer. It was found that, at realistic leak rates such contamination areas are concentrated within a few tens of meters around the leak path. The above leak path models, including any other model requiring overburden properties, benefited from a regional scale leak path model up to the surface as built in Petrel.

While having now a calibration point in the center of the development, via formation and sonic properties as acquired in the Radway 8-19 well, and the Quest Phase 1 seismic processing finalized, it was warranted to recalibrate time lapse seismic models to confirm the feasibility of detecting CO_2 plumes in the subsurface and to assess its accuracy. It was confirmed that the time laps seismic response of CO_2 in the BCS is robust to expected noise levels. The time lapse seismic response of CO_2 after a hypothetical leakage above the Lotsberg salt, now residing in either the Winnipegosis or the Cooking Lake, was found to be perhaps challenging but feasible.

All Gen-4 modeling activities, including the availability of new appraisal data confirmed the validity of key development decisions already made. Linking the subsurface to the surface components via Integrated Production System Modeling, it was confirmed that a Quest development consisting of 3 to 8 vertical injector wells, receiving CO_2 in dense phase via a 12" pipeline driven by a 14.5 MPa compression unit is a robust development under the remaining subsurface uncertainties.

TABLE OF CONTENTS

Page intentionally left blank

2. INTRODUCTION & OBJECTIVES

2.1. Introduction

To continue meeting the world's growing energy demand, while reducing greenhouse gas (GHG) emissions, several pathways must be pursued. Carbon Capture and Storage (CCS) is one of the six pathways that Shell is progressing along with increasing energy efficiency, low CO_2 fuel options, and advocating more effective CO_2 regulations, to reduce GHG emissions. The Athabasca Oil Sands Project Joint Venture (AOSP JV) owners – Shell Canada Energy (Shell), Chevron Canada Limited (Chevron) and Marathon Oil Sands L.P. (Marathon) – are advancing the front-end development work for a fully integrated carbon capture, pipeline and storage project in Alberta called the Quest CCS Project.

Quest is a fully integrated CCS project in the oil sands sector involving CO_2 capture at the Scotford Upgrader near Fort Saskatchewan, pipeline transportation northeast from Scotford and CO_2 storage in a deep saline formation zone. The project will:

- Capture and store CO_2 from the steam methane reformer units at the existing Scotford Upgrader and at the upgrader's expansion currently undergoing production start-up.
- The CO_2 will be compressed and transported via pipeline northeast of Scotford site
- The CO_2 will be stored underground (2,000 to 2,100 m) in a deep, highly saline aquifer formation (Basal Cambrian Sand).

On March 31, 2009, Shell submitted a Full Project Proposal (FPP) for the Quest Project on behalf of the AOSP Joint Venture Owners. Subsequent to this, the Government of Canada (GoC) announced the creation of a Clean Energy Fund that also made funding available for CCS projects. Shell was invited to submit the FPP to Natural Resources Canada, the administrators of the Clean Energy Fund, and did so on July 2, 2009.

Non-binding letters of intent were successfully negotiated with the GoA and the GoC for $865 million total funding (GoC $120 million; GoA $745 million), subject to the execution of binding funding agreements. Subsequent negotiations were successfully conducted and concluded on June 24th, 2011

Several regulatory submissions where prepared in November 2010 such as the D65, D56 and D51 applications and the OSCA on the capture plant. Subsequent Information Requests where answered during Q1 and Q2 of 2011. These regulatory submissions now setting the boundaries for the development of Quest, including the definition of some conformance parameters.

The capture, transport and injection of approximately 1.1 Mtpa of CO_2 is expected to begin towards the end of 2015. The Quest design case is for 25 years of capture and storage, which is linked to the operational life of the Scotford heavy oil upgraders. The CO_2 injection stream will be dehydrated, relatively pure (98%), and contains no H_2S.

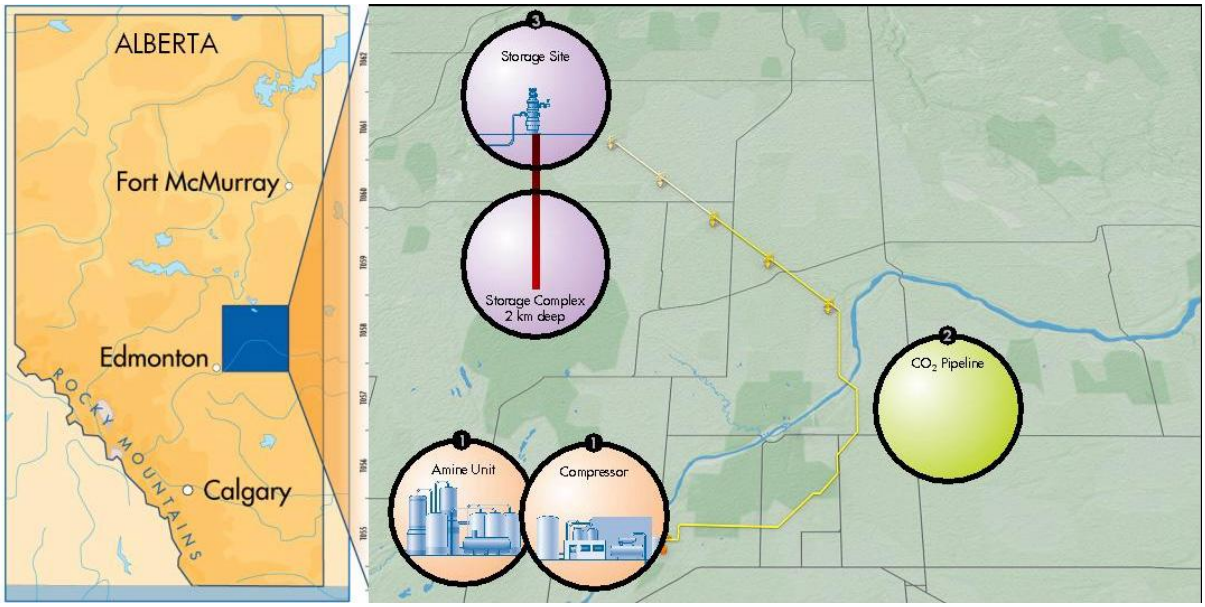

Figure 1: Schematic view of the Quest CCS Project in Alberta, Canada.

The Quest project is intended to store up to 1.2 million tonnes of year of CO_2 safely in the BCS formation from 2015 onwards. Design life has been set at 25 years, nominally linking the project to the remaining design life of the Scotford Upgraders.

As CCS projects are not commercially economic today, and certain aspects of the technology can be considered novel, in addition to the typical major project success factors there are a number of unique success factors that will require to be addressed.

- Deliver the project without harm to people (Goal Zero)
- Secure and maintain public support for Quest, particularly in the vicinity of the storage area (Thorhild & Radway)
- Secure a total of $865 mln of Federal and Provincial Government funding:
  - $745 mln from Government of Alberta
  - $120 mln from the Federal Government of Canada
- Store up to 27 mln tonnes of CO_2 over 25 years
- No CO_2 or BCS brine to 'leak' from the storage complex
- An MMV plan that is capable of demonstrating that no CO_2 or BCS brine has 'leaked' from the storage complex
- Handover of the site free and clear, post-closure to Government of Alberta
- Be considered to have fulfilled the extensive knowledge sharing obligations, and in particular de-risked the BCS as a major storage site for the Government of Alberta
- Breakeven at premise CO_2 price

- Access to multiple CO_2 credits have been negotiated to help close the economic gap whilst the CO_2 prices remain low compared to the cost of abatement.

2.2. Gen-4 Modeling Scope & Objectives

The Generation 4 modeling activities (referenced as Gen-4 in this document) reflecting the latest evolution of increasing subsurface definition and associated simulation of subsurface related outcomes directly impacting the successful development of Quest as defined in the last paragraph of the chapter 1 above.

The CO_2 plume uncertainty modeling, as an example, that was conducted during Gen-4 work has a direct impact on the definition of site conformance, on MMV activities and associated cost. To name another example. The pressure modeling as conducted using a Quest full-field model in Gen-4 verified our regulatory submissions, identified an opportunity to reduce the number of injection wells from a base case of 5 to 3 and helped to quantify the risk of potential leakage of highly saline brine at known legacy well locations. This work has provided the foundation for the Quest Storage Development Plan (Crouch, 2011)

As with previous generations of Quest subsurface models, the Gen-4 modeling activities were part of an iterative modeling strategy driven by increasing data availability and closely linked to the decision requirements of the Quest project timeline (Figure 2 below).

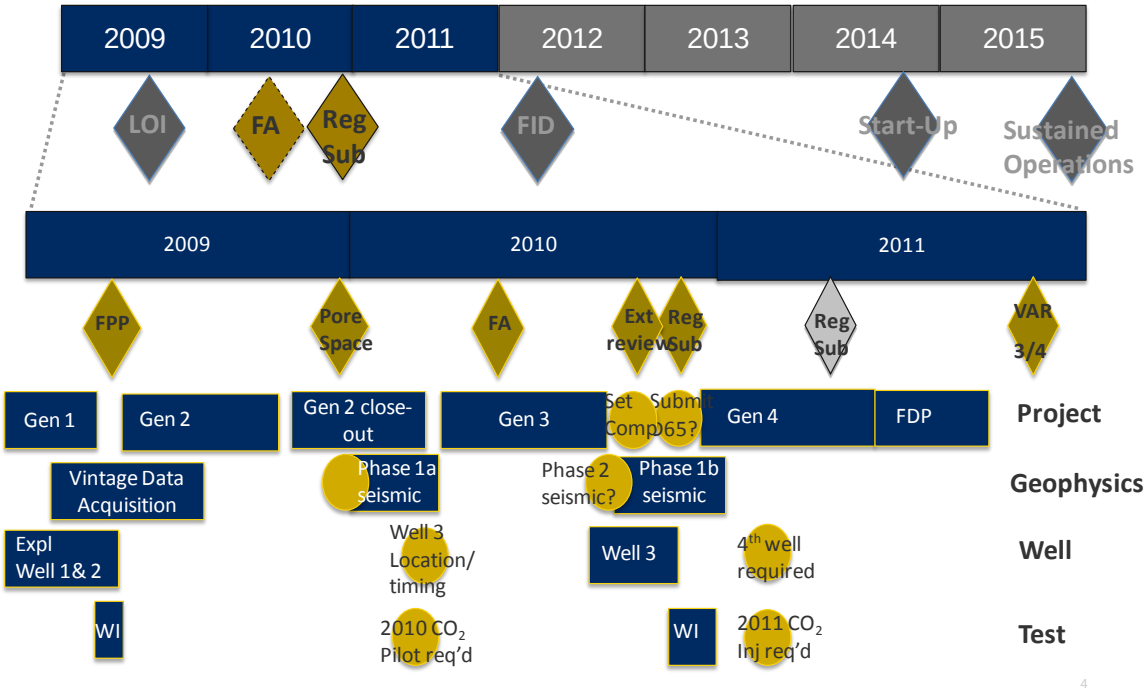

Figure 2: Quest project time line and major milestones (top time line) and subsurface activities and iterative modeling projects (zoom in below)

A detailed description of the iterative modeling strategy is attached in APPENDIX 1, including objectives, outputs and learnings.

Gen-1 models, as used in 2009, were essentially screening models based on regional data. Their outputs and findings supported the submission of the FPP (Full Project Proposal)

Gen-2 activities benefited from the availability of first results gathered at Shell appraisal wells (Redwater and Scotford wells) and additional legacy seismic improving the geological understanding of the storage complex significantly. These models provided input to the submission of the Exploration Tenure and also de-risked the Funding Agreement due to confirming the anticipated injector well count while having a more local calibration.

The results of both, Gen-1 and Gen-2 activities are reported in (Winkler, Quest CCS Project - Technical Feasibility and Forward Plans to FID, 2010).

The Gen-3 models, as built in 2010, focused on providing input to the Regulatory Submissions. Subsurface uncertainty was further reduced due to fully incorporating log and core date of the 2009/2010 Shell appraisal wells, the interpretation of the Phase 1A seismic survey and a HRAM (High Resolution AeroMagnetic) survey. A summary of this phase of modeling can be found in the Quest Generation-3 Integrated Modeling Report (Winkler, 2010)

The Gen-4 models and outcomes, as summarized in this report, focused on supporting select and define decisions of the Storage Development Plan while also providing subsurface-to-surface guidelines on operational aspects including MMV activities.

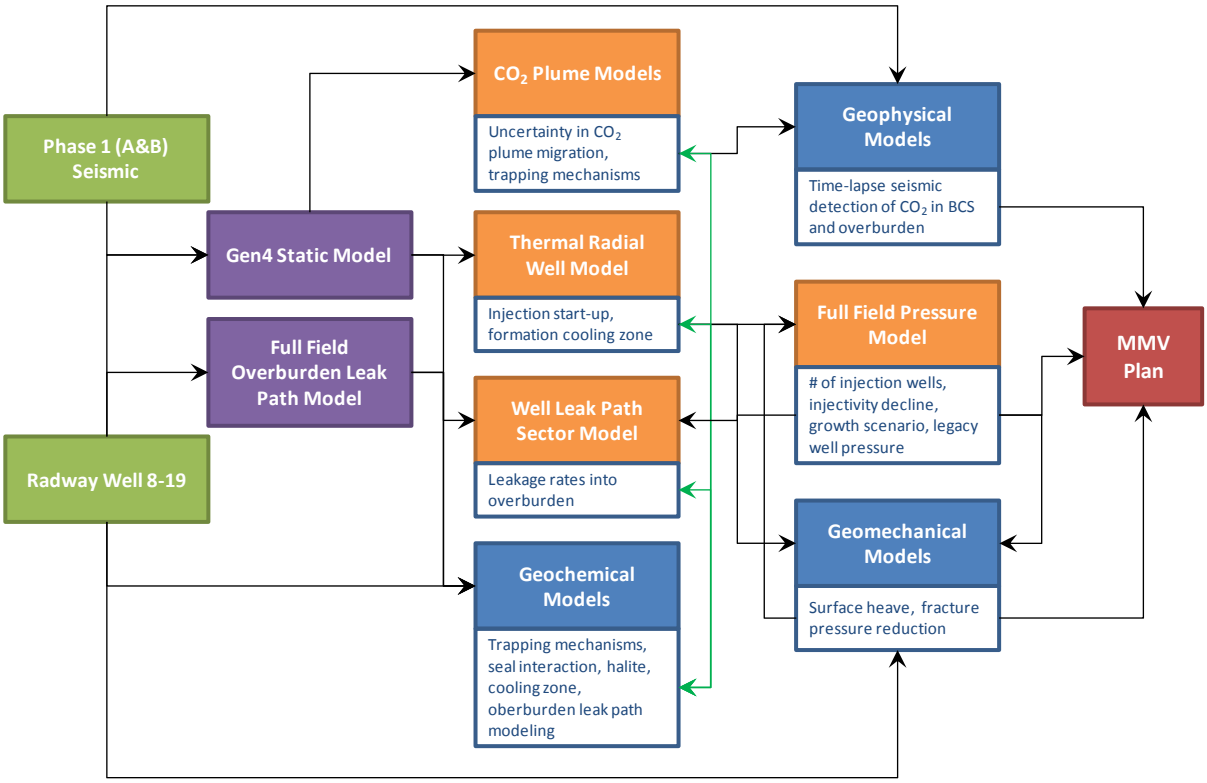

Figure 3: Gen4 data inputs, static, dynamic and "other" models including interdependency, outputs and synergy.

A high level summary of key Gen4 models, their inputs, interdependency and cross synergy is shown in Figure 3 above. Needless to say, the mentioned outputs are key inputs to the Quest Storage Development plan while also supporting the various regulatory submissions as well as the MMV plan.

3. PROPERTIES & UNCERTAINTIES

3.1. Conceptual Depositional Model & Facies Modeling

The Quest Gen-4 geologic model was designed to be representative of a ~350 m thick section of the subsurface at the base of the Western Canada Sedimentary Basin within the geological scale AOI (~180 km x ~190 km).

The Quest Gen-4 facies model was constructed to represent sediment deposition during a transgression upon the North American craton in which the broad Precambrian margin was slowly flooded by the Panthalassic Ocean from the present West - Southwest toward the Canadian Shield hinterland to the present East - Northeast. The initial deposition associated with this transgression manifests as the Middle Cambrian Basal Sandstone and Earlie formations, which are respectively represented by the Basal Cambrian Sand (BCS) and Lower Marine Sand (LMS) zones in the Gen-4 model).

The Gen-4 Environment of Deposition (EoD) facies model is constrained by:

- analogue literature addressing both coincident North American Cambrian sections as well as modern depositional systems
- interpretations of cores of this interval recovered at Radway 8-19, Redwater 3-4 and 11-32 and 5 additional well locations,
- A suite of 19 variable vintage well logs over the geologic AOI.

3.1.1. BCS Depositional Analogues

North American Lithostratigraphic Analogues

The Western Canada Sedimentary Basin (WCSB) Cambrian sequence is not unique, but rather the regional expression of a global Cambrian transgression associated with the Sauk II Subsequence of North America. Remarkably similar sequences of tidally influenced sheet sandstones lying directly atop Precambrian basement and below progressively more distal siliciclastic sediments wrap around an extensive portion of the North American Craton (Figure 4). Analogous lithostratigraphic equivalent formations to the WCSB Basal Cambrian Sand include the Flathead Formation of Wyoming and Montana (Miller, 1936), the Reagan Formation of Oklahoma, Kansas, and Nebraska (Howell et al., 1944), the Riley Formation of central Texas (Chafetz, 1978), the Lamotte Formation of Missouri (Ojakangas, 1963), the Mt. Simon Formation of South Dakota, Minnesota, Iowa, Wisconsin, Illinois, Indiana, and Ohio ((Howell, 1944); (Runkel A. C., 1998), the Potsdam Formation of eastern Ontario, southern Quebec, and New York (Otvos, 1966), and the Bradore Formation of south-eastern New Foundland and Labrador (Hiscott, 1984). These formations were deposited coincidentally as the Panthalassic and Iapetus Oceans slowly encroached on the equatorially positioned proto-North American continent, Laurentia, as extensions of each other, effectively creating a relatively thin but

laterally extensive sheet sandstone complex that lies at the base of much of the North American sedimentary column.

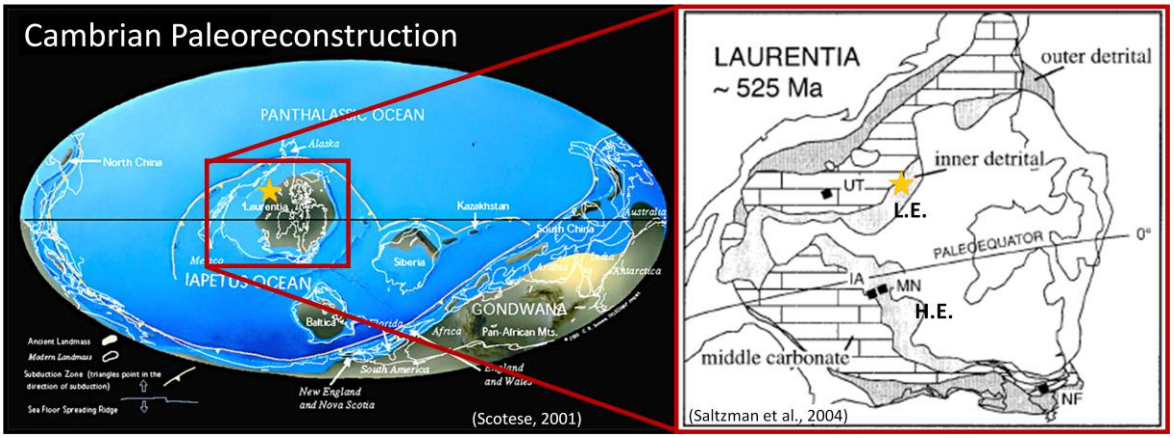

Figure 4: Cambrian Paleoreconstruction. Approximate position of Quest AOI is illustrated with gold star. The Lloydminster and Hollandale embayments are respectively denoted by "L.E." and "H.E." in the blown up Laurentia facies belt map at right.

Outcrop, core, and well log investigations of these formations inform the Gen-3 conceptual design and modeling of the Cambrian sequence. Common characteristics of these lower Paleozoic cratonic interior strata include their widespread but relatively thin (typically < 100 m) sheet-like geometries, extreme textural and mineralogical maturity, and pronounced lack of clay to silt-sized sediments ((Runkel A. C., 2007) and references therein). Plausible causes of these somewhat anomalous characteristics include a lack of Cambrian terrestrial vegetation induced fine-grained source material, exceptionally slow subsidence rates of Precambrian crystalline basins and associated reduced accommodation space, the existence of broad shallow bathymetry margins, and extremely low cratonic shelf gradients (Runkel et al., 1998, 2007). In concert these conditions effectively yielded basal Cambrian sandstones highlighted by extensive reworking of shoreface material and associated transport of scoured fine-grained material to exceptionally distant outer margin environments. A reasonable sequence stratigraphic interpretation of such a system necessitates facies belts that are both elongated in space and representative of a greater amount of time relative to the traditional intra-cratonic eperic sea deposition (Runkel et al, 2007; Figure 5).

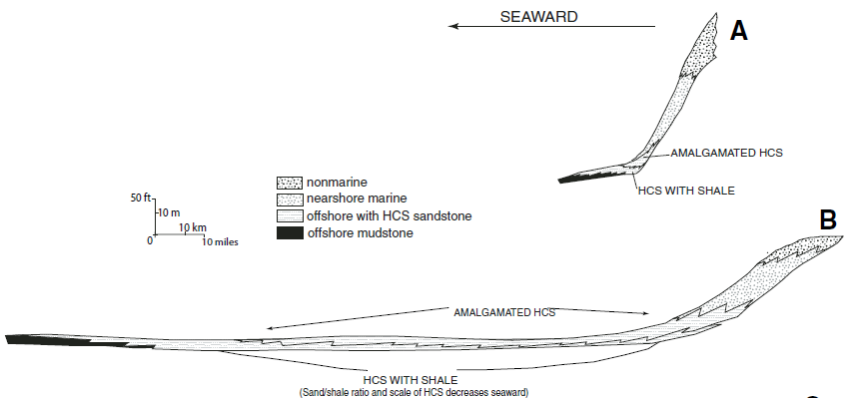

Figure 5: Idealized comparison of Cretaceous intra-cratonic eperic sea (A) and lower Paleozoic cratonic shelf margin (B) facies belt extents (Runkel et al., 2007).

The Mt. Simon formation of the Midwestern United States is particularly well suited as an analog to the WCSB BCS because it was deposited in a similar tectonic setting at approximately the same latitude. Reconstructions approximate that the Mt. Simon accumulated in a broad open embayment known as the Hollandale on the Southwestern coast of Laurentia, while the BCS was deposited in the Lloydminster broad open embayment on the Northern Laurentia margin (Figure 4). Both margins were characterized by a wide shallow cratonic shelf that likely never experienced water depths greater than ~100 m during Mt. Simon / BCS deposition (Runkel et al., 2007).

Outcrop, well log, and core constrained correlations of the Hollandale embayment Cambrian sequence illustrate Mt. Simon coarse-grained sandstone transgressive system tract sediments overlain by progressively more offshore finer-grained siliciclastic sediments and thin carbonate stringers of the Eau Claire and Bonneterre formations representative of the upper transgressive to highstand system tracts (Figure 6; Runkel et al., 2007). This sequence is consistent with a depositional model in which the broad shallow Precambrian margin was slowly filled by sediments characteristic of progressively more distal environments, beginning at base with fluvial sedimentation, continuing through a tide dominated shoreface environment in which the noted sheet sandstones were deposited, and culminating in low-energy offshore shelf deposition of fine-grained siliciclastics and carbonates (Figure 7). This sequence, which may represent ~4 Myrs of Cambrian sedimentation (Runkel et al., 2007), is mimicked in the Lloydminster embayment by coincident deposition of the BCS, Earlie, and Deadwood formations (Figure 8).

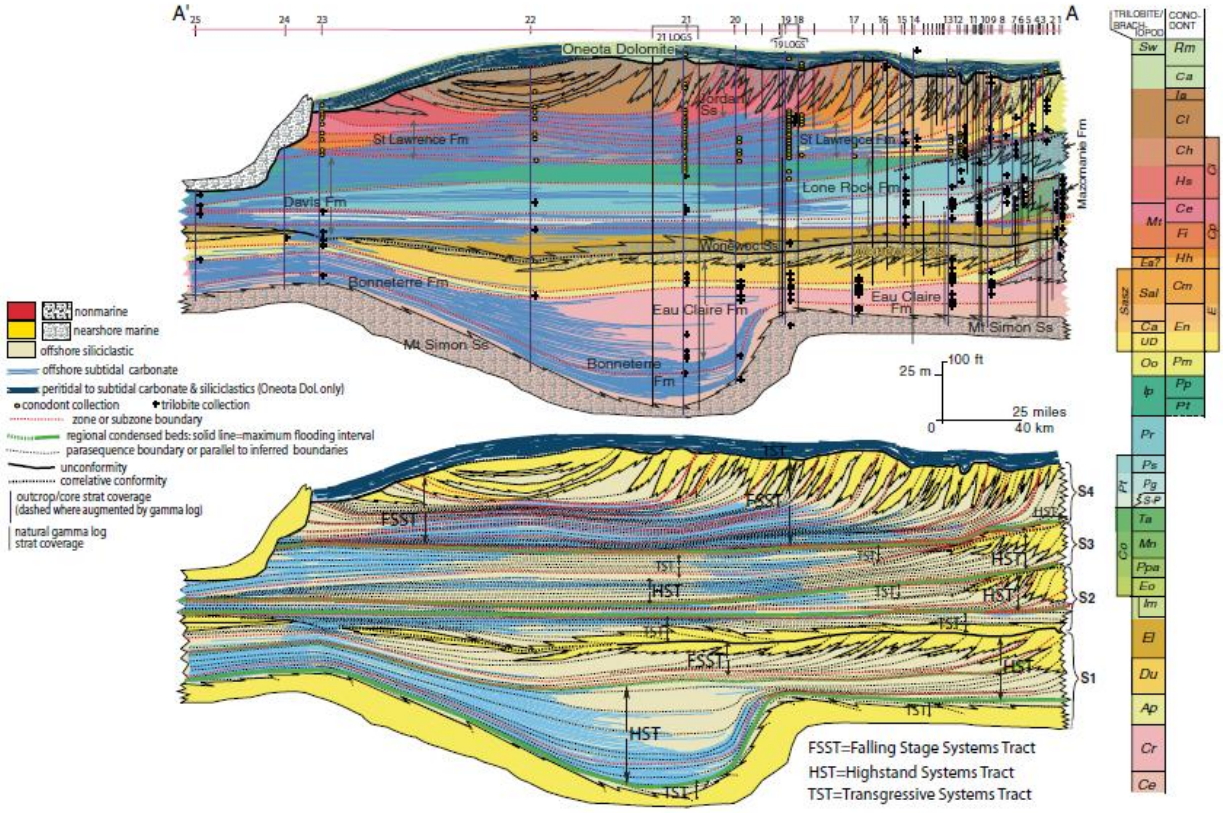

Figure 6: Stratigraphic cross sections of Middle Cambrian to Lower Ordovician rocks deposited on the Upper Mississippi Valley eperic ramp in the Hollendale embayment (Runkel et al., 2007).

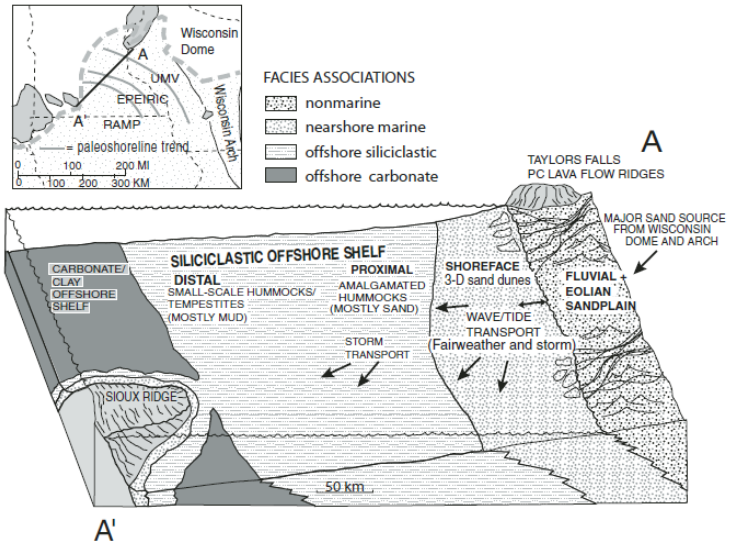

Figure 7: Depositional model of the Cambrian sequence.

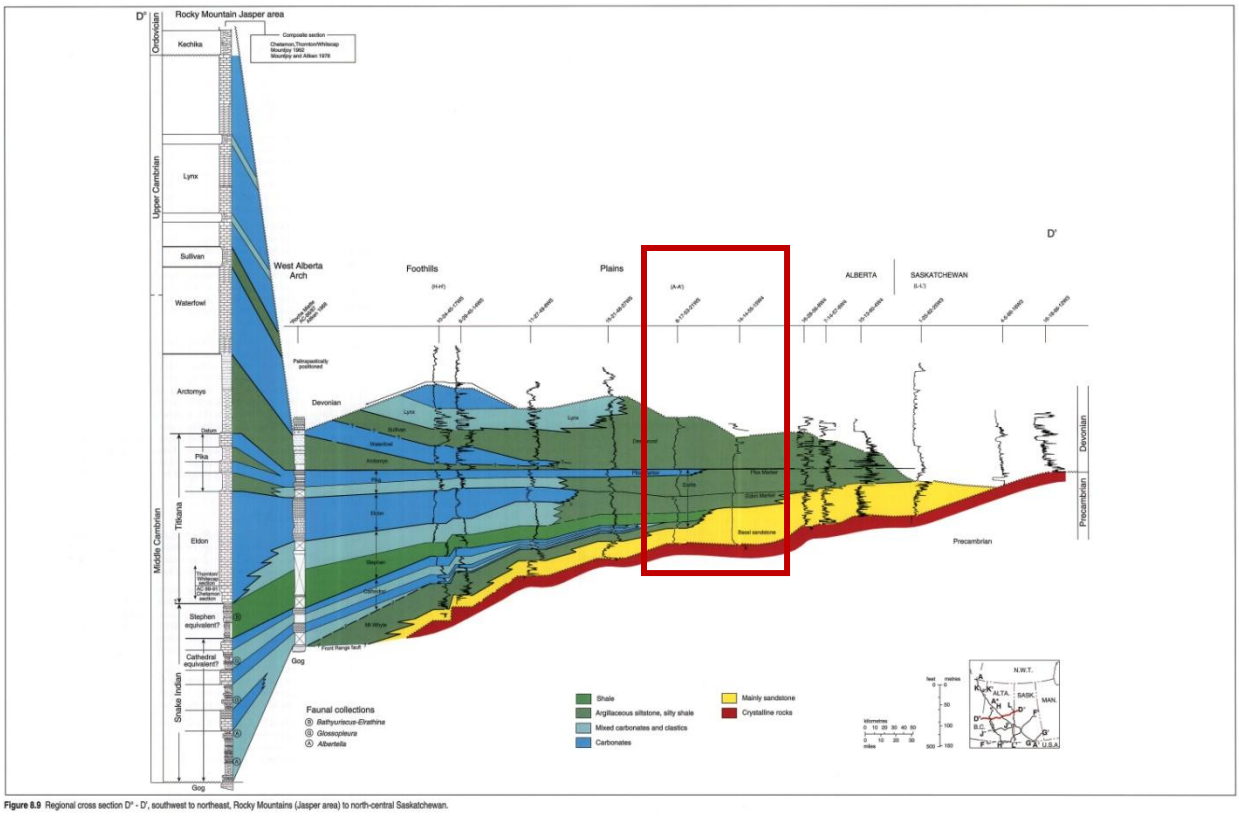

Figure 8: Cross section through the Western Canada Sedimentary Basin illustrating the Cambrian passive margin sediment sequence (Slind et al., 1994). Approximate extent of the Quest AOI is denoted by the red rectangle.

3.1.2. Modern Tide Dominated Margin Systems

Tidally influenced environments create some of the most complex depositional systems in the modern world because of the variable interaction of numerous physical, chemical, and biological processes. These include the influence of local bathymetry, river and tidal currents, wave energy and associated longshore currents, the brackish character of the water as it transitions from fresh river inputs to ocean salinity, and the impact this salinity transition imparts on the abundance and assemblage of bioturbating macrofauna (Figure 9) Dalrymple and Choi, 2007 and references therein). While tide dominated systems as a whole are a common phenomena of modern coastlines the world over (Figure 10), the degree to which the noted variables impact a given locality acts to delineate four distinct systems including those associated with river-mouths, open-ocean settings, heads-of-bays, and tidal-coasts (Figure 11). These systems are best thought of as a continuum that exists along a given continental margin as the climate and river influence, shelf width and depth, and coastal topography of that margin evolve both in space and time.

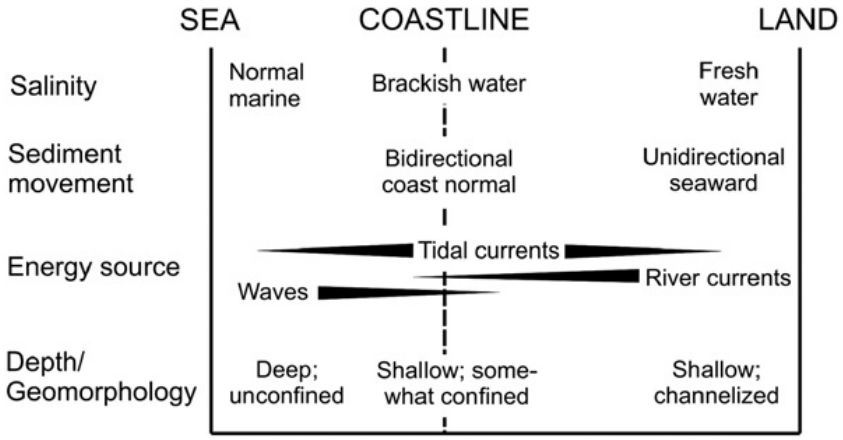

Figure 9: Coast-normal variation in the essential controls on sedimentation in the transition from purely fluvial settings ("land"), through the tide-dominated coastal zone, to shelf environments ("sea") (Dalrymple and Choi, 2007).

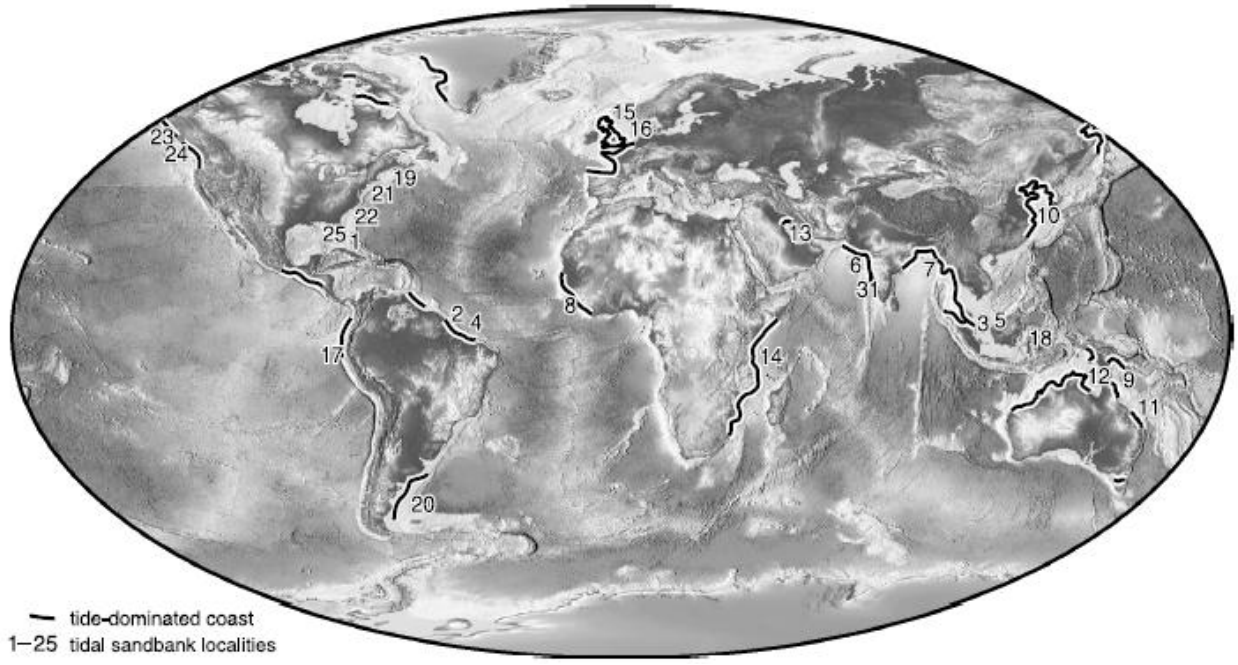

Figure 10: World map of tide dominated systems and as indicated by occurrence of tidal dune complexes (Wood, 2004). Numbers refer to locations studied by Off (1963).

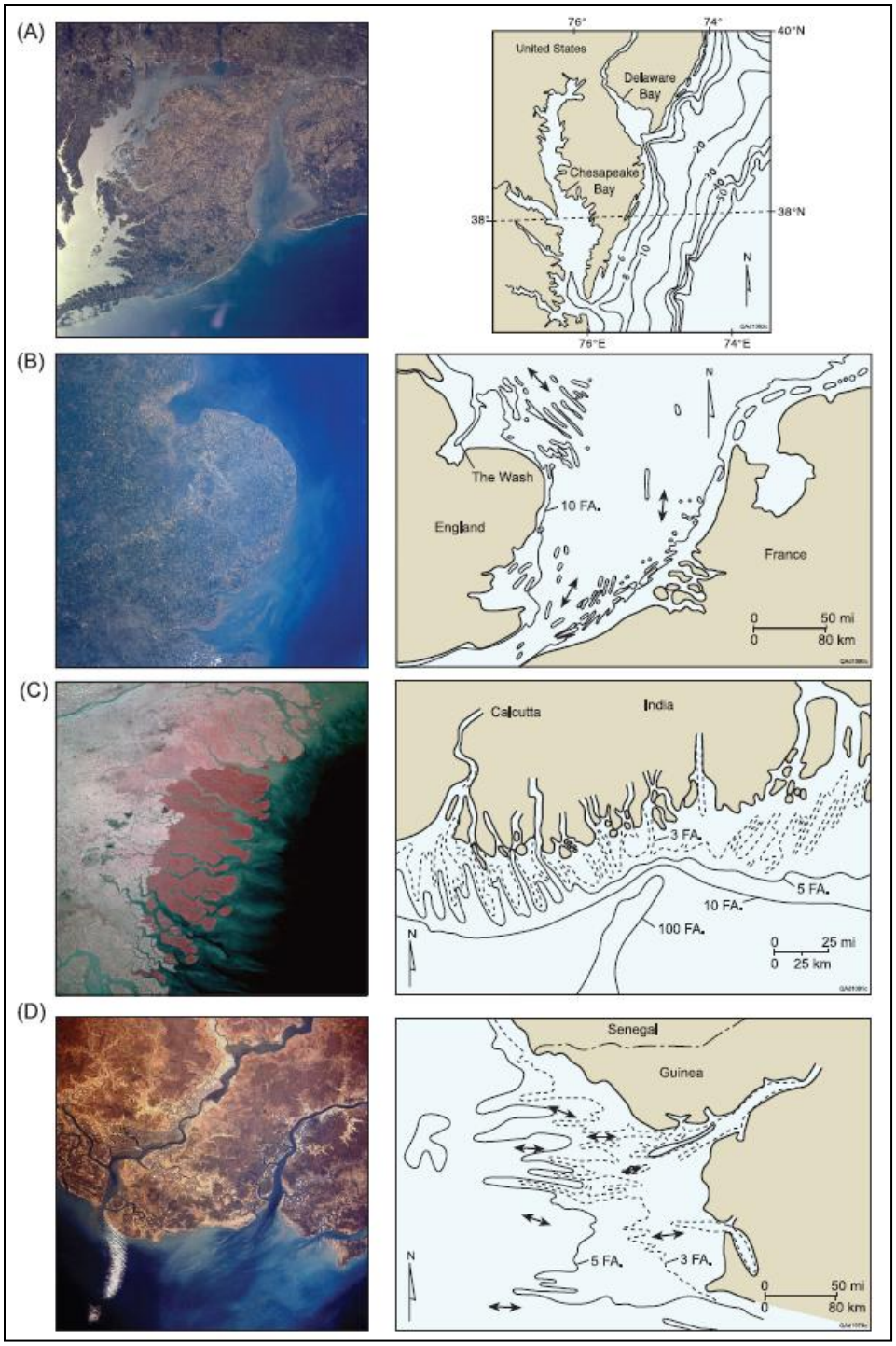

Figure 11: Examples of the four geomorphic classes for tidal sandbanks as defined by Off (1963) (Wood, 2004).

Figure 11 shows examples of different geomorphic classes for tidal sandbanks. Illustrated examples include: (A) river-mouth example showing the morphology of the mouth of the Delaware River, U.S.A.; (B) open-ocean example showing the Tongue of the Ocean area in the Bahamas at left and the southern North Sea at right; (C) head-of-bays example showing the Ganges Delta, India; and (D) tidal-coast example showing the coast of west Africa near the Senegal and Guinea-Bissau border. FA = fathoms.

The nature of sand bodies within these systems is similarly complex and broadly occurs as bed forms indicative of bars, flats, or channels. Formations such as the North American basal Cambrian sandstones that were subject to a slow transgression and therefore much reworking should be principally composed of amalgamated tidal bar forms. Although frequently used interchangeably, two scales of tidal bar forms are discernable in both modern and ancient settings. These include tidal sand bars, which are recognized as single-cycle, coarsening-upward, elongate sand features that are typically <5 m thick, <1.5 km wide, and < 10 km long, and tidal dune complexes (sometimes referred to as sand ridges) that are themselves composed of multiple cycles of tidal sand bar deposition and therefore can be significantly larger bodies on the order of <20 m thick, <5 km wide, and <60 km long ((Wood, 2004). Tidal sand bars consist of a series of dipping beds oriented toward the direction of dominant flow that are commonly intercalated with fine-grained sediments deposited during the low-energy portion of the tidal cycle ((Dalrymple, 2007) (Figure 12)). Erosion and re-deposition by subsequent tidal cycles yields bar forms and eventually compound dune complexes that exhibit complex multidirectional flow patterns and therefore tortuous reservoir flow conditions.

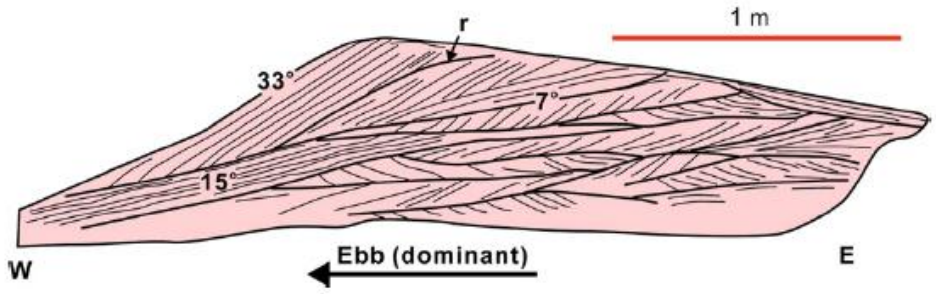

Figure 12: Internal structures of a small compound dune (Dalrymple 2007). Reactivation surface denoted by “r”.

Tidal channel width and curvature imparts a dominant control on both the growth style and shape of the resulting bar tidal bar forms. Where tidal channels exist as dendritic extensions of terrestrial riverine systems, the more nearshore tidal channels are relatively narrow and more sinuous, causing tidal bars to form as bank-attached point bars or alternate bars that exhibit a similar sinuosity (Wood, 2004); (Dalrymple, 2007) (Figure 13). However as the depositional setting becomes more increasingly dominated by marine conditions, tidal channels are relatively wide and straight, leading to more linear tidal bars oriented normal to shore and containing

morphological elements of the channels themselves (Wood, 2004; Dalrymple, 2007; Figure 13). Ultimately, both internal sand body architecture and external tidal bar form and tidal dune complex shape is a reflection of the influence of the multidirectional flow inherent to the tidal system and the relative position and current strength of adjacent river systems.

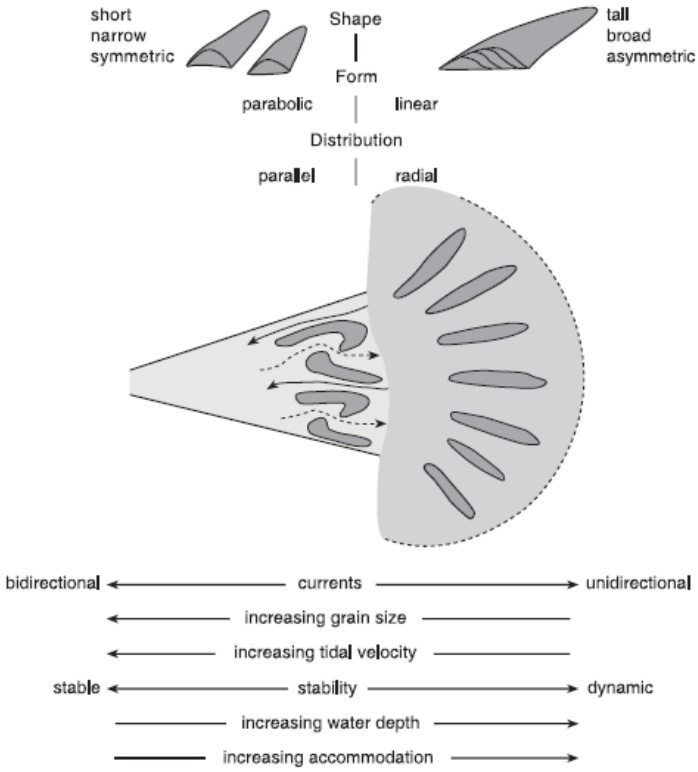

Figure 13: Idealized illustration of spatial variance of factors influential to the shape, form, and distribution of tidal sand bars (Wood, 2004).

3.1.3. Core Descriptions & Offset Well Correlation

Three independent core description studies were conducted on core from wells within the regional study area, including both Quest appraisal wells (11-32 and 3-4) and 5 additional wells of variable core recovery and quality (Table 1).

Table 1: Core description workers and thicknesses interpreted.

Well Name	**Desjardins, P.R. & Buatois, L.A. (University of Saskatchewan)**	**Farris, M. (Shell Int. E&P)**	**Kier, J. & Cormier, R. (Core Lab)**
	Described Section Thickness (m)		
SCL Radway 8-19	52.05		
SCL Redwater 11-32	37.42	29.89	205.90
SCL Redwater 3-4	35.57	-	-
Imperial Ardrossan No.1	6.13	-	-
Imperial Egremont 6-36	0.75	-	-
Imperial Clyde No.1	1.50	-	-
Imperial Baysel Riverdale 1-27	22.08	-	-
Imperial Dapp No.1	6.52	-	-

All three studies provided broadly consistent interpretations both in regard to each other as well as prior work on coincident North American Cambrian margin sequences. The results of Desjardins and Buatois were the principal source or the modeling because :

- it addresses cores from multiple well locations including all Quest appraisal wells
- the authors are amongst the world's experts in Western Canada Sedimentary Basin and Rocky Mountain Foothills Cambrian sequences.

In sum, Desjardins and Buatois describe 16 lithofacies, 6 independent lithofacies associations, and 4 Environments of Deposition (EoD), see Figure 14.

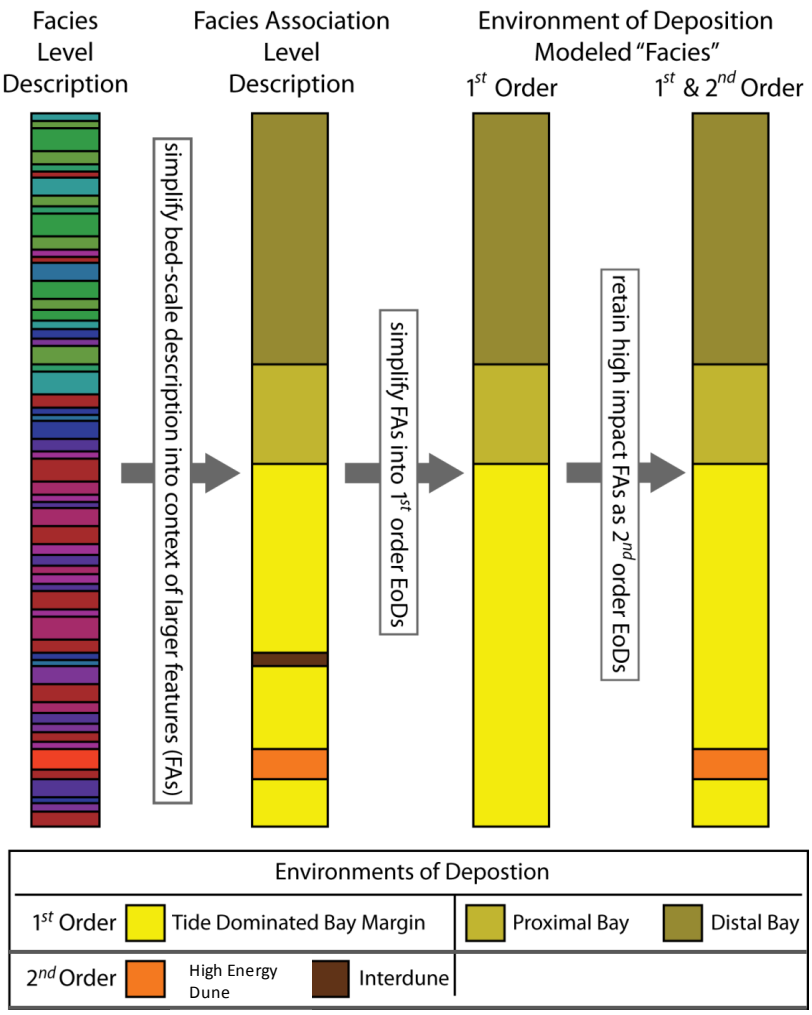

Figure 14: Core description hierarchy and facies modeling workflow.

3.1.4. Environments of Deposition

The environmental framework of MacEachern and Gingras (2007) for bay successions is adopted for this description. These authors distinguished restricted bays (embayments that have limited or intermittent connection to the open sea) and open bays (embayments having virtually unrestricted connection to the open sea).

The Lloydminster Embayment can be described as a large open bay in the cratonic interior, fringed to the west by a carbonate platform. Five main environments are recognized as:

1. Fluvio-influenced tide-dominated bay margin;
2. Tide-dominated bay margin;
3. Proximal bay,
4. Distal bay and

5. Offshore

The first three assemblages are formally included within the BCS, while the fourth and fifth assemblages occur in the lowermost Earlie Formation, or LMS. The distinction between the distal bay and offshore is based on the ichnologic content and is linked to a salinity gradient, however the offshore environment was recognized only in the regional core analysis (Desjardins and Buatois, 2010) and corresponds to a higher stratigraphic interval than the zones of interest for the Gen-4 models.

For the purposes of building the Gen-4 models the Cambrian transgression is described by sediments deposited in the following major environments of deposition (Figure 15; Figure 17):

1. Tide Dominated Bay Margin (TDBM)
2. Proximal Bay
3. Distal Bay

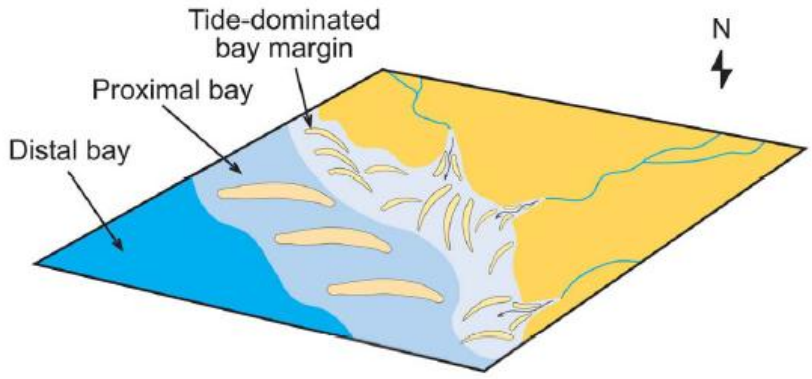

Figure 15: Major environments of deposition incorporated into conceptual and 3D facies model.

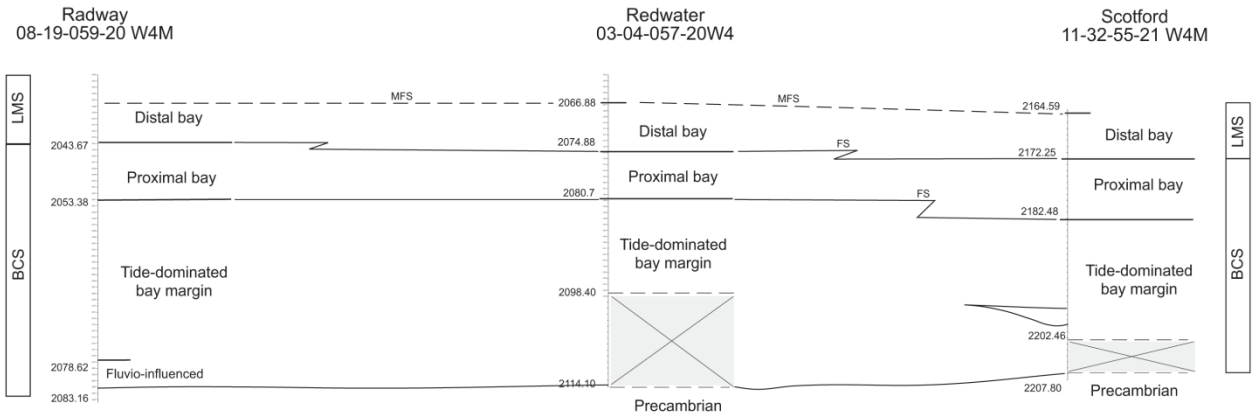

Figure 16: Correlation of all tree Quest Appraisal wells showing consistency in depositional style.

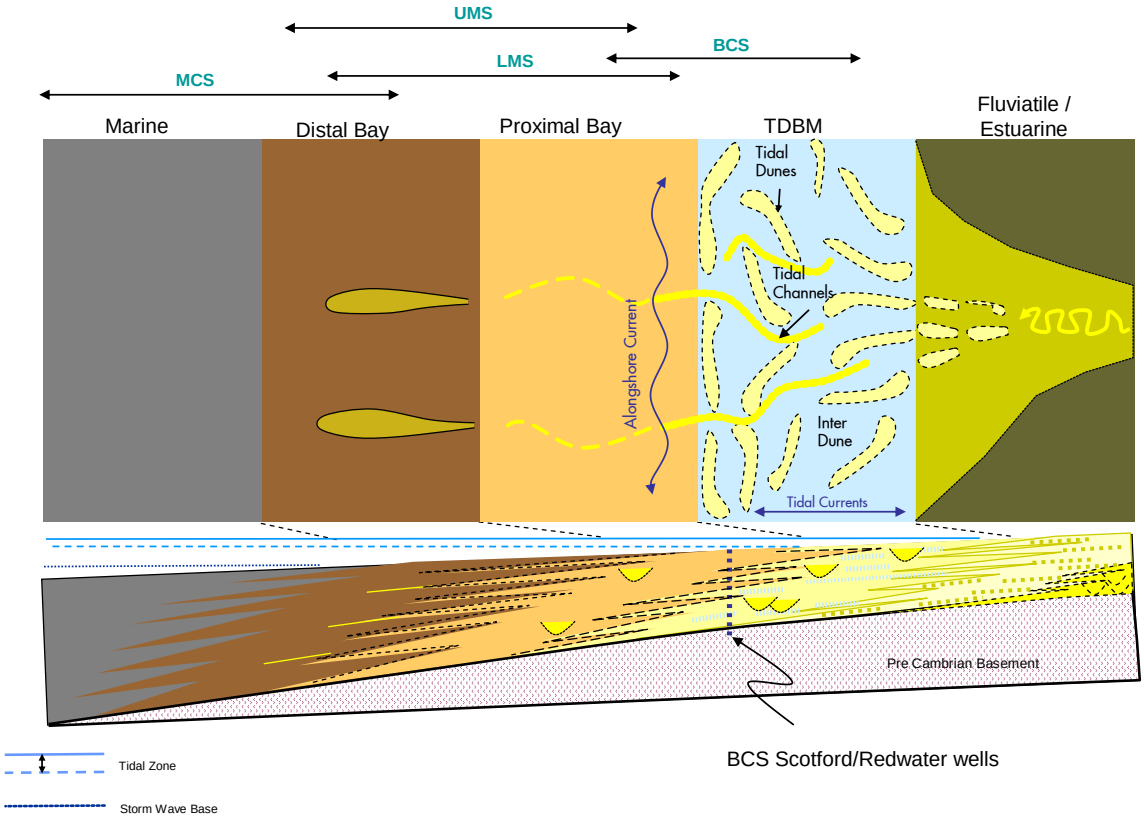

Figure 17: Quest 3D conceptual model of the major environments of deposition with map view showing relationships at time of deposition and cross section showing preserved sequence.

Tide Dominated Bay Margin (TDBM)

The TDBM EoD is comprised of sub-tidal dunes, inter-dunes and high energy dune sands frequently deposited in the most proximal position in the bay margin. This EoD records the highest NTG (~0.97 from FMI interpretation, see (Simone, 2011) and overall represents the best reservoir quality material within the Cambrian sequence.

Sub-tidal dune

Multiple compound cross-stratified packages record the migration and deposition of superimposed bedforms. Evidence of migration of ripples and storm events is present in core. The presence of thick intervals composed mainly of tidal dune core and toe/top lithofacies suggest these deposits were part of larger geomorphological elements, such as bars. FMI data from the Redwater 3-4 and Redwater 11-32 wells suggests that the orientation of the cross beds was oblique to perpendicular to the paleoshoreline. This distribution pattern supports the tidal-bar interpretation, as these are generally oriented obliquely to almost perpendicular to the

dominant tidal flow (Dalrymple, 2007). In between tidal bars, both low-energy interdunes areas or high-energy tidal channels can be present.

This dynamic environment ultimately yielded a highly complex sand body architecture at both the bed scale (e.g. multiple orientation toe and top sets) and dune scale (e.g. parabolic or sigmoidal dunes), and therefore, a torturous flow path in both the horizontal and vertical directions is expected. Sand body dimension estimates range from 460-3500 m long by 8-55 m wide and 0.2 – 1.2 m thick.

Inter-dune

These features should represent the lowest quality reservoir material in this EoD as they would have been exposed to the same episodic low energy suspension fall out of fines but a reduced concentration of sand relative to the tidal dunes. Whilst interdune is not explicitly modelled, the impact is captured in the model as the lower end of the relatively broad spectrum in reservoir quality of the TDBM environment.

High Energy Dune

This lithofacies association often occurs as erosively-based, 1–2 m thick, fining-upwards packages composed of coarse to very-coarse grained, cross-stratified sandstones that grade upward to overlaying medium- to coarse-grained cross-stratified sandstones with common mud drapes, finally capped by fine-grained, very thin- to thin-bedded heterolithic lithofacies or massive mudstone.

These fining-upwards packages record deposition by dunes in a higher-energy environment, possibly within confined areas or channels. The variety of lithofacies documents deposition by tidal dunes, located adjacent to or in the channels. Finer-grained heterolithic lithofacies record low-energy conditions that occurred after channel abandonment.

The lack of mud-drapes, visible amounts of feldspar, subangular nature of some of the grains in the lowermost interval suggests a fluvial-influence. However, the presence of *Planolites* burrows within the lower package indicates the presence of at least brackish-water conditions. Therefore it is interpreted that these deposits represent the most proximal position in the bay margin, and that there may have been connection to rivers draining into the marine embayment. This fluvial influence disappears as one moves up in the section.

The High Energy Dune facies (HED) represent the consistently highest quality reservoir material within the Cambrian sequence (See Reservoir Quality: Horizontal Permeability). Therefore these features, although significantly rarer than the other EoDs incorporated into the facies model, were explicitly retained in the facies modeling efforts. HED sand body dimensions are estimated to range from 5-15 km long by 0.25-1.5 km wide.

Sand Body Dimensions and Orientation

The TDBM texture represented in the model is designed to be a function of the antecedent topography of the Precambrian following the approximate orientation of the Pre-Cambrian Rimbey Block, which geophysical work indicates was marked by localized "bald highs" along its boundary during TDBM deposition (see Reservoir Connectivity section). The NE – SW axis of this basement block should then have created a topographic low and ultimately had a broad impact on reservoir quality and sand body geometries. This is reflected in the model via the use of a map to control sand body orientation derived from the trends in basement lineaments (Figure 19).

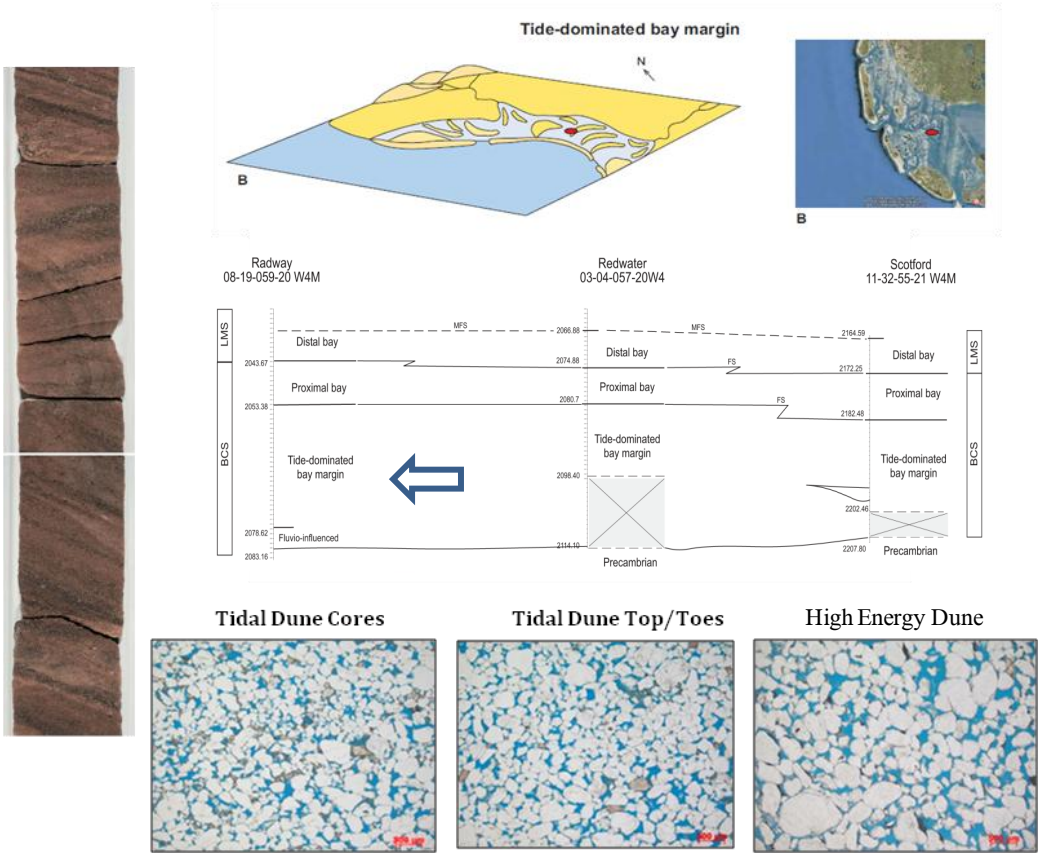

Figure 18: Facies associations and thin sections of the Tide Dominated Bay Margin interval.

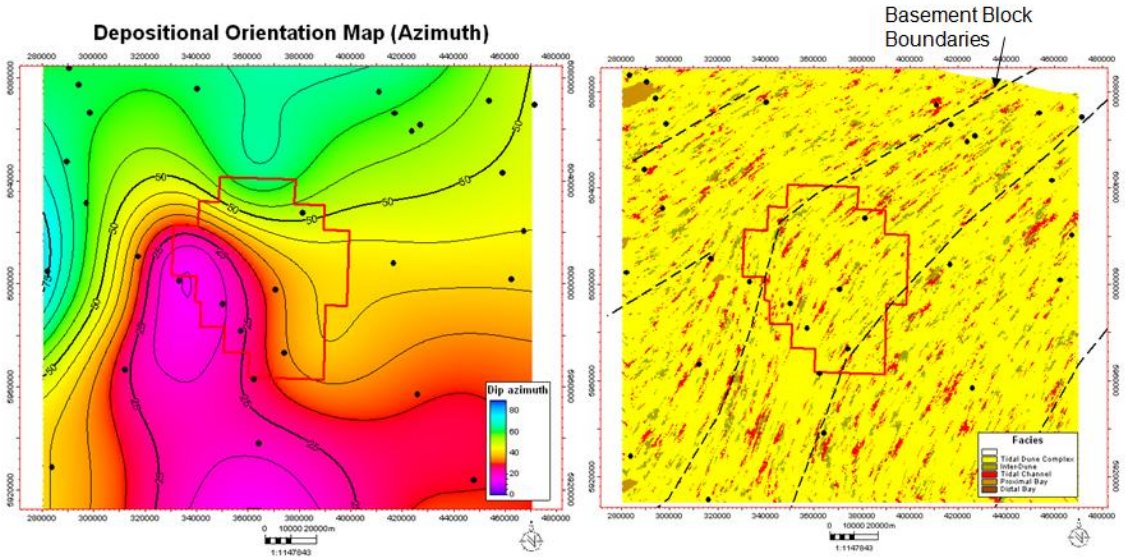

Figure 19: Orientation of Precambrian basement block boundaries were used to create an azimuth map to control TDBM 2nd order facies body orientations and reservoir quality variability.

Proximal Bay

This represents a deepening of water depth relative to the TDBM. Sediment deposition likely occurred near or below the fair weather wave base resulting in both a relatively high sand concentration but also an increase in the amount of clay to fine-silt sized material that dropped out of suspension (Figure 17).

Sand bodies, while certainly rarer than in the TDBM, should be larger in this EoD as fewer flow restrictions (i.e. tidal bars) should have yielded more uniform current distributions and ultimately allowed for sand bodies to splay out. While this EoD yielded a relatively high NTG (~0.93), and potentially horizontal flow pathways, the increased concentration of shale intercalations meands that vertical flow is highly restrictive.

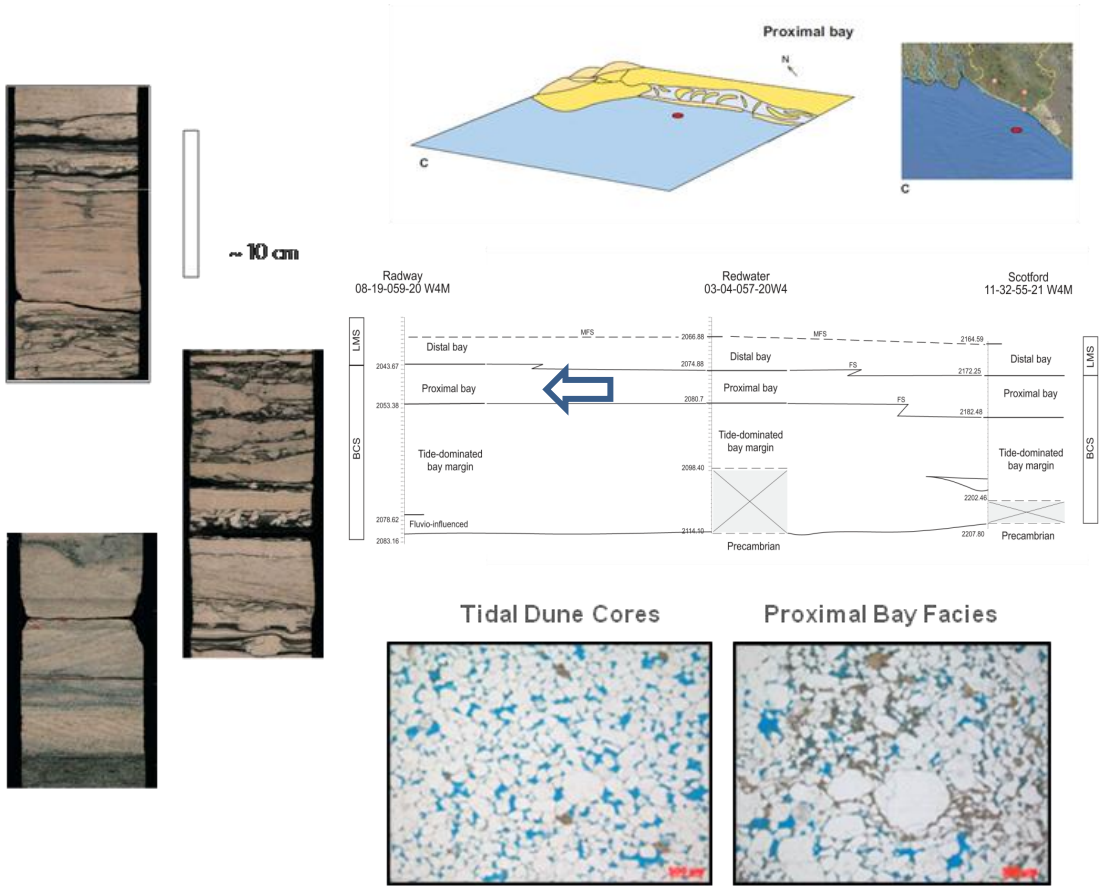

Distal Bay

This EoD represents the lowest energy system in the facies model. This facies is composed principally of fine-grained sediments deposited between the fair weather wave base and storm wave base (Figure 17) as the ocean continued to transgress upon the Canadian Shield to the NE. Sand deposition occurred as rare tempestite deposits during high energy storm events and likely had an even broader aerial coverage than similar deposits in the Proximal Bay.

The diminished sand deposition within this EoD and subsequent decreased NTG (~0.35-0.5) yields a very poor quality reservoir that acts principally as a barrier to flow in both the horizontal and vertical directions.

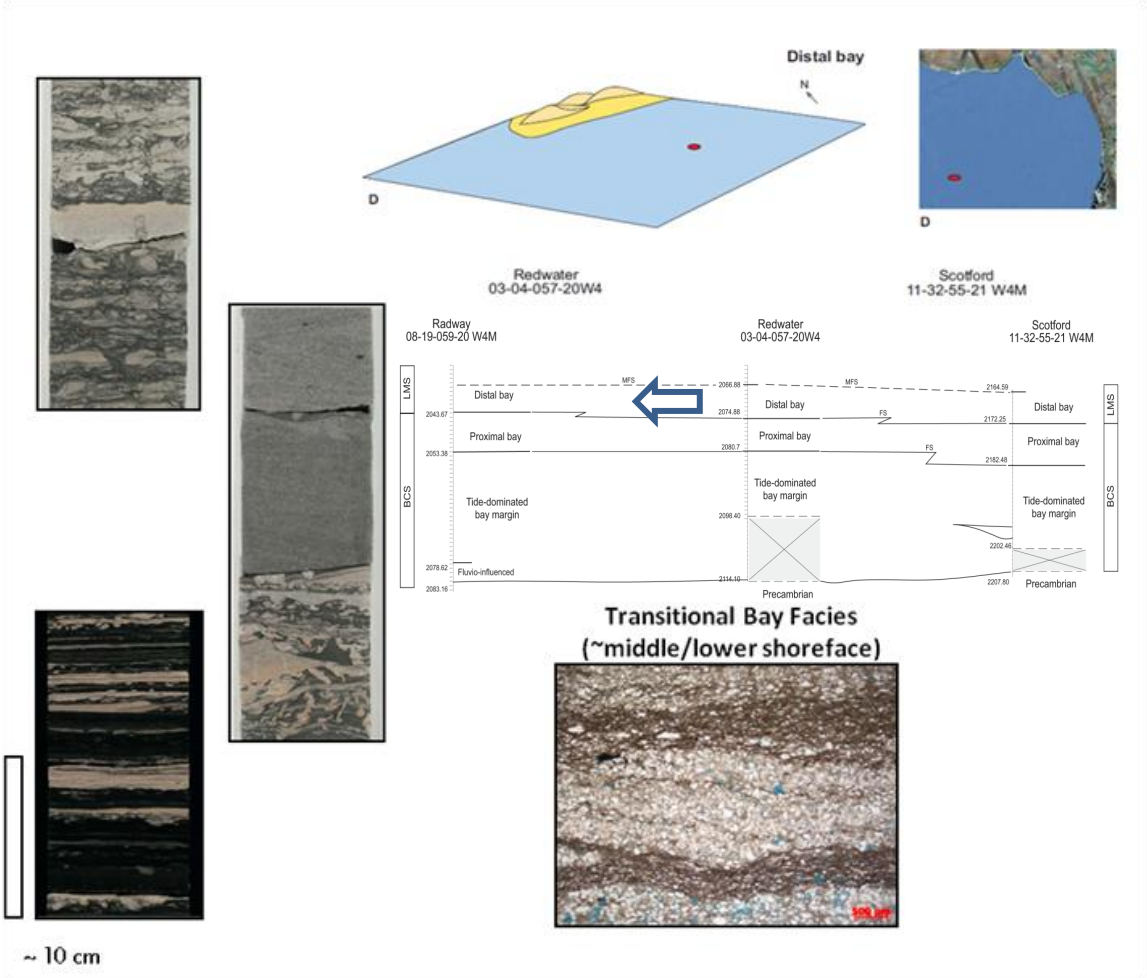

3.1.5. Offset Well Correlation

In sum, the sediments deposited during the Cambrian transgression within the interval captured by the facies model can be represented by a series of time transgressive facies belts that in broad terms illustrate a fining up grain-size sequence in which better quality reservoir material (TDBM) is progressively overlain by poorer quality material (the transition from PB to DB). Extension of the noted 1st Order EoD facies away from cored wells to offset wells across the geologic AOI was achieved qualitatively through log correlation (Figure 20). This effort yielded a suite of 19 wells that constrain the vertical and lateral extent of the 1st Order EoD facies belts over the geologic AOI.

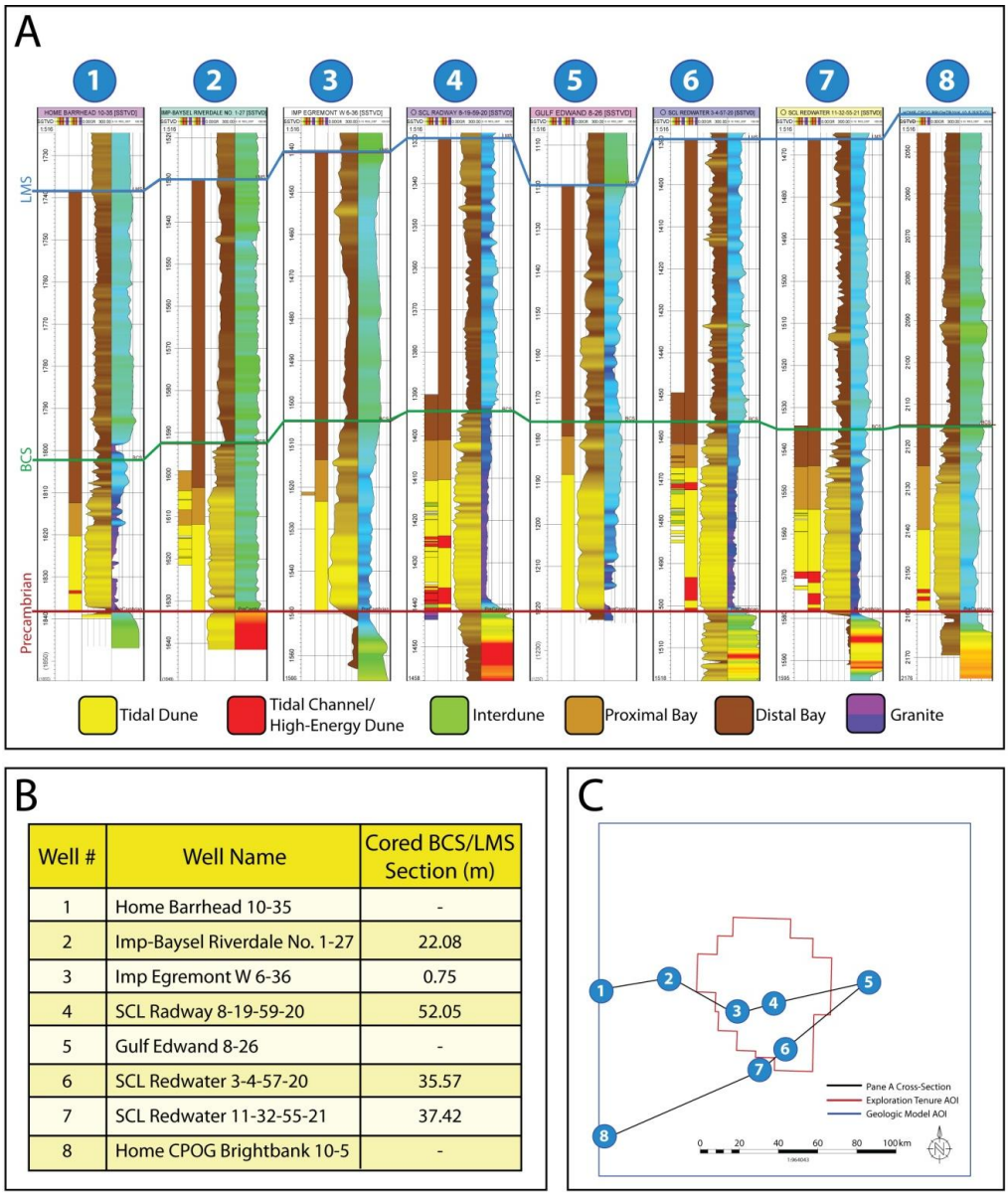

B

Well #	Well Name	Cored BCS/LMS Section (m)
1	Home Barrhead 10-35	-
2	Imp-Baysel Riverdale No. 1-27	22.08
3	Imp Egremont W 6-36	0.75
4	SCL Radway 8-19-59-20	52.05
5	Gulf Edwand 8-26	-
6	SCL Redwater 3-4-57-20	35.57
7	SCL Redwater 11-32-55-21	37.42
8	Home CPOG Brightbank 10-5	-

Figure 20: Offset well Environment of Deposition correlation.

Figure 20 shows a cross section with offset well correlation. Depicted in Pane A is the BCS and LMS model zone intervals (top BCS denoted by blue line; top LMS denoted by green line) of 6 wells (listed in Pane B) that lie roughly along depositional strike within the geologic scale AOI (illustrated by the grey rectangle in Pane C; note the red polygon in Pane C represents the Exploration Tenure AOI). Illustrated logs include from left to right, Facies Association descriptions of available cores (note variable core coverage), the 1st Order Environment of

Deposition interpretation from both cored and non-cored wells, Gamma Ray, and Deep Resistivity.

3.1.6. BCS Sandstone Texture and Composition

Grain size distributions within each core plug in the Redwater 11-32 and Redwater 3-4 wells were determined petrographically. The majority of the analyzed grains are upper medium (mU) size and mean measured sizes range from lower very-fine (vfL) to lower coarse (cL),. Most of the studied samples are bimodal in nature, as the majority of the sedimentary structures are cross-beds of different scales and geometries, or finely laminated heterolithic packages.

The majority of the studied sandstones are arenites, with original volumes of detrital clay content less than 10%. When present, detrital clay matrix appears as discontinuous rims covering the surface of the grains (pore-lining plus clay rim varieties; averaging 0.18%, with up to 2.33% of total rock volume); filling pores (average of ~0.50%, up to ~3.3%); or, most commonly, as thin laminas (average of 0.5%, up to 5.00%). There is an overall increase of total detrital clay matrix towards the top of the unit (Figure 21). The clay content trend is consistent with the observed tendency of mean grain size decreasing upwards within the studied interval. The clay content and grain size trends are direct responses to the transgressive event that dominated sedimentation patterns.

Framework composition is dominated by the presence of monocrystalline quartz , polycrystalline quartz, potassium feldspar and subordinate plagioclase. Minor components include lithic fragments that are represented mostly by metaquartzites, some finely crystalline granitic rock fragments, and phyllites. The framework suite observed in the Redwater 11-32 appraisal well is indicative of an overall plutonic to highgrade metamorphic source area, consistent with the sourcing of sediments from the meta-volcanics and meta-sediments of the Pre-Cambrian crystalline basement. A plot of framework compositions and associated mean grain sizes reveals that quartz content tends to increase with increasing grain size (Figure 22).

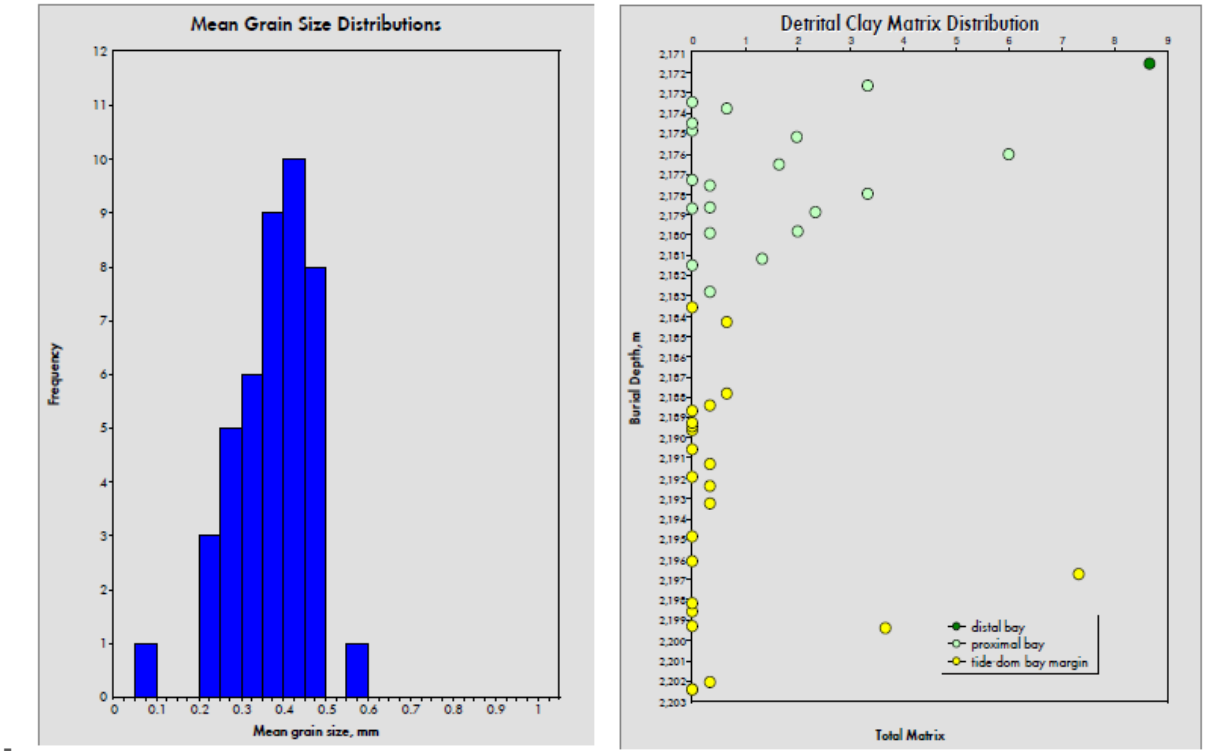

Figure 21: Left: Frequency histogram of Mean Grain sizes . Right: cross plot of total detrital clay vs. depth (Redwater 11-32 BCS samples).

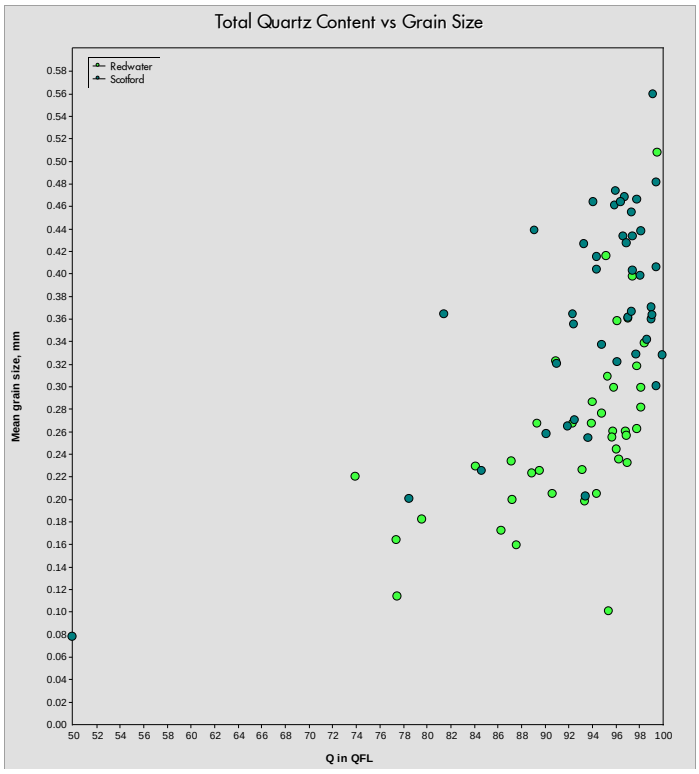

Figure 22: Mono-crystalline quartz content as a function of grain size, Redwater 11-32 and 3-4 wells.

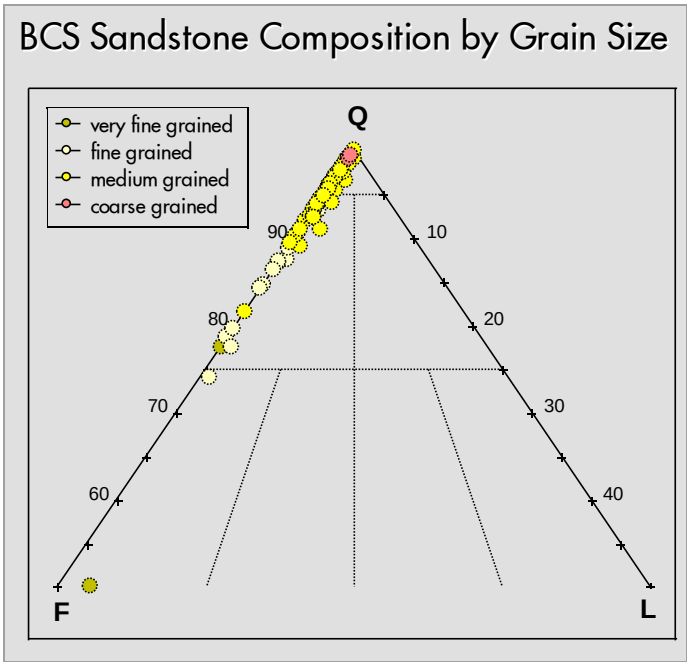

Figure 23: Compositions of BCS samples and associated mean grain sizes. in both Redwater 11-32 and 3-4 wells. Q: quartz; F: feldspar; L: lithic fragments. Based on Folk 1968 classification.

3.1.7. Geologic Model Structural Framework

The Quest Gen-4 geologic model was designed to represent a wedge of the subsurface located at the base of the Western Canada Sedimentary Basin within a "geological scale" AOI (~180 km x ~190 km) that thins from ~350 m in the southwest to 0 m thickness in the northeast where two erosional unconformities join. For an outline of the static and dynamic model AOI's, including well calibration inputs see Figure 120.

The Gen-4 Geological Model structural framework describes the Cambrian age section of the Western Canadian Sedimentary Basin (WCSB) and includes a small portion of the Pre-Cambrian basement, see Figure 24.

Property modelling is restricted to only the BCS and the LMS as these are the only zones that are exported to the reservoir simulator.

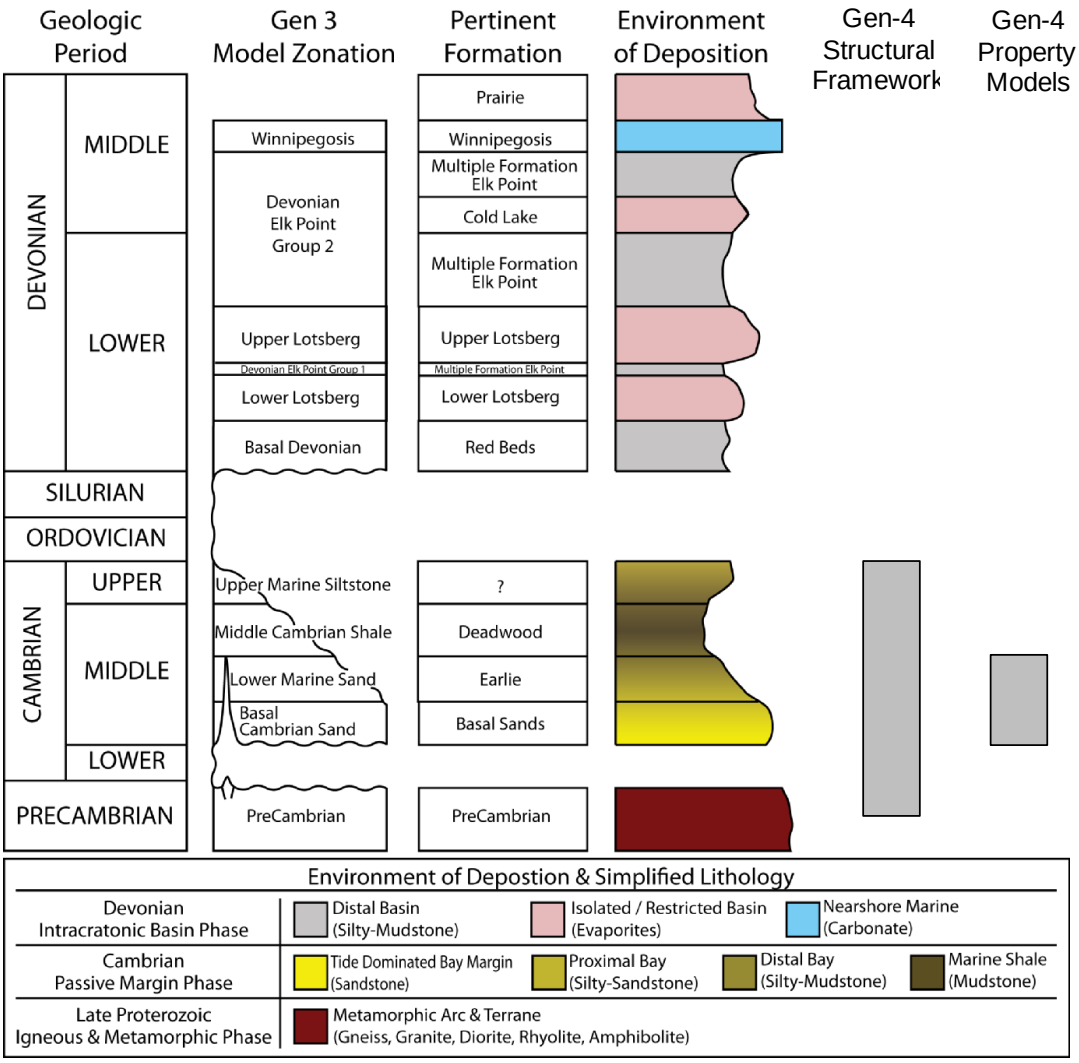

Figure 24 - Overview of the Quest Storage Complex showing structure and property modelling captured in Gen-4.

The grid resolutions per zone is shown in Table 2

Table 2: Gen-4 Geological Model Grid Resolution

Zone	Z Resolution	XY Resolution
UMS	all 1 Layer	250 x 250 m
MCS		
LMS	Bottom 10m: 10 layers (~1m/layer) Rest: 10 layers (~ 5m/layer)	
BCS	50 layers (~ 0.8 m/layer	
Pre-Cambrian	50 m Interval 1 layer	

The grid is oriented at 45° to align cell geometry with the regional dip azimuth as seen at top basement. This same orientation is used in the Pressure and Plume models.

3.2. Static Formation Properties

This chapter describes the key formation and fluid properties utilized in the various Gen-4 models, the manner in which properties were modeled and the uncertainty range in each. The reader is typically referred to discipline specific reports for a more comprehensive description of the input data, data analysis and justifications for the uncertainty ranges carried in the Gen-4 models.

3.2.1. Facies

A 3D facies model was constructed to condition the distribution of reservoir quality properties. The model is defined at the scale of Environments of Deposition.

A complete description of the various facies present in the models can be found in section 3.1. The only component of the facies varied across the Gen-4 realizations is the spatial arrangement of the High Energy Dune (HED) sub-facies of the Tide Dominated Bay Margin environment of deposition.

3.2.1.1. 1st Order - Environment of Deposition

The 1st order facies model describes the Environments of Deposition (EoD) within the LMS and BCS zones; Tide-dominated Bay Margin (TDBM), Proximal Bay (PB) and Distal Bay (DB). The modelling workflow is described below:

1. EoD facies log digitized at each well in the AOI from logs and/or core.
2. EoD facies log upscaled into the Geological Model grid using “Most Of” option.

3. Truncated Gaussian Simulation With Trends algorithm used to distribute facies between wells.
    a. Facies transitions mapped through well data (see Figure 25).
    b. Define variogram to describe “feathering” of facies transitions
4. QC results to ensure consistency with wells and the conceptual geologic model.

Truncated Gaussian Simulation With Trends (TGSwT) is a stochastic algorithm that allows the user to model the inter-fingering character of lateral facies changes. The transgressive sequence contains three environments of deposition that reflect the proximal to distal trends in reservoir quality and that likely have an interfingering profile in cross section. A variogram is used to describe the character of the inter-fingering relationships.

Table 3 lists the variogram settings used in TGSwT facies modeling.

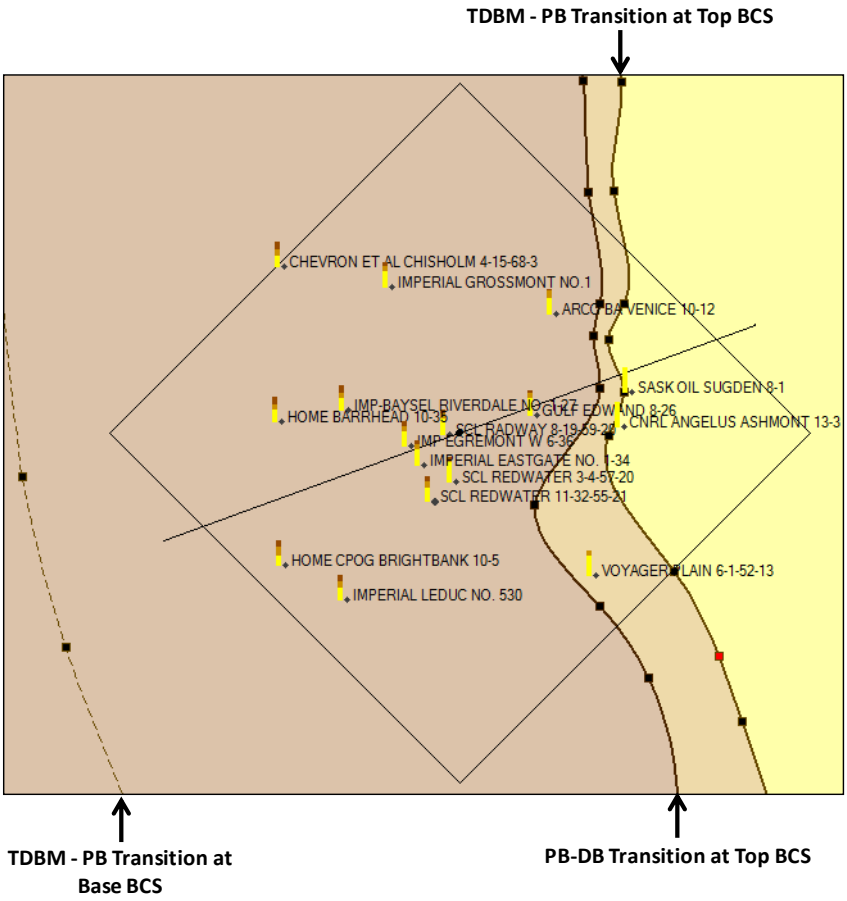

Figure 25 Mapping Facies transition locations using the TGSwT algorithm in Petrel.

Table 3 - Variogram settings for EoD facies modeling

Variogram Settings	
Type	Gaussian
Sill	1.0
Nugget	0.01
Major Direction	40000
Minor Direction	10000
Vertical	1
Dip	0
Variance	0.001

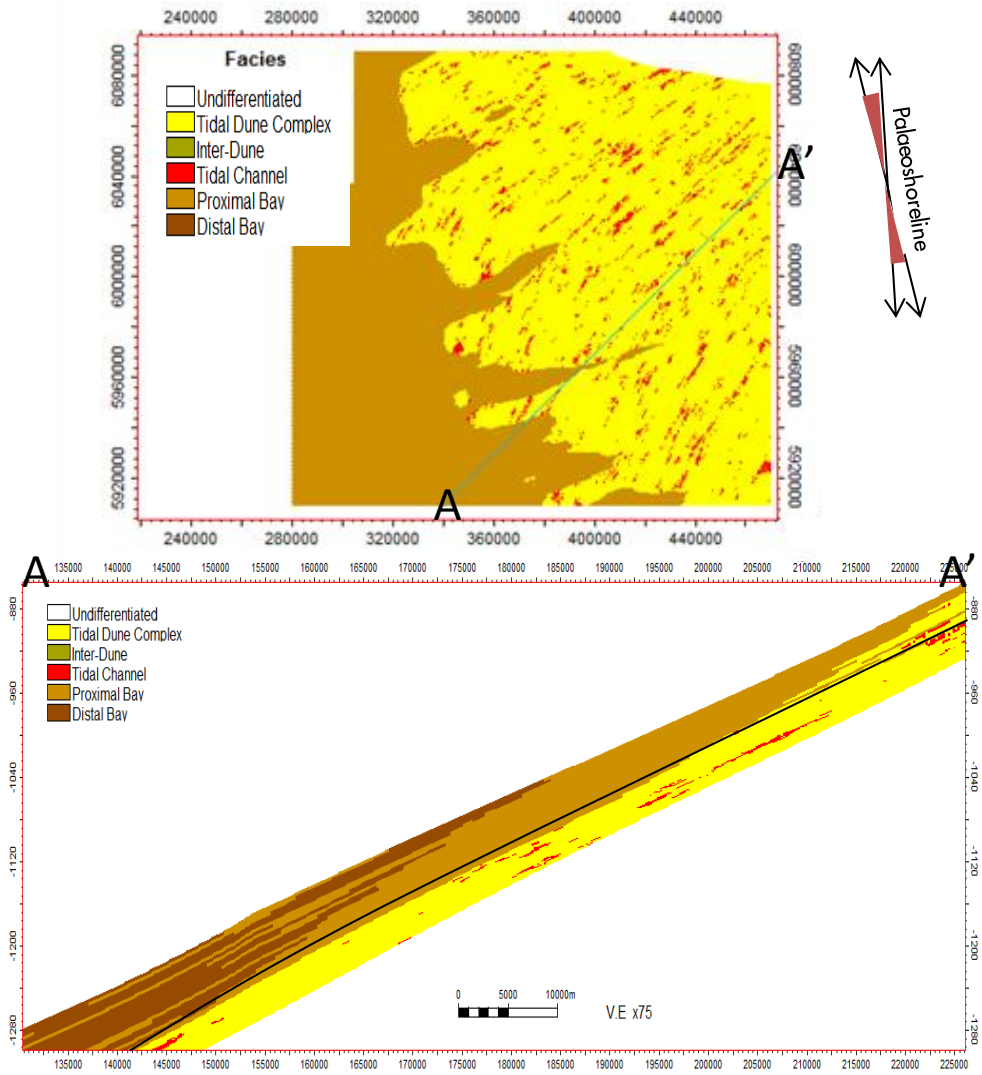

Figure 26: BCS and LMS EoD (1st and 2nd Order) Facies Model in Petrel. Black line in cross section is the BCS/LMS zone boundary straddling the transition from TDBM to Proximal Bay facies.

The variograms have been defined via an iterative work flow to ensure that a reasonable visual result is produced that does not contain obvious artifacts associated with the location of well control points. There is little in the published literature to support the definition of these facies relationships. The influence of local specific variables such as the basement topographic variation and regional dip come into play.

The major EoDs straddle defined zone boundaries, see Figure 26. The lateral and vertical arrangement of facies over the time of deposition results in the BCS and LMS containing a varying proportion of each facies as shown in Table 4.

Table 4: EoD facies proportions per model zone.

Zone	TDBM %	Proximal Bay %	Distal Bay %
BCS	67	20	13
LMS	3	14	83

3.2.1.2. 2nd Order – High Energy Dune (HED)

The HED facies has been found in core from all three appraisal wells and is consistently composed of the best reservoir quality as observed from core plug data. It is not possible to discriminate HED facies from the other facies via just the well logs. The BCS conceptual depositional model states that the best quality reservoir is most likely developed in a more proximal location relative to the palaeo shoreline and indeed, some of these sands may actually be reflecting an element of fluvial deposition. Therefore with the current conceptual model of a drowned topography this facies is expected to be preferentially developed in the lower portion of the BCS, just above the top of the Pre-Cambrian basement.

The HED facies in the model is used to condition the location of the highest quality reservoir properties as these represent the high permeability intervals that are likely to act as possible thief zones for CO_2 during injection and migration. The distribution pattern of HED is therefore a possible control on the CO_2 plume geometry during and after injection. The BCS conceptual model suggests that the proportion of HED decreases with increasing distance above the top Pre-Cambrian as water depth is increasing and energy level are decreasing. This conclusion may be incorrect and so the alternative case states that there is no preferential development at base and that HED is equally likely to occur at any level within the TDBM environment, see Figure 27.

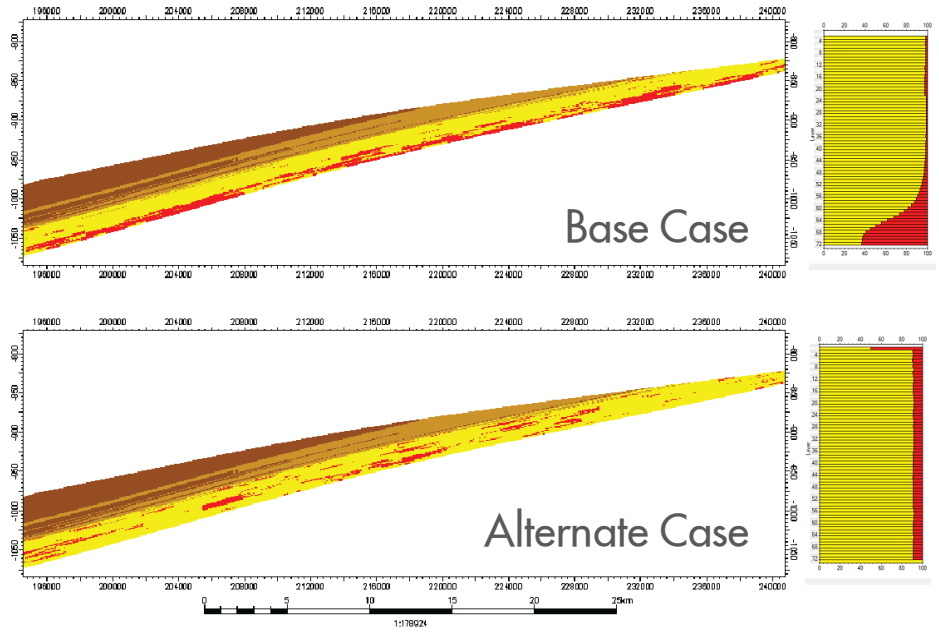

Figure 27: HED distribution pattern uncertainty in the Gen-4 models.

The three appraisal wells have the following proportions of HED within the TDBM environment:

- Redwater 11-32 = 10%
- Redwater 3-4 = 5%
- Radway 8-19 = 20%

Figure 28 shows the probabilities of these well outcomes at any location in the Quest AOI for different proportions of HED within the model. With only 5% HED in the model (Red CDF) the result at Radway 8-19 (red vertical line) is highly unlikely at less than 5% likelihood of occurrence. At 15% HED concentration (Green CDF) the result at Redwater 3-4 (yellow vertical line) is also very unlikely with an approximately 10% chance of finding Redwater 3-4 well properties in the model . At 10% HED content, either with a vertical trend (light blue CDF) or without (dark blue CDF) the probabilities of all three wells are within the range of expectation, i.e. P10 – P90. Hence 10% HED content was selected as the proportion of HED in the TDBM to include in the model.

3.2.1.3. Facies Uncertainty

Table 5 lists the way in which the uncertainty in the distribution of HED is captured in the Gen-4 models.

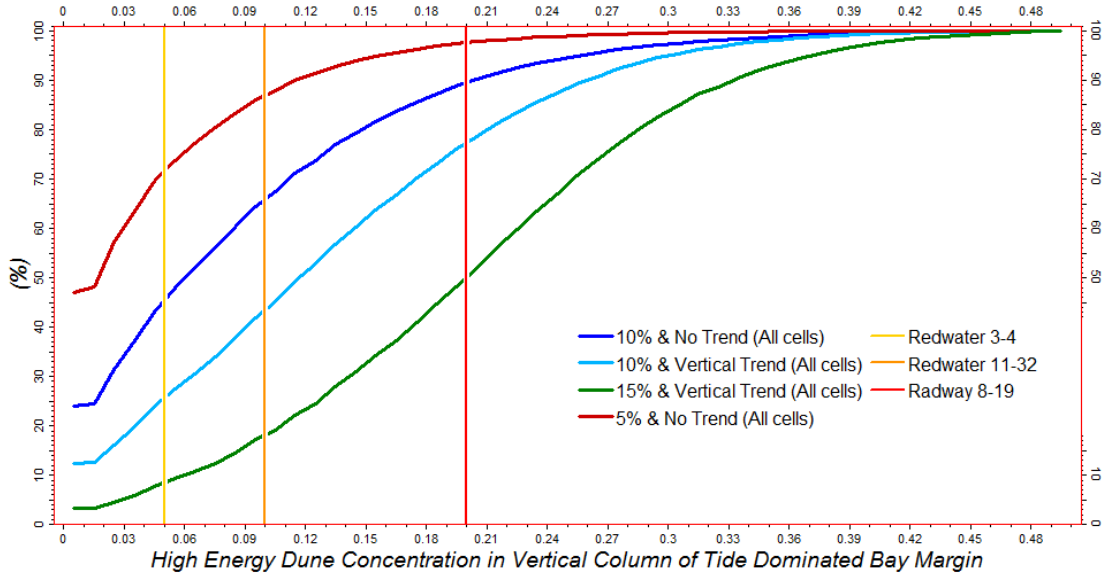

Figure 28: Appraisal Well HED concentration probabilities from models with a range of HED concentrations

Table 5 - Range of Uncertainty in HED Facies Distribution

Case	Vertical Arrangement	Proportion
LOW	Random	10% of TDBM
MID	Vertical Trend	

3.2.2. NTG

NTG is handled in the static models by assigning a constant value to all grid cells of a particular facies.

Each facies has a range of constant NTG that can be assigned to it. The determination of NTG at the Quest appraisal wells is described in detail in Petrophysics Report (Simone, 2011) where various independent techniques were compared against one another – core description, core photo analysis, FMI, Thomas Stieber (TS) V_{sand} from well logs.

The final NTG range carried in the Gen-4 models is derived from TS V_{sand} logs provided by the petrophysicist. The TS V_{sand} logs were arithmetically upscaled into the Geological Model grid.

The P90/P50/P10 outcomes from V_{sand} cumulative probability distributions for each facies (using the three Quest appraisal wells) were used to determine the H/M/L constants for Tide Dominated Bay Margin (TDBM) and the Proximal Bay (PB) facies.

As seen in Figure 29 the Low case NTG from the CDF in TDBM is 0.8. This was further discounted to 0.75 to reflect the inherent uncertainty in the estimation of NTG from the Thomas Stieber V_{sand} methodology, i.e. the measurement uncertainty. It can be shown that the NTG impact of diagenetic precipitates observed in core at Radway (~2% of BCS gross thickness) is relatively insignificant compared to the TS measurement error, see Figure 30.

The Distal Bay (DB) NTG range was defined by ranking the mean V_{sand} of that facies in each well. This is because the Distal Bay is expected to be significantly more continuous in character than the other two facies thus the mean at the Radway 8-19 well is presumed to be representative and is taken as the Mid Case.

The final NTG range per facies is shown in Table 6.

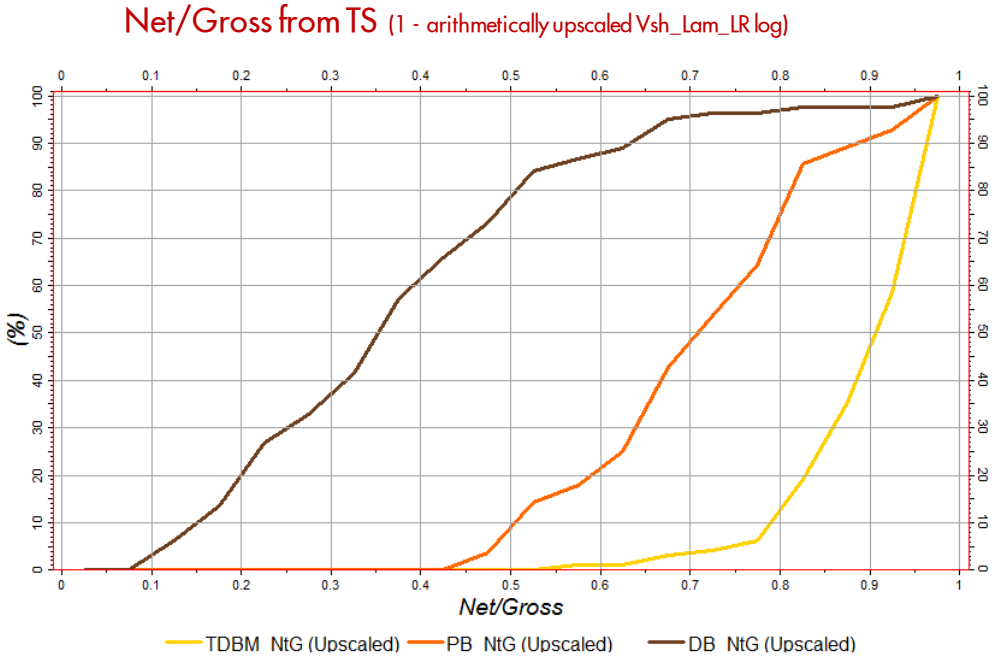

Figure 29: Cumulative Probability of NTG (Upscaled TS Vsand) for each facies at all Quest Appraisal wells

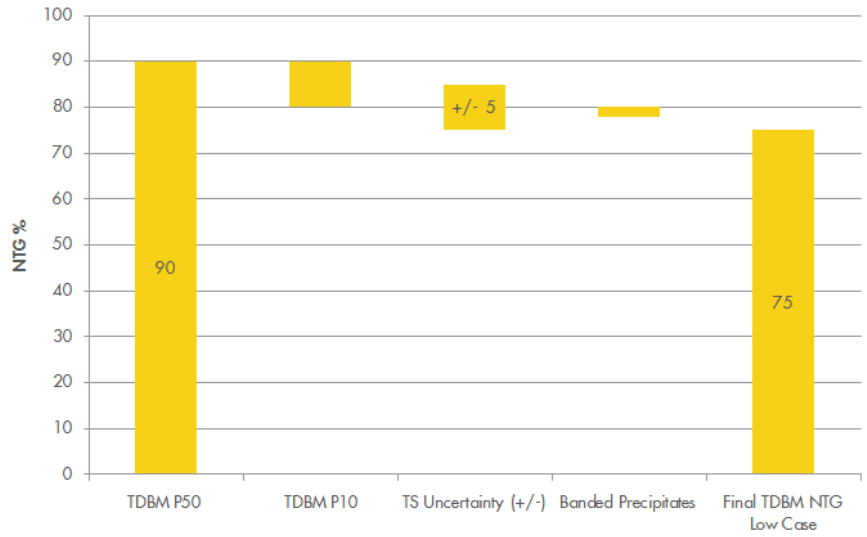

Figure 30: Washing line plot recording how the final Low Case NTG constant was arrived at for the TDBM facies.

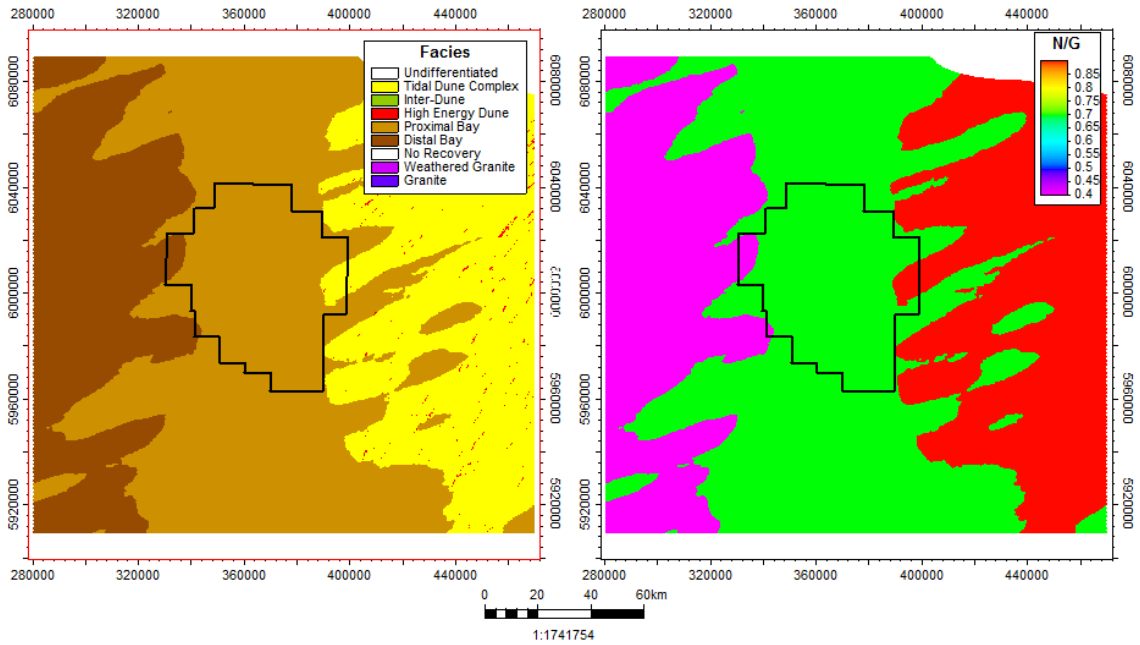

Figure 31: Slice through the Geologic model (K=34) with the Mid Case NTG model reflecting facies changes.

Table 6: Gen-4 NTG Uncertainty

Case	TDBM	PB	DB
LOW	0.75	0.50	0.3 (Driven by 11-32 result)
MID	0.90	0.70	0.4 (Driven by 8-19 result)
HIGH	0.95	0.90	0.5 (Driven by 3-4 result)

3.2.3. Porosity

The porosity property is stochastically distributed within the Geological model with the frequency distribution constrained by upscaled logs and the Facies model.

The input to the porosity modeling is the set of base case porosity logs provided by the Petrophysicist. The calculation of porosity logs across all wells of interest and the manner in which petrophysical uncertainty is determined is described in detail in the Petrophysics Report (Simone, 2011).

3.2.3.1. Petrophysical Uncertainty

To maximize the use of all legacy well data found during the GEN 2 regional study, all wells were classified based on data availability, quality and vintage into three different groups:

- **Group 1**: This group consisted of the most modern wells in the region, including the three Quest appraisal wells, with all evaluation logs available: GR, Caliper, Density, Neutron, Resistivity, PEF.
- **Group 2**: This group consists of wells drilled between 1958 and 1991, with incomplete data sets but with a sonic log available for the evaluation.
- **Group 3**: A variety of wells (dated and new) with very limited data. (Old LN and SN logs, with visual Porosity assessed from cuttings)

The classification of wells facilitated the application of the most suitable petrophysical evaluation technique consistently on each well group. A larger uncertainty in the property estimation was associated with the less reliable groups of data (i.e. group 2 and group 3).

Base Case porosity logs and a table of porosity uncertainty magnitude for each well group were provided by the petrophysicist (see

Table 7).

Low and High case porosity logs were calculated in Petrel by simply applying the appropriate +/- bulk shift to the base case porosity log depending upon the assigned group for that well.

Table 7 - Porosity Uncertainty vs. Well vintage. Low Case = Base case – bulk shift. High case = base case + bulk shift.

Well group / Wells	+/- σ (v/v)
Group 1	0.0136
Redwater 11-32	0.007
Redwater 3-4	0.007
Radway 8-19	0.007
Group 2	0.028
Group 3	0.028

3.2.3.2. Geologic Uncertainty

There is uncertainty in the way porosity may be distributed between the wells. The wells in the Quest AOI and surrounding region are spaced far apart, usually 15km or more. This results in significant uncertainty in the volume around a well for which that well can be considered representative.

The porosities observed at the Radway 8-19 well were at the high end of the range of expected outcomes based on Gen-3 predictions. The average porosity at that location was significantly higher than predicted by the compaction depth trend derived from other wells. This suggests that there is either:

- a very high level of variability in reservoir quality at any depth over the AOI, or
- that there is an additional, higher frequency trend to reservoir quality distribution in addition to the regional depth trend.

Plotting the results of the three appraisal wells as shown in Figure 32 it is clear that there is a significant change in reservoir quality between the 11-32 well in the SW (blue) and the 8-19 well in the NE (yellow) and that the gradient of porosity decrease with increasing depth far exceeds the regional depth trend. And yet, at similar depths in the BCS as the 8-19 well there are other wells with significantly poorer average porosity.

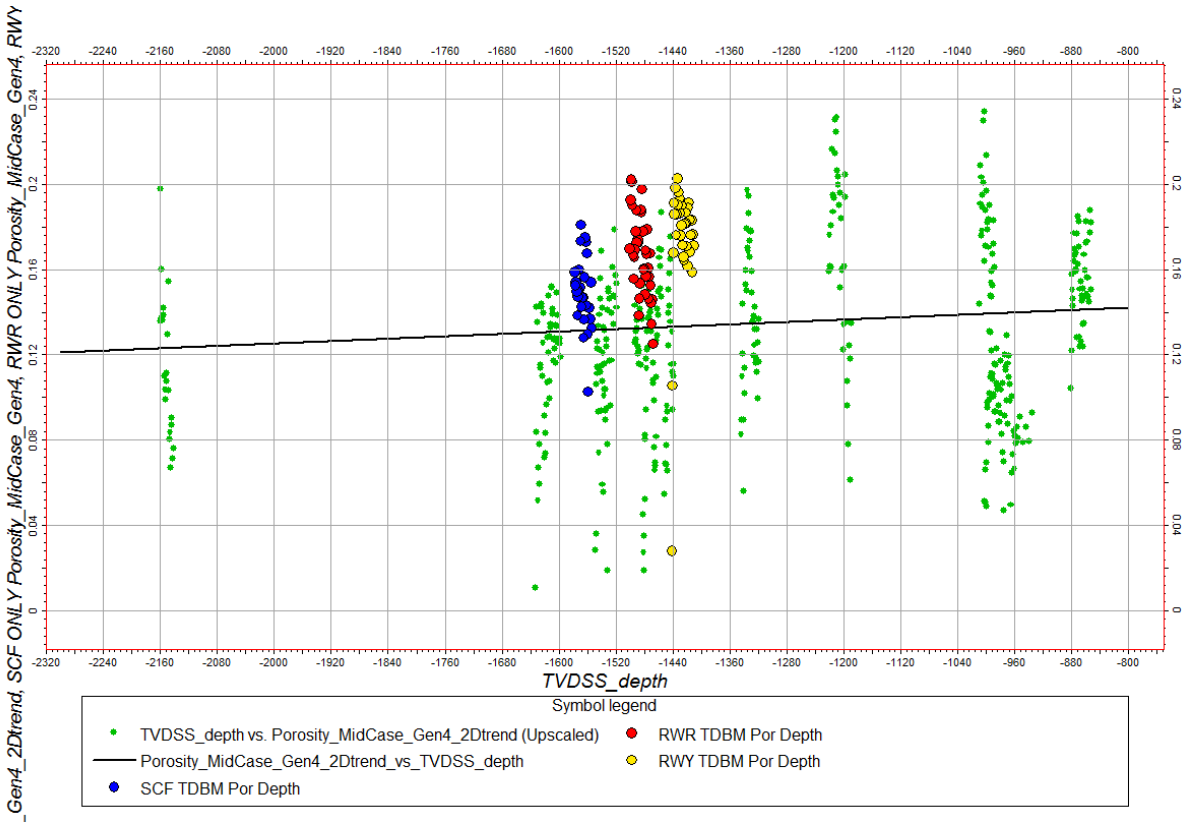

Figure 32: Upscaled porosity logs vs. depth for all wells (green) showing regional compaction trend (black). Note the three Quest appraisal wells highlighted to show the obviously stronger trend between these wells. SCF (SCL Redwater 11-32, Scotford) RWR (SCL Redwater 3-4, Redwater), RWY (SCL Radway 8-19, Radway).

A 2D aerial trend was identified for average porosity in the TDBM facies within the BCS. This trend can be used to explain the differing reservoir quality across the region, see Figure 34. It suggests that better BCS reservoir quality is typically present in locations along the NE-SW trending major axis of the Pre Cambrian Rimbey and Lacomb blocks (Figure 34). The mapping of 2D and 3D seismic over the Quest AOI and the location of known areas of missing BCS over Pre-Cambrian basement highs in the South (e.g. at the Westminster Hairy well) suggests that the Rimbey and Lacomb blocks were relative lows and thus a natural focus for sands deposition in the Cambrian. As such these blocks offered the greatest accommodation space in which to accumulate sediment, being bounded by the relative basement highs to the NW and the SE along the Snowbird Tectonic Zone (STZ) and the Red Deer Lineament (RDL) respectively, see Figure 33.

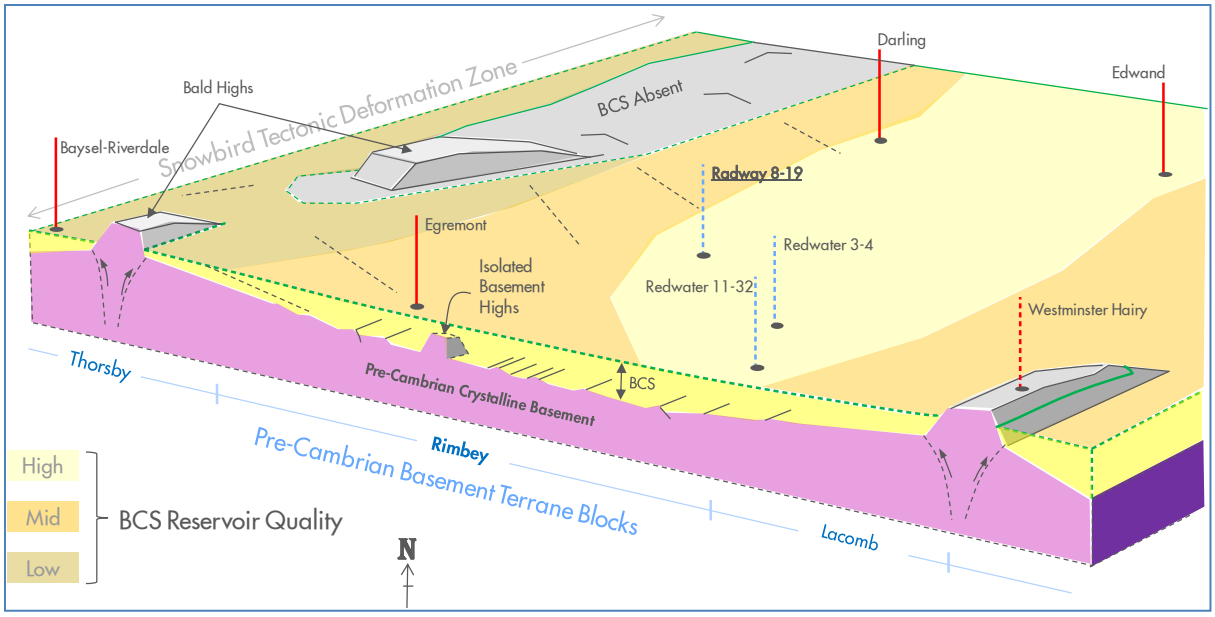

Figure 33: Conceptual image (not to scale) of the BCS interval sitting on top of Pre-Cambrian Topography looking North. Te BCS thins towards basement highs in the North and South East.

The coarsest and most proximal, and possibly fluvial, sands are expected to be found towards the base of the BCS and would be expected to be preferentially developed in the basement lows. This trend suggests that, within the Quest AOI, better reservoir quality is likely to be found in the eastern half of the license with poorer reservoir quality towards the West, as observed by the Egremont-1 well.

The 2D trend map is the result of gridding up the residuals between mean porosity at wells in the TDBM Vs. Predicted Mean from the Regional Depth Trend. The gridding of these residuals was accomplished via kriging and the use a long range anisotropic variogram oriented to align with the NE-SW structural trend of the Pre-Cambrian basement.

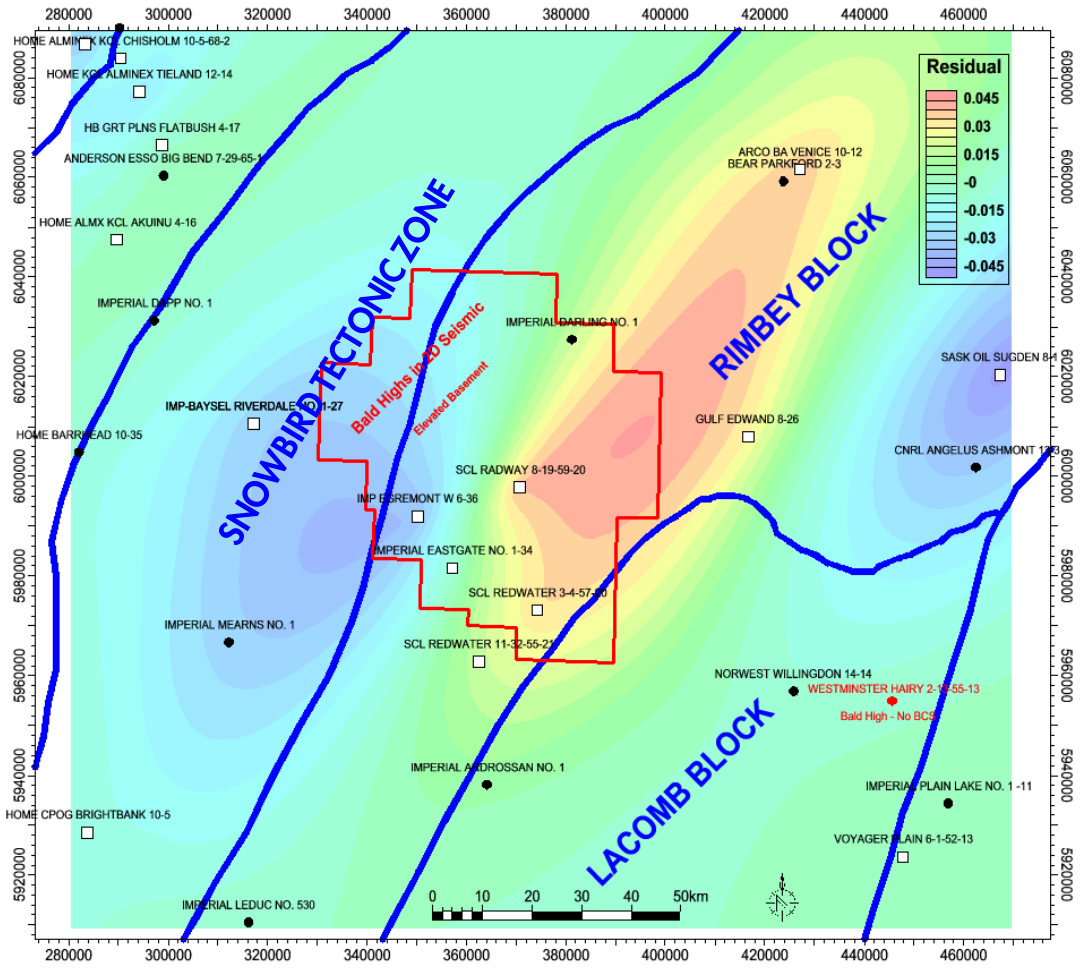

Figure 34: 2D Trend Map (gridded residuals to depth trend) for conditioning TDBM Average Porosity. Pre-Cambrian Basement Block boundaries from aero-magnetic interpretation overlain (blue). White squares are gridding control points.

The underlying approach for incorporating porosity and underlying uncertainty, in the Gen-4 models is summarized in Table 8. The associated probability density functions of the porosity within the BCs and LMS are displayed in Figure 35 and Figure 36, respectively.

Table 8: Porosity Uncertainty in Gen-4 Geological Model.

Case	Logs	1D Trend	2D Trend
LOW	Low	*Yes*	No
MID	Mid	*Yes*	*Yes*
HIGH	High	*Yes*	*Yes*

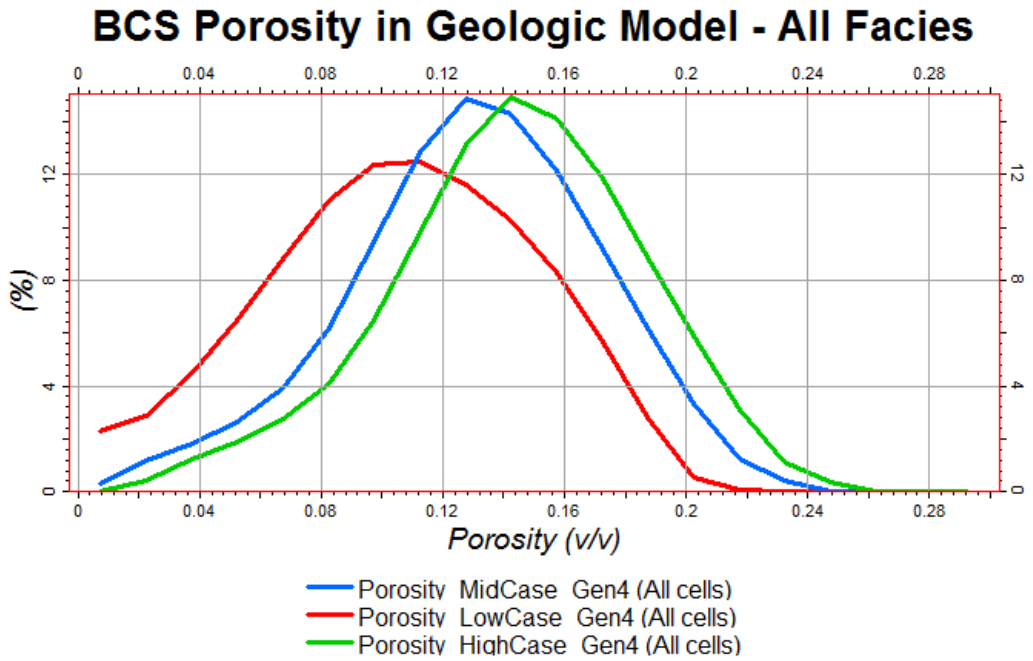

Figure 35: Probability density function of high, mid and low cases of the BCS porosity.

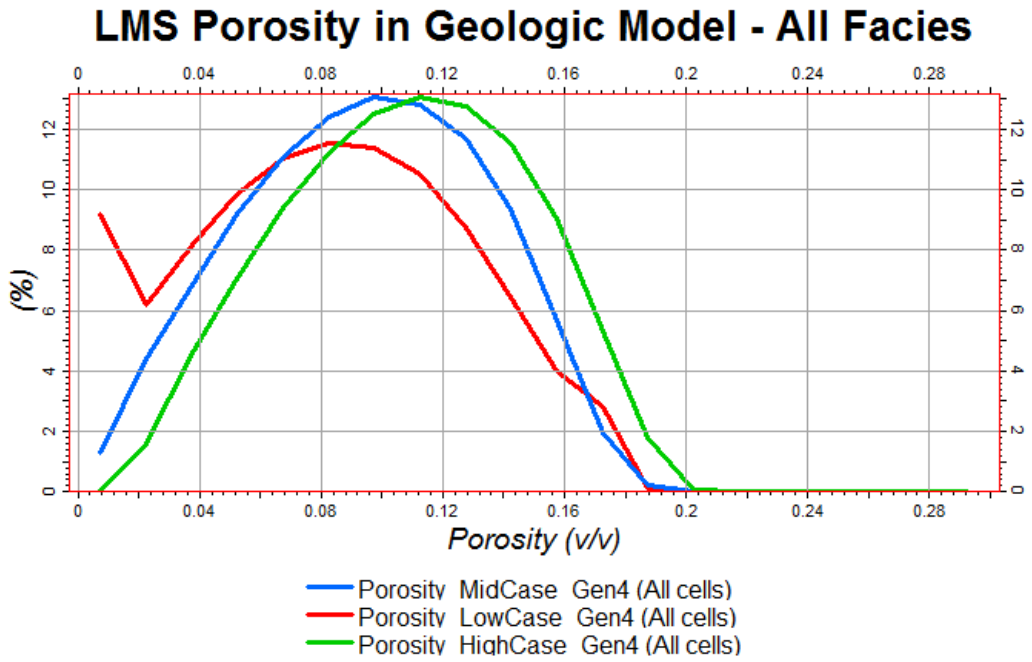

Figure 36: Probability density function of high, mid and low cases of the LMS porosity.

3.2.4. Permeability

3.2.4.1. Horizontal Permeability (kh)

The permeability at wells is derived using the same methodology in the Gen-4 modeling workflow as was used previously in Gen-3 modeling, the use of a regression between porosity and permeability core plug data. Please refer to petrophysics report (Simone, 2011) for a comprehensive description of how the permeability relationship was derived.

The function relating permeability to porosity is:

$$K = 4E9 \times POR^{8.976}$$

Figure 37 shows the function plotted against the input core plug data. The function is based on Swanson means calculated for several porosity bins and thus corrects for the natural bias associated with the logarithmic distribution of permeability. The porosity bins and associated Swanson means are not shown on the plot.

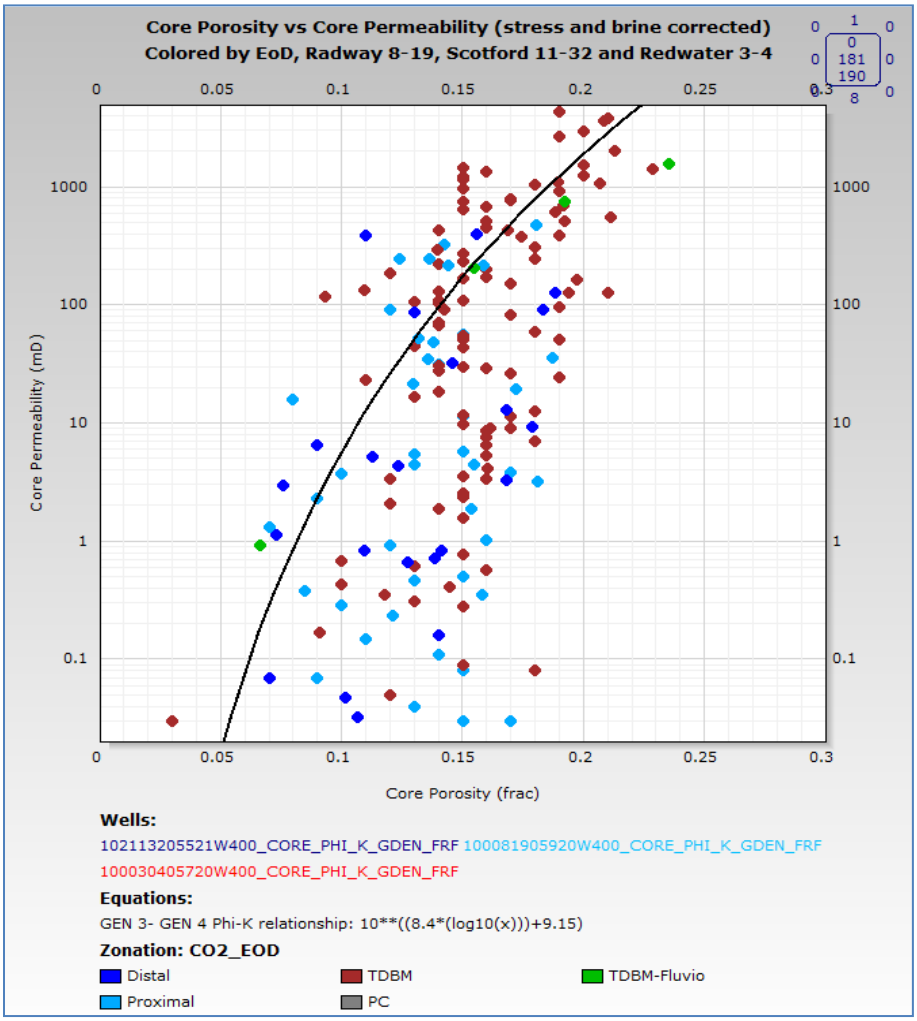

Figure 37 - Core plug porosity and permeability with the Gen-3 function (black) used in Gen-4 models.

The high, mid and low case porosity logs are transformed via the same function into permeability logs, hence the uncertainty in horizontal permeability is directly proportional to the uncertainty in the porosity - Low case porosity logs are used in combination with the associated low case permeability logs when constructing a low case reservoir quality model and vice versa for the high case.

Permeability is distributed stochastically in the model using the porosity model as a trend. The resulting probability distributions, including the high-, mid- and low cases as used in the various subsurface realizations are shown in Figure 38.

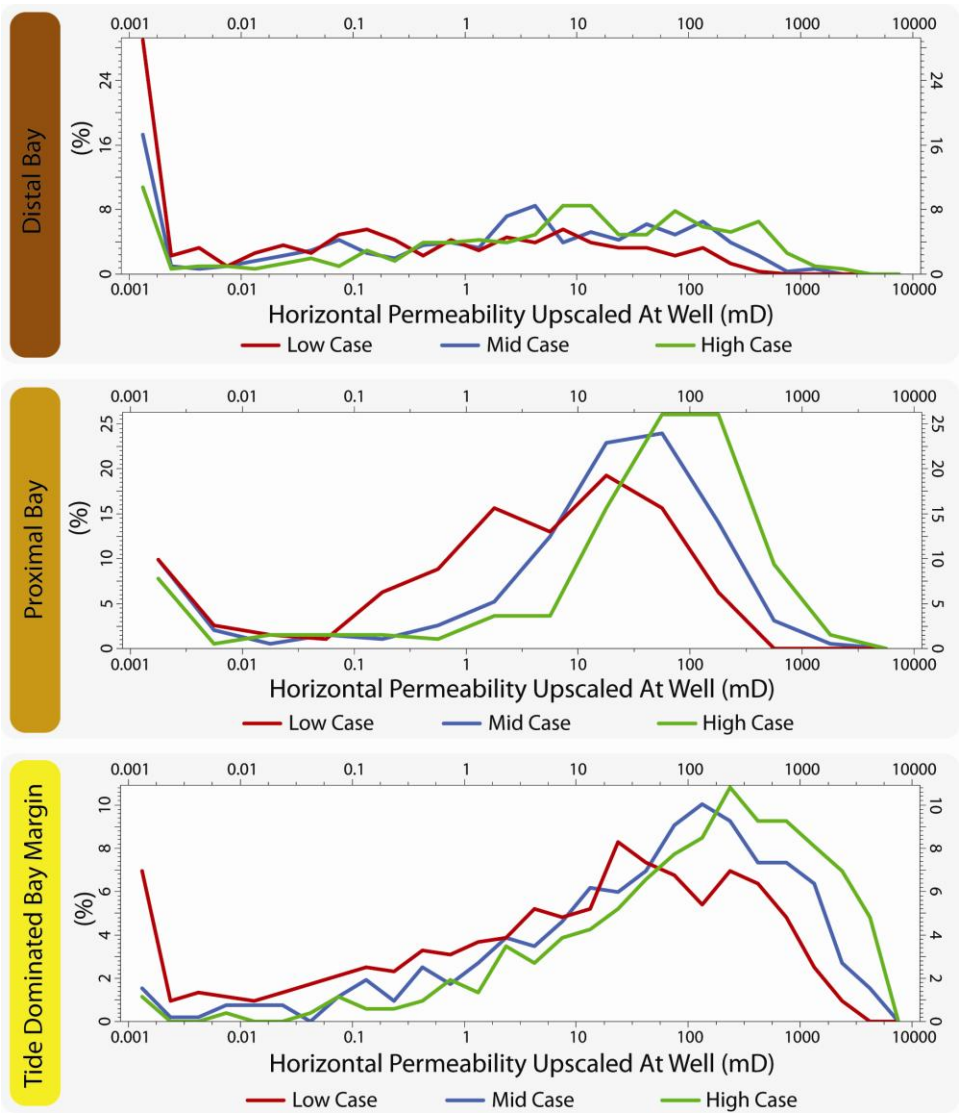

Figure 38: Permeability distribution in the static model as function of the depositional environment.

Different cut-offs were applied after modeling to limit the maximum horizontal permeability that was permitted in different facies in different cases. The cut-offs are summarized in Table 9.

Table 9: Permeability cut-offs as applied to depositional facies and property ranges.

Case	Maximum Kh Cut-offs (mD)
LOW	TDBM: 3000 PB: 1000 DB: 500
MID	TDBM: 5000 PB: 5000 DB: 5000
HIGH	TDBM: 5000 PB: 5000 DB: 5000

3.2.4.2. Kv/Kh

Vertical permeability is a key control on the geometry of a CO_2 plume. The uncertainty in vertical permeability is controlled by two different components, with a range for each being captured by the Gen-4 models.

1. Horizontal Permeability (Kh)
2. Kve/Kh ratio

The uncertainty in the horizontal permeability is discussed above.

The uncertainty in the Kve/Kh ratio is also represented in the models. The cell scale effective vertical permeability is calculated in the static model via the use of work by (Begg, 1985). The equation used in this work is similar to the often cited "Begg & King" transform in that it accounts for the effect of vertical flow baffles (impermeable layers) that may exist internal to a cell on the total vertical permeability of that cell. This value is referred to as *effective vertical permeability* (*Kve*). The approach used differs from the original Begg & King work in that it allows for 2D permeability anisotropy (i.e. horizontal versus vertical) of the reservoir sands. The equation (reconfigured to solve for Kve/Kh) is as follows:

$$\frac{Kve}{Kh} = NTG \cdot \left[(1 + F \cdot r_{mean}) \cdot \left(\left(\frac{Kv_{sand}}{Kh_{sand}}\right)^{-1} + F \cdot r_{mean}\right)\right]^{-1} \quad (1)$$

- *NTG* = concentration of material in a cell that is amenable to flow (following the above noted methodology),
- *F* = frequency of occurrence of baffles to vertical flow (per meter)
- r_{mean} = *average baffle radius*
- Kv_{sand}/Kh_{sand} = ratio of vertical to horizontal permeability of the material considered as "net" in the NTG workflow (i.e. "clean" sand).

The NTG is discussed in chapter 3.2.2. The F and t_{mean} distributions are conditioned by the FMI log interpretation on the 11-32 and 3-4 appraisal wells. Kv_{sand}/Kh_{sand} is a constant per facies and based on vertical core plug data from appraisal wells..

A slight adaptation was made in the Gen-3 and Gen-4 models to permit uncertainty in the input assumption on the mean baffle radius (r_{mean}). It is considered geologically reasonable to assume that thicker intervals of non-net in a well would typically correspond to greater lateral extents of that non-net around the well than thinner intervals. Thus the original r_{mean} term is expanded to relate baffle radius to mean baffle thickness (t_{mean}) via a ratio of both (l_{ratio}).

The adapted equation takes the form:

$$\frac{Kve}{Kh} = NTG \cdot \left[\left(1 + F \cdot (t_{mean} \cdot l_{ratio})\right) \cdot \left(\left(\frac{Kv_{sand}}{Kh_{sand}}\right)^{-1} + F \cdot (t_{mean} \cdot l_{ratio})\right)\right]^{-1} \quad (2)$$

Each parameter of the adapted Kve/Kh formula is calculated at the Quest appraisal wells, at the cell scale based on up-scaled log data.

Once all parameters are defined in the cells at the appraisal well locations the Kve/Kh is calculated for those cells. The Kve/Kh ratio is then stochastically populated into all remaining cells in the model honoring the frequency distributions (per facies) as seen at the appraisal wells.

The Kve/kh property distribution is loosely correlated to the porosity model via a correlation coefficient of 0.75. This implies that cells with higher porosities are more likely to have higher Kve.

When assessing Kve/kh uncertainty the F, t_{mean} and Kv_{sand}/Kh_{sand} distributions are fixed in all uncertainty cases. The NTG varies as described in the NTG section above. The l_{ratio} is varied to reflect the significant uncertainty in the presumed lateral continuity of the flow barriers identified in the FMI logs. Thus the Low case Kve/Kh ratio assumes that the baffles are longer than the base case while the high case ratio assumes the baffles are shorter than the base case (see Table 10).

Table 10 Range of mean baffle thickness Vs. width ratios used in modeling effective Kv.

Case	l_{ratio} Thickness:Radius
LOW	1000:1
MID	250:1
HIGH	100:1

3.3. Dynamic Formation Properties

3.3.1. Relative Permeability and Capillary Pressure

Gen-4 relative permeability models and capillary pressure models were based on updated analyses, using the Gen-3 Quest Mineral Oil – Brine SCAL experiment data. For the relative permeability Corey model, the key difference from Gen-3 is the use of imbibitions relative permeability experiment data to define the Corey exponents (curvatures) of the CO_2-brine primary drainage relative permeability curves, rather than using drainage relative permeability experiment data. This change was made for the following reasons:

- The ambiguity of the primary drainage experiment data.
- The new methodology can capture the upside uncertainty better than the Gen-3, when comparing with the literature analog end point data in Figure 39.

Table 11 summarizes the resulting uncertainty range in Corey exponents of the Gen-4 drainage curves. The key difference in the capillary pressure model, in comparison to the Gen-3 models, is the introduction of the low and the high case models, while slightly updating the base case capillary pressure model. Figure 40 illustrated the low, mid, high case Gen-4 capillary pressure curves for the Quest representative permeability range.

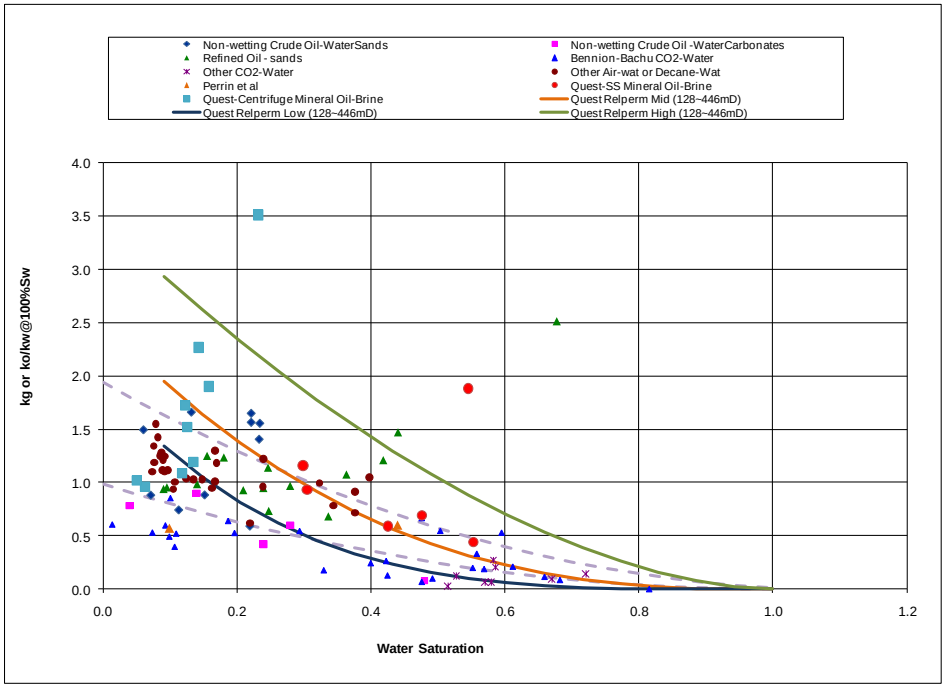

Figure 39: Representative Perm Class Quest H-M-L Primary Drainage Rel. Perm. Curves vs. Quest End Point Measurements and Literature Analog End Point Data

Table 11 Corey Exponent Uncertatiny

Corey Exp.	n_o	n_w
Gen4 Low Case	3.75	3.88
Gen4 Base Case	2.625	4.804
Gen4 High Case	1.73	5.28

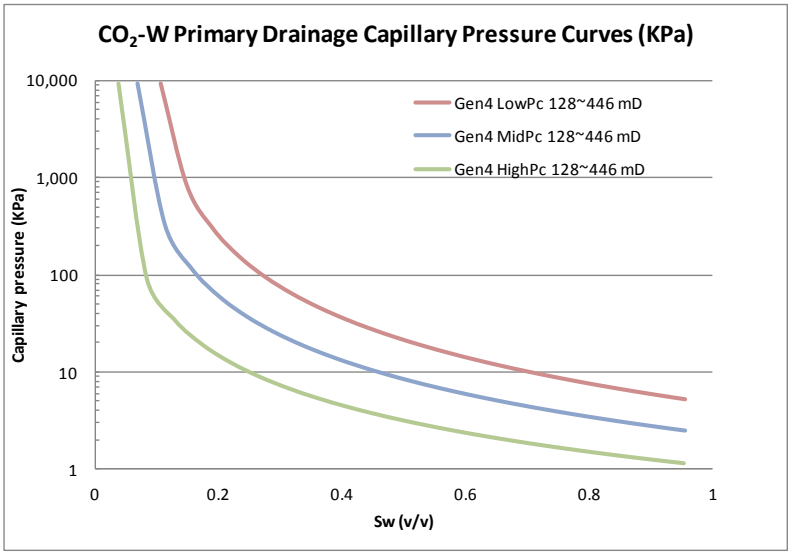

Figure 40: Quest Primary Drainage Capillary Pressure Uncertainty

Permeability Class

Similar to Gen-3, the Gen-4 relative permeability and capillary pressure models were implemented in the simulations by defining various rock classes as a function of rock permeability. Table 12 gives the range of permeability in those rock classes.

Table 12 Permeability Classes

Perm Class	MinK, mD	MaxK, mD	MidK, mD
1	0.85	3	1.59
2	3	10	5.57
3	10	36	19
4	36	128	68
5	128	446	239
6	446	1500	818

Capillary Pressure Models

Low case, base case and high case capillary pressure functions were derived based on fitting the Quest primary drainage capillary pressure experiment data. Those functions and parameters are summarized in APPENDIX 2.

Figure 41 illustrates the low case, base case and high case supercritical CO_2 - brine primary drainage capillary pressure model results.

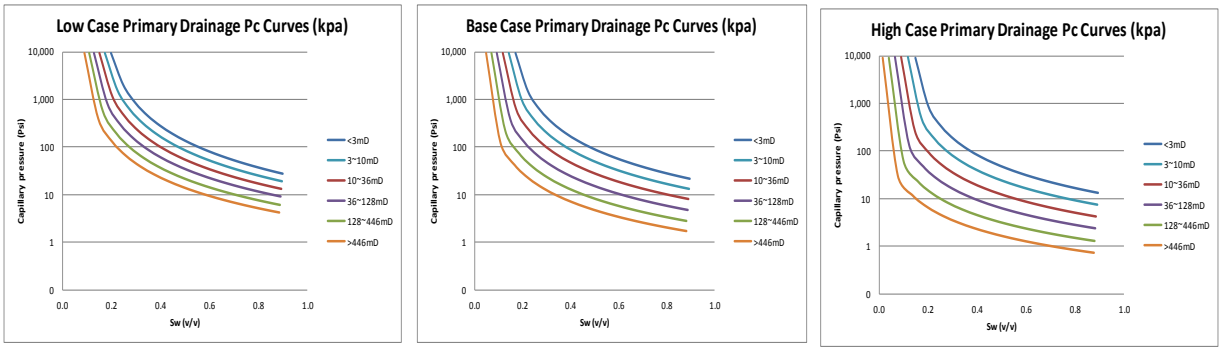

Figure 41: Quest Gen-4 Low, Base, High Case Supercritical CO2-Brine Primary Drainage Capillary Pressure Models

Effect of Capillary Pressure on Relative Permeability

The capillary pressure model was used to set the irreducible water saturation (Swirr) for each rock class. Since the irreducible water saturation is also a parameter in the Relative Permeability Corey Model, it directly impacts the CO_2 end point relative permeability (Kroi@Swirr) and the max residual CO_2 saturation (Sor) in the imbibition process. With the Corey exponents of the Corey Model unaffected, the variation in the irreducible water saturation will still cause the a shift of the relative permeability curves.

The Gen-4 low case and high case capillary pressure models introduce such variations (about +-3 saturation units) to the irreducible water saturation defined by using the base case capillary pressure model. Hence, the relative permeability inputs are different once the different capillary pressure models are used.

Figure 42 illustrated the effect of Gen-4 capillary pressure model on the drainage relative permeability curves. For this plot, the base case relative permeability Corey model was used.

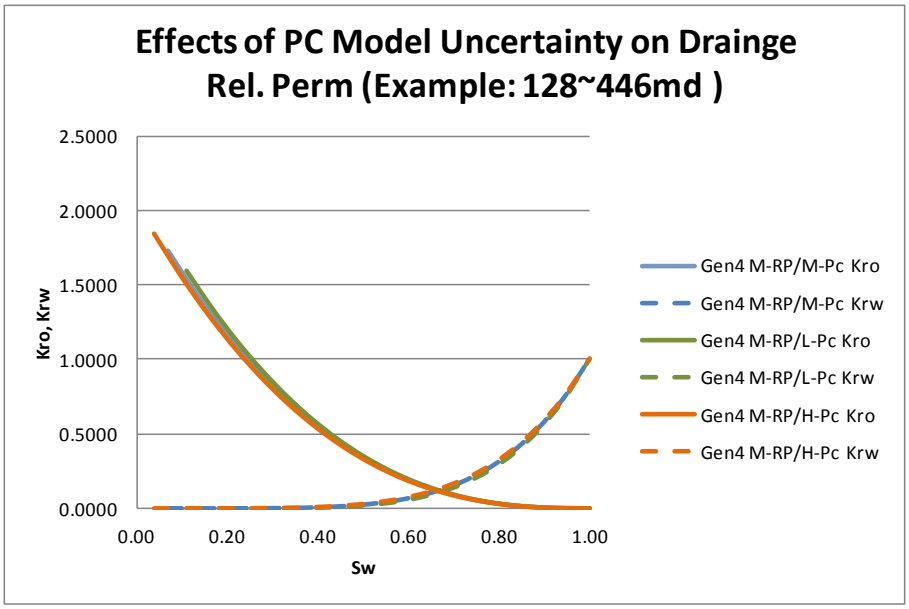

Figure 42: Effect of Capillary Pressure on Drainage Rel. Perm. Model

Relative Permeability Corey Model Parameters

The relative permeability Corey model is an empirical model. For an Oil-Water (or Supercritical CO_2 – brine) system, the Corey functions for the drainage cycle (inject CO_2 to displace reservoir brine) can be found in APPENDIX 3.

GEM, the chosen dynamic simulator, requires the drainage Corey model inputs and the max imbibitions residual CO_2 saturation (Sor) as the hysteresis input. With those inputs, the imbibition relative permeability scanning curves of CO_2 are computed in GEM using a modified form of Land's equations. The hysteresis of water, the wetting phase, and the hysteresis of capillary pressures were not modeled, as experience shows very little effects of such physics on the modeling results.

Corey exponents in the Corey Model are functions of the wettability index. Corey exponents and the uncertainty are independent from the capillary pressure model used. See Table 11 for the Corey exponent uncertainties in the Gen-4 relative permeability Corey Models.

It should be noted that, Swirr is however determined by the capillary pressure model used.

Other Corey model parameters, like Kroi, Sor, vary largely from the low case to base case to high case of the Corey models. To a small extent, they are impacted by the applied capillary pressure model as discussed in the section above.

Hence, combining the low, mid, high cases of relative permeability Corey models together with the low, mid, high cases of the capillary pressure models, results in total of nine permutations for the relative permeability and capillary pressure inputs as outlined in APPENDIX 3.

Relative Permeability Model Scale-down and Absolute Permeability Scale up

The Kroi and $Krwi_{\_drain}$ values in the Corey models (APPENDIX 3) must be scaled down because GEM reservoir simulator requires a normalization of the relative permeability end point (Kroi or Krwi) to a value of 1. Corey exponents, Swirr and Sor in those tables are not affected by the scaling process. The additional table in APPENDIX 3 summarizes the scaling factors and the resulting Kroi and $Krwi_{\_drain}$ for the relative permeability Corey models as finally applied in GEM.

It should be noticed that when such down-scaled relative permeability models are applied, the absolute permeability values in the simulation model must be correspondingly scaled up in order to compute correct effective permeability values for the simulation.

3.3.2. Pore Pressure and Temperature

MDT pressures in the BCS interval were recorded in the recent appraisal wells Scotford 11-32, Redwater 3-4 and Radway 8-19. The data form a very consistent pore pressure gradients (Figure 43), indicating very similar fluids in the BCS formation at a single pore pressure gradient across a vast area. Given that the center of the development is close to the Radway well, the pressure gradient of 11.691kPa/m from the Radway well MDT test was applied to determine the initial BCS formation pressure in the model, equating to 20.465Mpa at 1431.32mTVDss(2078mTVDKB).

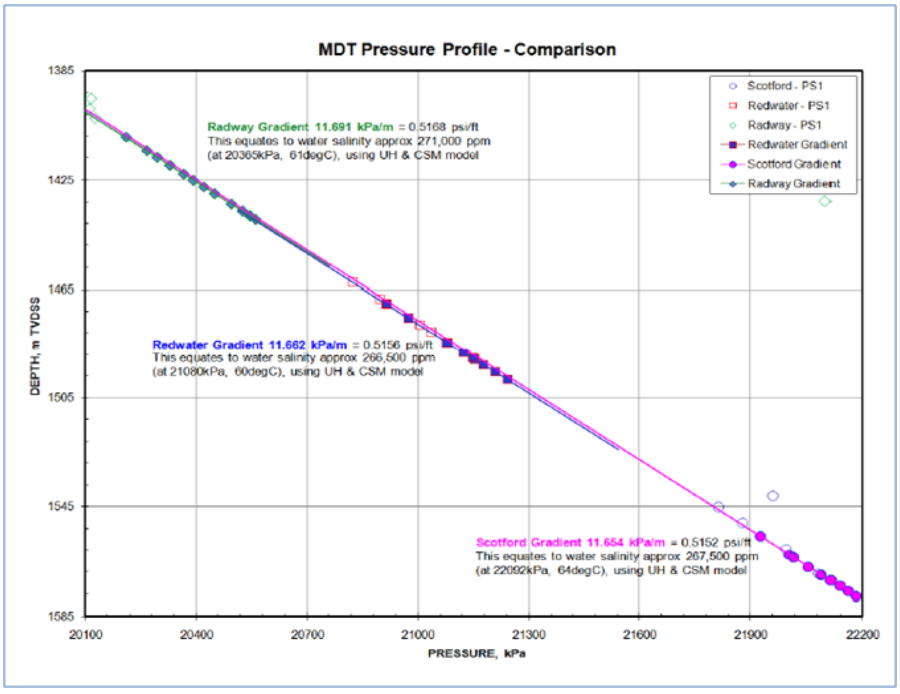

Figure 43: Quest Appraisal Wells Pressure Gradients

The temperature estimate, made from all three MDT runs (pre-tests and post-sampling) suggested a formation temperature of approximately 60°C at the depth of the BCS. This was applied consistently as initial formation temperature in all of the Gen-4 models. Further local calibration using the DTS reading as recorded in the Radway 8-19 well confirmed the regional temperature gradient as displayed in Figure 44, suggesting an initial formation temperature of the BCS of 65°C instead of 60°C.

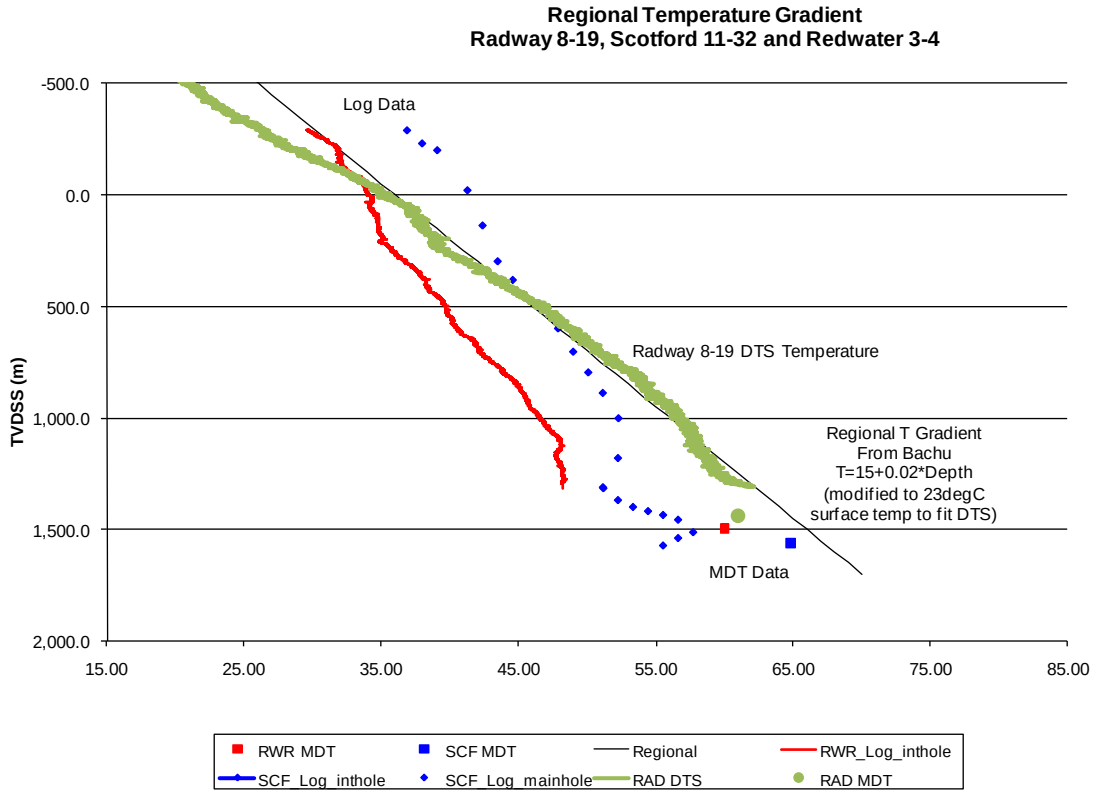

Figure 44: Quest appraisal wells, temperature vs. depth

This 5°C difference may be attributed to the fact that the MDT, even after hours of fluid sampling, has not reached thermal equilibrium, however from all practical purposes of Gen-4 modeling, this 5°C difference between assumed formation temperature and true formation temperature is insignificant.

3.3.3. Aquifer Flow Direction and Velocity

The following work was undertaken to help discuss any potential influence on CO_2 migration away from Quest Injector wells by aquifer flow within the BCS storage complex. If deemed valuable the resultant flow direction and velocity could be incorporated into reservoir models for further assessment on its influence. The aim of this work was to gain an understanding of a representative range of flow velocities that the AOI may be subject to, and not to narrow down an exact velocity leaving open ambiguity to the input variables, and undetermined ranges of uncertainty.

Values of pore velocity were calculated using a range of hydraulic and reservoir parameters taken from Quest well appraisal work used in the Gen-3 and Gen-4 modeling program. High, base, and low case water levels were calculated using the range in formation fluid densities listed in Table 13. Water levels are calculated using pressure and depth of recorded pressure, fluid density, and acceleration due to gravity. These calculations are made utilizing a very large range to gauge sensitivities so to ensure an understanding of the range of uncertainty for such a large area. The area mapped covers 45 townships by 40 ranges shown in Figure 45. They may be subject to change as new data comes to light.

Three wells (two Quest and one non-venture well were used to calculate water levels representative of the Quest AOI. Please see Figure 45 below:

Michigan Wisconsin Pipeline Company (MICH):	100/07-06-065-04W5/00
Quest Redwater (Redwater 03-04):	100/03-040-057-20W/00
Quest Scotford (Redwater 11-32):	102/11-32-055-21W4/00

(Bachu S. , 2009) created a regional Basal (which includes the BCS) water level map from approximately townships 65 to 100 and Ranges 0W4 to 25W4. The three resultant water level scenarios from the Quest and non-venture wells labeled above were used to extend the Bachu study southward. Figure 45 thru Figure 47 show the water level maps. Flow vector directions were drawn at right angles to lines of equal potentiometric surface. The vectors measured out between 25 and 300km in length while making sure to pass through the AOI. Variations in vector length were used in calculations to attempt higher potentially representative ranges in velocity. Multiple scenarios were created using the water level maps a range of reservoir parameters giving high, base and low case flow rates.

Pore velocity was calculated according to Darcy. Flow was calculated through $1m^2$ of porous media being proportional to permeability and the drop in water level (pressure) between two points, and inversely proportional to length between the two water levels, viscosity, and porosity.

Basal Cambrian Sand porosity, permeability, and fluid viscosity ranges were taken from the Quest Gen-3 modeling parameters to calculate flow rates along the vectors (see Table 14).

Results

- Flow vectors taken from resultant potentiometric surfaces showed an East to Northeastward flow direction. This flow is up dip flow and may add to buoyancy effects.
- Results showed a range of flow velocities from 0.3cm to 39cm per year with an average of ~1cm per year. Good in-line with the above estimate, (Bachu S. H., 1986) made calculations on basin scale pore velocity with results of 0.006cm/yr to 79cm/yr with an average of 0.8cm/yr

Table 13: Formation Fluid Properties & Resultant Water Levels.

Table of Calculated Water Levels BCS			
MICH	**High**	**Expected**	**Low**
	560	540	482
Water Density kg/m3	1157	1194	1230
Temperature (C)	78	68	58
TDS (ppm)	285767	336196	386625
Pressure (kPa)	26913	26913	26913
Redwater 03-04			
Water Level (mTVDSS)	418	372	319
Water Density kg/m3	1129	1157	1191
Temperature (C)	68	58	48
TDS (ppm)	232.7549	269	315.2668
Pressure (kPa)	20826	21070	21243
Redwater 11-32			
Water Level (mTVDSS)	418	376	321
Water Density kg/m3	1129	1157	1191
Temperature (C)	68	58	48
TDS (ppm)	232.7549	269	315.2668
Pressure (kPa)	21961	21070	21243

Table 14: Reservoir and Fluid Properties with Resultant BCS pore velocity for a given Vector.

Parameter Range for Flow Calculation through 1m2								
Scenario	**k (mD)**	**Porosity (frac)**	**Viscosity (mPa.s)**	**Fluid Density (kg/m3)**	**ΔP (kPa)**	**Distance (km)**	**Velocity (cm/yr)**	**Vector Direction**
High Velocity	500	0.11	1.13	1191	1614	45	39cm/year	95 - 125° (ESE - SE)
Mid Velocity (Expectation)	50	0.15	1.155	1157	2935	250	1cm/yr	70 - 95° (ENE - E)
Low Velocity	20	0.19	1.18	1129	821	70	0.3cm/yr	70 - 95° (ESE - SE)

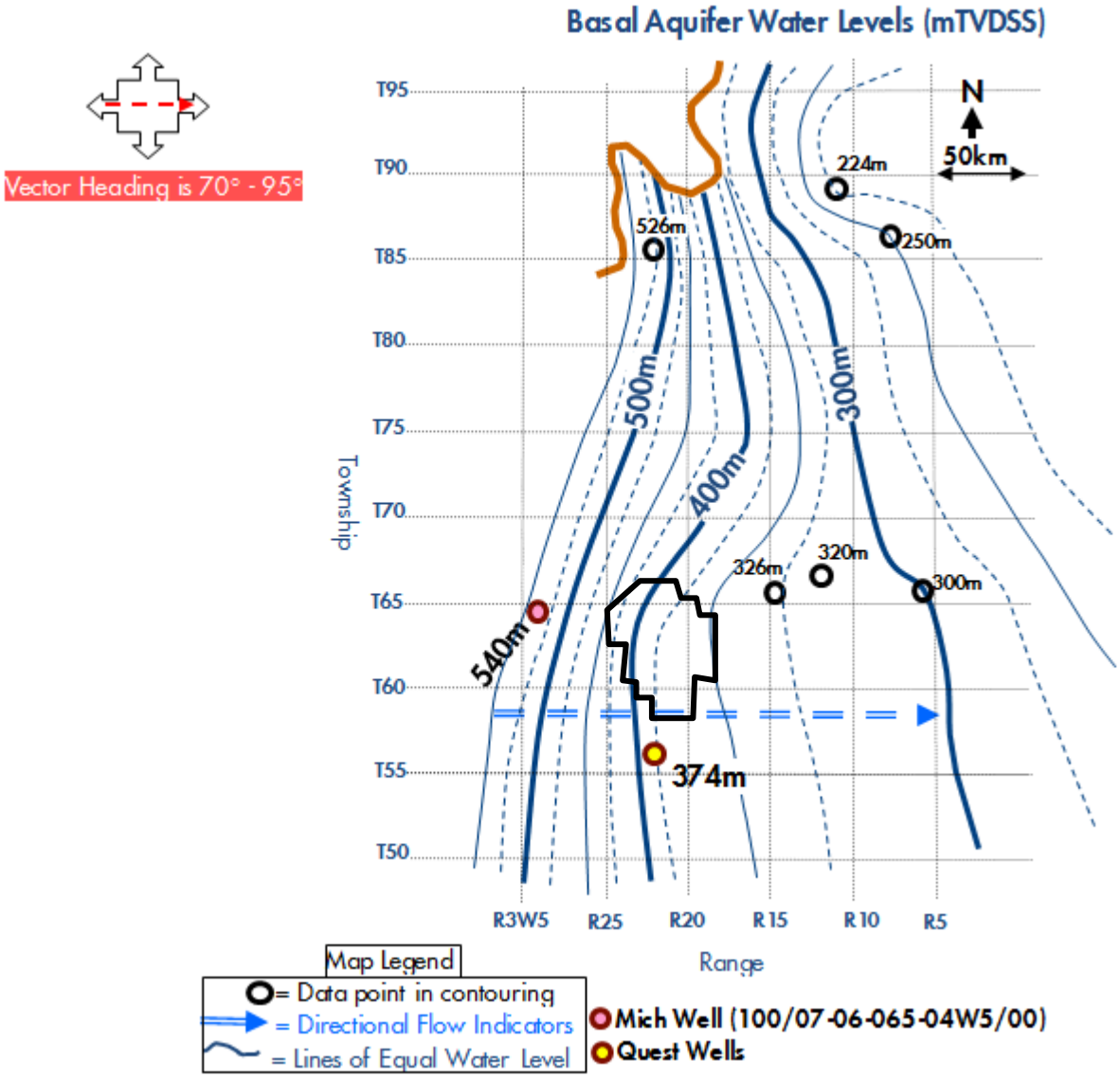

Figure 45: Base Case Water Levels drawn from amalgamating the Bachu etal. 2009 Basal Aquifer water level map with three wells in the Quest area. The Quest wells were close enough together and similar enough in resultant water level(s) to be represented by one data point. Note the 250 km vector (hashed blue) represented as hashed blue arrow. The black outline is the Quest AOI.

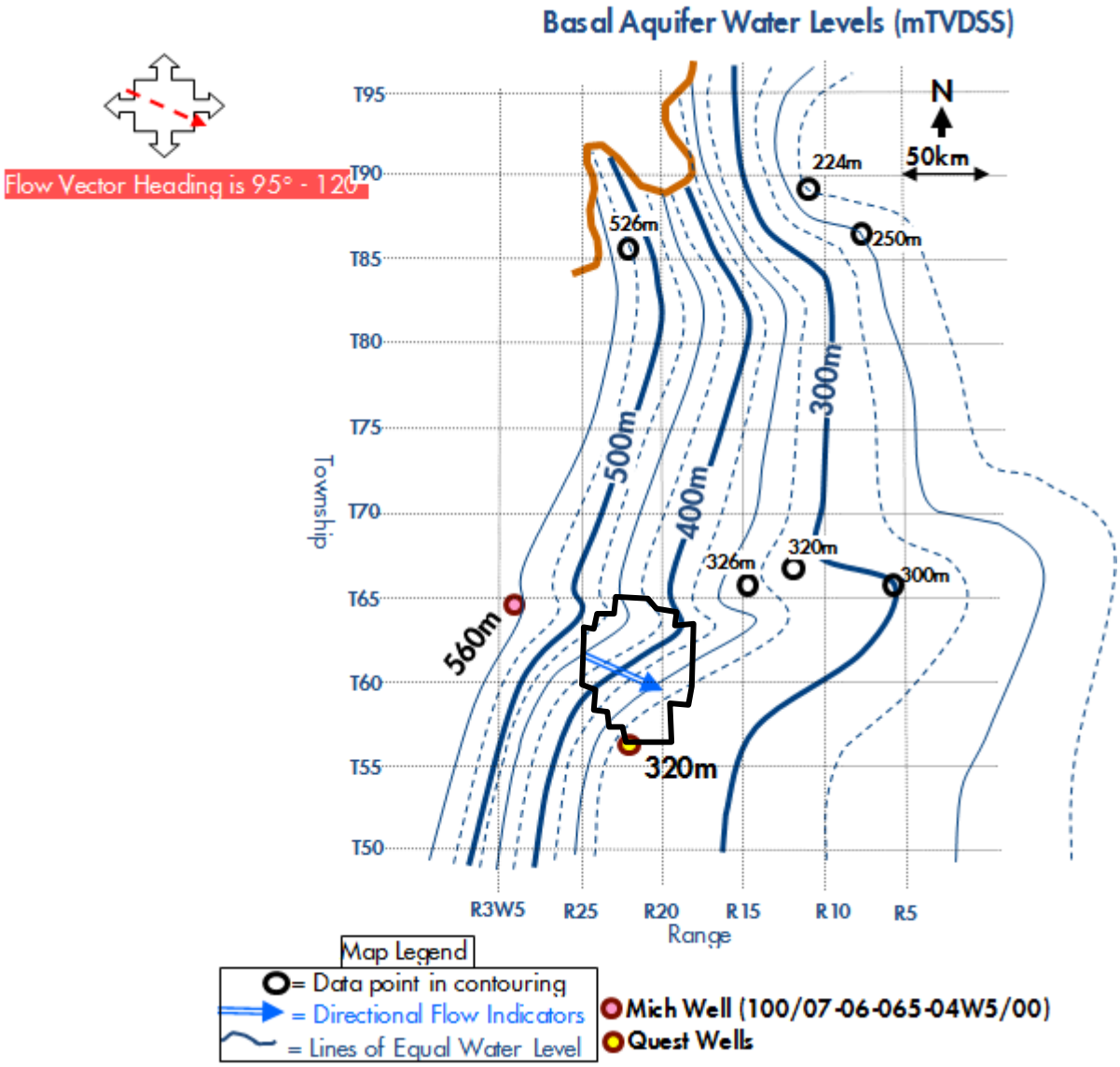

Figure 46: High Flow Water Levels drawn from amalgamating the Bachu etal. 2009 Basal Aquifer water level map with three wells in the Quest area. The Quest wells were close enough together and similar enough in resultant water level(s) to be represented by one data point. Note the 45 km vector represented as a blue arrow.

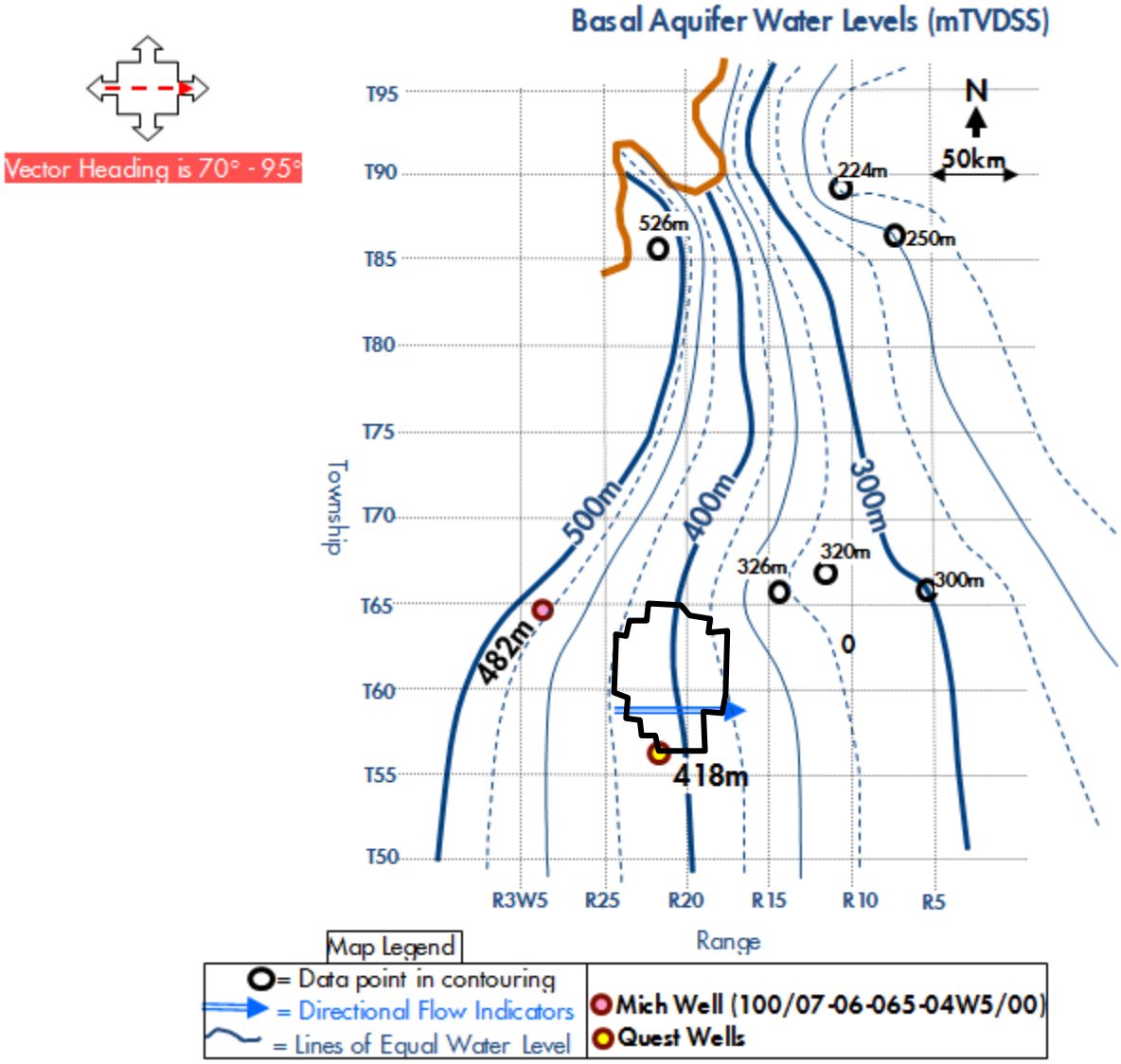

Figure 47: High Flow Water Levels drawn from amalgamating the Bachu etal. 2009 Basal Aquifer water level map with three wells in the Quest area. The Quest wells were close enough together and similar enough in resultant water level(s) to be represented by one data point. Note the 70 km vector represented as a blue arrow.

3.4. Fluid Properties

3.4.1. CO_2 Properties and Contaminants

The CO_2 injected at Quest will have a high purity of 99.2% under normal operations. Its physical properties are almost identical to the pure CO_2, hence, pure CO_2 was used as the injection component in all Gen-4 models.

Table 15: Composition of the injection stream under normal operations.

Total Stream composition	Normal Mol %	Upset-Mol %
CO_2	99.2%	95%
CO	0.02%	0.15%
N_2	0.00%	0.01%
H_2	0.68%	4.27%
CH_4	0.09%	0.57%
H_2O	<52 PPM	52 PPM

3.4.2. Formation Brine

The in-situ brine salinity measured from the Radway well fluid samples was first reported to be 328,000 mg salt per liter brine, and later reported after detailed geochemical analysis to be 315,000 – 320,000 mg salt per liter brine or 262,000 – 267,000 mg salt per kg brine. These measurements are similar to and within the range of the Scorford well sample results, which varies from 256,000 – 277,000 mg salt per kg brine.

The initial value of 328,000 mg salt per liter brine used in the model is considered representative of the reservoir in-situ salinity and has been consistently used in all Gen-4 modeling activities, except if stated otherwise.

The reservoir fluid density and viscosity are calculated within the GEM software using the most appropriated correlations available according to the above reservoir water salinity input. The density and viscosity values are then compared to the lab measurement results of the Radway well and Scotford well samples. The density is also compared to pressure gradient from MDT measurements.

The Rowe-Chou correlation (Rowe, 1970) is used in GEM to calculate brine density based on salinity and at specified pressure and temperature. The correlation is developed for wide ranges of temperature, pressure and salt concentration, which are summarised in Table 16.

The brine density calculated at reservoir condition is 1190 kg/m3, which is nearly the same as what is measured in the Radway well samples and only slightly higher than that from the Scotford well samples. This is also consistent with the MDT pressure measurements at the Radway, Redwater, and Scotford wells, which are plotted in Figure 43. The density of 1190 kg/m3 is equivalent to the pressure gradient of 11.7 kPa/m.

Table 16: Applicable ranges of the Rowe-Chou and Kestin correlations for aqueous density and viscosity.

Property	Aqueous Density	Aqueous Viscosity
Temperature	0-175	25-150
Pressure (MPa)	0-34	0.1-35
Concentration (ppm)	0-250,000	0-350,000

The reservoir brine viscosity is calculated in GEM using the Kestin correlation (Kestin, 1981), which is developed for wide ranges of temperature, pressure and salt concentration shown in Table 5. The calculated viscosity of 0.98 cp is also within the range of lab measured data from the Radway and Scotford samples from 0.76 to 1.18 cp.

4. SINGLE WELL RADIAL MODEL

This Single Well Radial Thermal model focussed on calibrating the injectivity in the larger full field pressure models and quantifying the expected zone of cooling around the injectors. IPSM modelling [ref] has shown that CO_2 will arrive at the wellhead at approximately only 5^oC due to heat exchange with the ground while being transported via a buried pipeline to the injection site. Therefore with injection of CO_2 the reservoir temperature in the near well bore of the injectors is expected to drop from initial conditions at around 60^oC to some 20^oC -30^oC depending on injection rates and cumulative injected volume. Since reservoir cooling the viscosity of CO_2 and fluids and is known to result in reduced formation strength and may reduce fracture gradients in the reservoir, it is important to quantify the areal extent of this cooling zone.

4.1. Objectives

The construction and calibration of injectivity through radial well models wells has the following objectives:

1) Establish benchmark injectivity for a simplified and reproducible permeability profile using an isothermal radial well model with fine gridding around the well.
2) Derive a permeability and/or skin correction factor from thermal radial well models to be incorporated in the full field isothermal pressure models that can represent the increased viscosity of CO_2 and resulting reduced injectivity due to the cooling effect around the injector.
3) Quantification of the relationship between area of extent of cooling around the injectors and cumulative injected volume for a range of reservoir scenario's (low, mid and high case permeability and various permeability profiles) varying rate and some of the key parameters that determine heat influx from the over and under burden.
4) Carry out a sensitivity analysis on the CO2 related parameters with uncertainty to evaluate the impact of these uncertainties on the start-up of an injector.
5) The benchmarked injectivity from the radial well model should be used to guide the local grid refinement strategy in the full field isothermal pressure model to ensure that modelled pressures in the near well bore region approximate the pressures that can be realistically expected in the field.

4.2. Model Setup

4.2.1. Input Data

Basic reservoir properties such as depth, porosity and horizontal permeability are based on the Radway 8-19 well logs, with kv/kh based on Gen-3 statistics where the Begg & King methodology was adopted. All model input data will be documented in this section, and discussed in the following subsections:

- Depth, porosity, permeability
- Kv/Kh
- Relative permeability and capillary pressure curves
- Reservoir and over/under-burden thermal properties
- Reservoir fluid properties

The following is a summary table of the basic input data for the radial, layer cake, thermal model. Inputs that vary by layer including permeability and porosity are documented in APPENDIX 4 for completeness. For consistency these basic properties, at the well location of the Radway 8-19 well, have been shared across the various models of the Gen-4 activities, including the CO_2 plume models, pressure models and geochemistry modelling.

Table 17: Summary of basic input data for the radial thermal model.

Property	Units	Value
Reservoir reference depth	m	2078
Temperature at ref. depth	deg. C	60
Initial Pressure at ref. depth	kPa	20465
Gross Thickness	m	43
Net-to-Gross		1
Net Thickness	m	43
Permeabiliy	mD	Layer
Kv/Kh		0.01
Porosity		Layer
Rock Compressibility	1/kPa	1.45E-07
Salinity	Ppm	328,000
water compressibility	1/kpa	2.77E-07
BHP Constraint	kPa	26,000
Wellbore radius	m	0.108
Perforation		all
Skin		10
Injection BHT	deg. C	20
Water Density	kg/m3	1190
Water viscosity	cp	0.98

Depth, porosity, permeability

Porosity and permeability of the radial thermal model have been directly incorporated from the petrophyscical evaluation of the Radway 8-19 well, including the description of the depositional facies. The inputs have been re-sampled to a 1m sampling rate, reflecting the layer thickness of the model. The perforation interval for injection was selected to be the Tide Dominated Bay Margin (TDBM) except the bottom two layers, consistent with general field development strategy.

The average permeability for the entire model is 682 mD, with 894 mD for the TDBM interval and 955 mD for the perforation interval.

Kv/Kh

A Kv/Kh ratio of 0.01 is used as shown in the properties summary table for the vertical permeability. This represents a mid-case value based on the previous Gen-3 statistics. This was a necessary choice due to the parallel nature of the Gen-4 work streams. This Kv/Kh ratio was subsequently confirmed as a representative number for the purpose of the study after finalizing the evaluation of the Radway 8-19 well and updating the Gan-4 static model.

Relative permeability and capillary pressure curves

As with the Kv/Kh above, the Gen-3 base case relative permeability was used for the radial thermal model while the Gen-4 relative permeability was being updated while incorporating additional lab data. The relative permeability and capillary pressure table that best fits the Radway 8-19 permeability range (279 mD – 1036 mD) is attached in the format of the CMG GEM input deck (APPENDIX 4).

Reservoir and over/under-burden thermal properties

Reservoir and over/under-burden thermal properties including heat capacity, heat conductivity and density for the rock, reservoir fluid and injected fluid are required for the thermal modelling. An extensive literature search was conducted, combined with field data providing the rock type/mineral content information to determine the thermal properties and uncertainty ranges (Lonergan, 1994) (Willis, 1994).

The rock types based on majority mineral content in each zone are summarized in the following table. The main injection zone, BCS, is mainly quartz sand or sandstone, with the over burden, LMS, being mainly siltstone and the underburden, the basement being crust.

Table 18: Formation and main rock type for thermal modeling

Formation	Assigned Rock Type
LMS	Siltstone
BCS	Sandstone
BCS	Quartz Sand
Basement	Crust

A detailed list of the thermal properties of the above rock types, as used in the thermal models is attached in APPENDIX 4, including high, mid and low values for heat capacity, rock density, heat conductivity, as well as thermal expansion coefficient, which is not used in this thermal modelling exercise.

The base case BCS quartz sand properties are used for the study. The data uncertainty ranges are relatively small, except the thermal conductivity that showed a wider range. The sensitivity of the thermal conductivity on cooling effect was later investigated using the analytical method, which showed insignificant cooling zone variations.

Reservoir fluid properties

Key fluid property values including reservoir water salinity, density and viscosity are listed in the basic input data summary table Table 17. Consistent with the other Gen-4 modeling activities, brine and CO_2 properties have been used as introduced in chapter 3.4 on fluid properties.

4.3. Boundary Conditions

The single well radial, layer cake model is set up with reservoir properties based on data from the Radway well, which is located at the middle of the planned development. Analytical infinite aquifer boundary condition, the Carter-Tracy model in GEM is applied for fluid flow at the model boundary.

Heat transfer to (/from) over- and under-burden as well as model boundary are modelled, using HEAT-LOSS key word with thermal and fluid properties stated in the above sections.

4.4. GEM Thermal Modeling

As the thermal modelling functionality in GEM is relatively new and it is the first time used, the following functionality has been included to capture thermal effects in the GEM models:

- The energy balance calculation includes heat conduction and convection within the reservoir rock and fluids as well as heat loss to the surrounding. The following is a direct quote from the GEM 2010.10 technical manual.
- The heat loss to the over- and under-burden is calculated heat diffusivity model by Vinsome and Westerveld, which is also quoted from the GEM2010.10 manual below for easy reference.

A detailed description of the underlying physics of both additions can be found in APPENDIX 4.

A benchmark exercise was performed to compare the simulated cooling zone using the GEM Thermal model, a STARS model and a TOUGHREACT model, which showed almost identical cooling zone size and very similar temperature distribution after 10 years of CO_2 injection, adding confidence about the validity of the new add-on to the GEM simulator.

4.4.1. Model dimension and grid size selection

A two-step model dimension and grid size sensitivity study was conducted to select proper model and grid sizes for the thermal radial modeling as well for providing guidance for plume model dimension requirement. In the first step, three models were compared, and the areal and cross section of the models with grids are displayed below:

1. 4 km radius, 30 “r” division (coarse grids)
2. 10 km radius, 75 “r” division (coarse grids)
3. 10 km radius, 600 “r” division (fine grids)

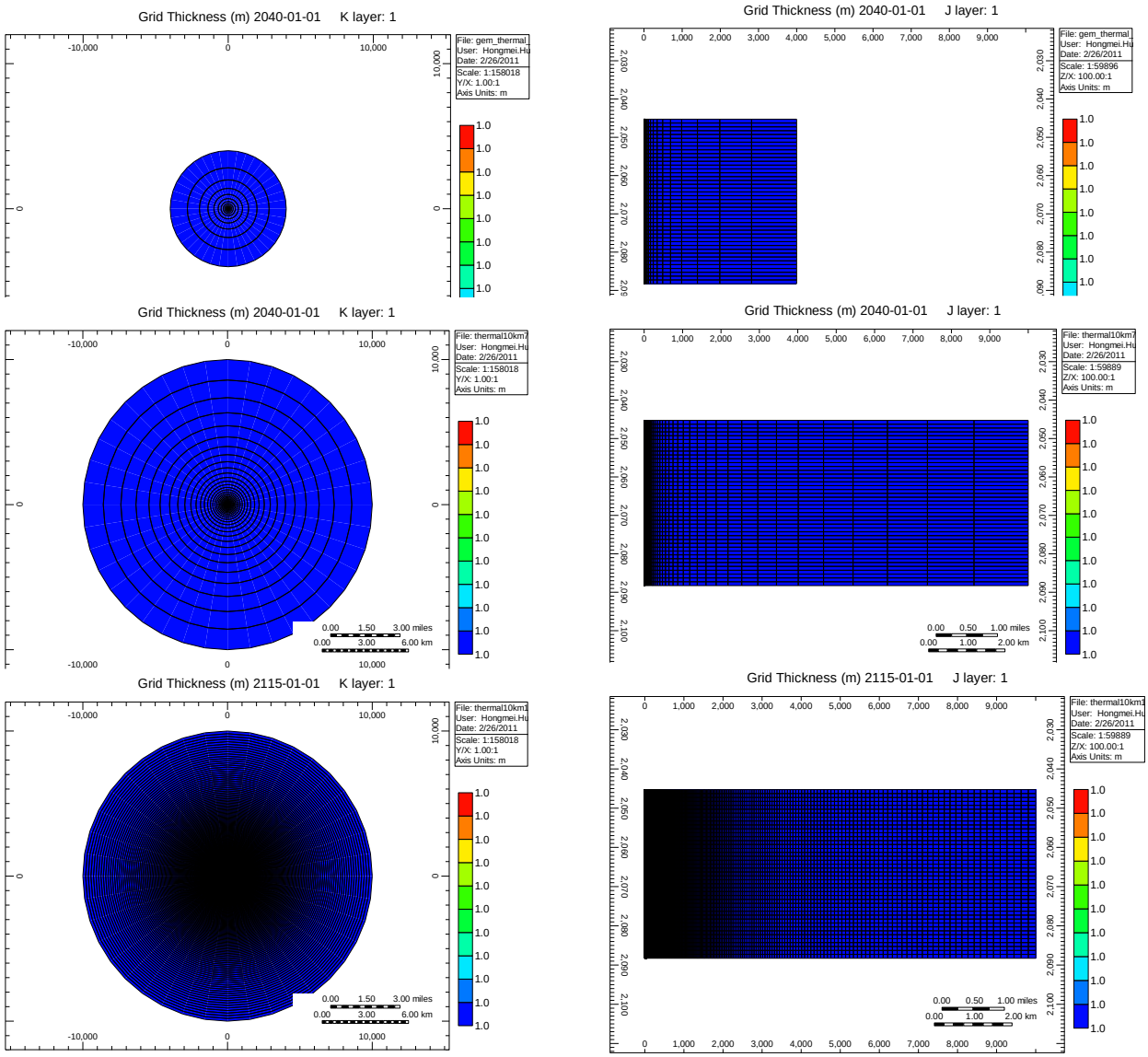

Figure 48: Areal and cross sectional display of the three models for model dimension and grid size sensitivity study (Top Model 1., Middle Model 2., Bottom Model 3. as described above)

The three models with the same properties and boundary conditions are simulated rate controlled to allow for injection of 1.08 Mt of CO_2 per year over 25 years while scaling well rate to the number of assumed injection wells, where required. For model comparison, the injection rate of the three models are plotted in Figure 49 below (in solid lines.) There is a significant difference shown between the 4 km radius model and the 10 km radius model. The percentage difference is plotted as the pink dotted line, which shows around 10% difference at early years to near 20% at later years. The rate difference between the two 10 km radius models with coarse and fine grids is smaller, less than 3%, showing at the blue dotted curve.

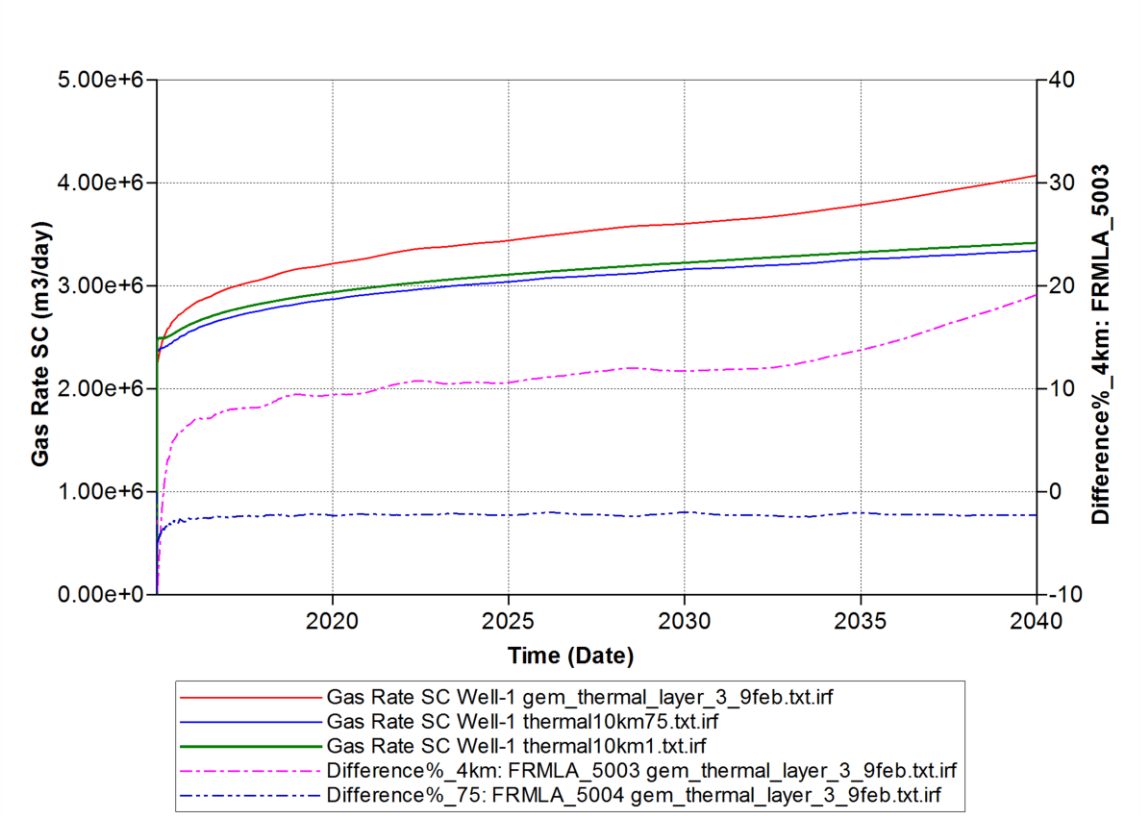

Figure 49: Gas rate plot showing large difference between the 4 km and 10 km radius models, and smaller difference between the coarse and fine grids 10 km radius models

To determine what is an appropriate model dimension and grid size for the study, further models were examined with increased model radius from 4 km and various grid sizes for each model dimension, as the second step. Besides those examined in the first step, 6 km radius models and 8 km radius models with different "r" divisions are compared. The following model results are shown in the gas rates plotted, in the order of gas rates from highest to lowest, top curve to bottom curve.

1. 4 km radius, 30 "r" division
2. 6 km radius, 45 "r" division
3. 6 km radius, 75 "r" division
4. 8 km radius, 60 "r" division
5. 8 km radius, 75 "r" division
6. 10 km radius, 600 "r" division
7. 10 km radius, 75 "r" division

The results showed that the 8 km radius models produced very similar injectivity as the 10 km models, and the two different grid sizes of the 8 km radius models produced nearly identical injectivity. It is concluded that, with appropriated grid size, the modeled injectivity reaches the "true" answer when the model radius is 8 km or greater. To minimize simulation time, a model with the smallest dimension and coarsest grid size acceptable would be selected for the study. In this case, the 8 km radius in dimension and 60 "r" division in grid size are selected for this study.

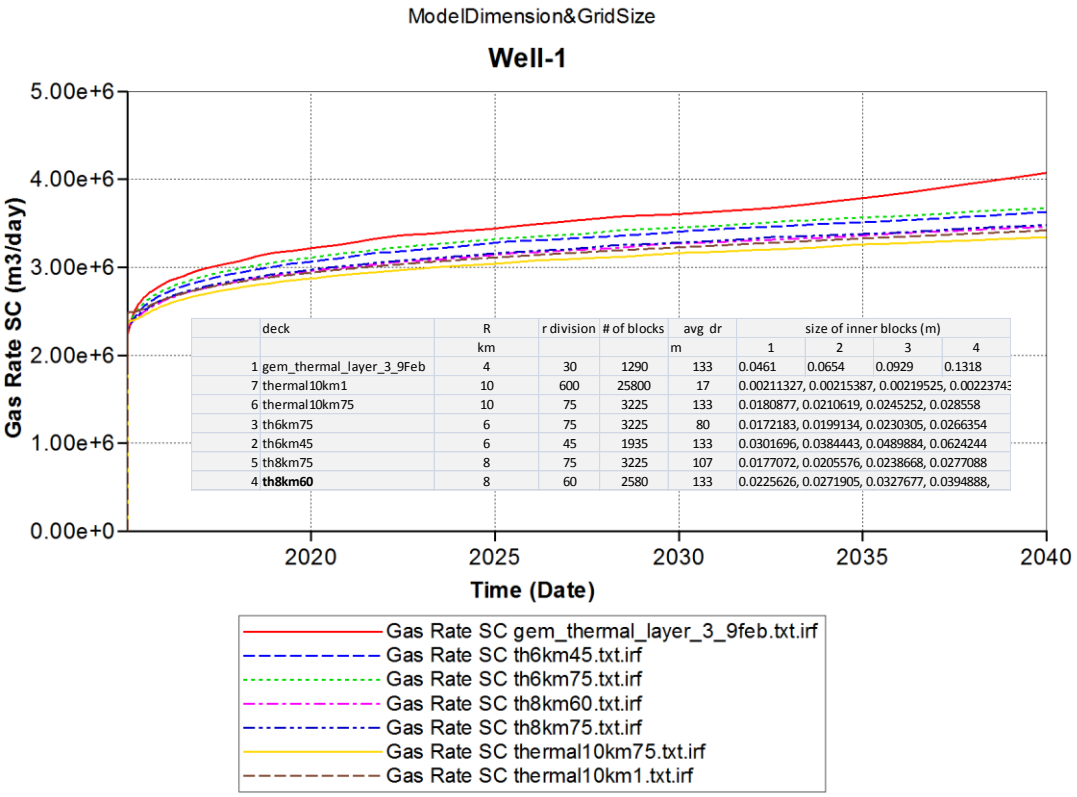

	deck	R	r division	# of blocks	avg dr	size of inner blocks (m)			
		km			m	1	2	3	4
1	gem_thermal_layer_3_9Feb	4	30	1290	133	0.0461	0.0654	0.0929	0.1318
7	thermal10km1	10	600	25800	17	0.00211327, 0.00215387, 0.00219525, 0.0022374			
6	thermal10km75	10	75	3225	133	0.0180877, 0.0210619, 0.0245252, 0.028558			
3	th6km75	6	75	3225	80	0.0172183, 0.0199134, 0.0230305, 0.0266354			
2	th6km45	6	45	1935	133	0.0301696, 0.0384443, 0.0489884, 0.0624244			
5	th8km75	8	75	3225	107	0.0177072, 0.0205576, 0.0238668, 0.0277088			
4	**th8km60**	8	60	2580	133	0.0225626, 0.0271905, 0.0327677, 0.0394888,			

Figure 50: Gas rate plot showing near identical results when model is 8 km or greater in radius and grid size is fine enough – 60n"r"division for the 8 km radius model

4.4.2. Thermal Effect

4.4.2.1. Injectivity reduction due to cold injection

Using the above described input and analytical infinite aquifer boundary condition, the 8 km radius model with 60 "r" division has been simulated in GEM for as a thermal model and an isothermal model, both rate constrained to allow for the injection of 1.08 Mt of CO_2 per year over 25 years, including having rate scaled to the number of injection wells.

The injection rates from the two models are plotted in the graph below (Figure 51) The red solid curve at the top is the rate from the isothermal model, where the injected CO_2 is assumed to be at reservoir temperature, 60 degree C. The blue dotted curve just below is the injection rate from the thermal model, where the injected CO_2 is assumed to be at 20 degree C. The percentage difference in the injection rates between the two models are shown as the dotted green curve at the bottom. About 5 – 8% difference in injectivity is shown between the two models with the thermal model showing lower injection rate.

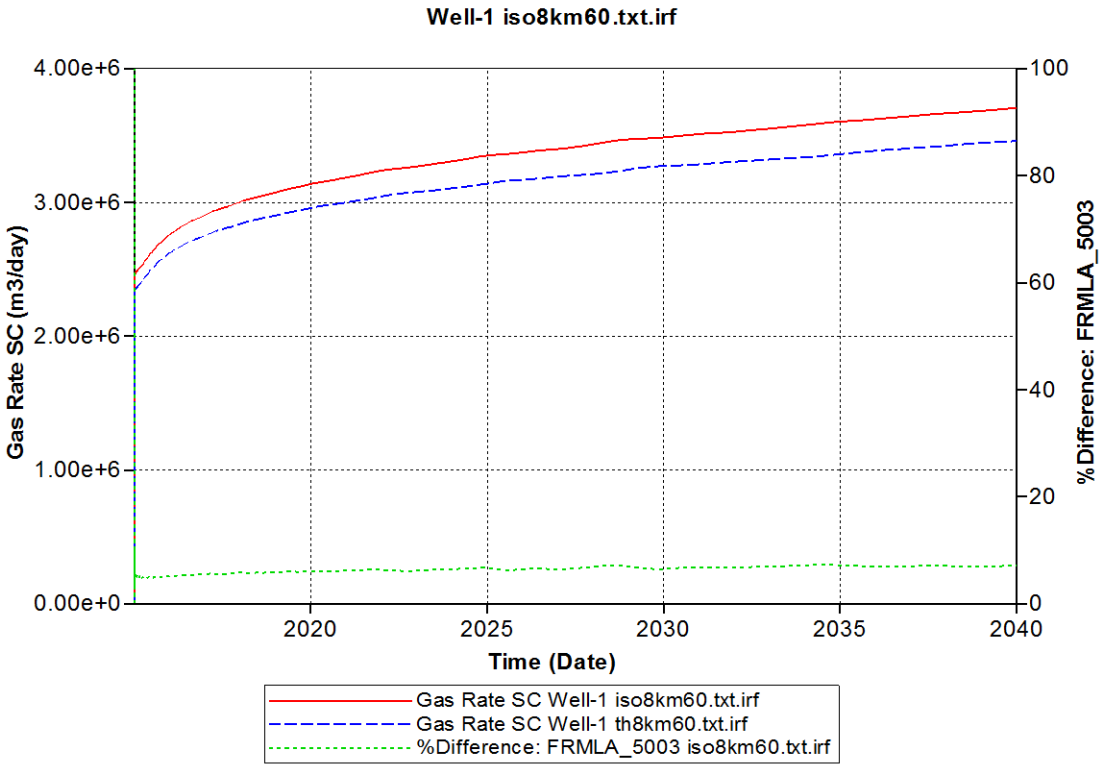

Figure 51: Injection rates of and percentage difference between the isothermal and thermal models.

4.4.2.2. Cooling zone estimation

Due to the injection of cold CO_2 the reservoir temperature around the well bore will be lowered. This cooling effect may also cause thermal stress to the reservoir rock, and therefore affect its geomechanical properties such as fracturing pressure. The size of the cooling zone and temperature distribution need to be estimated to provide basis for geomechanical calculations as well as for MMV strategy.

A range of injection rates were simulated for estimating the cooling zone variation with injection rates and volume. The injection rates covers a practical range of possible average per well injection rate, i.e. from one half of the total target rate to one tenth of the total target rate.

The modeling period includes 25 years of injection followed by a long shut-in period with a total simulation time of 1000 years.

The following panels in Figure 52 display temperature distribution of the cross section at years 10, 25, 50, 100, 500, and 1,000, of the one half rate case. The second panel from the top on the left shows the cooling zone at the end of the 25 year injection period extends to approximately 350 m in radius from the well bore. There are some residual cooling effects remaining showing at years 50 and 100.

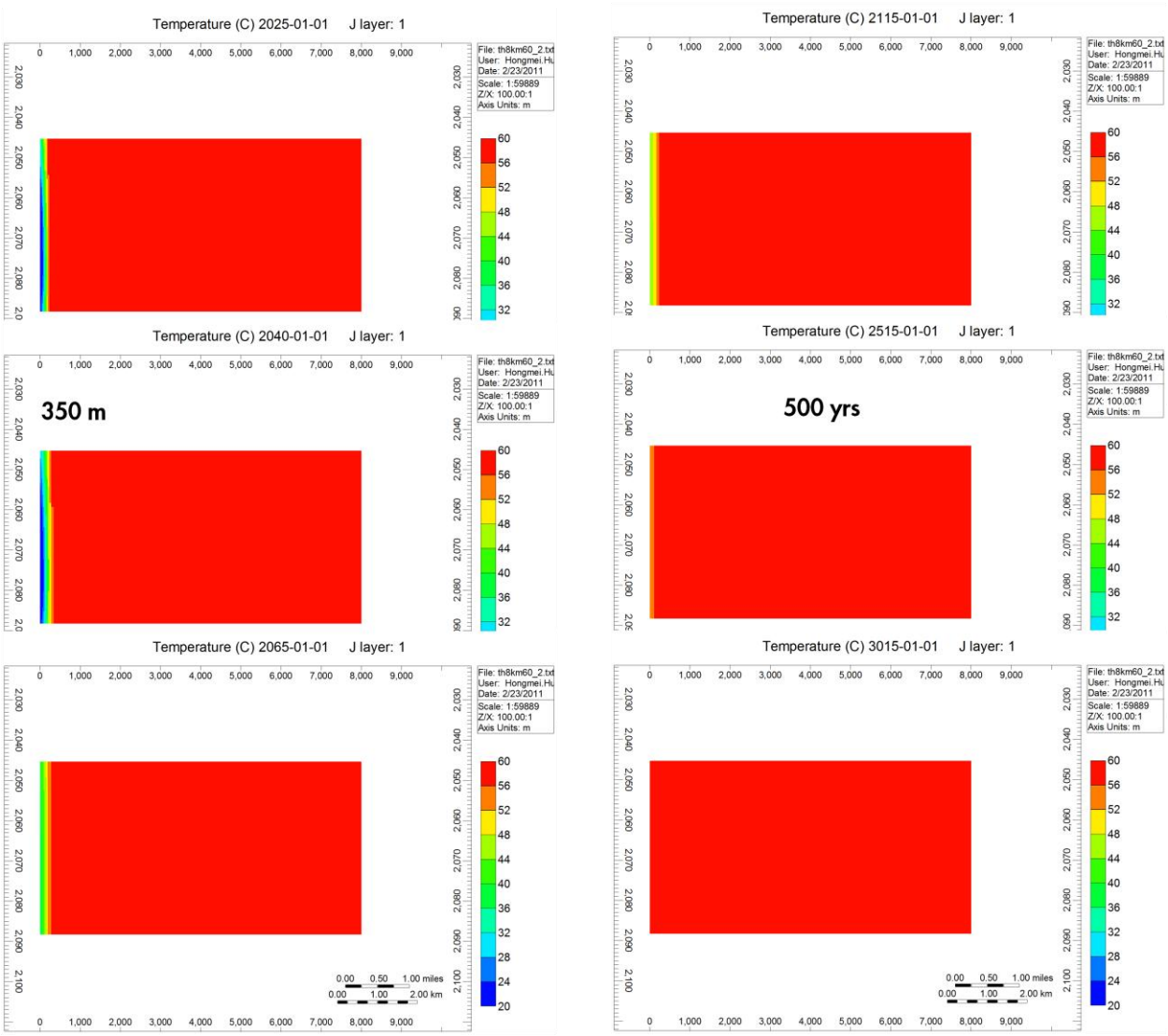

Figure 52: Cross sections showing temperature distribution of the modeling results at an injection rate at one half of the total target rate (10, 25, 50 years - left from top to bottom; 100, 500, 1,000 years – right top to bottom)

The cooling zone radius at year 10 and year 25 of all four injection rate cases are summarized in the following table. At the end of 10 year injection, the cooling zone ranges from approximately 130 m in radius for the one tenth of target injection rate case to 230 m in radius for the one half of target injection rate case. At the end of 25 year injection, the cooling zone ranges from approximately 160 m in radius for the one tenth of target injection rate case to 350 m in radius for the one half of target injection rate case. The results are summarized in Table 19 below.

Table 19 Summary of cooling zone radius at the end of 10 year and 25 year injection

Injection Rate (fraction of target rate)	Cooling zone radius at 10 years (m)	Cooling zone radius at 25 years (m)
1/2	230	350
1/3	190	320
1/5	170	190
1/10	130	160

In addition to the GEM simulation, some simple hand calculations were also completed to provide a sense check on the cooling zone estimation and sensitivities. This was accomplished by performing an energy balance calculation based on the same heat capacity data of the rock, brine, and CO_2 used in the simulation and temperature, porosity and saturation assumptions similar to those in the simulation. The cooling zone size calculated is closely comparable to the simulated results. Analytical calculations were done for the cooling zone temperature recovery time and sensitivities. One dimensional unsteady state heat conduction solutions for three geometric shapes including cylinder of infinite length, sphere, and slab were tested for the temperature recovery process. The analytical calculation confirms that it is likely that a small area near the wellbore region could remain at lower temperature than the rest of the reservoir for a relatively long time, tens of years or longer. Sensitivity studies shows that CO_2 makes the thermal recovery period much longer due to its low conductivity to heat.

4.5. Conclusions

In summary, key conclusions with regard to thermal effect on the injectivity and cooling zone estimation are

1. Well injectivity reduction due to cold CO_2 injection is within 10% (5 – 8%) compared to isothermal modeling results. This effect is largely due to increased fluid viscosity as a result of lowered temperature. This effect may be relatively small compared to some other modeling uncertainties including geological uncertainties and the grid size effect if coarse grids are used, which is usually the case in full field pressure modeling; more so compared to the effect of thermal stress caused reservoir fracturing pressure reduction
2. Cooling zone size extends to a few hundred meters from the well bore and is relatively small in comparison to both, the pressure front and CO_2 plume sizes. The estimated cooling zone radius and temperature distribution as a function of injection time and injection volume have been provided for geomechanical calculations of the thermal stress effect and for MMV strategy consideration.

5. GIVENS AND CONSTRAINTS

5.1.1. Compressor & Pipeline Size

During the Gen-3 activities the General Allocation Package (GAP) within the Integrated Production Modeling (IPM) toolkit was used to confirm a compressor with a 14.5 MPa discharge pressure is sufficient to provide the necessary wellhead and bottom hole pressures to inject the minimum 1.2 MT/yr CO_2 required for the Quest CCS project under the conditions studied (100% up-time of facilities and injection).

Quest's integrated injection modeling system includes the integration of the surface network with the well model. An example diagram of Quest's GAP network can be found in Figure 53. The temperature-pressure operating envelop and associated CO2 phase behavior is shown in Figure 54.

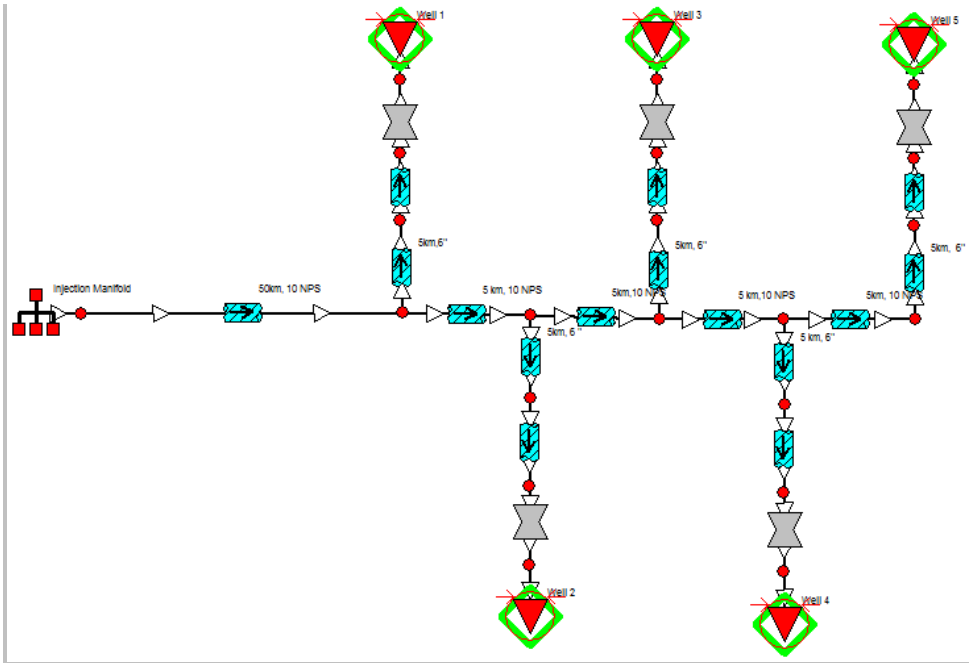

Figure 53: Example of Quest GAP network connecting surface components and wells

GAP was used to model the pressure and temperature losses across the pipelines from the compressor (i.e. Injection Manifold) to the wellhead (i.e. Well 1). This available wellhead pressure and temperature was then used by a Prosper well model to model the bottom hole pressure and temperature at the top perforation.

The changes in pressure and temperature throughout this injection process are illustrated in the CO_2 phase envelope below, which shows CO_2 remaining in the liquid or supercritical phase at all times. The arrows in the phase envelope indicate the direction of flow from the compressor, through the pipelines to the wellheads, down the wellbore and into the reservoir.

Already during the Gen-3 modeling a four and five well count scenario was compared against a 10, 12, and 16 inch nominal pipeline size. A seven well count scenario with a 10 inch NPS pipeline was compared against 3.5" and 4.5" tubing. A winter and summer scenario for a

31°C and 60°C compressor discharge temperature were modeled to capture the range of realistic temperature losses attainable from the compressor to the wellhead. To ensure a 14.5 MPa compressor could deliver sufficient injection pressures in each of these surface scenarios, the Gen-3 low case reservoir permeability of 20-50 md was used in the well model.

GAP modeling shows a 14.5 MPa compressor discharge pressure more than adequate to provide the necessary wellhead and bottom hole pressures to inject the minimum 1.2 mtpa CO_2 required for the Quest CCS project for all the surface scenarios modeled.

Whilst a 10" pipeline would provide adequate capacity, the decision was made to move forward with a 12 inch pipeline in the base case. This permits additional capacity to be added to the system at a later date should the opportunity arise.

The detailed results of this study can be found in the "Quest IPSM Compressor Design Modeling Results" report. (Clark, 2010).

5.1.2. Well Type

All Quest appraisal wells are vertical, including the Radway 8-19 well which will be kept as an injector well.

Intensive modeling was done to determine to what extent a deviated or horizontal well would bring substantial benefit, versus the additional costs and risks they carry. The full modeling comparison can be found in the Quest Wells Conceptual Completion Design document (Hugonet, 2011), in which the following observations are made:

- Inflow/outflow modeling shows adequate injection for vertical, deviated, and horizontal well types for the Quest CCS project.
- Deviated wells provide minimal increase in injection rates over vertical wells.
- Horizontal wells deliver a substantially higher injectivity than deviated or vertical wells, but are more difficult to drill, complete, and operate.

The current reservoir characterization suggests that vertical wells are sufficient to provide the required injectivity during the project lifetime, and are therefore carried as the base case well completion type.

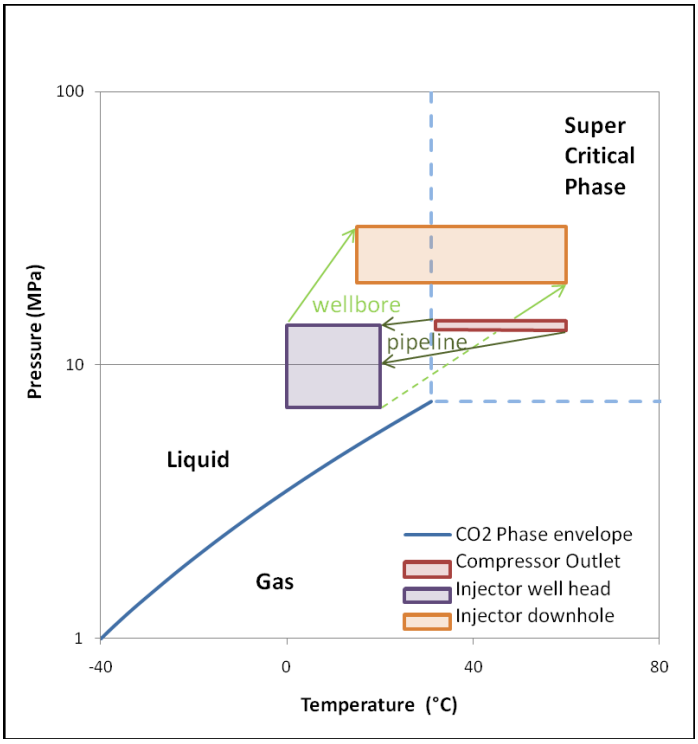

Figure 54: Quest CO_2 phase changes expected from surface compressor outlet to injector bottom hole conditions

5.1.3. Bottom Hole Pressure (BHP) Constraint

5.1.3.1. Regulatory requirements and additional safety margins

Regulatory requirements state that the maximum BHP in an injection well must be no more than 90% of the formation fracture pressure to avoid hydraulic fracturing.

High levels of confidence are required due to Quest being a CCS demonstration project with high demands on long term safe disposal and storage of CO_2. Therefore, as the Lower Marine Sands (LMS) which is the first formation overlying the BCS storage formation has the lower fracture gradient the Quest project team has chosen to provide an additional safety margin by selecting the fracture extension pressure of the Lower Marine Sands (LMS) as the BHP limitation. This provides an additional 15% safety margin, because the LMS fracture extension pressure was measured at 17.4 kPa/m versus 20.6 kPa/m in the BCS. The Quest project team feels this is a more appropriate constraint, as the first barrier to loss of containment is the avoidance of fractures propagating into the overburden and the LMS is the first formation above the BCS in that sequence.

Based on the above, the bottom hole injection pressures for the commercial well design and the D65 regulatory application wills will be limited to 90% of the lowest observed fracture extension pressure in the LMS at 17.4 kPa/m. For a top BCS reservoir depth in Well 8-19 at 2,041.3 m MD this corresponds to a bottomhole pressure constraint of 32 MPa (90% safety factor already applied). An illustration of this, very conservative, BHP constraint estimate is illustrated in Figure 55 below.

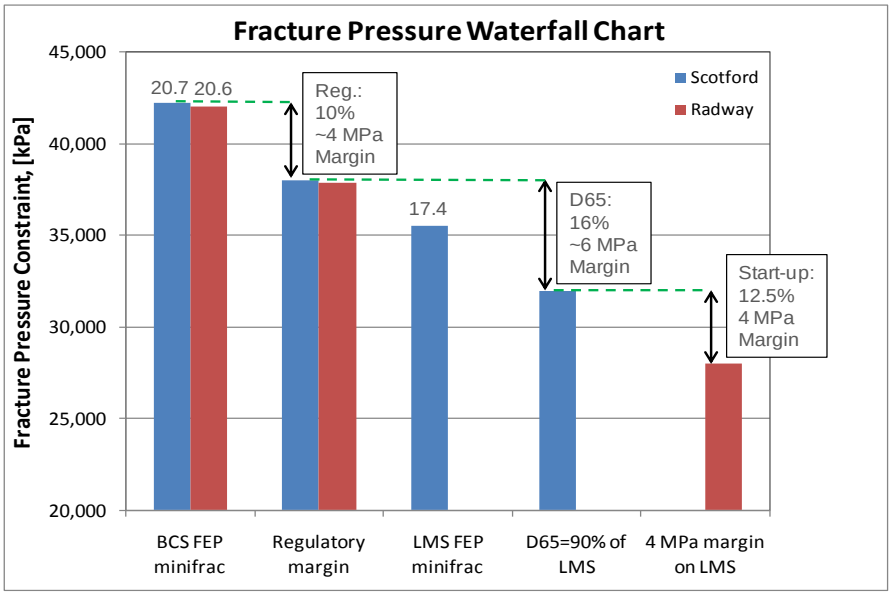

Figure 55: The impact of regulatory requirements and operational aspects on the injection pressure constrain.

Since cooling of the near well bore region changes the stress field, an effort was made to calculate the expected reduction in fracture pressure. Using the thermo-elastic properties of sandstone under the pressure and temperature conditions as encountered in the BCS resulted in an estimate of fracture pressure reduction of up to 4.5 MPa within in the BCS. For details of this calculation see APPENDIX 5.

A Radway Core calibrated geomechanical model, within its own range of uncertainty, confirmed this result (chapter 10.2 and (Tare, 2011)) and showed a temperature induced stress reduction to 27 – 32 MPa at the Radway 8-19 location. Combining the regulatory and operational aspects of an injection bottom hole pressure limit, the following BHP ranges (Table 20) have been applied in the Gen-4 models.

Table 20: Range of Maximum BHP permitted in injection wells.

Case	Max BHP (MPa)
High	32
Mid	28
Low	26

5.1.4. Well Bore Skin

Well injectivity is a function of well bore skin. Typically, the total well bore skin consists of four parts as shown in the formula below.

$S = S_{mech} + S_{geom} + S_{pp} + D*Q$

S_{mech} mechanical skin; S_{geom} geometric skin; S_{pp} partial penetration skin; D rate dependent skin factor (non-Darcy skin factor).

With the given of having selected a vertical well design for development, the geometric skin is zero. Limited perforation causes partial penetration skin $S_{pp.}$ In the Gen-4 models carried out, the injectors were simulated with only the bottom 30m of the BCS sand perforated, basically only the identified TDBM (Tide dominated bay margin) facies perforated. That results in 67% partial penetration, assuming the average BCS sand thickness of 45m. S_{pp} is not a direct input parameter in the simulation model, but a result of the partial penetration extent and the sand connectivity, especially vertically, at the well location.

S_{mech} and D are, however, direct simulation input parameters. Like any other input parameters in the model, they carry the ranges of uncertainties. Based on benchmark studies, 4-10-15 was used as the mechanical skin range and an intentionally large non-Darcy skin factor, D, range of 0.35 – 2.12 – 17.66 day/MMm^3 (0.01-0.06-0.5 day/MMscf) was used to flag the severe non-Darcy effect, if any.

Severe reduction of well injectivity due to the non-Darcy flow is judged unlikely in Quest. The reasons are below:

- The low to moderate single well injection rate planned in Quest: 3-8 development wells, single well rates are likely less than 0.85 MMm^3/d (30 MMscf/d) as in the 2-well scenario.
- Base case non-Darcy skin factor, D, leads to the non Darcy skin (= base case D*rate per well) of only 1.8 and lower, if the single well rate is 0.85 MMm^3/d or lower (30 MMscf/d or lower) in the 2+ wells scenarios. This non-Darcy skin has small impact on the well injectivity.
- High case non-Darcy skin factor, D, leads to the non-Darcy skin of 15 in the 2-well case, 10 in the 3-well case and and 6 in the 5-well case. These non-Darcy skin values were high. However given the 3~5 well development plan, these non-Darcy skins are not too high to fail the wells to deliver the total field injection target. Hence, the non-Darcy effect is still less likely an issue.

The possibility of severe well injectivity reduction due to strong non-Darcy effect does exist, but it is low. Nevertheless, it is recommended to keep the well rate below 0.85 MMm^3/d (2-well scenario) to minimize the non-Darcy effect. Note: as long as the total field rate can be achieved, use the lowest fair share rate for each injection well.

5.1.5. Mechanical Skin

The Gen-4 well mechanical skin range of 4-10-15 represents an increase from the Gen3 range of 4-7-10. The Alberta producer mechanical skin database and the SCL Redwater 11-32-55-21 well base case skin of 7 from the water injection test interpretation were the foundation for the Gen-3 mechanical skin range. The increase of such a skin range in Gen-4 resulted from two reasons:

- Water injection wells tend to have notorious mechanical skins relative to the producers. Even for acid gas injectors in Alberta, the cases were seen occasionally.
- Quest Radway 8-19-59-20 well water injection test showed higher skin. History matching the water well test data indicates a skin of 10 or higher.

Hence, a widened mechanical skin range of 4-10-15 was taken in Gen-4, in order to capture the risk of drilling and completion damage to the formation.

5.1.6. Non-Darcy Skin

Supercritical CO_2 has a high density of 0.72 g/cm^3 at 20MPa and 60^{o}C, but low viscosity of 0.06 cp, close to gas. The unique fluid properties make supercritical CO_2 prone to inertial flow, or non-Darcy flow. Some non-Darcy flow behavior was indeed observed at the Gen-3 stage when attempting to perform supercritical CO_2 – brine steady state relative permeability experiments at the BTC lab on Quest core samples. The experiments were then adjusted to quantify the non-Darcy coefficient β, 1/ft. Additional in-depth efforts have been made during the Gen-4 modeling work to define the non-Darcy contribution to wellbore skin, including an assessment of related uncertainties. This included a re-assessment of Non-Darcy coefficient β literature data, recalibration of our own experimental database while also reflecting on the accuracy of D-β correlations.

An in-depth discussion of this work within this report would not be practical, however it is summarized and reported in (Doe, 2011).

5.1.6.1. Non-Darcy skin and its impact on Quest well injectivity

As per the definition, Non-Darcy Skin = non-Darcy skin factor * well rate = D * Q. Table 21 below lists the possible occurring non-Darcy skin values for Quest wells.

Table 21 Possible Non-Darcy Skin in Quest

Non – Darcy Skin, D * Q			
	D = 0.35 day/MMm3 (0.01 day/MMscf)	D = 2.12 day/MMm3 (0.06 day/MMscf)	D = 17.66 day/MMm3 (0.5 day/MMscf)
Q= 0.85 MMm3/d (30 MMscf/d) 2well case	0.3	1.8	15
Q = 0.57 MMm3/d (20 MMscf/d) 3well case	0.2	1.2	10
Q = 0.34 MMm3/d (12 MMscf/d) 5well case	0.12	0.72	6
Q = 0.21 MMm3/d (7.5 MMscf/d) 8well case	0.075	0.45	3.75

The main conclusions on potential non-Darcy flow effects on well injectivity at Quest can be summarized as followed:

- The non-Darcy skins (= D*Q) are assessed low (<2) for the given base case D value (2.12 day/MMm^3).
- The high well count and low well rate cases (e.g. the 5-8 well scenario) is unlikely to be impacted much by the non-Darcy effect.
- Low well count and high well rate cases, e.g. a hypothetical the 2-well scenario, could be affected by high non-Darcy skin (~15). However, such a low well count scenario corresponds to good rock quality and reservoir connectivity, hence, the well

injectivity is unlikely constrained by the non-Darcy flow due to sufficient permeability. Moreover, 3 – 5 wells were proposed in Gen4 as the development base case. The range of this well count is considered confident to withstand the risk of well injectivity reduction due to possibly severe non-Darcy flow effect.

Nevertheless, the risk of well injectivity reduction due to severe non-Darcy flow exists, even though small. Therefore, the well planning and operation should be warned of this risk. The best mitigation is not to inject too high rate, e.g. > 0.85 MMm3/d (30 MMscf/d), down to a single well.

6. CO2 SATURATION MODELING

This chapter discusses the division of the Gen-4 modeling effort designed to provide constraints for answers to key regulatory and MMV questions centered on predicting where and at what rate a given volume of CO_2 might migrate following injection into the subsurface given both a range of possible reservoir properties and development scenarios.

6.1. Objectives & Workflow

The CO_2 saturation modeling objective was to provide a much better understanding of the uncertainty and controls on CO_2 distribution within the subsurface away from any injector well. The insights from these models inform SDP and MMV decisions related to demonstrating conformance, i.e. demonstrating that observed subsurface behavior is within the range of expectation.

Conformance is demonstrated via the use of various sensor technologies. A variety of MMV technologies are anticipated to be employed to provide verification that the subsurface is performing within the range of expectation. Part of this involves having a confident assessment of *where* injected CO_2 has moved to over time. As all sensor technologies have a limit of detection it is important to be able to interrogate modeling results using appropriate limitations of resolution for each MMV technology. Models then show what a particular MMV technology can resolve as it relates to observing saturation changes in the aquifer. This then allows quantification of the residual uncertainty in the MMV signal as the model also shows what may *not* be resolved.

The primary metric that is reported in this modeling exercise is the *maximum plume extent away from an injector*, typically referred to as *plume size.* This implies a distance and an orientation and is subject to the definition of how one defines the "edge" of a CO_2 plume.

This metric is important as it impacts the regulatory process. The project is required to inform landowners around the project whose property may be impacted by CO_2 injection at a nearby location. The understanding on plume size uncertainty better informs this process.

6.1.1. Modeling Strategy

The modeling of CO_2 saturation distribution is complicated by:

- The number and range of subsurface uncertainties
- The dynamic interactions and inter-relationships that exist between various subsurface uncertainties and migrating CO_2.
- Uncertainty in the gross volume of CO_2 that may be injected down any well over the life of the project
- Practical simulation run-times to achieve acceptable results in the required timeframe.

The overall strategy to assess the uncertainty in maximum plume length was to run a Monte Carlo probabilistic approach, simulating multiple random subsurface realizations to assess plume size distribution and supported by a sensitivity study to understand the relative impact of all the various individual subsurface uncertainties.

All subsurface uncertainties were assigned three outcomes, high, mid and low. The combination of different outcomes for different uncertainties permits definition of unique subsurface realizations.

Uncertainty outcomes for the CO_2 Saturation models are all driven by the contents of the Geological model.

A small scale sensitivity study was performed to better understand the relative impact of each of the uncertainties and to identify which could be ignored due to their negligible impact.

6.1.2. Gridding

6.1.2.1. Static Model

A 10 x 16km grid was constructed by taking a sector from the large area Geological Model. This sector only covers the BCS zone. The sector is re-gridded at a resolution of 25 x 25 x 1m to give a total cell count of over 18 million cells.

Reservoir quality properties are distributed in this model and subsequently up-scaled to a coarser resolution dynamic model with a total of just fewer than 1 million cells.

6.1.2.2. Dynamic Model

The full scale dynamic model only models the BCS sand interval and has an area dimension of 10km x 16km. The size of the model was determined based on two considerations:

- 8km radius is the recommendation from the single well radial models, aiming to correctly predict the well injectivity to certain extent.
- 10km x 16km is anticipated to be bigger than most CO_2 plume sizes from most realizations to be simulated.

The sensitivity study exercise used a 5 x 5 km grid that contained properties up-scaled from the static model grid described above. This model used a constant grid size of 50 x 50 x 2m and was restricted to the BCS zone. Results of the sensitivity study are presented in section 6.5.1 Maximum Plume Length.

Extremely small models (e.g. ~1km radius) can result in unsustainable well injectivity due to the small tank size and highly elevated reservoir pressure, even with analytical infinite aquifer boundaries. Small models can be free from the unsustainable well injectivity issue, but can cause over estimation of well injectivity. This is because analytical infinite aquifer boundaries, when compared to the numerically modeled aquifer in a big-size model, acts as a faster pressure sink and leads to a lower reservoir pressure when injecting same rate of CO_2. Hence, the max injection rate potential of the well is higher in a small-size model than in a big-size model. According to the radial well modeling results the effect of model dimension on well injectivity does not become insignificant until the model size is around 8km radius or larger.

A variable resolution grid, also known as “tartan gridding” was applied into the CO_2 saturation dynamic model to address the following objectives:

- Accurately predict well injectivity, CO_2 saturation change and plume front movement by using find grids extensively in the model.
- Avoid using Local grid refinement on multiple cells for the extensive fine-grid requirement.
- Keep the total cell count as low as possible to have a reasonable computing time.

Applying local grid refinement on multiple cells is not a practical solution in the modeling. It leads to long computing time and convergence problems, as evidenced during some of the Gen-3 pressure modelling. Tartan grids in the Gen4 saturation model can handle both fine grids and coarse grids in the same model. A 8km*10km region of high resolution grid

(50m*50m*2m) was deemed appropriate to meet the accuracy requirements in injectivity prediction and the resolution requirement for CO_2 saturation changes. Grid resolution decreases gradually towards the boundaries of the model. The max cell size is 250m*500m at the corners of the model. The fine gridding area (50m*50m*2m) is off centered by 1km to the up-dip direction to accommodate the preferential CO_2 plume migration up-dip as the result of the buoyancy force. Figure 56 illustrates the tartan gridding in the Gen4 saturation model.

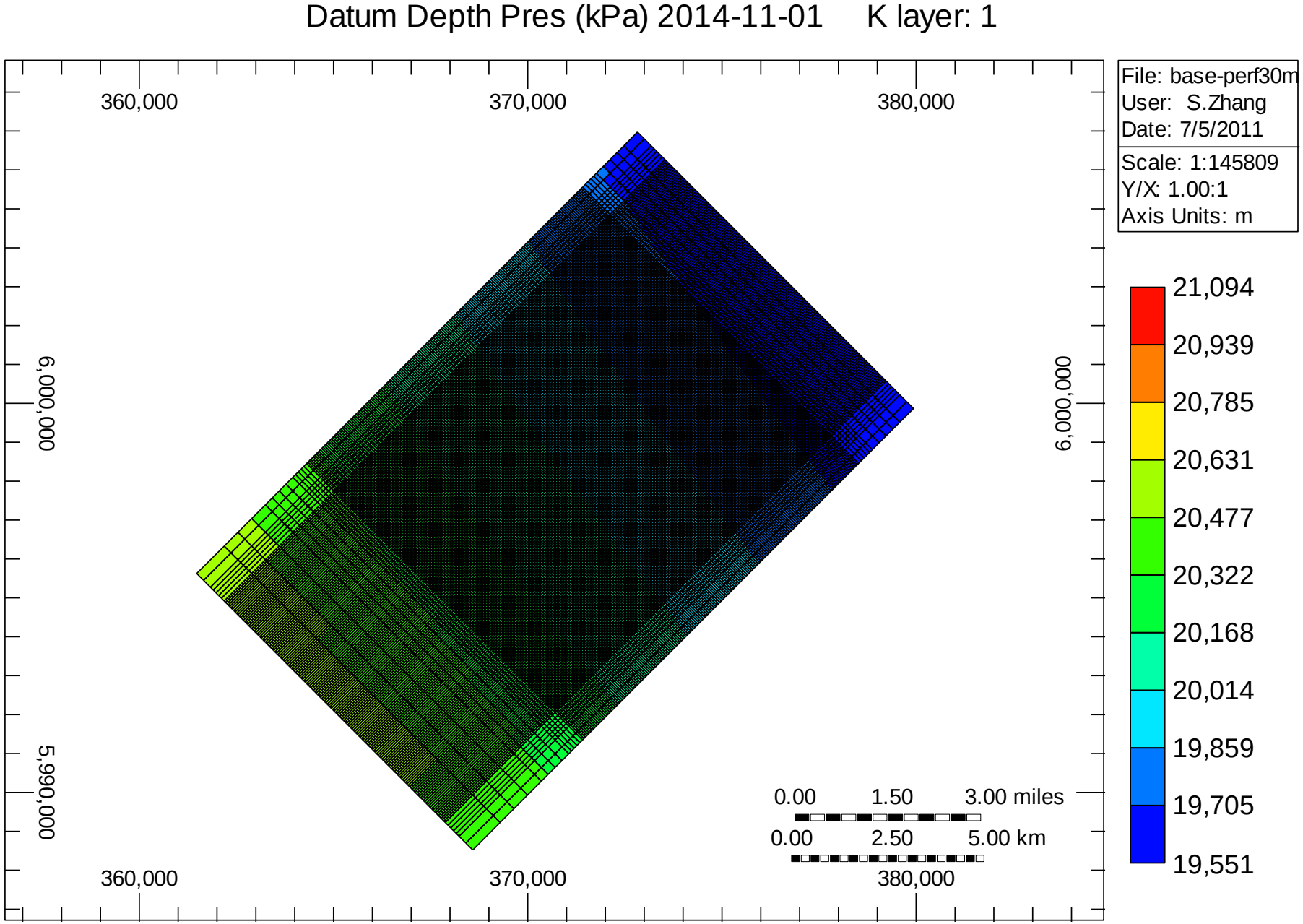
Datum Depth Pres (kPa) 2014-11-01 K layer: 1
360,000
370,000
380,000
6,000,000
5,990,000
File: base-perf30m
User: S.Zhang
Date: 7/5/2011
Scale: 1:145809
Y/X: 1.00:1
Axis Units: m
21,094
20,939
20,785
20,631
20,477
20,322
20,168
20,014
19,859
19,705
19,551
0.00 1.50 3.00 miles
0.00 2.50 5.00 km

Previous Page: Figure 56 – Variable resolution (Tartan Gridding) in the dynamic plume models

6.2. Uncertainties

6.2.1. Facies

Facies were re-sampled directly from the Geological Model from the same location as the plume sector model. Cells in the fine plume model are assigned the same facies as the cells they are co-located within the coarse Geologic Model.

- High and Mid Case = Vertical Trend in HED Distribution
- Low Case = Random distribution of HED facies

6.2.2. NTG

Constants were assigned to all cells with the same NTG as per the Geologic Model and as described in section 3.

6.2.3. Heterogeneity

The range of uncertainty in heterogeneity is controlled by applying the appropriate variogram settings in the porosity modeling. The range of variogram dimensions is as described in section 3. The heterogeneity uncertainty can be thought of as the reservoir architecture as it is driven by the 3D pattern of porosity, which in turn controls permeability, see Figure 57 below.

It was recognized that one stochastic realization of porosity may give very different simulation results for plume size compared to another stochastic realization made with exactly the same inputs. For this reason a "seed sensitivity" study was carried out to ensure that the impact of the purely stochastic character of the models could be accounted for. The workflow for achieving this involved simulating multiple realizations of the same properties constructed using exactly the same inputs, but only allowing the seed number of the realization to change. The realization with plume behavior that was the closest match to the mean plume behavior from all realizations was selected as the "Type" realization to use in all further modeling for that level of heterogeneity. Thus there are three "Type" realizations of heterogeneity, one each for the high, mid and low heterogeneity cases. The workflow is closely linked to the generation of the range of porosity and is shown in Figure 58.

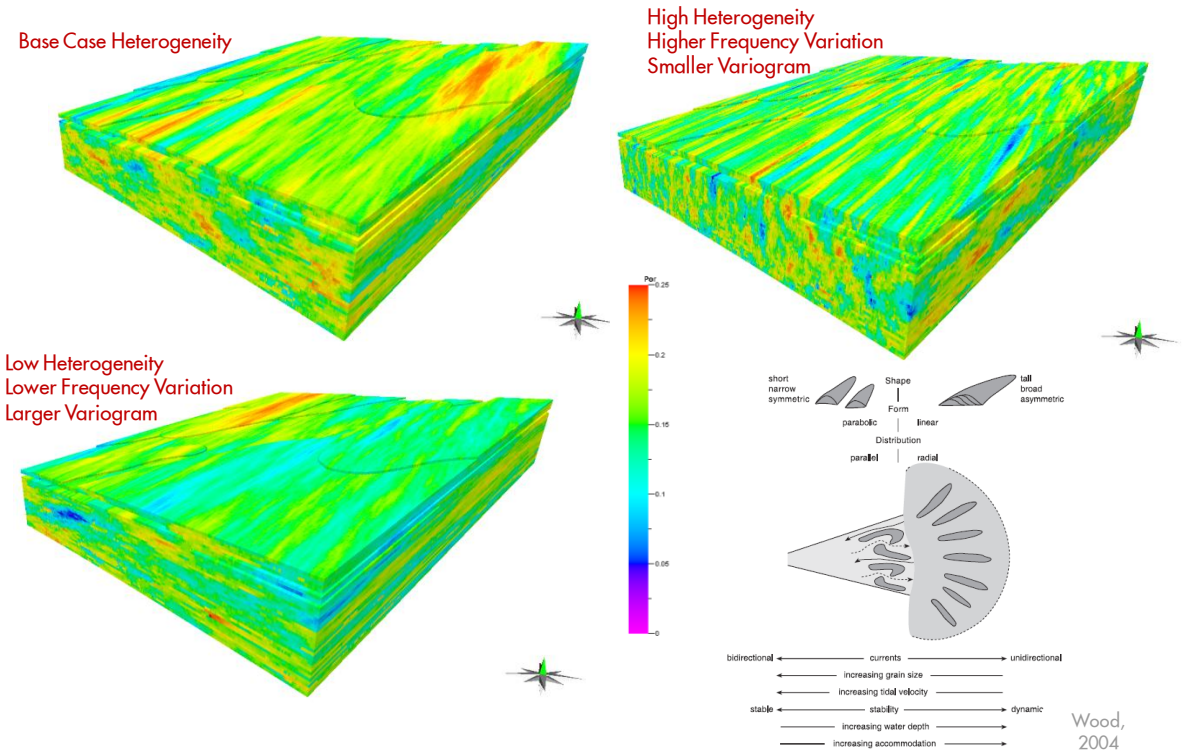

Figure 57: Type realizations of Heterogeneity Cases with illustration from Wood (2004) that explains how uncertainty in distance from shore drives uncertainty in dune physiology.

6.2.4. Porosity

A high, mid and low case porosity property is generated for each of the cases of heterogeneity. The workflow for achieving this consistently without allowing the stochastic nature of the properties to influence the comparability results is shown in Figure 58.

The mid case porosity honors a local distribution of values from the large area geological model. The high and low porosity cases are simply bulk shifted by 2pu up or down respectively. The bulk shifting preserves the 3D reservoir architecture that also impacts the simulation result. It was critical to keep reservoir architecture constant when running different cases of porosity. Steps 7 – 10 in the workflow in Figure 58 describes the process by which the reservoir architecture is controlled.

It was also important to maintain control over the porosity at the injector well location. Varying reservoir quality at that location would make it difficult to compare and contrast results from different realizations. The manner in which this was achieved is described in Figure 58, steps 5 and 6.

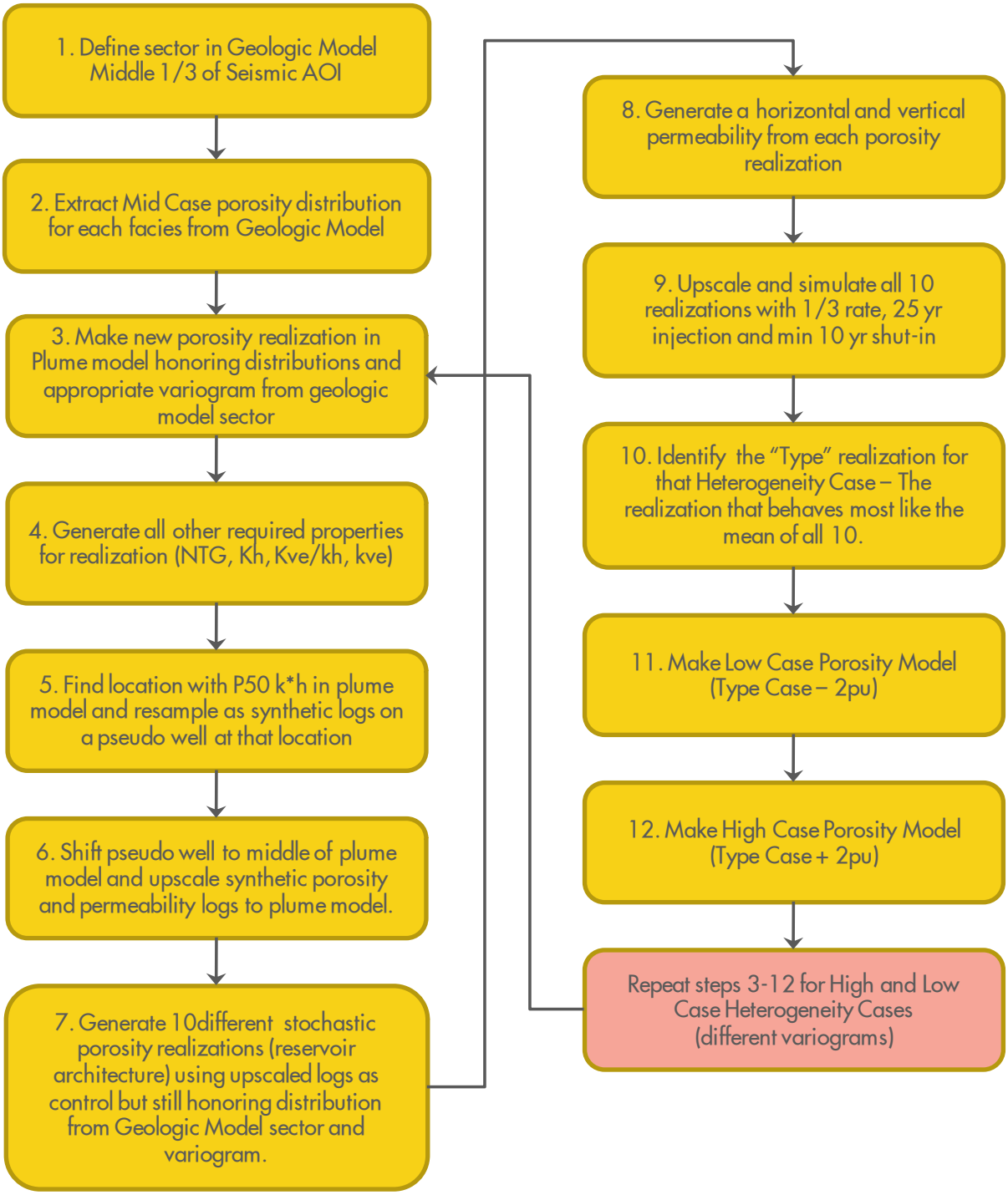

Figure 58: Workflow for generating high, mid and low Porosity cases for each of the high, mid and low Heterogeneity cases.

6.2.5. Horizontal Permeability (Kh)

The Kh is not sourced from the Geologic Model in the same manner as the porosity properties. Where kh is stochastically distributed in the Geological Model and uses the porosity property as a trend, in the plume models the Kh is calculated directly from the porosity property via the porosity-permeability regression from the petrophysical analysis or core plug data (see section 3 and the petrophysics report (Simone, 2011). This results in there being no scatter when porosity and permeability are cross plotted together. This simplification is considered acceptable as it provides for one less stochastic seed uncertainty

aspect of the reservoir architecture that would need to be accounted for in the overall modelling workflow.

6.2.6. Baffle Ratio and Vertical Permeability (Kv)

Vertical permeability is calculated within the Geological Model using the methodology described in section 3. This results in a low, mid and high case Kve/kh property derived using different ratios relating shale bed thickness to width (the Baffle Ratio parameter) along with other inputs. This property is then used to calculate the effective vertical permeability by multiplying the horizontal permeability by the kve/kh.

For the Plume Models a frequency distribution for low, mid and high Kve/kh for each facies is extracted from a sector of the Geological Model. The sector is the 3D seismic AOI. In the Plume Models these distributions are then used as part of the input to the stochastic modelling of kve/kh, with variograms appropriate to the Heterogeneity Case in question.

The Kve/kh property is always loosely correlated to porosity in the modelling (correlation coefficient of 0.75) and as a result it needs to be re-distributed every time the porosity model is updated, i.e. ten random realisations of porosity require 10 further associated realisations of kve/kh.

Step 4 of the workflow shown in Figure 58 describes where the kve/kh property is re-calculated when identifying a "Type case" porosity realisations to define the heterogeneity cases.

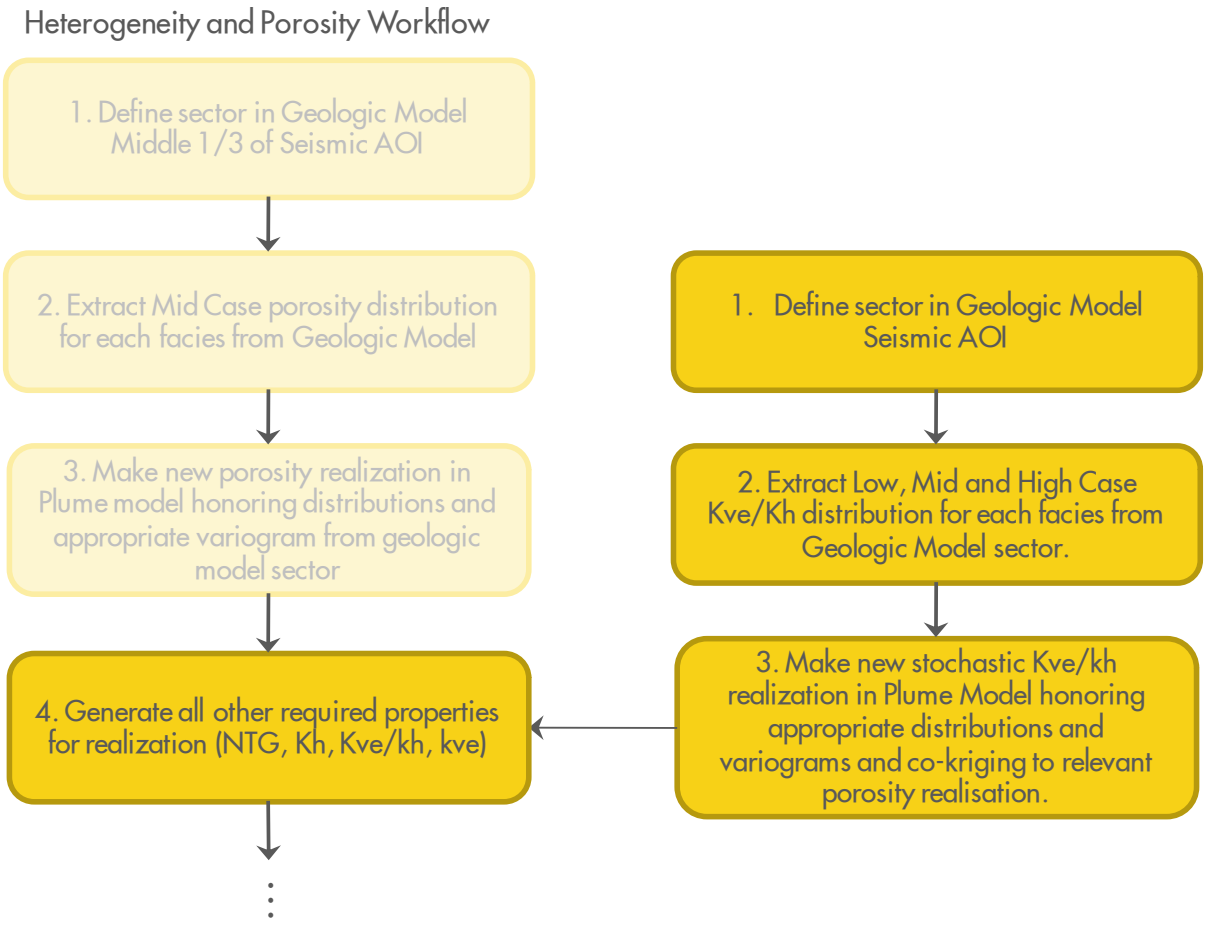

Figure 59: Workflow for modeling range of kve in Plume Model linking to workflow shown in Figure 58

6.2.7. Structure and Reservoir Fabric Orientation

The direction in which a plume migrates away from a well depends on:

- Stratigraphy dip angle and azimuth – plumes move up-dip under buoyancy forces.
- Reservoir Heterogeneity orientation – preferred flow path direction

Regional structural dip is very low – averaging 0.3° on a NE-SW azimuth. Local variations result from underlying basement topographic variability as observed in 3D and 2D seismic. Other subtle contrasts associated with deposition may also introduce more local variation in dip angle and azimuth around injectors. No uncertainty in the structural dip is carried in the models.

The actual orientation of the reservoir fabric is uncertain. Whilst the conceptual model describes shore line normal or oblique sand bodies, it is impossible to rule out the possibility of shore line parallel sand bodies around some of the injectors.

It was considered impractical to try and simulate a range of different reservoir fabric orientations. A conservative approach was assumed by aligning both the reservoir fabric and structural dip vectors so that preferential flow paths and buoyancy forces complement each other. In this way we can be confident that the plume is highly unlikely to travel any further than the model predictions. Combining a different reservoir fabric orientation within the same structural framework would result in the buoyancy force moving the plume up-dip at the same time as it attempts to follow the reservoir fabric along strike. This should result in an overall smaller plume compared to aligning both vectors.

The maximum plume extent calculated from the simulation models is used to define the radius of a circle around any injector well. The area of the circle represents the uncertainty in the location of the actual plume. This is considered a fair reflection of the range of uncertainty on plume migration behavior in the pre-injection phase of the project. The first data from MMV sensors that can "see" the plume, such as 4D seismic should significantly reduce the range of uncertainty.

6.2.8. Dynamic Uncertainties

The uncertainties in dynamic parameters and conditions listed below all impact the CO_2 plume migration to variable degrees.

- Relative permeability
- Capillary pressure
- Rock compressibility
- Boundary conditions
- Injection rate (1/3, 1/5, 1/8 of the field rate)
- Skin

For detailed discussions in dynamic properties and uncertainty ranges, including relative permeability, capillary pressure, rock compressibility and fluid properties, please refer to Chapter 3. For skin uncertainties, please look into Chapter 5 on constraints.

Boundary conditions (infinite aquifer or pressure boundaries due to well interferences) and different well rate target (1/3, 1/5, 1/8 of the field rate) were added to the list here. Boundary conditions impact the pressure field, and therefore influence the CO_2 plume movement. Well injection rate influences the pressure field as well as the fingering tendency of the CO_2 due to the big mobility contrast with brine. Consequently the CO_2 plume shape and size can vary.

Effects on the CO_2 plume from the above listed dynamic parameters and conditions, except for fluid properties and skin, were assessed in the small scale sensitivity study to prioritize which ones need to be included in the full scale plume modeling. Skins as a near-wellbore uncertainty, have no impact on the overall pressure field, and hence are not expected to impact the CO_2 plume migration at field scale.

Operational uncertainties such down-time or cycling injection of water and supercritical CO_2, were not in the scope of this CO_2 saturation modeling study.

6.3. Subsurface Realizations

In order to assess the maximum plume length uncertainty a number of unique subsurface realizations were constructed. Each one is a different combination of the various uncertainty outcomes discussed above.

A total of sixteen realizations were simulated. Thirteen of these are purely random combinations of subsurface uncertainty outcomes, with the caveat that the 13 at least cover the range of relative permeability and porosity uncertainty (Table 22). The remaining three realizations were deterministically selected based upon the insights of the sensitivity study on small models and represent a low, mid and high case. This allows a look back comparison to be made of our ability to predict the subsurface realizations expected to result in P10,P50 and P90 equivalents for maximum plume length.

Table 22 - Subsurface realizations for determining maximum plume length probability

	Random Realizations										Deterministic Realizations		
	1	2	3	4	5	6	7	11	12	13	Low	Mid	High
Porosity	HIGH	HIGH	MID	LOW	HIGH	MID	HIGH	MID	MID	LOW	MID	MID	LOW
Baffle Ratio (Kve)	MID	MID	MID	MID	MID	HIGH	MID	MID	HIGH	HIGH	LOW	MID	HIGH
NTG	MID	MID	LOW	LOW	LOW	HIGH	HIGH	MID	HIGH	MID	LOW	MID	HIGH
Heterogeneity	LOW	LOW	HIGH	HIGH	MID	MID	HIGH	MID	LOW	MID	HIGH	MID	LOW
HED Facies Trend	MID	LOW	LOW	MID	LOW	MID	LOW	MID	MID	LOW	MID	MID	MID
Capilary Pressure	HIGH	LOW	LOW	HIGH	MID	HIGH	MID	LOW	LOW	MID	LOW	MID	MID
Relative Permeability	MID	MID	HIGH	MID	HIGH	MID	HIGH	LOW	LOW	LOW	LOW	MID	MID

6.4. Plume Metric Calculators

6.4.1. Maximum Plume Length

The reservoir simulator lacks the capability to automatically calculate maximum plume size. The maximum plume sizes measured from the thirteen simulated subsurface realizations form the basis of calculations of plume size probability carried out in an Excel spreadsheet tool called the Plume Length Dashboard (PLD). The objective of this tool is to allow for efficient, consistent, and repeatable production of plots and values of interest (e.g. plume lengths at given times and conditions, dates when various realizations and/or probability cases project to meet given distance thresholds, etc…) with various degrees of flexibility.

The input to the PLD is a series of data tables that record maximum plume extent from an injector well for a range of different minimum saturation cut-offs and across the full range of simulation time steps. The saturation cut-offs define the plume edge. A separate data table file is created for each subsurface realization. The workflow for generating the input to the PLD is shown in Figure 60 and shown graphically in Figure 61.

Following the dynamic simulation of any realization in CMG-GEM a series of saturation time step properties are imported into Petrel that describe the injection and shut-in periods to the end of the simulation. A novel Petrel script called the Plume Length Calculator, written by the Quest subsurface team, is applied to all simulated realizations as per step 5 in Figure 60 and illustrated in Figure 61.

1. Set a property filter to only show the CO_2 plume (cells with CO_2 saturations greater than selected minimum cut-off)
2. Identify grid cell in plume at furthest distance from injector.
3. Record time step, distance and saturation cut-off in an internal spreadsheet
4. Repeat for all time steps and for all saturation cut-offs.
5. Export internal spreadsheet as text file to chosen location.

The saturation cutoffs used in calculating maximum plume length results was 5%, 10%, 15%, 20%, 25%, 30%, 35%, 40%, 45%, and 50%. The data tables generated by the Petrel script are then loaded into the PLD.

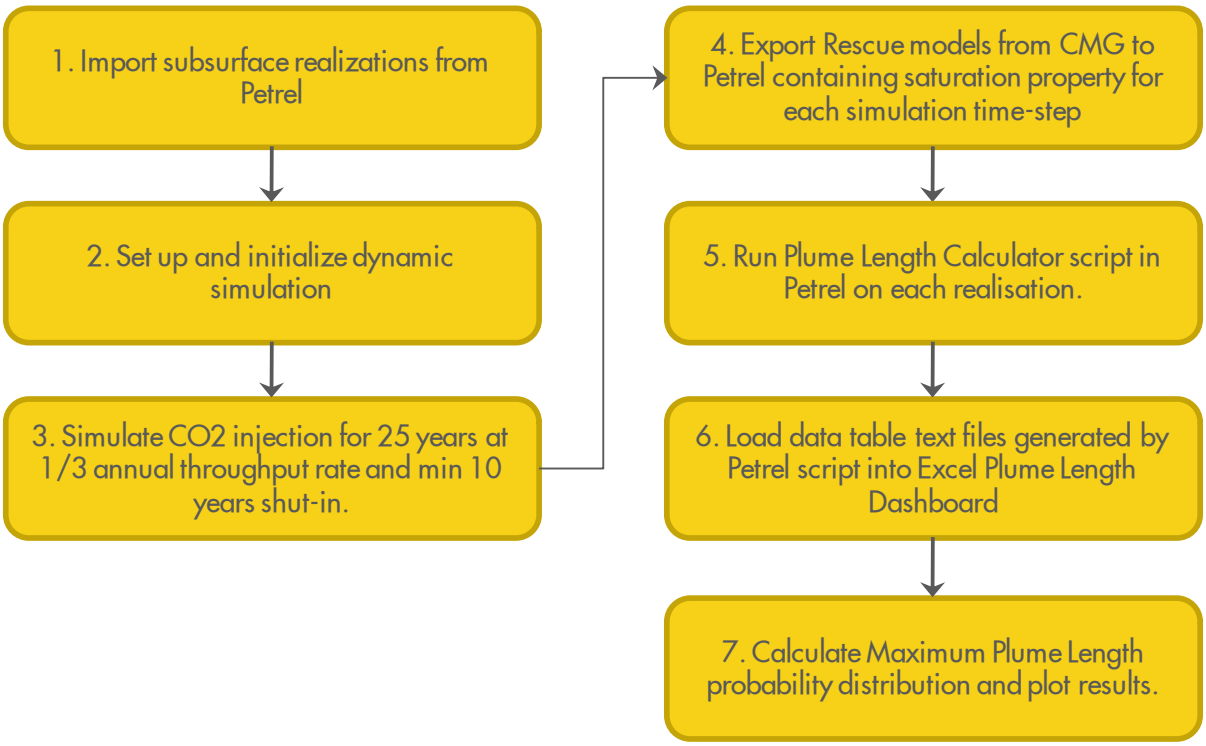

Figure 60- Plume Length Probability calculation workflow

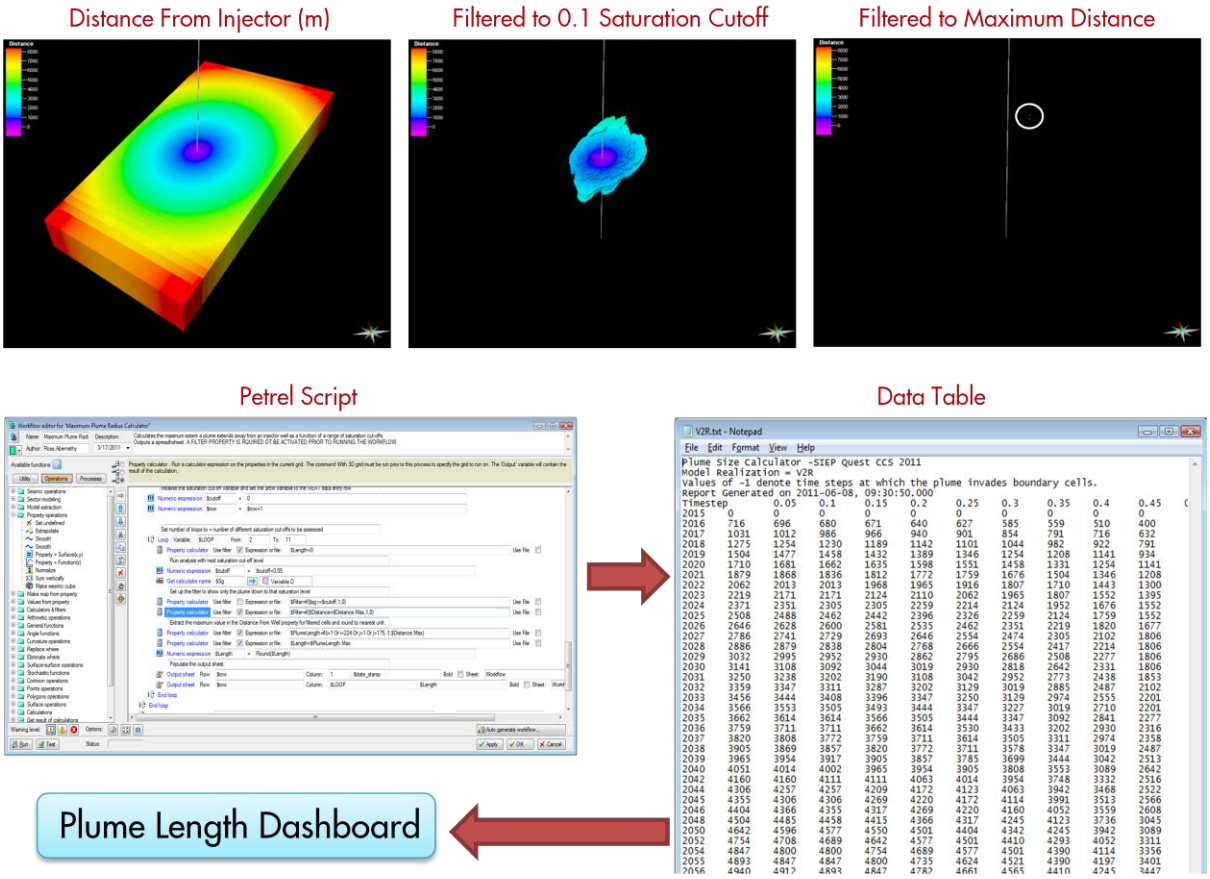

Figure 61 - Workflow for determining maximum plume length from simulation results

The PLD presents results in three panels with a large amount of control offered to customize the data that is used as input and the display of calculated results such as discrete probability outcomes such as P10, P50 and P90 estimates of maximum plume length, see Figure 62 - Figure 64.

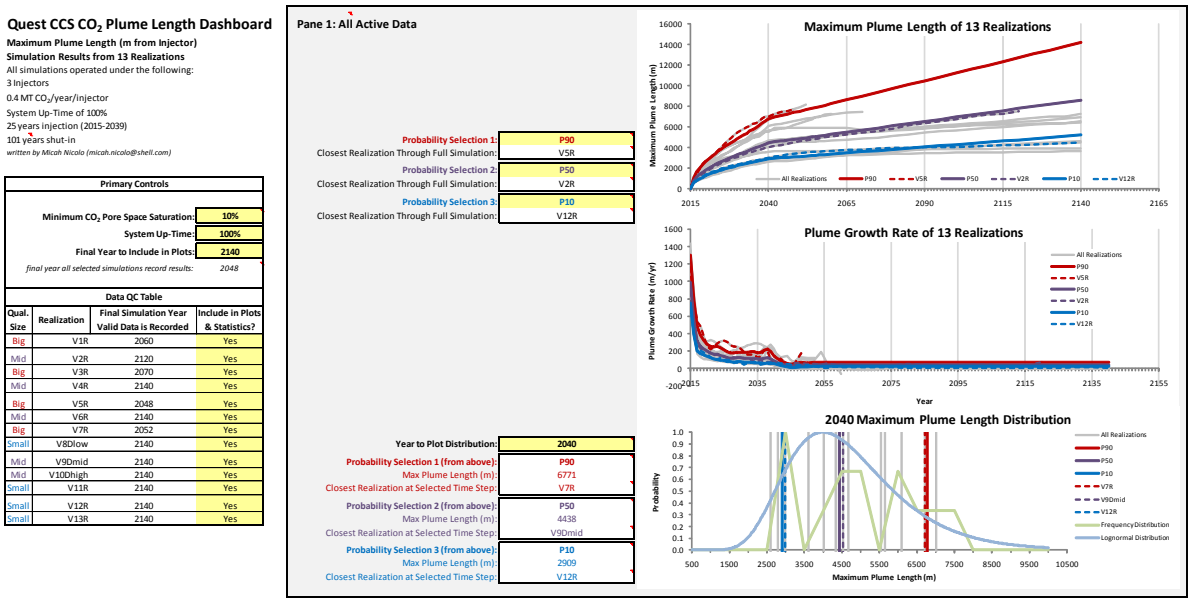

Figure 62 - Quest PLD panel 1: plotting controls, plots of length vs time and realisations PDF.

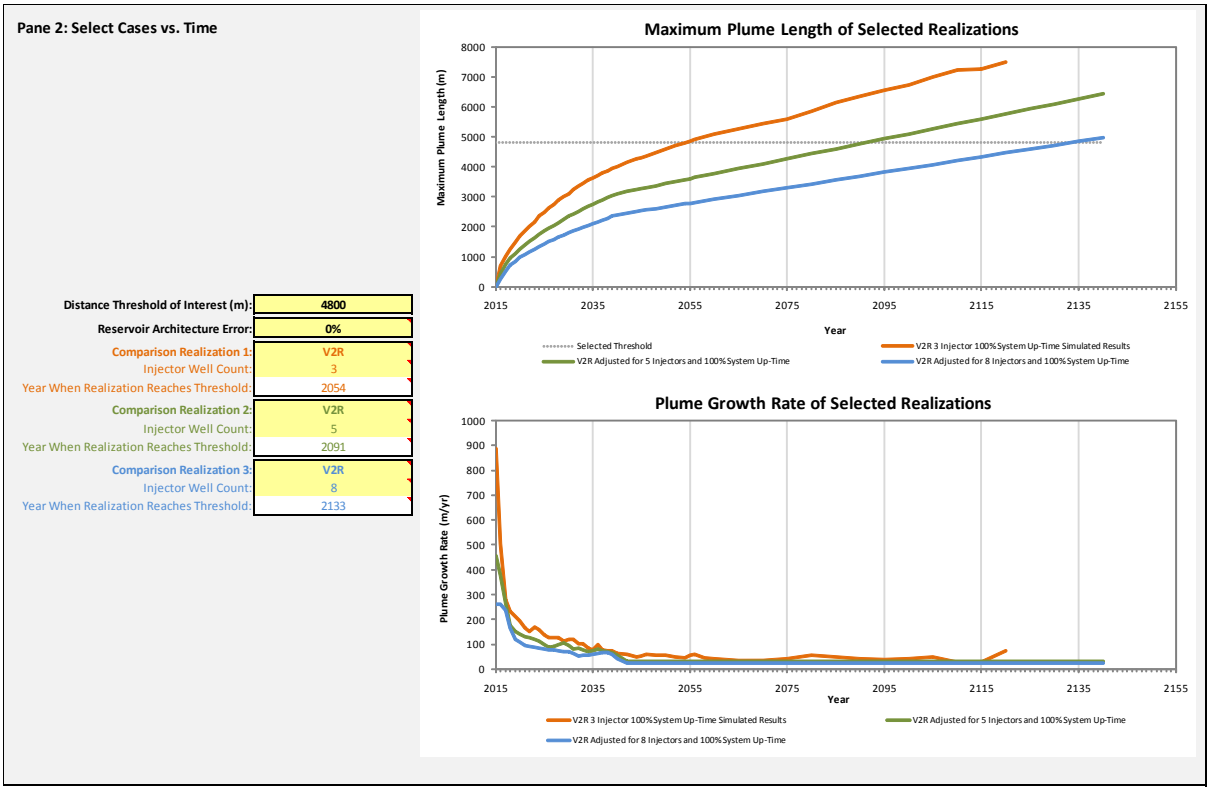

Figure 63 - Quest PLD Panel 2: plots of selected realisations/probability outcomes in length and rate of growth vs time.

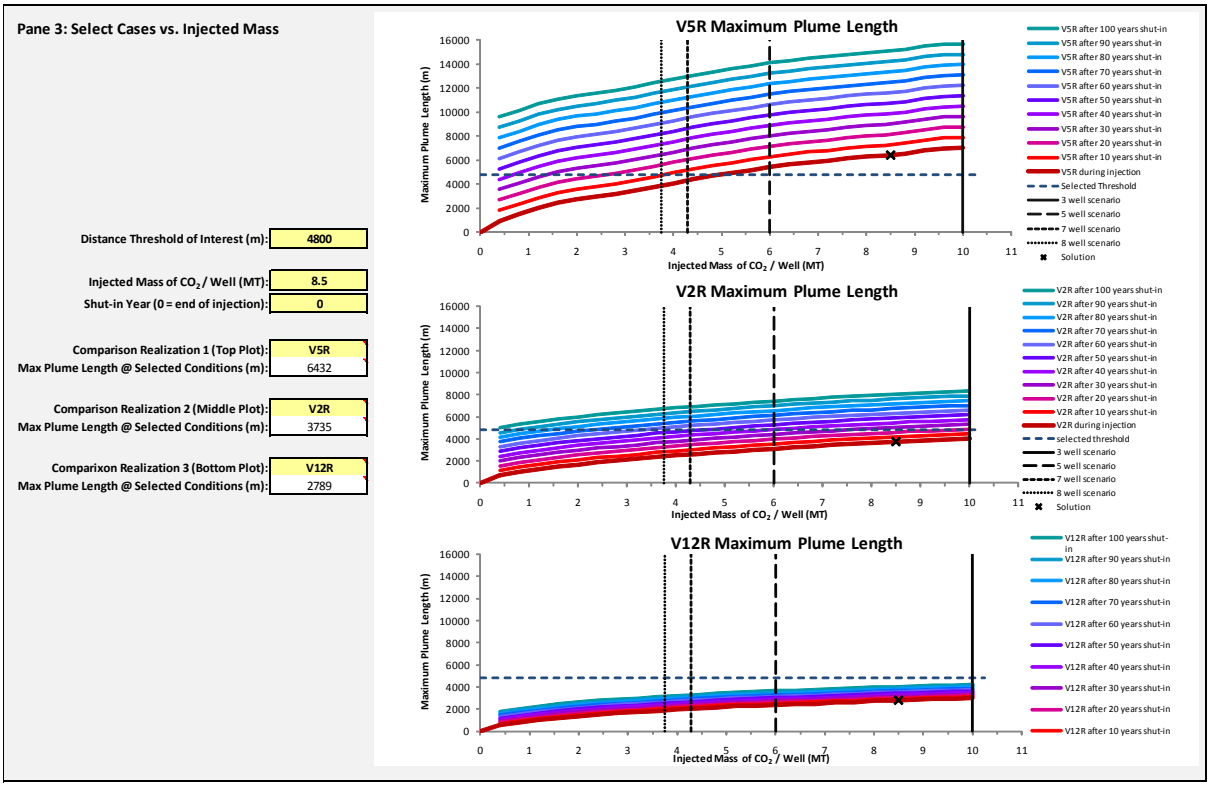

Figure 64 - Quest PLD Panel 3: Plume length probability vs. injected volume

6.4.2. Plume Volume

Plume length alone is an important metric, however it is also important to understand the potential impact associated with stating that a plume is present at some distance from an injector well. The volume of CO_2 that is present at different distance from an injector is a complementary metric in this case.

Similar to the maximum plume length metric, in order to generate a plume volume metric, a novel Petrel script was written that adopts the following workflow:

1. Set a property filter to only show the CO_2 plume (cells with CO_2 saturations greater than selected minimum cut-off)
2. Identify grid cells in plume at required distance interval from injector, e.g. 2001-2500 m away from the injector
3. Record the time step, total CO_2 volume within distance interval and saturation cut-off used in an internal spreadsheet.
4. Repeat for all time steps and for all saturation cut-offs.
5. Export internal spreadsheet as text file to chosen location.

This workflow is illustrated graphically in Figure 65. Once all the volume data tables have been generated they are imported into an Excel tool titled the *Plume Volume Dashboard (PVD)*. The Petrel script executed this on all realizations and all time steps exported from CMG for bins of 500 m, from 0-500 m to 9001 – 9500 m away from an injector.

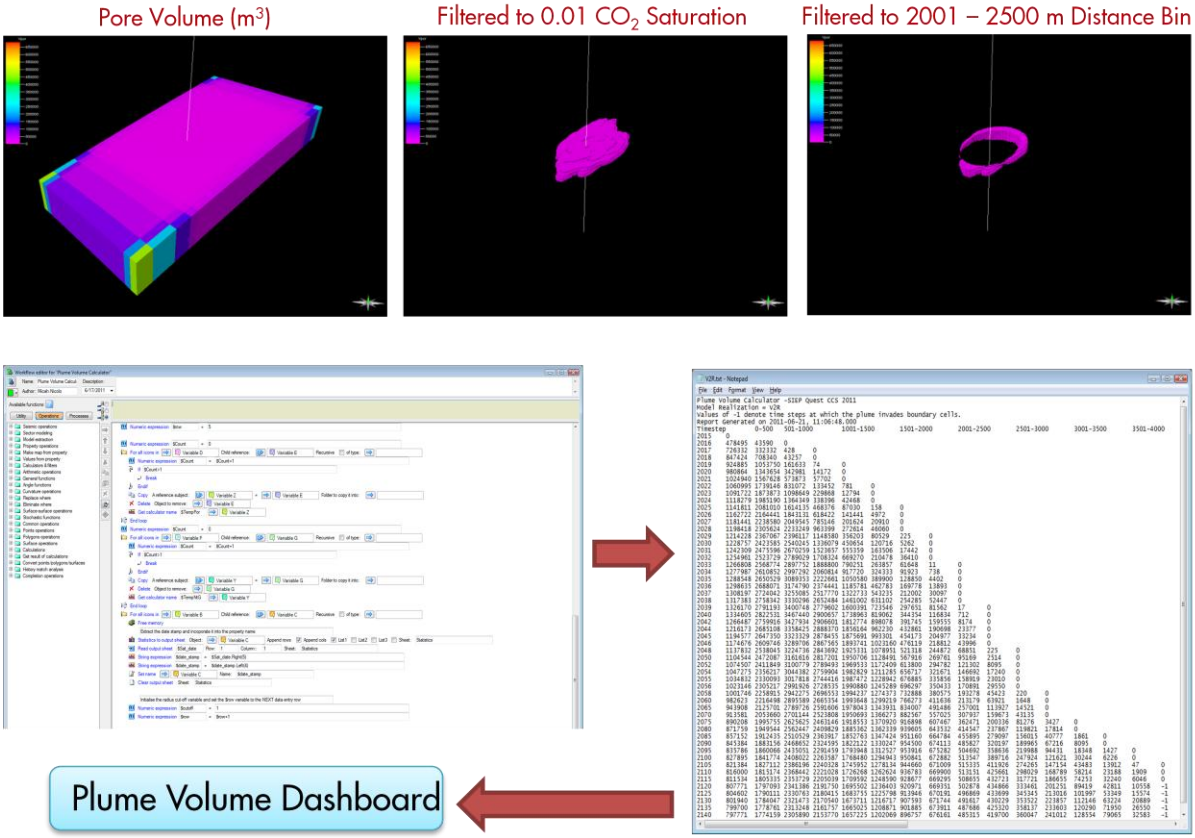

Figure 65 - Workfow for calculating CO_2 volume at discrete distances from the injector well.

The PVD tool (Figure 65) is intended to be used in concert with the Plume Length Dashboard, and because the metric itself was considered less critical than the maximum plume length, this tool received considerably less attention and by consequence is less

sophisticated than the Plume Length Dashboard. This is particularly true in terms of probability distribution calculations and analysis. However, this workbook does provide several useful plots and pieces of information.

6.5. Results

6.5.1. Maximum Plume Length

6.5.1.1. Sensitivities

6.5.1.1.1. Heterogeneity Impact

The small scale sensitivity study could not adequately account for the impact of heterogeneity on the maximum plume size. This is due to the scale difference between plumes resulting from only 3 years of injection and the correlation length of reservoir properties in the model. To fully appreciate the impact of heterogeneity the plume must interact with a representative amount of variability in the model during the simulated period. In the small scale sensitivity study the plumes were only interacting with a narrow sample of the total variability in the model as the plume was typically within the range of the variogram, the area heavily influenced by the variability present at the injection well location, see Figure 66.

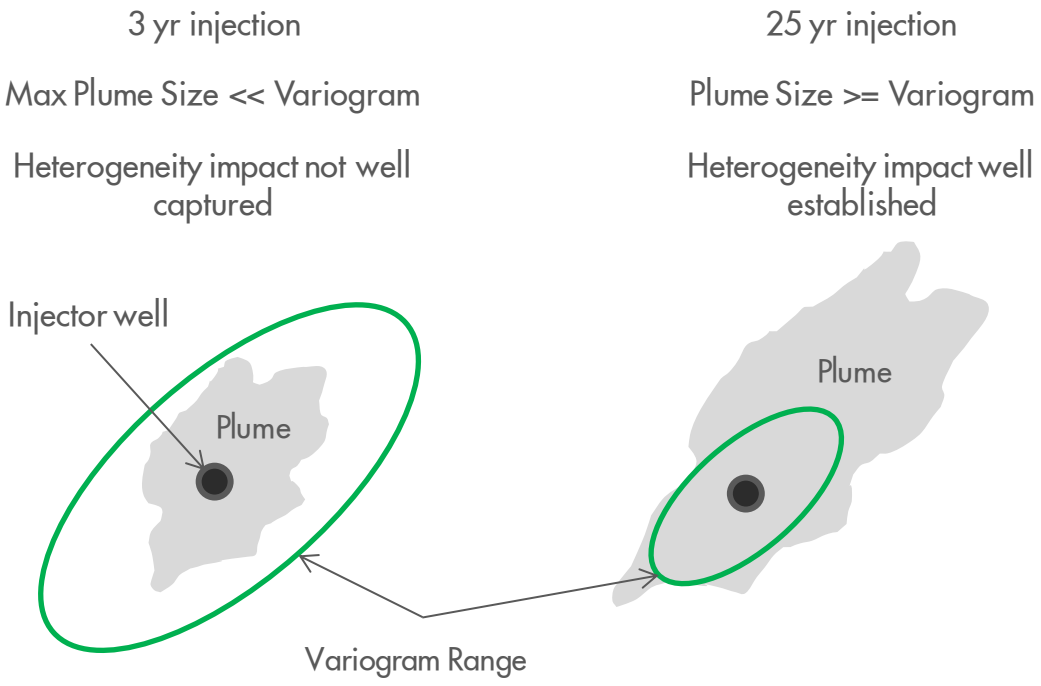

Figure 66 – Schematic concept of plume size versus heterogeneity correlation length controlled by the variogram used in porosity modeling.

The true impact of the range of modeled heterogeneity on the maximum plume size could only be assessed on the full size plume models and using the full 25 years of injection time. The workflow that is used to identify the "Type realization" of porosity to use for any case of heterogeneity also permits the uncertainty in plume size as a function of the heterogeneity to be assessed. This resulted in plume sizes that interacted with a much broader range of the model variability.

This shows that:

- The heterogeneity uncertainty introduces approximately 14% uncertainty around the best estimate of maximum plume size from the mid case heterogeneity.
- The uncertainly in 3D reservoir architecture has a significant impact on the eventual plume geometry regardless of the absolute magnitude of porosity or permeability.
- This has important implications for conformance as it is impossible to accurately predict fine scale reservoir architecture around an injector.

The sensitivity study also quantified the uncertainty in the best estimate of maximum plume length that results from each of the heterogeneity cases. This is the result of simply changing the seed in the stochastic algorithm to give a different 3D arrangement of porosity that still honors all the input constraints and variogram, see the right hand panel of Figure 67. The stochastic seed introduces an average of 14% uncertainty around the best estimate of maximum plume size for each case of heterogeneity, with the high heterogeneity having closer to 17% uncertainty.

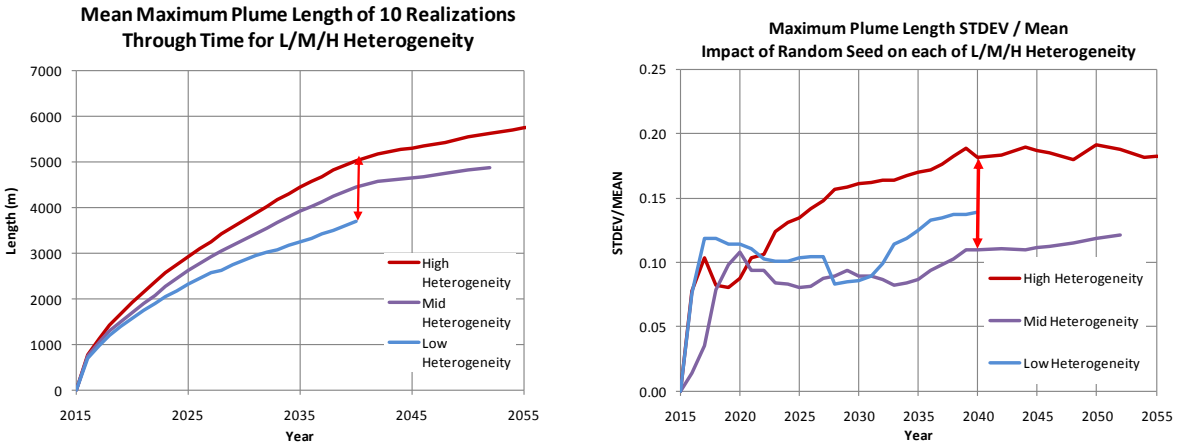

Figure 67: Impact of Heterogeneity uncertainty on plume size at end of injection. Left: Mean maximum plume length from 10 different stochastic realisations, average +/- 14% around mid case. Right: Uncertainty around mean maximum plume length for each heterogeneity case, average is also +/- 14%.

6.5.1.1.2. Pressure Interference Sensitivity

Differential pressure is the driver to enable CO_2 flow in the formation. Hence, the difference in the pressure field will cause the variation of CO_2 plume. This sensitivity evaluation shows negligible effect of the pressure field variation on the plume size.

The CO_2 saturation models used the infinite analytical aquifers as the boundary conditions, assuming no interference with other wells. However, pressure interference does exist in reality when multiple injectors are injecting at the same time. A no-flow boundary between two adjacent injectors is the approximate to such pressure interference conditions. To evaluate the effect of well pressure interference on CO_2 plumes, case A and B, in Table 23, with adjusted boundary conditions were simulated to mimic the well pressure interference in the realistic world. For an injector with two neighboring injectors, boundaries at NW and SE side of the model were changed to no-flow boundaries. For an injector with one neighboring injector, only the SE boundary of the model was changed to no-flow.

Table 23 Pressure Interference Sensitivity Model Cases

Case	Reality Scenario	Boundary Conditions in the model	Well Distance to the no-flow boundary	Model Parameters
A	Center injector scenario	• Infinite aquifers NE and SW • No-flow boundaries NW and SE	2.5 km (assume same injection rate per well)	• 10km*16km tartan grid model • Well rate – 1/3 of field target rate • Injection – 25yr • Shut-in – 100yr
B	Outer injector scenario	• Infinite aquifers NE, SW and NW • No-flow boundary SE	2.5 km (assume same injection rate per well)	

The resulted CO_2 plumes were compared to the base case model result, as seen in Figure 68. The plume shape in layer 8 at 2050 was not distorted by the placement of no-flow boundaries, either on two sides or on only one side. Relative to the base case with no well interference, the addition of one side no-flow boundary (outer well scenario) only slightly offsets the plume, and the two-side no-flow boundaries (center well scenario) only slightly elongate the plume. The reservoir fabric (heterogeneity) has the dominant effect on the plume shape and plume size. The pressure interference impact on plume size is considered negligible.

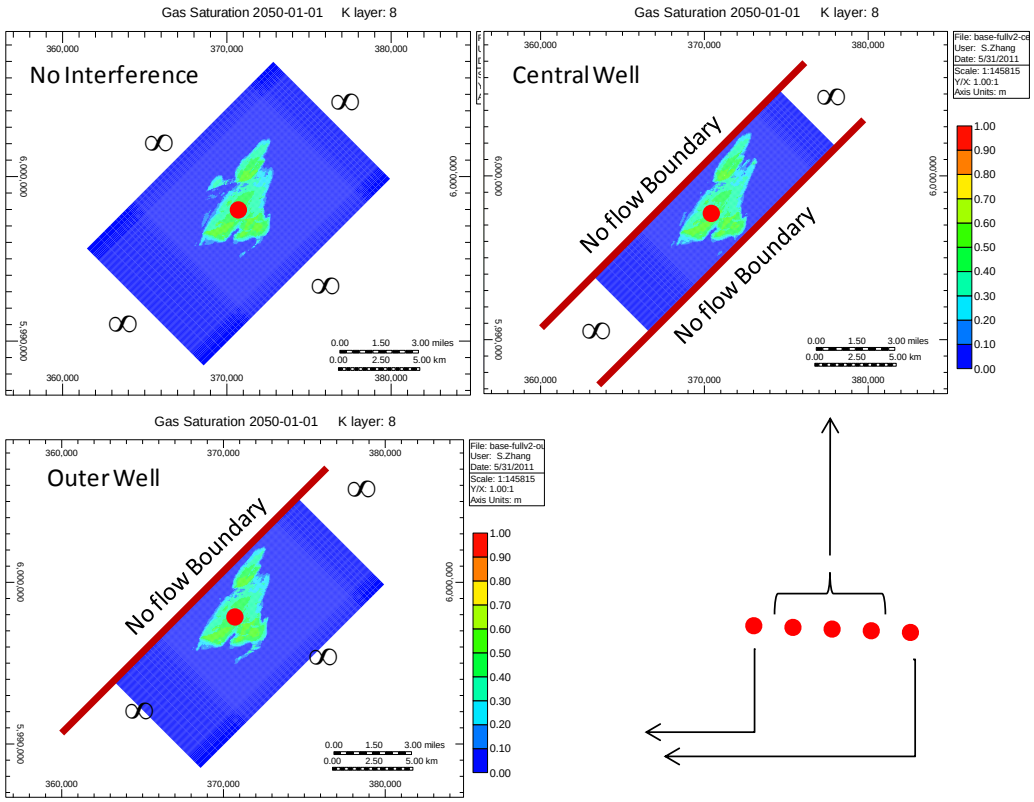

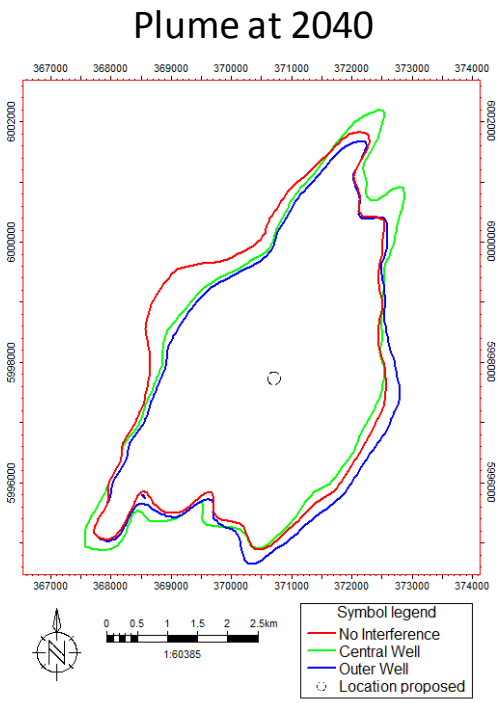

Figure 68: Effect of Well Interference on CO_2 plume.

6.5.1.2. Probability

The following charts illustrate the range of uncertainty in maximum plume length where plume edge is defined at 10% CO2 saturation. The range of uncertainty is large and is heavily driven by the range of uncertainty in the relative permeability. Further studies that can reduce the range of uncertainty on relative permeability will have a significant impact on the results.

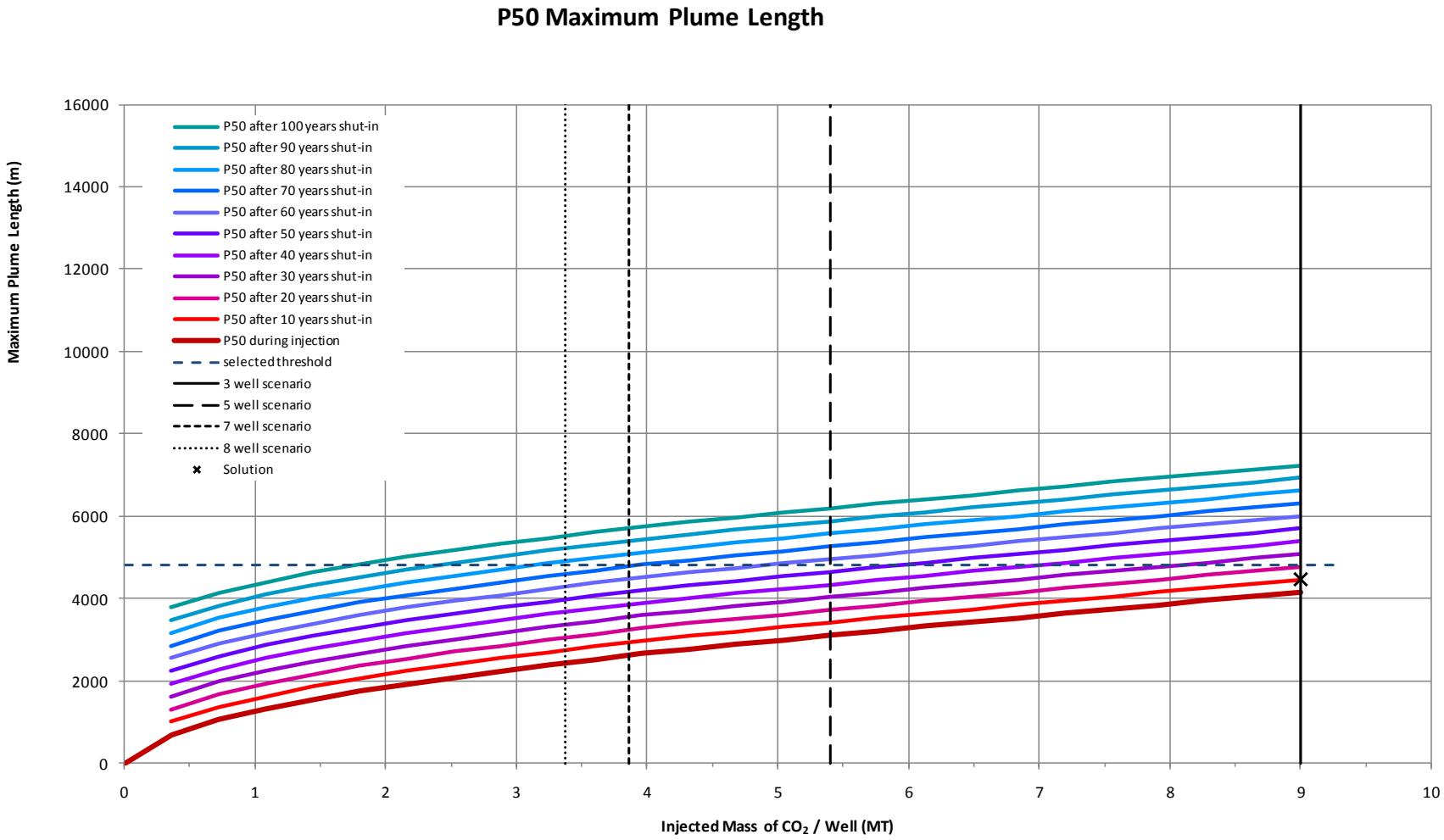

Figure 69 - P50 Maximum Plume Length plot. Solution (X) marks a hypothetical three well case, ten years after injection has stopped.

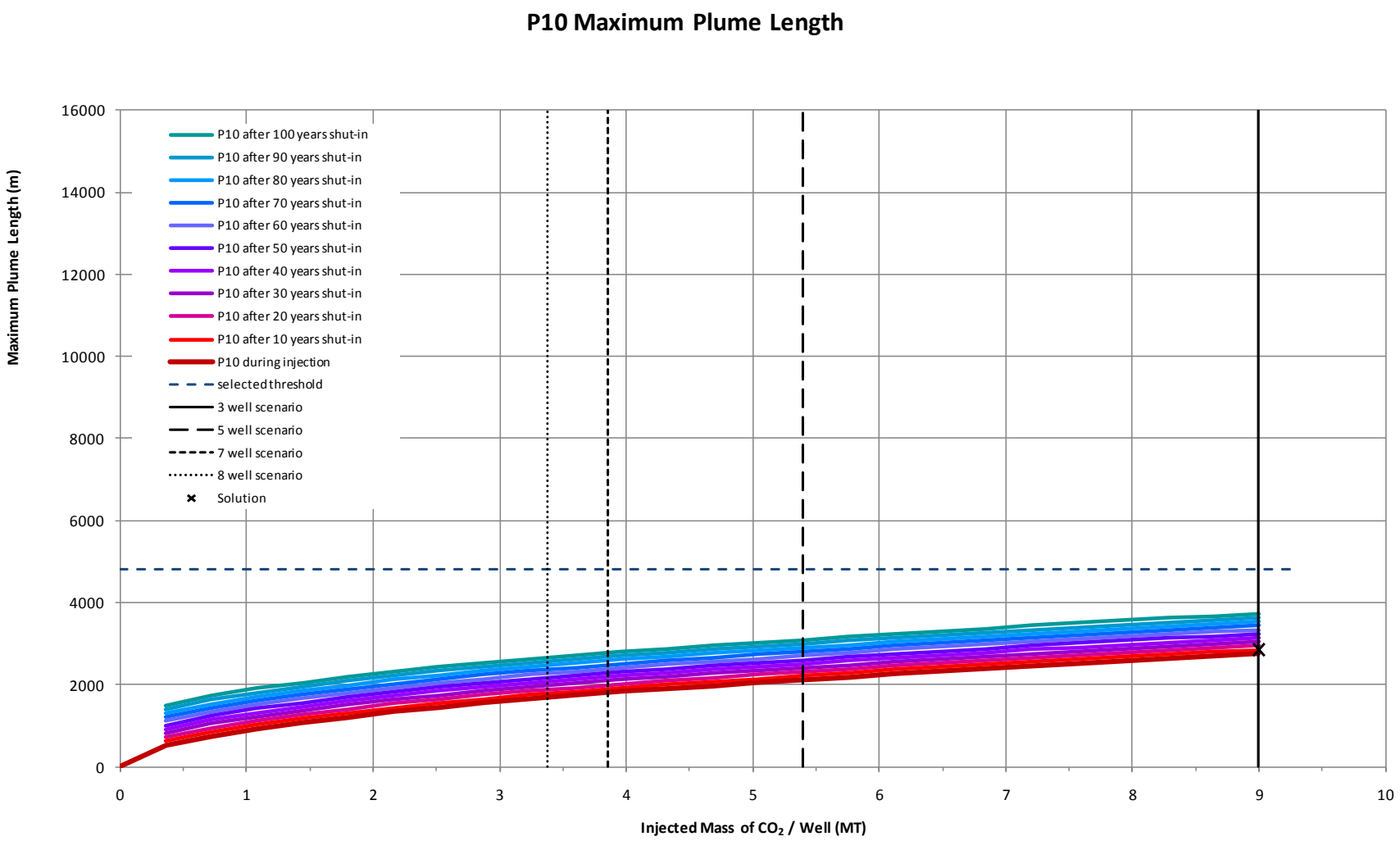

Figure 70 - P10 Maximum Plume Length plot. Solution (X) marks a hypothetical three well case, ten years after injection has stopped.

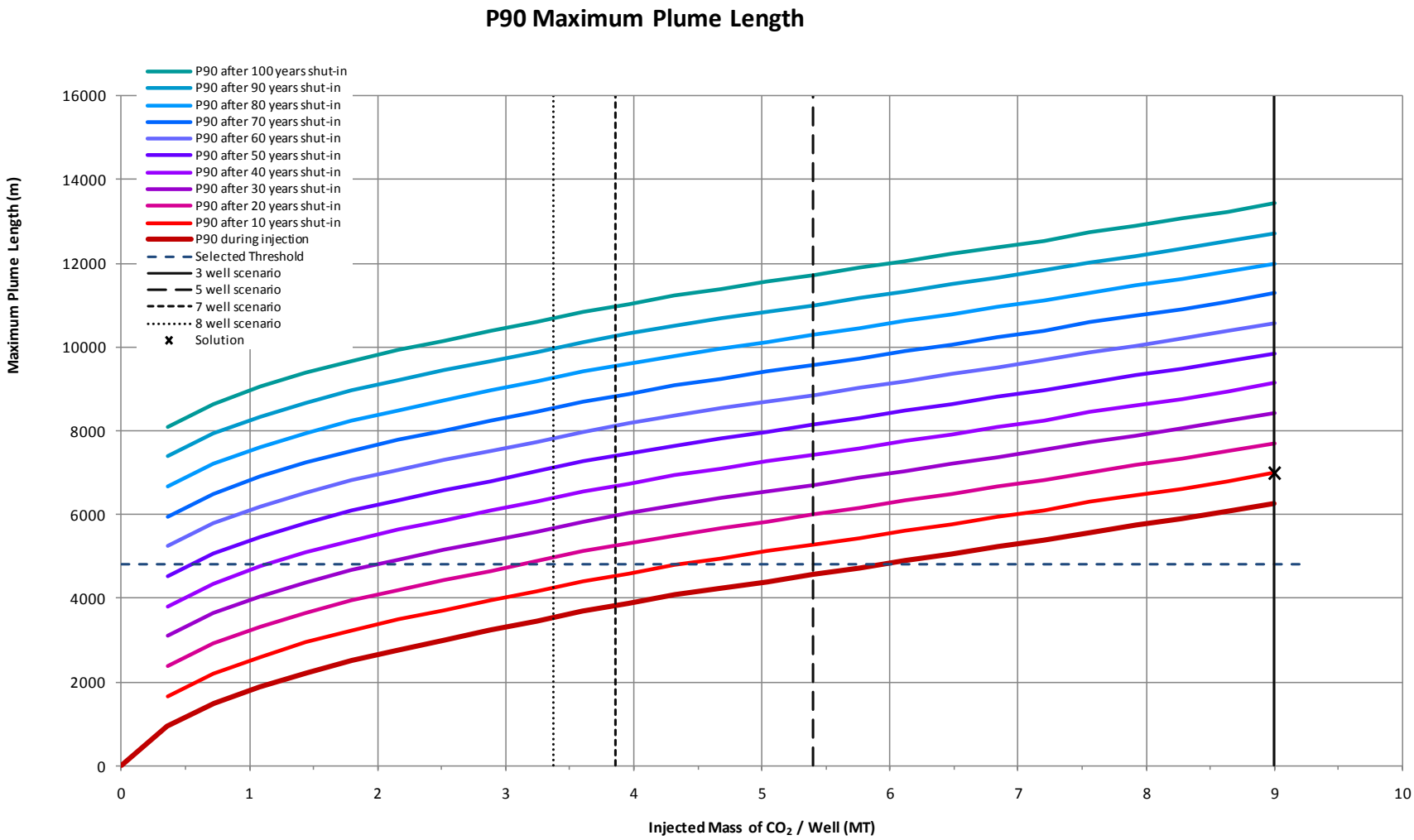

Figure 71: P90 Maximum Plume Length plot. Solution (X) marks a hypothetical three well case, ten years after injection has stopped.

6.5.2. Property Sensitivities

A separate set of simulations were also systematically conducted to evaluate the relative impact of each static and dynamic uncertainty listed below.

- Porosity and permeability
- Baffle Ratio (ratio of Shale Bed Radius to bed thickness, impacting Kv/Kh ratio most)
- Variogram
- Net to Gross (NTG)
- Vertical distribution of high energy dune (HED)
- Relative permeability
- Capillary pressure
- Rock compressibility

To allow for a fast understanding of the key sensitivities a, 5km*5km fine-grid (50m*50m*2m) saturation models were used for this set of sensitivity runs, as well as the 1/5 of the field injection rate for the well, 3-yr injection and 20-yr shut-in.

Changing only one variable at a time in the model, meant that a total of 16 models were built and simulated. Figure 72 shows the max plume length results with time from all cases.

Compressibility uncertainty, even though a wide range (0.725E-7 Kpa^{-1} – 1.45E-7 Kpa^{-1} – 7.25-7 Kpa^{-1})was simulated, shows zero impact on the plume results Figure 73. Since compressibility directly influences the pressure field, the zero effect of compressibility on the plume also infers that variations in the pressure field, either caused by boundary conditions or by injection rate, only have very limited or negligible impact on the plume.

In the cases with low vertical permeability, namely Baffle ratio-high and Porosity-low cases, the CO2 plume grows very fast through high permeability layers in the injection phase, then dramatically slows down or even stops growing in the max plume length once in the shut-in phase, Figure 74. This is because the low vertical permeability greatly restricts the vertical migration of CO_2, as it undermines the buoyancy effect. In the injection period, CO2 flies through the high permeability (lowest resistance) layers to end up with a big plume length. Once in the shut-in period, the CO2 in each layer could only grow through the diffusion process, as additional CO2 supply through vertical layer communication is so limited.

Even with the base case vertical permeability, the growth of max plume length in the shut-in phase is far slower than that in the injection phase (Figure 74, Figure 75). This is because in the shut-in period, capillary and gravity forces dominate the CO_2 migration, rather than the viscous force (pressure) that dominates the injection phase. Capillary pressure and gravity forces are stable forces, hence the speed of max plume length growth is close to linear in the shut-in phase.

A tornado plot (Figure 76) at the end of the 3-yr injection simulation highlights the rank of the impacts from individual variables.

- Tier 1 variables are, Baffle ratio, porosity and permeability and relative permeability.

- Tier 2 variables are, the variogram (although as discussed in the previous section this is because a 3 year injection period is too short for the interaction between the CO2 plume and the variogram to be felt therefore this was re-examined using the full injection period), NTG, capillary pressure and HED.

However, the relative impacts of individual variables are strongly time dependent, except for the capillary pressure (Figure 77). Given a longer time, the impacts of relative permeability and variogram grow bigger and become more important than the Baffle ratio and the porosity and permeability at the end of 20yr shut-in. As a matter of fact, tornado plots made at any time slice are very different. This time dependency of tornado sensitivity is not a total surprise given the different driving forces in the injection and shut-in phases. However, the magnitude of the time dependency is very much unexpected. The increasing trend of variogram impact vs. time (Figure 77) indicates that the impact of the 3D geological complexity depends on the interaction area between the injected CO_2 and the rock matrix. Longer time and more injection volume could possibly enlarge the impact of variogram, compared to the other sensitivity variables.

The time dependency of the sensitivities also challenges the idea of scaling up the plume size results from 3-yr injection to those with 25-yr injection. An attempt was made to analytically scale up the 3yr injection plume size results to those after the 25yr injection. Then the same geological model but in the 10km*16km scale and tartan-grid was simulated for 25yr injection and 100yr shut-in. The analytically predicted max plume length vs. time is unsatisfying, compared to that from the actual model result (Figure 78).

Overall, this set of property sensitivity runs, conducted on the model scale of 5km*5km and for shorter injection and shut-in simulation time, provides the following insights:

- Baffle ratio, porosity and permeability, relative permeability and variogram are the tier 1 sensitivity variables for the max plume length. The impacts from NTG, capillary pressure and HED are far less. The max plume length is not sensitive to the uncertainty in rock compressibility, which also indicates the insensitivity to the pressure field variations caused by the boundary conditions or by the injection rate difference.
- The max plume length sensitivities to individual variable uncertainties are time dependent. Because the driving forces are different from the injection phase to the shut-in phase. Meanwhile, the impact of 3D geological complexity (variogram) depends on the CO_2-rock interaction area which associates with the injection volume and time.
- The CO2-rock interaction area and the impact of 3D geological complexity can't be analytically predicted to the satisfying standard. Hence, analytically scaling up the plume length results from the small injection volume (3yr injection) runs to those with larger injection volume (25yr injection) is not satisfying.

As a result of this property sensitivity study, another set of large CO2 saturation models in the 10km*16km scale and with tartan grids were constructed to obtain the max plume length results from simulating the 25yr injection and 100 yaer shut-in. Those large saturation models were also used to assess the uncertainty range in the plume length. See previous chapter for detailed discussions.

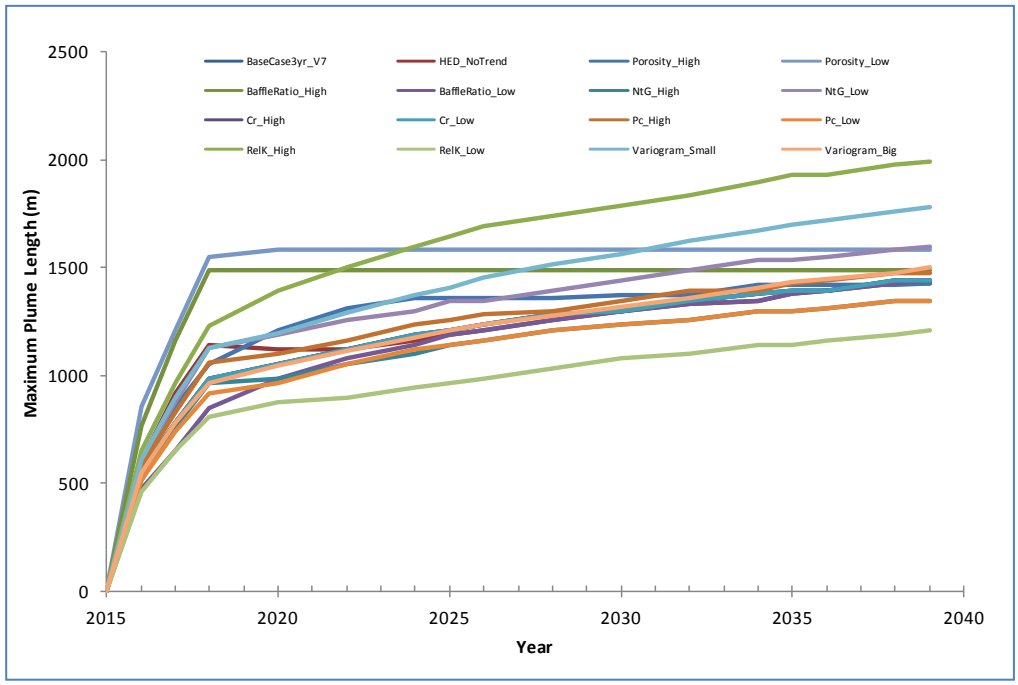

Figure 72: All property sensitivity model results for maximum plume length

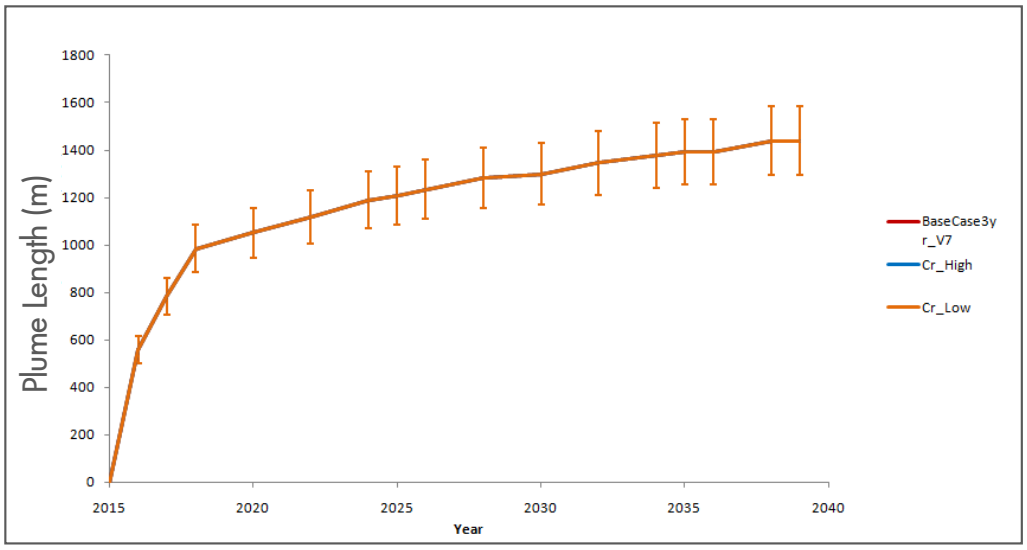

Figure 73: CO_2 plume insensitive to Rock Compressibility Uncertainty

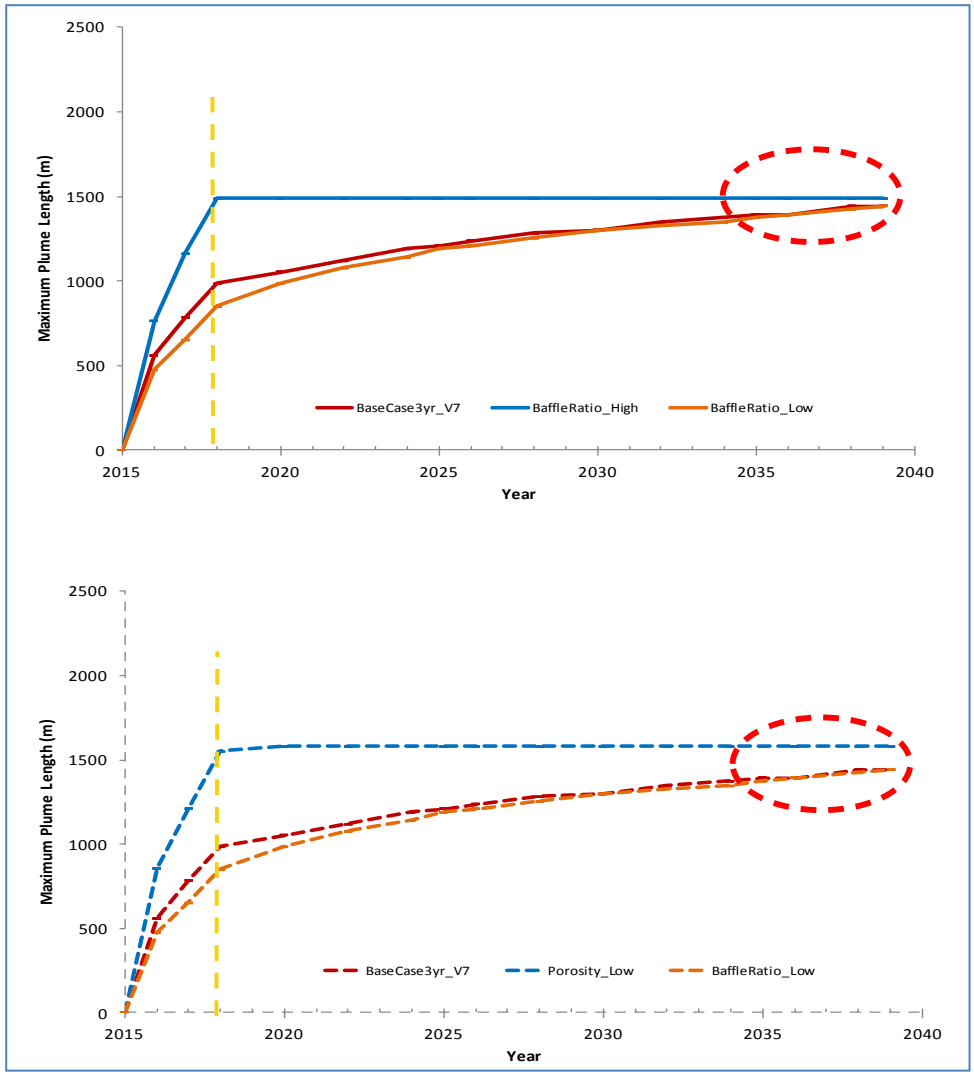

Figure 74: Sensitivity to Kv related uncertainties.

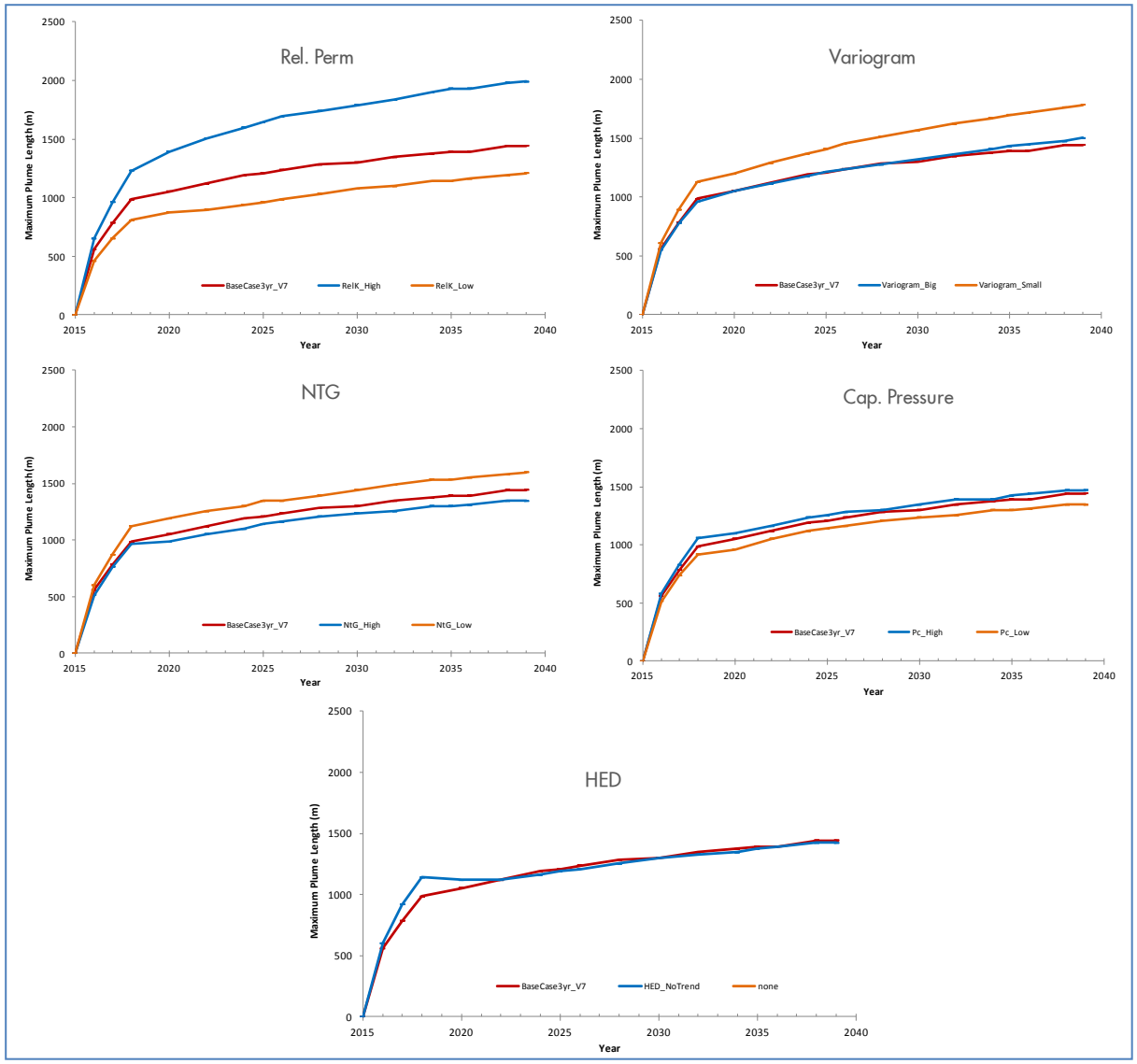

Figure 75: Sensitivities to Other Properties Uncertainties

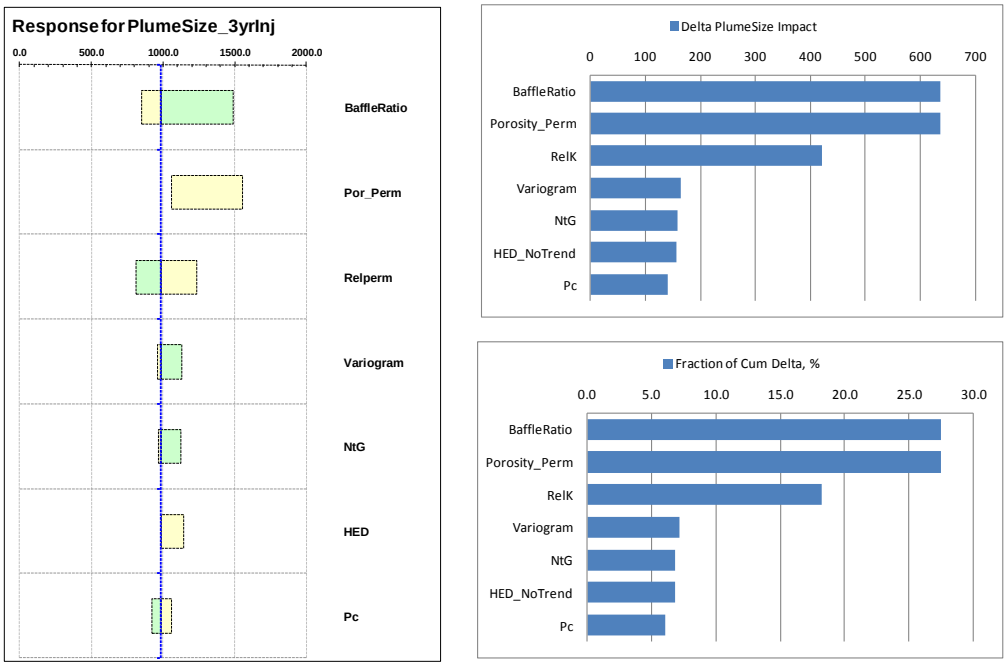

Figure 76: Sensitivity Tornado Plot (at the end of 3yr Injection)

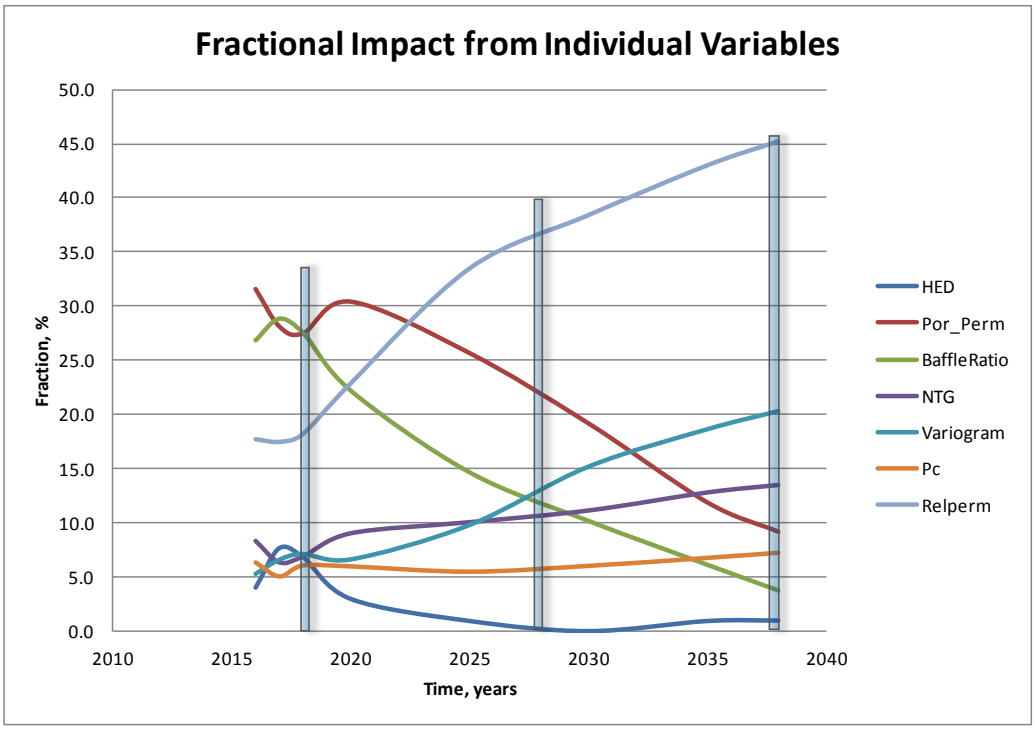

Figure 77 - Time Dependency of Properties Sensitivities

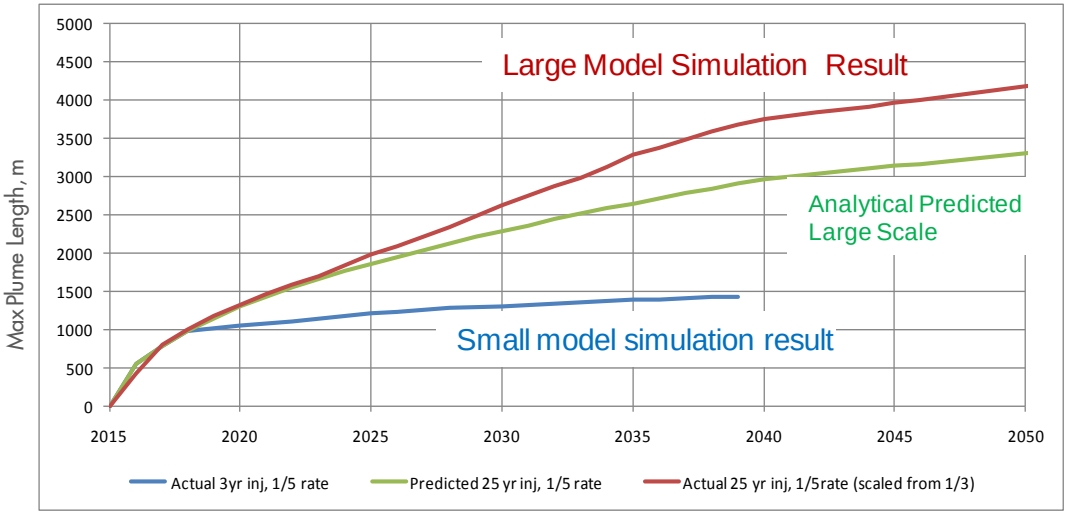

Figure 78: Miss-fit of an Analytical Prediction of Max Plume Length

6.5.3. CO2 Trapping Quantities

The injected CO_2 stays underground in at least two phases. A certain amounts of CO_2 is dissolved in formation brine and remaining in the aqueous phase, while the majority remains in a distinct supercritical phase even at a time scale of 100 years post shut-in (Table 24, Figure 79). Mineral trapping is expected to be insignificant, even at long exposure times due to the clean nature of the BCS sandstone and its mineral storage capacity has been reported in the Quest Feasibility Report and Gen-3 report previously (Winkler, 2010). Residual trapping (hysteresis), local capillary pressure trapping (high capillary entry pressure at poor permeability barriers) and CO_2 dissolution into brine are therefore the CO_2 trapping mechanisms in the subsurface (Figure 79). Table 25 gives a summary of trapped CO_2 from the plume length base case V9 and P10-V11R, P50-V2R, P90-V5R cases. It shows that 50%~70% of injected CO_2 could have been physically trapped in the storage formation by 2140, that is one hundred years shut-in after the 25-year injection.

Table 24: CO_2 Storage in Phases

100-year shut-in after 25yr-injection	P10-V11R	P50-V2R	P90-V5R	Basecase-V9R
Total Injected CO2, gmol	2.27E+11	2.27E+11	2.27E+11	2.27E+11
CO2 dissovled, mol	1.02E+10	1.71E+10	1.92E+10	1.39E+10
Supercritical CO2, mol	2.17E+11	2.10E+11	2.08E+11	2.13E+11
Dissolved CO2, %	4%	8%	8%	6%

Table 25: CO_2 Trapping

100-year shut-in after 25yr-injection	P10-V11R	P50-V2R	P90-V5R	Basecase-V9R
Total Injected CO2, gmol	2.27E+11	2.27E+11	2.27E+11	2.27E+11
CO2 dissovled, mol	1.02E+10	1.71E+10	1.92E+10	1.39E+10
Trapped CO2, mol	1.32E+11	1.39E+11	1.29E+11	1.05E+11
Total trapped CO2, %	62%	69%	65%	52%

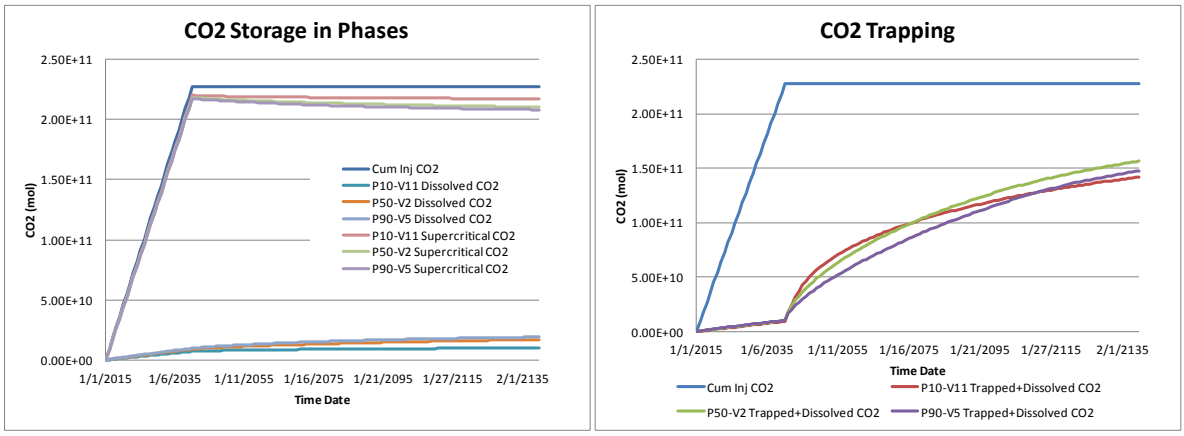

Figure 79: CO2 Phase Storage and Trapping

7. PRESSURE MODELING

7.1. Objectives & Modeling Strategy

The Gen-4 Pressure Modeling is designed to validate the number of wells that may be required to successfully inject 27 Mt of CO_2 into the BCS over a period of 25 years given the range of subsurface uncertainty. In addition to development size the Pressure models also assist in defining the scope of the MMV plan by providing a range of expected pore pressure increase that may be expected at older legacy well that penetrate the BCS and that present the largest containment risk.

The focus of Gen-3 modeling in 2010 was the determination of the well count range. The Gen-3 models were constructed prior to the drilling and analysis of the Radway 8-19 well and the acquisition of the full area of 3D seismic date over the development AOI. The Gen-3 modeling showed that between 3 and 10 wells should be sufficient to achieve the target injection volume across a broad range of subsurface scenarios. With the addition of the 8-19 well in the centre of the development and increased seismic coverage the aim for Gen-4 is to validate, and if possible narrow the range of uncertainty in well count given the new data.

The same modeling strategy was adopted in Gen-4 as that used in Gen-3, with the definition of scenario's in a "solution space", combinations of different development options with different subsurface realizations to assess how well the development performs given the subsurface uncertainty.

The subsurface realizations are defined by the two key uncertainties, Reservoir Quality and Reservoir Connectivity, each with a high, mid and low case outcome, see Figure 80. The combination of different outcomes describes a broad range of subsurface realizations sufficiently covering the current range of subsurface uncertainty.

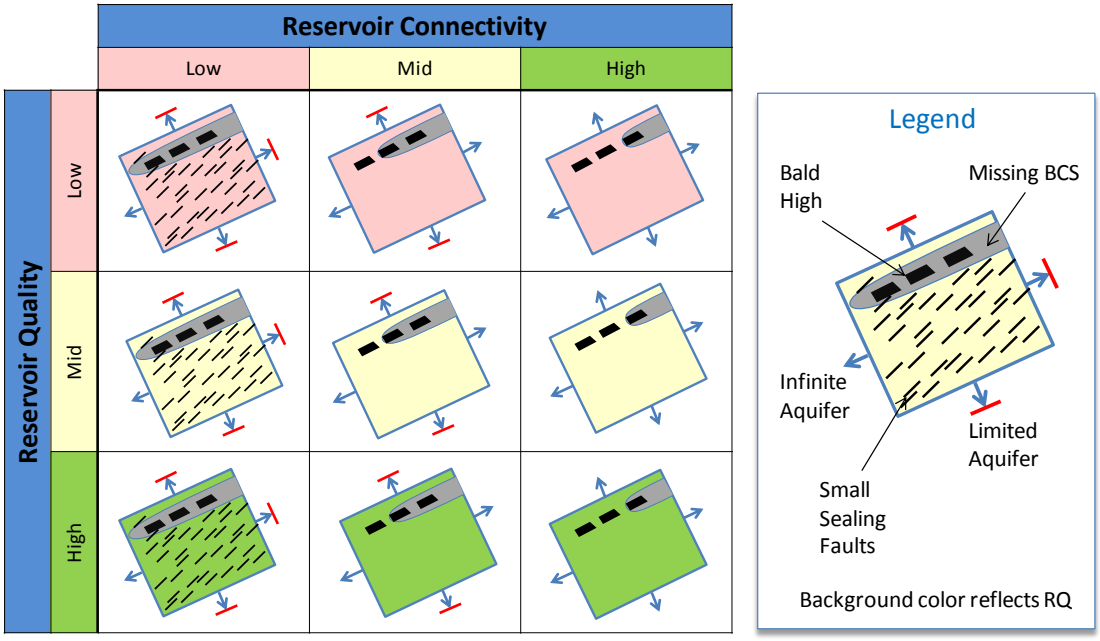

Figure 80: Gen-4 Pressure Modeling Realization Matrix with schematic representations of the subsurface realizations

Not all realizations are simulated as the learning's from one can often be used to infer the result of running other simulations.

A range of dynamic related parameters are also tested as sensitivities, typically around the reference case realization of Mid Reservoir Quality, Mid Connectivity.

7.2. Structural Framework

The Pressure model grid is simply a re-gridded sector from the larger area Geological models. The zonation and structure of the BS and LMS is identical in both models. The Pressure model was re-gridded to a coarser resolution in all zones to allow for practical simulation times. Layering in the Pressure model follows a proportional scheme targeting mean thickness in the BCS and lower portion of the LMS of 4m and 10m in the rest of the LMS. The total number of grid cells in the Pressure model is 313,600 down from a total of 10.1 Million in the Geological model over the same zones and AOI.

Table 26 - Grid statistics comparison for Pressure and Geological Models

Model	Cell Count (Pressure Model AOI and Zones)	Grid XY Resolution	Mean Layer Thickness		
			BCS	LMS Lower	LMS Upper
Geological	10.1 M	250 x 250m	0.8 m	1m	5.2m
Pressure	0.31 M	750 x 750m	4m	5m	10.2m

7.3. Uncertainties

7.3.1. Reservoir Quality

All of the various reservoir quality properties are constructed in the Geological model as described in Section 3 and are up-scaled into the coarse Pressure Model grid. See Table 27 for a summary of up-scaling methods for different properties. Table 28 below shows the subsurface property combinations leading to the various reservoir quality cases.

Table 27: Reservoir Quality Up-scaling Methods from the Geological Model

Property	Upscaling Method
NTG	Arithmetic Average
Porosity	Arithmetic Average, NTG Weighted
Kh	Flow Based Up-scaling (IJK Tensors)
Kve	

Table 28: Reservoir Quality uncertainty configuration for simulated Pressure Model subsurface realizations

Property	Reservoir Quality Case			
	Low Low*	**Low**	**Mid**	**High**
NTG	Low	Mid	Mid	High
Porosity	Low	Low	Mid	High
Kh	Low	Low	Mid	High
Kve/Kh	Mid	Mid	Mid	Mid
HED Facies	Mid	Mid	Mid	Mid

7.3.2. Reservoir Connectivity

Following reservoir quality properties up-scaling from the geological model the various components that describe the relevant Reservoir Connectivity realization are added into the dynamic model prior to export to the simulator:

- Basement Features
  - Bald Highs through BCS and LMS
  - Elevated basement region in BCS
  - Isolated basement highs in the BCS

- Small Sealing Faults

The parameters for the connected aquifers are set up within the simulator and reflect the connectivity configuration within the model, see Figure 81.

Table 29: Reservoir Connectivity uncertainty configuration in the pressure model subsurface realizations.

Component	**Reservoir Connectivity Case**		
	Low	**Mid**	**High**
Elevated Basement	Low	Mid	High
Bald Highs	Yes	Yes	Yes
Isolated Highs	Yes	Yes	Yes
Sealing Faults	Yes	No	No
Connected Aquifers	3 of 4 restricted	2 of 4 restricted	All infinite

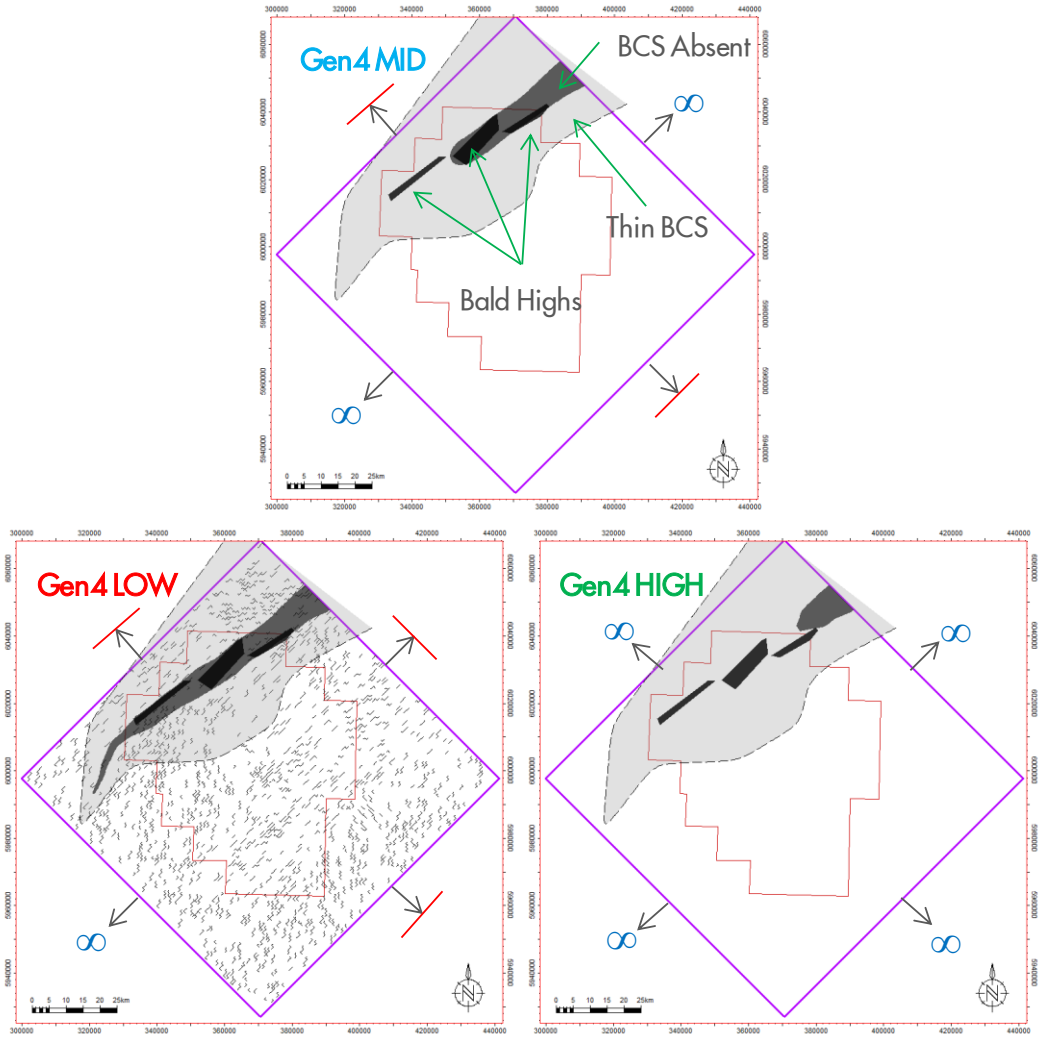

Figure 81: Gen-4 range of Reservoir Connectivity capturing BCS thinning and pinch out, faulting and connected aquifer.

7.3.2.1. Basement Features

The region of elevated basement observed on 3D seismic and some 2D lines is added into the BCS zone of the model. The well spacing in the North of the Quest AOI is very large. Between the well penetrations the seismic suggests that the basement is elevated compared to the top Basement surface that results from simply gridding up the available well tops. Hand contoured isochores were constructed that describe a thickness of Basement to add onto the top of the basement as it exists in the model framework, see Figure 82.

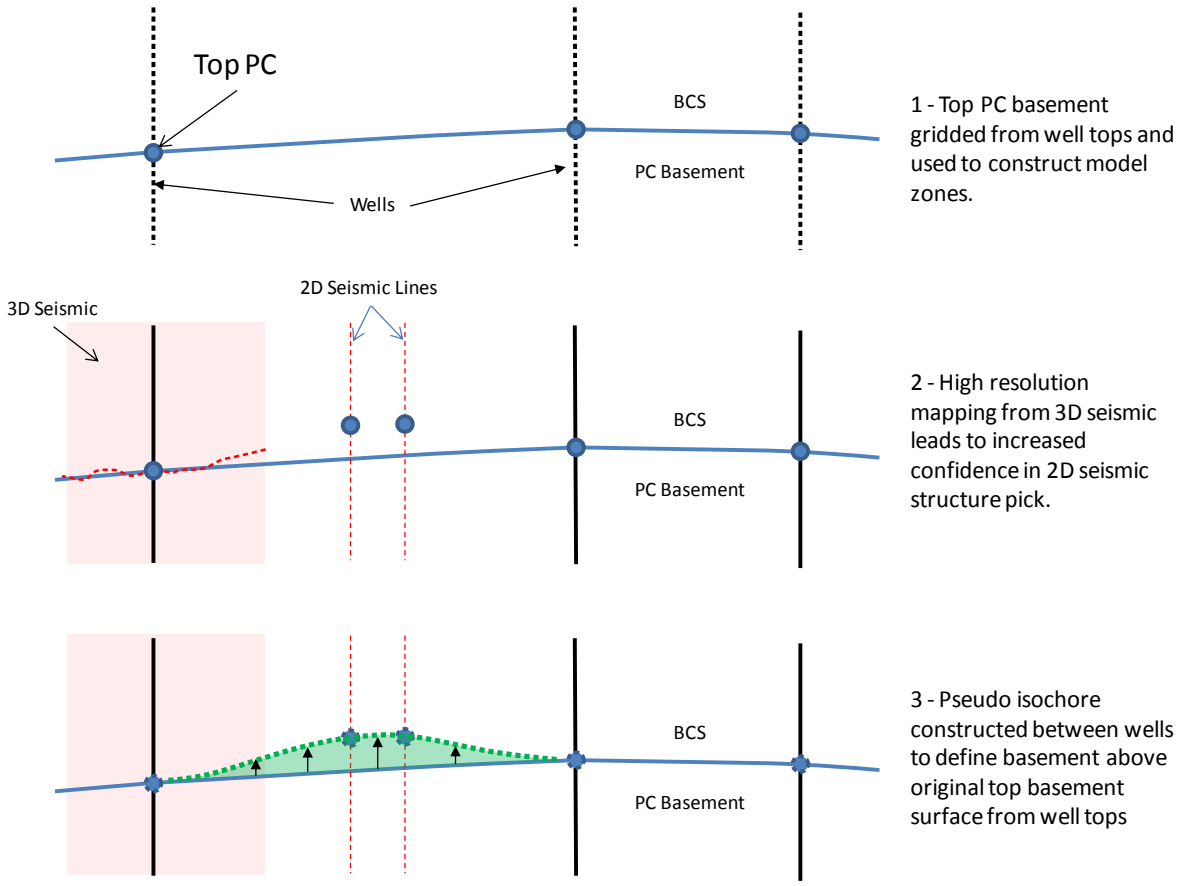

Figure 82 - Workflow to define elevated basement between wells in the Pressure Models after property upscaling.

The cells in the BCS that are within this region are given basement properties, i.e. no NTG, no porosity or permeability, see Figure 83.

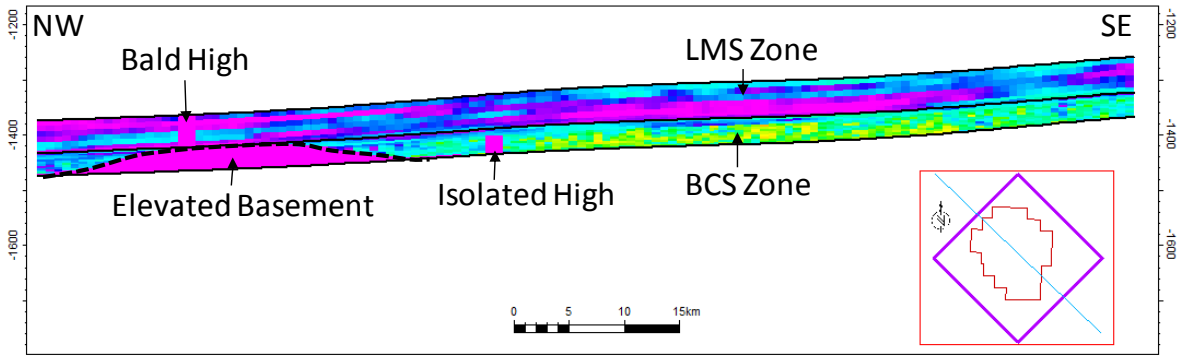

Figure 83 - Elevated basement region in the BCS (purple = no porosity) in the Low Connectivity realization.

The range of uncertainty in the degree of thinning of BCS over the basement high is captured via 3 alternate isochore maps which result in different extents of region where the BCS is completely missing due to pinch out against the elevated basement, see Figure 81.

7.3.2.2. Bald Highs

Bald Highs are areas of basement where both the BCS and LMS are assumed to be missing.

The typical interpreted faults on the 2-D data have throws with a maximum of about 20 meters. An exception is the larger transgressional style faulting on the north end of the 2-D data area. These faults, with throws of up to 100 meters appear related to the aero magnetically-defined Rimbey Terrain Block boundary and Snowbird Tectonic Zone. The majority of the Quest AOI overlies the Pre-Cambrain Rimbey magmatic arc, a small Southeastern portion that sits atop the Lacomb metamorphic belt and a small Northwestern portion deposited over the Thorsby Terrane. According to Ross et al. (1989), the Thorsby is an accreted terrane, the Rimbey is a continental-margin magmatic arc , and the Lacomb is a zone along the front of the Hearne Archean Province (Chen, 2005).

The correlation of fault interpretation on multiple 2D lines is consistent with the shape of the Rimbey – Thorsby terrain boundary on HRAM and published regional gravity/magnetic data.

Lateral changes in fault throw suggest a series of en-echelon faults. The resultant structural highs are thought to be 1-2 km wide and several km long, with a maximum relief of about 100 meters and possibly part of flower structure “pop ups” typical of the transgressional structural style. Figure 85 shows a key seismic line crossing these faults. These are informally referred to as “bald highs” and interpreted as being palaeo-islands at the time of BCS/LMS deposition which were subsequently drowned by the marine transgression. The offset legacy well Westminster Hairy-1 penetrates a similar bald high to the East of the Quest AOI. This well showed shallow Pre-Cambrian basement with a missing BCS/LMS section. The bald high at Westminster Hairy-1 is also associated with a Pre-Cambrian terrane block boundary. The Basal Cambrian Sands are expected to be missing over these highs in the Quest AOI. Because of their relatively large relief compared to the thickness of BCS/LMS, these features may present a slightly higher MCS top seal risk due to possible thinning of the MCS over the bald high or possibly differential compaction-driven faulting at the edges of the bald high, see Figure 86.

From the seismic interpretation of reflector geometry the bald high fault block edges appear rounded off, likely due to exposure and erosion.

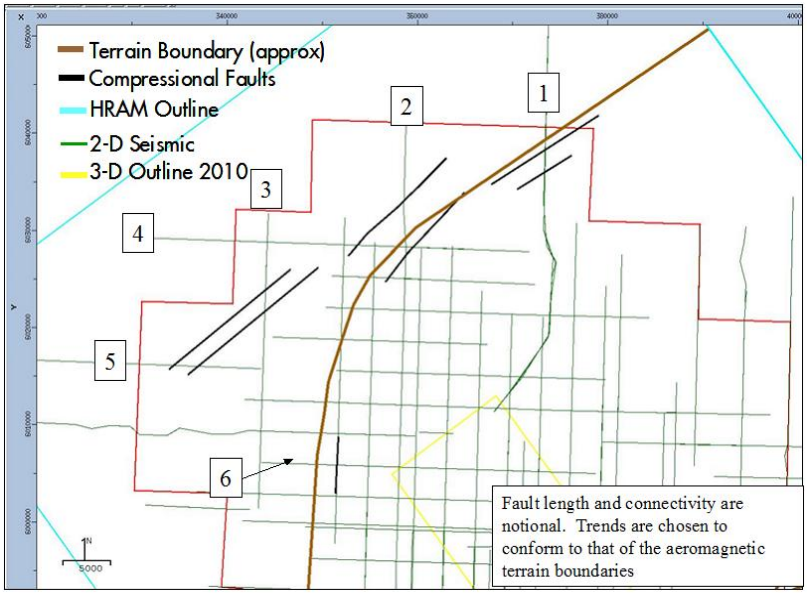

Figure 84 - Mapping of north Rimbey block faulting on 2D lines.

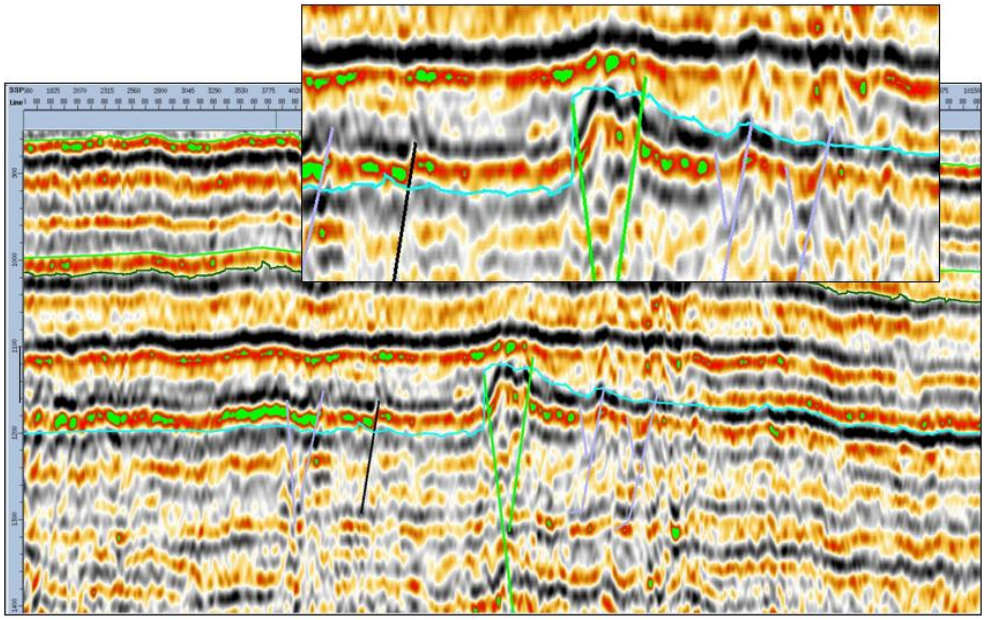

Figure 85: 2D line (line #1 on Figure 84) showing "bald high" and change in reflector configuration, suggesting missing BCS and LMS over the elevated area of basement. The blue pick is top Pre-Cambrian basement.

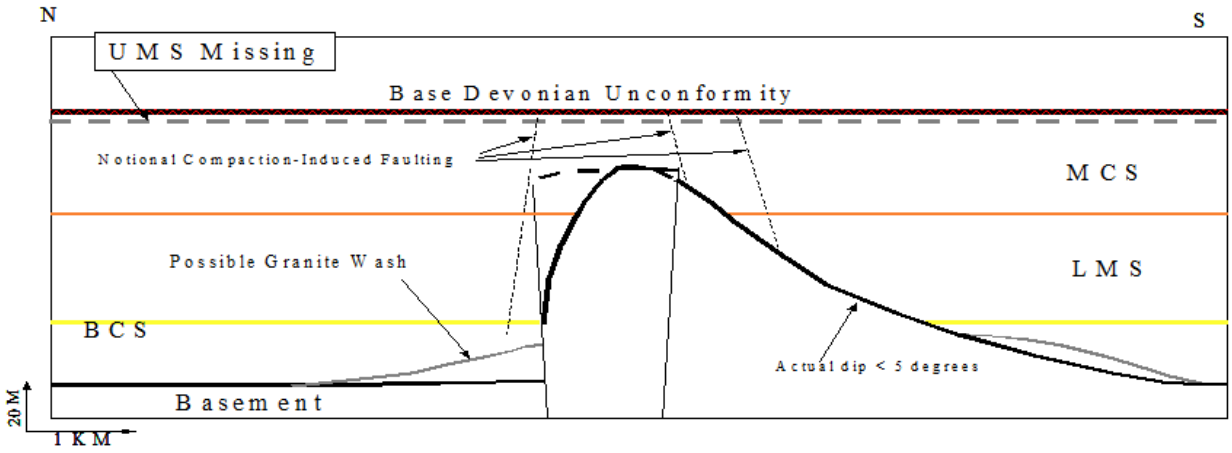

Figure 86: Schematic interpretation of the line shown in Figure 85.

7.3.2.3. Isolated Highs

Isolated basement highs are added to the model to honor the basement topography observations from the 3D seismic. These are small areas of elevated basement that do not fully cut-out the BCS, but do systematically thin it, see an example in the cross section shown in Figure 83 and locations of all highs in Figure 87.

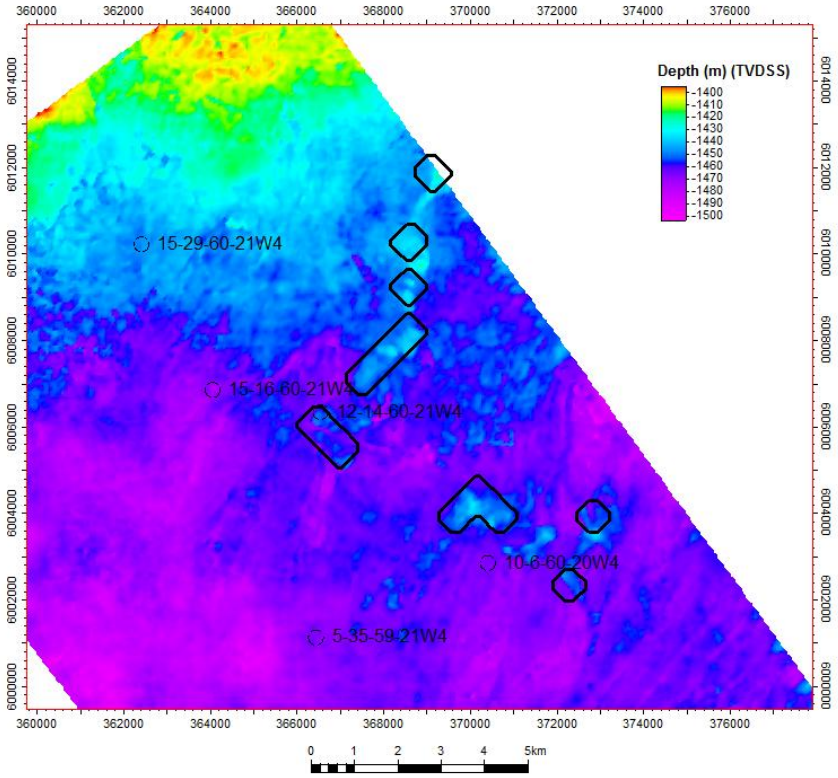

Figure 87: Top PC elevation map from 3D seismic with the location of isolated basement highs in Gen-4 Pressure models (black outlines).

7.3.2.4. Small Faults

Faults are added to the grid as simulation faults in Petrel. These are located deterministically within the area of the 3D seismic, as mapped at top basement. Outside of the 3D seismic AOI the faults are generated using a stochastic technique and trends to control where faults are preferentially developed and their strike azimuth. The location of all faults in the model is shown in the lower left panel of Figure 81.

The fault location probability trend is derived from High Resolution Aero Magnetic (HRAM) data. The HRAM map used is a 5km high-pass filtered derivative of the Total Magnetic Intensity data (TMI reduced to pole). This map shows a *qualitative* correlation between density of faults as picked in the seismic data and the HRAM amplitude and patterns, see Figure 88. The assumption was that, beyond the area of the seismic, the patterns in the HRAM data were indicative of faulting density and dominant azimuth trends see Figure 89 and Figure 90. Areas bounded by pink polygons in Figure 90 have a higher probability of containing faults.

The workflow for inserting the faults into the model is as follows:

1. Pick a random location in model to start a fault
2. Generate a random number between 0 and 1
3. Keep the fault if:

a. The probability trend has a value of 1 at that location (Figure 90, right) AND the random number is less than or equal to 0.8.

Or

b. The probability trend has a value of 0 at that location AND the random number is less than or equal to 0.2.

Otherwise return to step 1.

4. Make the fault polygon by picking a random length from the input distribution and assigning an azimuth from the value of the azimuth trend map at that location (Figure 89).
5. Resample the fault polygon into the grid as a simulation fault.

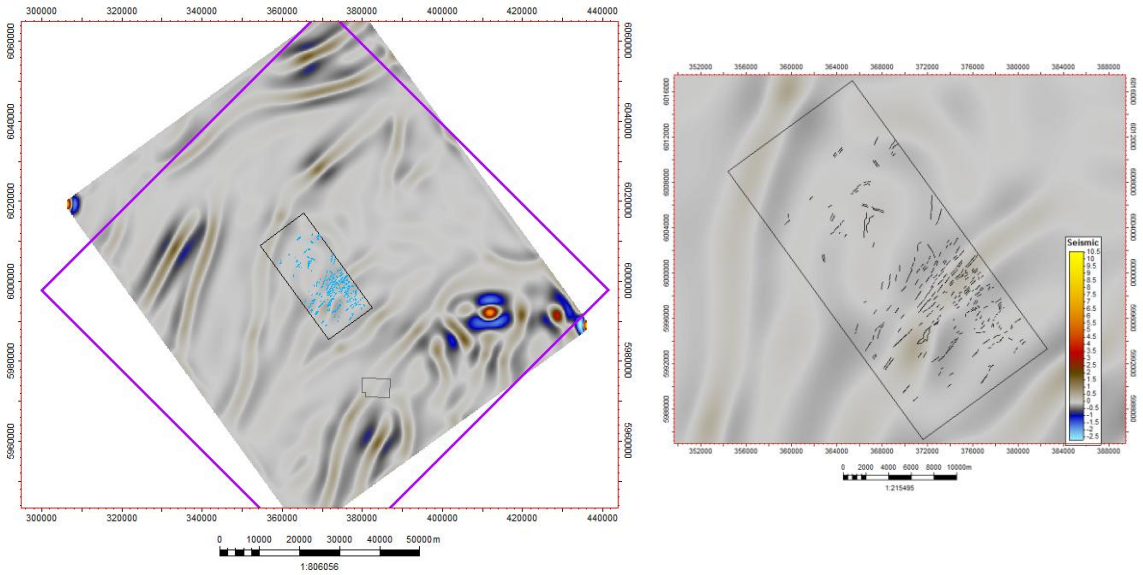

Figure 88 - Left: HRAM data and mapped faults at top basement. Right: Zoomed in view over 3D seismic AOI showing qualitative match between fault density and azimuth with HRAM pattern.

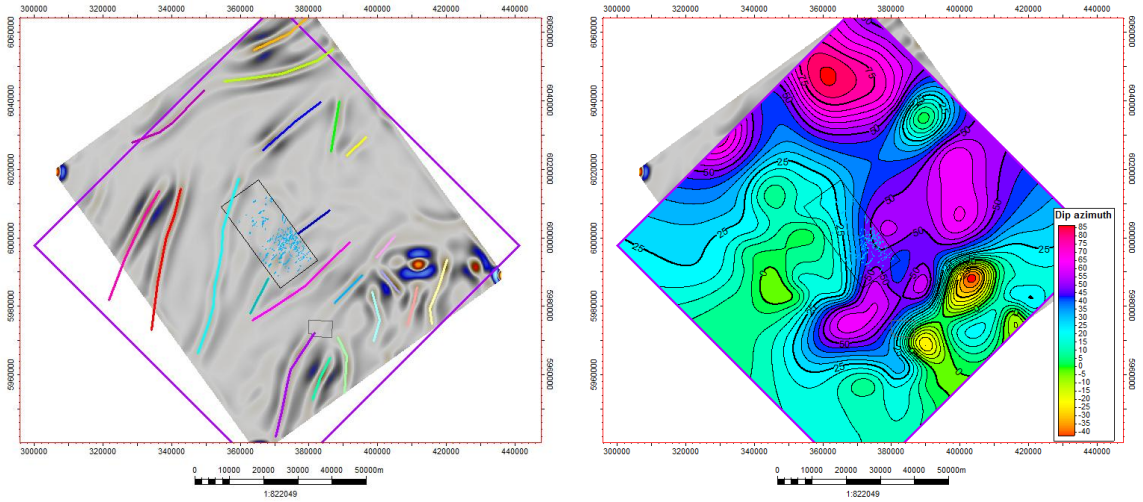

Figure 89: Left - HRAM data with digitized orientation lines. Right - Fault Azimuth trend map from digitized orientation lines.

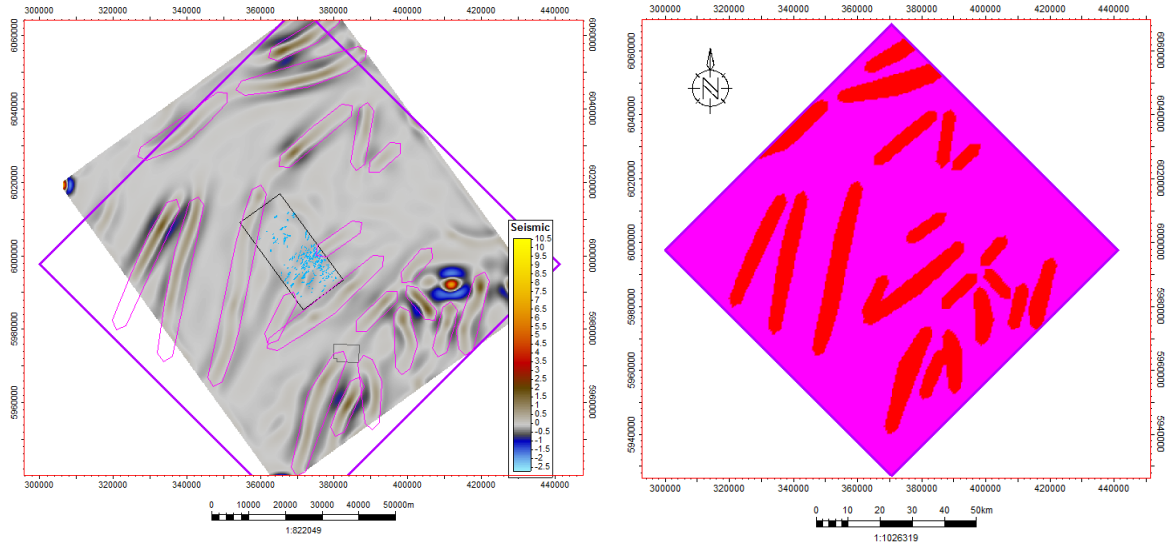

Figure 90: Left - HRAM data with digitized boundaries (pink) reflecting areas with presumed higher probability of fault presence. Right - Probability Trend Map used in fault modeling workflow (red=1, pink=0)

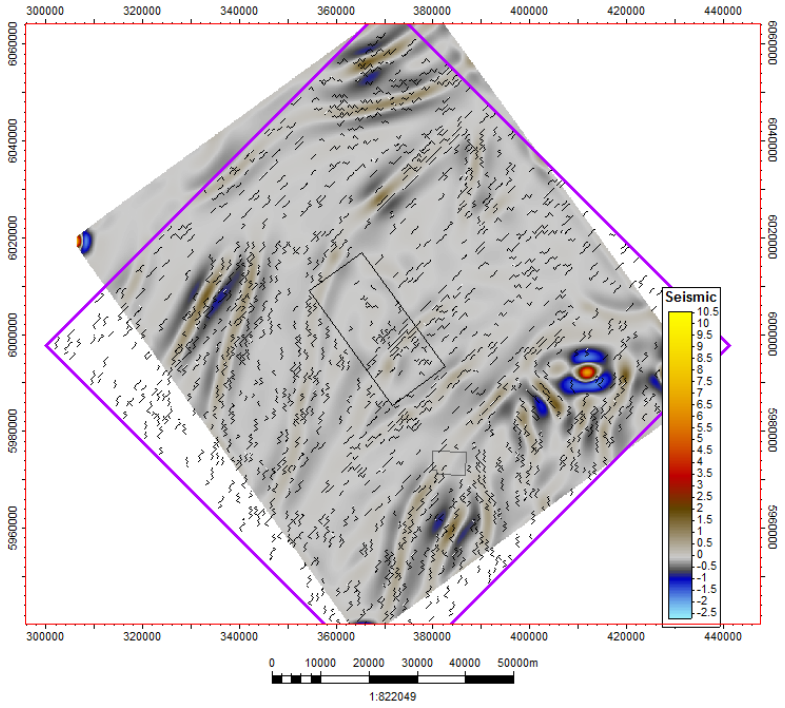

Figure 91: HRAM data with all simulation fault locations overlain. Note that the faults in the 3D seismic AOI in the centre of the model are deterministically inserted and appear in context with the surrounding region.

Faults are set to sealing only in the Low Connectivity case realizations. The faults are completely open to flow in the mid and high case connectivity realizations. This is to reflect two parameters:

- the fact that the maximum throw on the faults is less than the BCS thickness.
- The faults are mappend on the pre-cambrian basement there is no accompanying expression on the map of the “top BCS”.

7.3.3. Dynamic Sensitivities

The various parameters that may be varied in the pressure simulation model are:

- Relative Permeability
- Capillary Pressure
- Mechanical Skin
- Non-Darcy Skin
- Pore Volume Compressibility

For the purposes of assessing well count across scenarios, where a development option is tested against a subsurface realization, the dynamic parameters are typically maintained at

base case levels. Sensitivities are mainly run around the mid reservoir property-mid reservoir connectivity (expectation) realization to investigate the impact of one or more parameters having different outcomes. For details on the range of uncertainty for each dynamic parameter see chapter 3.

7.3.3.1. Bottom Hole Pressure (BHP) Constraints

In-line with the all other Gen-4 modeling activities an mid case injection bottom hole pressure constraint of 28 MPa has been assumed with a low value of 26 MPa and a high value of 32 MPa. The operational and regulatory rational for the mid case and associated ranges are described in chapter 5.1.3.

7.4. Subsurface Realizations

The subsurface realizations are defined by the two key uncertainties, Reservoir Quality and Reservoir Connectivity, each with a high, mid and low case outcome, see Figure 92 and as described above. The combination of different outcomes describes a broad range of subsurface realizations, sufficiently covering the current range of subsurface uncertainty.

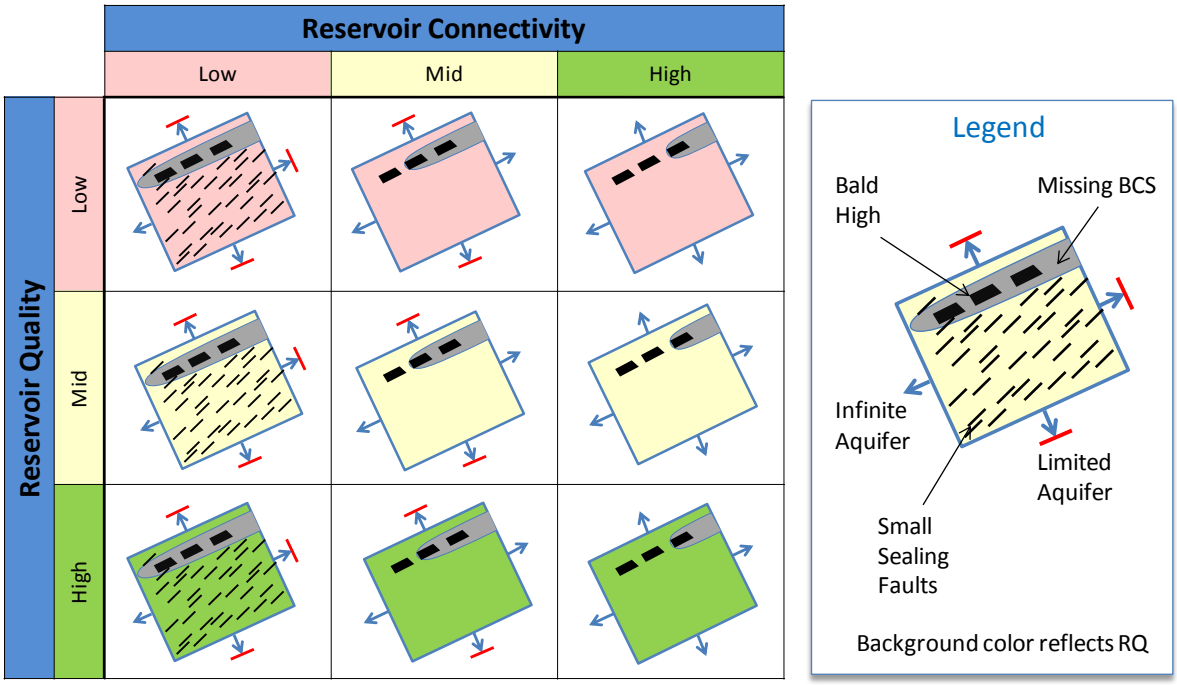

Figure 92: Gen-4 Pressure Modeling Realization Matrix with schematic representations

Not all realizations are simulated as the learning's from one can often be used to infer the result of running other simulations.

Table 30- Reservoir Quality uncertainty configuration for Pressure Model subsurface realizations

Property	Reservoir Quality Case		
	Low	Mid	High
NTG	Mid	Mid	High
Porosity	Low	Mid	High
Kh	Low	Mid	High
Kve/Kh	Mid	Mid	Mid
HED Facies	Mid	Mid	Mid

There is a positive skew in the NTG uncertainty range, with the Low case being significantly less than the mid case in the TDBM facies, see Section 3.2.2 on NTG. The compound probability of a realization that combined low NTG, porosity and associated permeability was considered extremely small and therefore not representative of a reasonable low case outcome (P90 equivalent). For this reason the Low Case Reservoir Quality realizations still uses mid case NTG, whilst the High Case Reservoir Quality realization uses high case NTG.

Table 31: Reservoir Connectivity uncertainty configuration for Pressure Model subsurface realizations.

Component	Reservoir Connectivity Case		
	Low	**Mid**	**High**
Elevated Basement	Low	Mid	High
Bald Highs	Yes	Yes	Yes
Isolated Highs	Yes	Yes	Yes
Sealing Faults	Yes	No	No
Connected Aquifers	3 of 4 restricted	2 of 4 restricted	All infinite

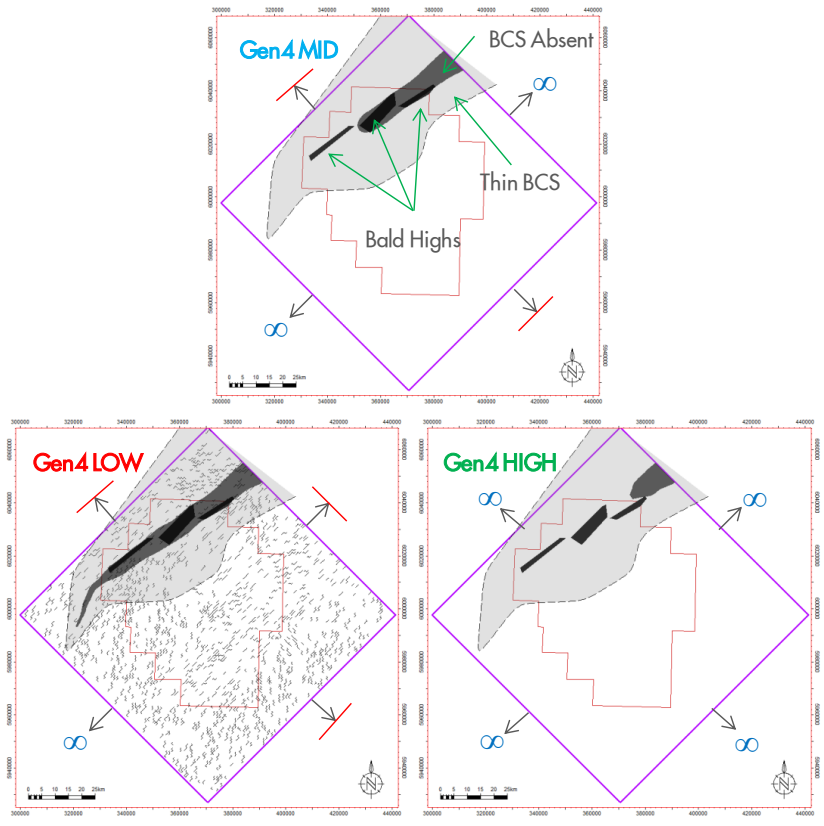

Figure 93: Gen-4 range of Reservoir Connectivity capturing BCS thinning and pinch out, faulting and connected aquifer.

7.4.1. Realization Probability

To give some context to the simulation results it is important to provide some assessment of the probability of any particular subsurface realization occurring. This allows better use to be made of simulation results in decision making. The probability of each of the subsurface realizations is shown in Table 32. This table assumes base case dynamic parameters. Sensitivities around the relative permeability, BHP constraint and skin will further reduce these probabilities.

Table 32 - Compound Probability of Gen-4 Pressure Model subsurface realizations.

Reservoir Connectivity			L	M	H
			0.2	**0.5**	**0.3**
Reservoir Quality	L	**0.3**	0.06	0.15	0.09
	M	**0.4**	0.08	0.2	0.12
	H	**0.3**	0.06	0.15	0.09

Reservoir Quality Outcome Probability

- Low: 0.2
- Mid: 0.5
- High: 0.3

There is a skew to high side in the probability across the three outcomes. This reflects the higher probability that there is likely to be some impact of basement topography on the distribution of reservoir quality in the BCS. Such a trend is incorporated into the mid and high case reservoir quality models but is absent in the low case. See Section 3.2 for more on the determination of the trends used in the property modeling.

Reservoir Connectivity Outcome Probability

- Low: 0.2
- Mid: 0.5
- High: 0.3

There is a skew to high side in the probability across the three outcomes. This reflects the low probability that there are a lot of sealing faults within the BCS and LMS that would restrict the ability of the aquifer to dissipate pressure induced by injection. The latest 3D seismic interpretation suggests that Pre-Cambrian faulting probably does not impact the BCS and equally is likely not present over most of the 3D seismic. Even if faulting were present, for all

those faults to be completely sealing in such a high NTG system is seen as improbable. The probability of the high case outcome reflects the considered opinion that such large pore volumes are rarely in perfect communication. The exact cause may not be known, but there is likely some reason for less than perfect connectivity on a regional scale.

7.5. Development Concepts

The range of development concepts or options for Quest has been significantly reduced following the outcome of Gen-3 modeling and the submission of the D65 regulatory application which was required to describe the development scheme being applied for. As a result the Gen-4 study was tasked with validating the selected concept given the updated range of uncertainty following the drilling of the Radway well 8-19 and acquisition of greater seismic coverage.

7.5.1. Development Givens

The following list describes the development "givens" in Gen-4:

- Well Type – vertical wells only
- Well Locations/layout– as per D65 + 3 additional priority locations selected from the 3D seismic as two of the original well locations carried in D65 were considered less attractive due to proximity to isolated pre-cambrian basement highs or the major pre-cambrian basement high to the NW
- Pipeline size – 12 inch NPS
- Compressor Size – 14.5 MPa output
- BHP limit of 28MPa with the potential to increase to 32 MPa.

For more details on reasoning behind those selections refer to chapter 5.

The only remaining uncertainties in the development concept are:

- Number of wells - how many of the eight specified need to be drilled
- Pipeline length – can wells all be located south of the Radway 8-19 location to reduce pipeline length?

In addition to the given parameters of the development concepts as mentioned above and rationalized in Chapter 5, and used consistently across the various subsurface modeling work streams, the pre-selected injector well locations where used in the pressure models for consistency with the regulatory submissions.

7.5.1.1. Well Locations

To progress the Directive-65 (D65) regulatory submission a total of five well locations were defined during the course of the Gen-3 modeling in 2010. These locations were based largely on the availability of surface access and, if located within the 3D seismic available at that

time, against the seismic to choose locations away from faulted basement areas. Following the delivery and interpretation of the complete re-processed seismic coverage these 5 well locations were re-validated. The interpretation on the completed seismic survey showed that two of the original 5 locations were sub-optimally located relative to basement topography and thickness of BCS.

The BCS is observed to thin towards the North onto a region of elevated basement as described above in 7.3.2 above. The 15-29 location was considered at risk of low BCS thickness. The 12-14 location was found to be located on an isolated basement high that likely has very thin BCS at that location. Given these findings further three locations were identified that met criteria for surface location, for interpreted BCS thickness and for distance from Pre-Cambrian faulting in the seismic.

The final locations of wells in the model and in the preferred order of utilization are as follows, see Figure 94 (to be confirmed after ongoing landowner engagement at the moment of writing this report):

1. 8-19-59-20W4 (Radway, already drilled)
2. 7-11-59-20W4
3. 5-35-59-21W4
4. 15-16-60-21W4
5. 10-6-60-20W4
6. 15-1-59-21W4
7. 15-29-60-21W4
8. 12-14-60-21W4

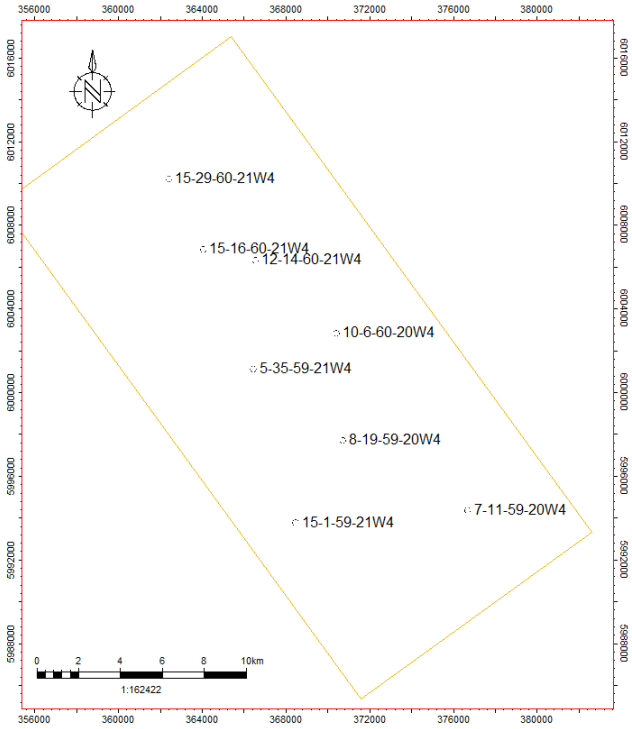

Figure 94: Gen-4 Well Locations (pending final confirmation after landowner consultation)

7.5.2. Local Grid Refinement

The pressure models are relatively coarse for the purpose of adequately describing far field pressure response in the reservoir; however, a finer scale grid is required to allow the simulator to model both the pressure profile and the relative permeability changes near the wellbore. This is critical during the initial injection period as a delay to flush out a 750m grid block can take an artificially long time, which overstates the associated BHP's required which can affect the assessment on well count requirements. For this purpose it was determined that nesting 3x3 grid refinements is the most efficient way of drilling down to refined near well grid blocks. The table below (Table 33) summarizes the effect of this approach on grid size per level of nesting.

Table 33: Block Size For Nested 3x3 Local Grid Refinements.

Nest Level	Local Grid Refinement	
	Block Structure	Block Size (m)
No LGR	1x1	750
Single - LGR1	3x3	250
Double - LGR2	3x3,3x3	83
Triple - LGR3	3x3,3x3,3x3	28
Quadruple- LGR4	3x3,3x3,3x3, 3x3	9

Figure 95 illustrates the convergence of BHP and block pressure for the Radway 8-19 well for the Mid-Mid realization. It can be seen that a significant improvement is made with just a single LGR. Although a double nested LGR scheme is adequate for the purpose of getting early injection rates a triple nested LGR scheme was utilized for all realizations as illustrated in Figure 96.

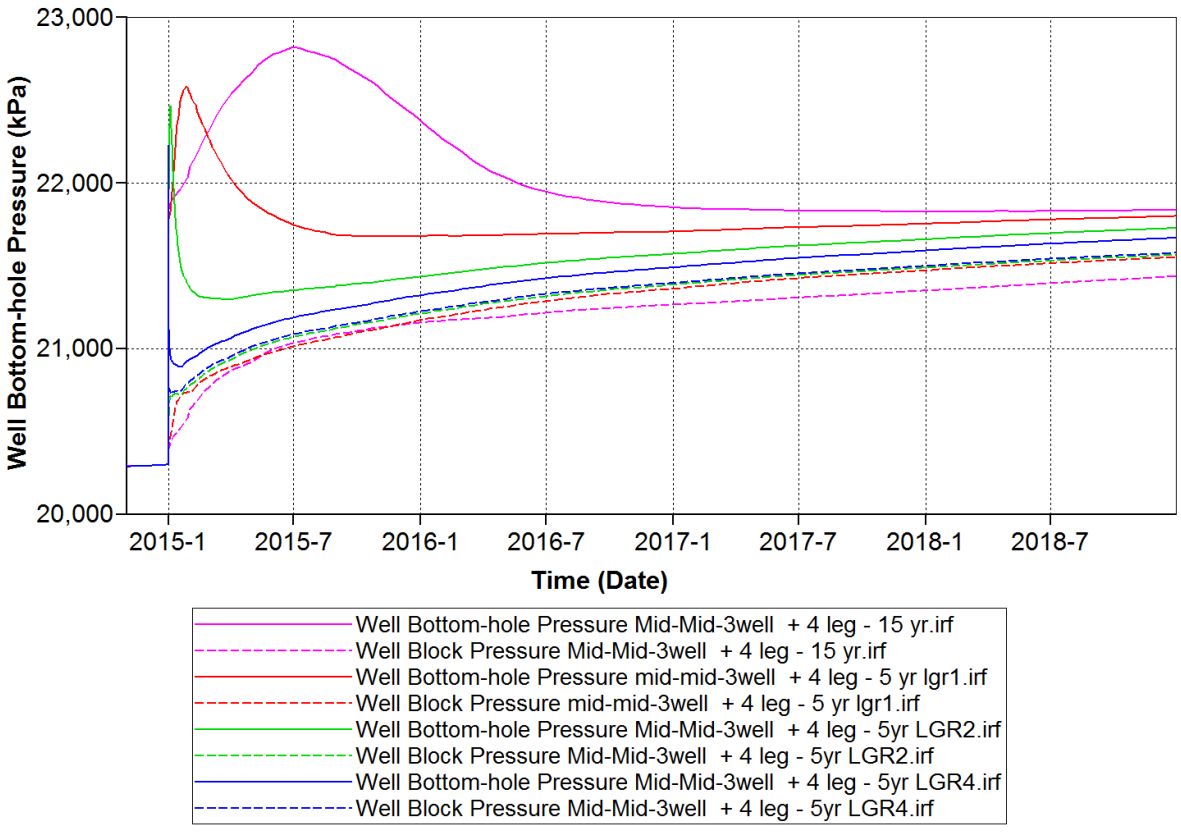

Figure 95 – Radway 8-19 LGR sensitivity Plot for LGR1, 2, & 4.

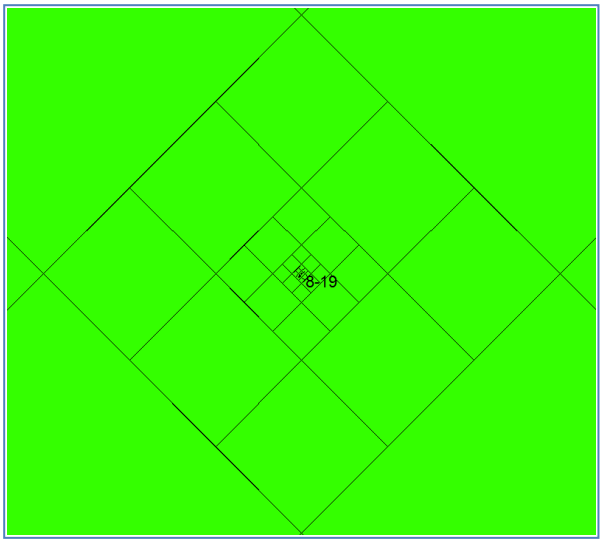

Figure 96 - A triple nested 3x3 LGR resulting in a matrix of 28 x 28 m grid blocks surrounding the well.

7.6. Solution Space

The Gen-4 Solution space captures the results of combining a subsurface realization with a particular development concept and assessing well count. By running numerous combinations in the dynamic simulator a robust estimate of the required numbers of wells can be derived. In principle the development concept that meets the required performance across the full range of subsurface uncertainty is the optimum solution. If a particular concept only fails against a highly unlikely subsurface outcome it may still be selected as the most robust concept.

Quest CCS - Generation 4 Reservoir Modelling

				Base Case		Growth		Urban Planning
				1	2	5	6	7
Pipeline Size (Inches)				12	12	12	12	12
Compressor Size (Mpa)				14.5	14.5	14.5	14.5	14.5
BHP Constraint (Mpa)				28	29	28	32	28
Throughput (MM T/yr)				1.08	1.08	2.4	3 - 10	1.08
Neighbor Developments?				No	No	No	No	Yes
Rationale				3-8 well development	3-8 well development with an additional 1 MPa of max BHP	Quest to accommodate injection of larger volumes at higher rates.	Quest to accommodate injection of much larger volumes at higher rates.	Combined ACOby competing developments.
Schematic Layout 3 Well Tested Inferred 5 Well Tested Inferred 8+ well Tested Inferred				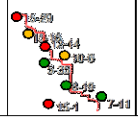	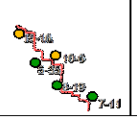	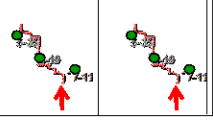		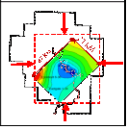
	Relization	Static	Dynamic					
A		MID-MID Base Case Mid Properties Mid Connectivity	L	Sensitivity	Sensitivity			
			M	Base Case: 3 well		30 MMT additional capacity	150 MMT additional capacity	1500 km2 required; 30x50 km
			H					
B		MID-HIGH Mid Properties High Connectivity	L					
			M					
			H					
C		Mid-LOW Mid Properties Low Connectivity	L					
			M	Base Case: 3 well				
			H					
D		LOW-MID Low Properties Mid Connectivity	L					
			M	8+ wells; need to step out locations to distribute pressure				
			H					
E		LOW-HIGH Low Properties High Connectivity	L					
			M					
			H					
F		LOW-LOW Low Properties Low Connectivity	L	Most Wells				
			M	8+ wells; need to step out locations to distribute pressure	5 wells			
			H					
G		HIGH-MID High Properties Mid Connectivity	L					
			M					
			H					
H		HIGH-HIGH Tank High Properties High Connectivity	L					
			M					
			H	Least Wells				
I		HIGH-LOW High Properties Low Connectivity	L					
			M					
			H					

Figure 97: Quest Gen-4 Solution Space linking subsurface realizations to development concepts.

7.7. Results

A primary objective of Gen-4 modeling effort is to assess the potential for achieving sustained injectivity in the presence of current subsurface uncertainty. The number of injector wells required at Quest is a critical component of the development plan and associated economics.

The range of wells required to mitigate the range of subsurface uncertainty is 3 – 8 vertical injection wells.

Gen-3 modeling suggested a range of between 3 and 10 wells as being necessary depending upon the subsurface realization. Gen-4 modeling involved integration of the recently drilled and tested Radway 8-19 well and the acquisition of the full area of 3D seismic over the development AOI. Gen-4 results now show that the range of wells required is slightly less than Gen-3 with only 3 wells being the expectation, and 5 wells being probable. Low probability cases, primarily with reservoir properties considerably poorer then the Radway well, could extend the well count to 8 or more wells. It should be noted that the Basis Of Design and Storage Development Plan have a 5 well scenario as the base case with an opportunity to reduce this to 3 wells pending the results of the development well 2 & 3 to be drilled in 2012. (Crouch, 2011)

Further evaluation of the expectation case concludes the following:

- Less than a 3MPa delta pressure is required to successfully inject 27 Mt of CO_2 into the BCS over a period of 25 years.
- There is significant potential growth in the current AOI:
    - More than double the current volume targets of CO_2 could be injected into the expectation case wells.
    - Alternatively an increased injection rate of up to five times the base case could be utilized.
- The approved AOI is sufficient area that potential offset sequestration schemes are not a concern for the current volume targets.
- In all cases except the low reservoir property cases the BCS pressure at legacy wells never reached a level where it can potentially overcome the static head and lift BCS brine into ground water.

7.7.1. Number of Injection Wells Required

Injectivity modeling over the full range of reservoir realizations has demonstrated that all considered reservoir scenario's can provide sufficient initial injectivity with three to five injection wells. The Solution Space shown in the previous chapter presents all the probable scenarios arising from the combination of subsurface realizations and development concepts. A few key cases that support the opening statement will be elaborated in this section.

As the majority of the aquifer area (10 000 km^2) influencing the injectivity of the wells are intrinsically modeled there is little impact observed by adding limited or infinite analytical aquifers to the edges of the model as discussed in the previous chapter. For robustness the

analytical aquifer extensions were therefore turned off for all runs discussed here. Once the project is operating with final well count it is recommended that the aquifer extends be revisited in detail as they will have a significant impact on closure conformance.

Expectation Case:

In the Mid reservoir property and Mid reservoir connectivity scenario, three wells are more than adequate to sustain an injection plateau of 1.08 Mtpa for 25 years without ever reaching bottom hole pressure constraints. This is illustrated in Figure 7.13 & 7.14.

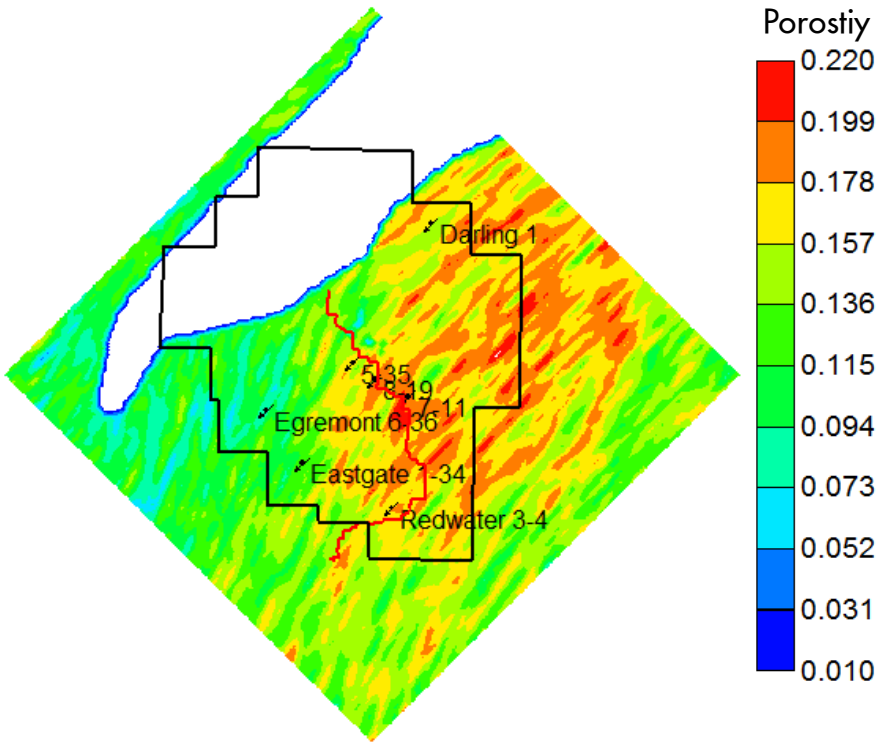

Figure 98: Expectation case reservoir property & reservoir connectivity scenario map

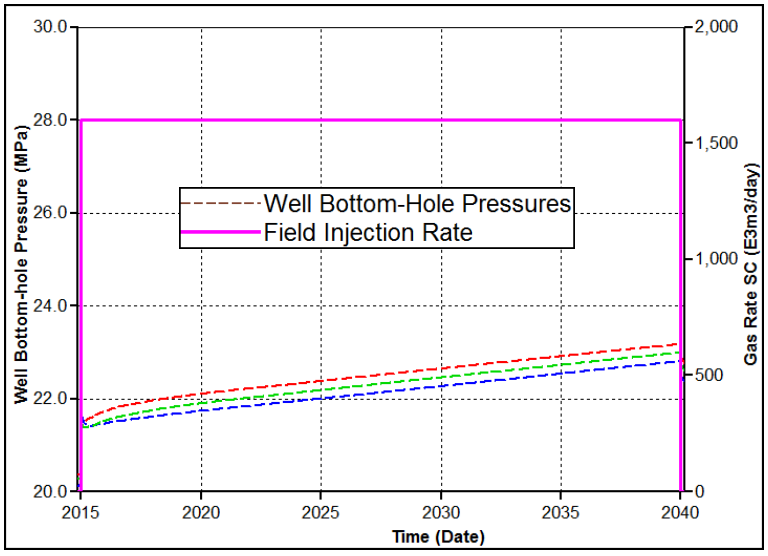

Figure 99: 25 year FBHP forecast for a three injection well development in the base property and base connectivity scenario.

The expectation case realization can successfully inject the required volume of CO2 in a 25yr period with only the Radway well. However this is an unrealistic outcome as more than one well will be drilled to overcome uncertainty and reliability risk. At least a second well is required to provide backup injection in case the first well is shut-in for operations reasons. However, without certainty that the second well will be as good as the Radway well and if the next wells had reservoir properties closer to either the Scotford and Redwater wells then it would be unable to handle the full injection rate, therefore, a third well is needed. Furthermore, confirmation of reservoir quality on a larger scale is required prior to commissioning the project to ensure we have sufficient well count. Therefore a continued appraise while develop strategy has been adopted starting with a total of 3 wells.

Low-Low Case:

In the low reservoir property and low reservoir connectivity scenario, five injection wells are more than adequate for start-up and will be able to sustain an injection plateau of 1.08 Mtpa for 13 years before reaching a bottom hole pressure constraint of 28 MPa. This is illustrated in Figure 101 and Figure 102. If for some reason we misjudge the results of the first 3 wells and end up in the low-low realization we will observe very high injection pressures at the well and have approximately 5 years to add additional wells.

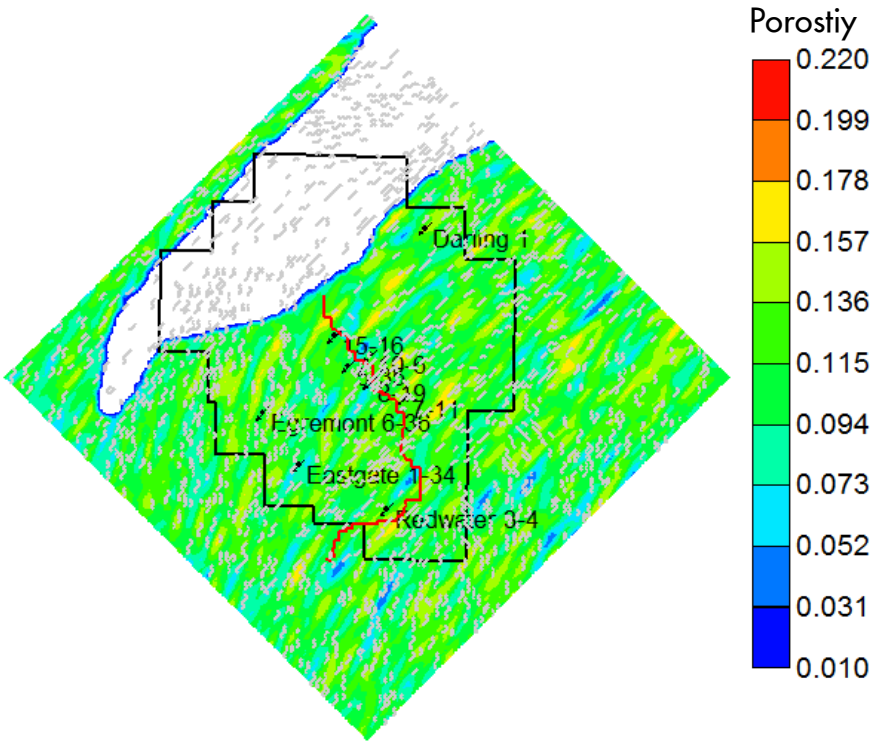

Figure 100: Low property and low connectivity scenario map.

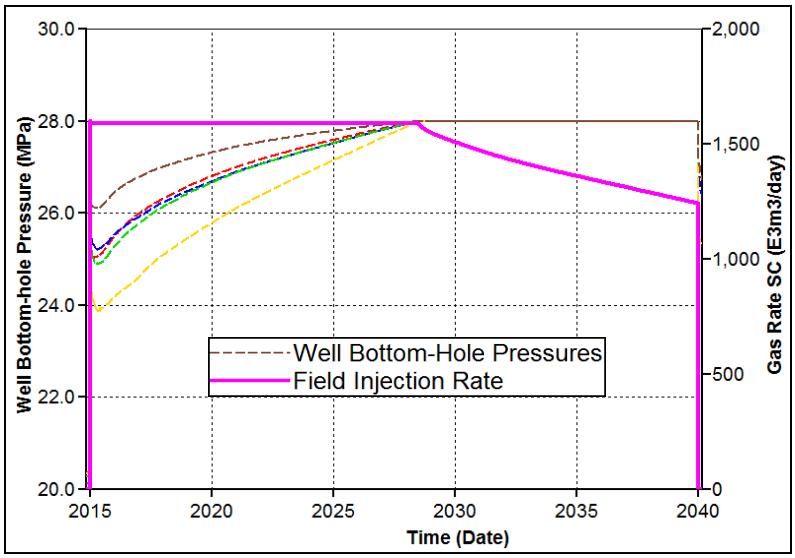

Figure 101: 25 year FBHP forecast for initial five injection wells in an eight well 2 phase development in the low property and low connectivity scenario.

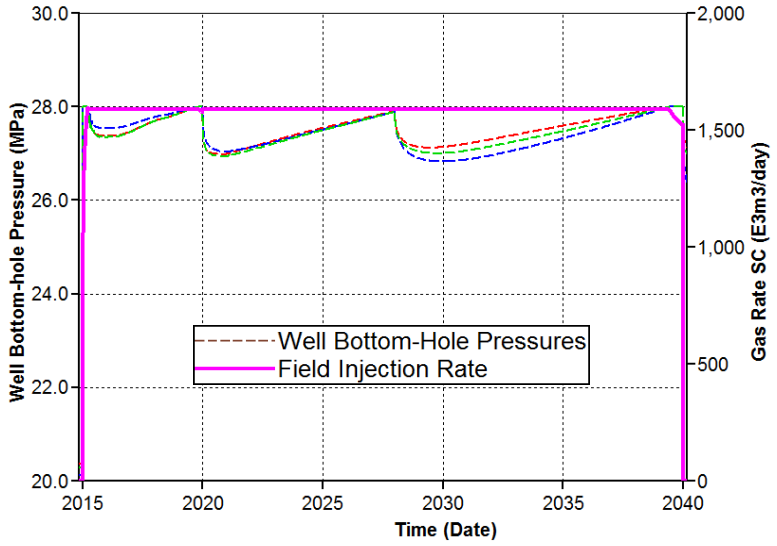

Figure 102: 25 year FBHP forecast for initial three injection wells in an eight well 3 phase development in the low property and low connectivity scenario.

7.7.2. Injectivity declining with time

The low reservoir property and low reservoir connectivity scenario illustrated in Figure 100 is an example of a reservoir realization that could result in declining injectivity with time. Other scenarios that could have a similar effect are:

- A gradual build-up of well bore damage or increasing skin could be another reason, but this is expected to be at least partially reversible through well intervention (i.e well bore clean-up or acid stimulation).
- Increasing CO2 viscosity with decreasing temperatures and increasing non-Darcy skin with increasing well rates were also investigated with marginal impacts.

All of the above impacts can be mitigated by increasing injection pressure. Only in the low reservoir property and low reservoir connectivity scenario low-low realization, after 13 years of injection, when we reach our maximum FBHP do we need to consider other measures. The declining injectivity in the low-low scenario is the result of a combination of limited aquifer connectivity and a low BCS reservoir storage capacity. There are two potential mitigations to pressure build-up in the BCS:

1) by spreading out the injection wells over a larger area (i.e infill drilling on the perimeter of the development)
2) the most effective way to address a shortage of storage capacity is to increase that capacity by lifting the bottom hole pressure constraints from the current 28MPa BHP constraint to the 32 MPa BHP requested from the ERCB in the D65 Regulatory submission.

These two mitigations to declining injectivity, infill drilling and increasing BHP constraints are illustrated in Figure 103 and Figure 104 respectively. Note that the eight wells used in Figure 103 were the wells applied for and that strategic placement of perimeter wells could reduce required well count.

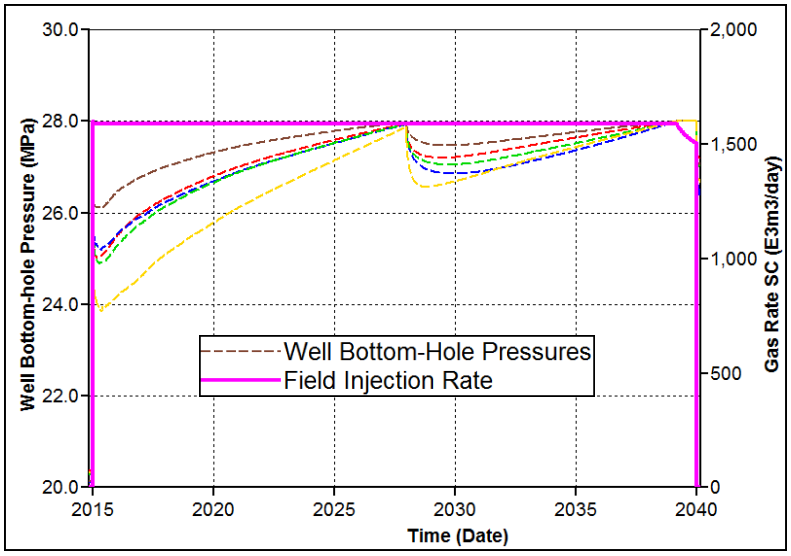

Figure 103: 25 year FBHP forecast for a five injection well development ramping up to eight injection wells in 2028 in the low property and low connectivity scenario.

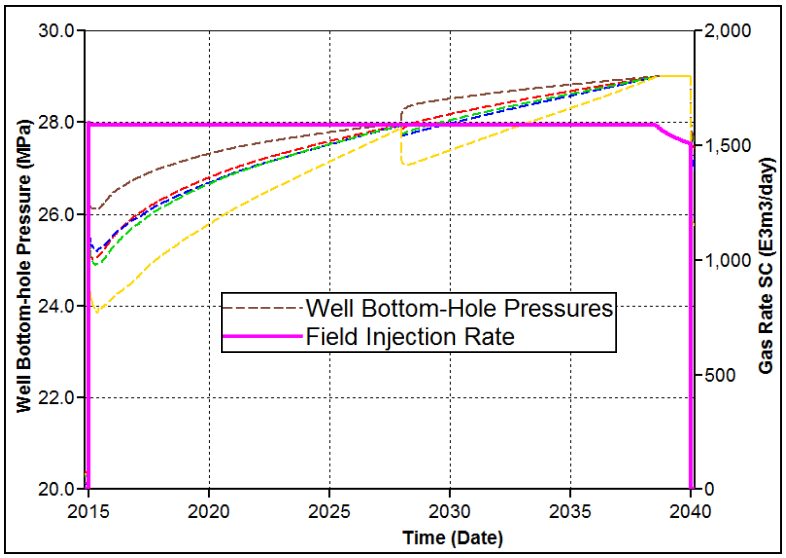

Figure 104: 25 year FBHP forecast for a five injection well development at a 28 MPa BHP constraint ramping up to 29 MPa between 2028 and 2039 in the low property and low connectivity scenario.

7.7.3. Growth Scenario

There is allot of potential for further CO_2 sequestration within the in the current Pore Space Tenure AOI. The industrial heartland around Fort Saskatchewan has the potential for considerable volumes of additional CO_2. This can be realized by either continuation of injection of 1.08 Mtpa past 2040 or by increasing the injection rates. The compressor and pipeline have been designed to have spare capacity in the event of the expectation case realization. A mid reservoir quality, low reservoir connectivity, mid dynamic property realization with 3 injection wells was ran at 1.08 Mtpa for 75 years as illustrated in Figure 105. A mid reservoir quality, mid reservoir connectivity, mid dynamic property realization with 3 injection wells was ran at 5.2 Mtpa for 25 years as illustrated in Figure 106.

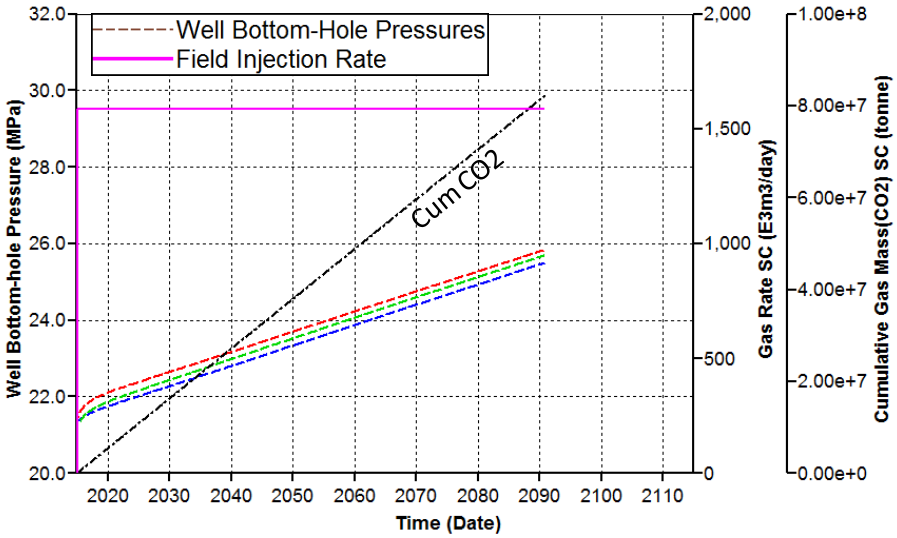

Figure 105: 75 year FBHP forecast for a three injection well development injecting 1.08 Mtpa in the mid property and mid connectivity scenario.

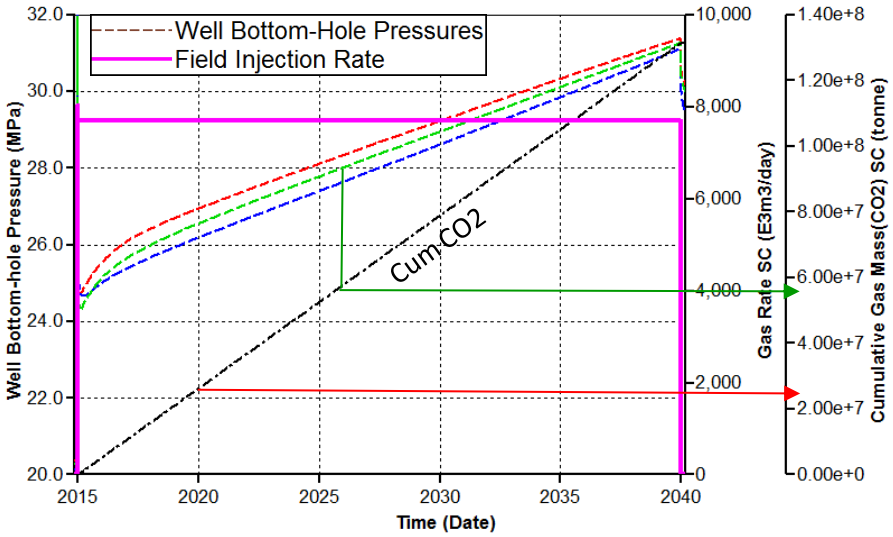

Figure 106: 25 year FBHP forecast for a three injection well development injecting 5.2 Mtpa in the mid property and low connectivity scenario.

These two figures imply:

- that the 1.08 Mtpa rate can be maintained for about 100 years before approaching the maximum BHP; it would seem prudent to increase the rate to utilize this asset.
- Or that the targeted 27 Mt's could be injected at 5.2 Mtpa in about 5 years (red arrow); this leaves an additional 20 years to sequester 5 times as much CO_2. It should be noted that we hit the 28 MPa bottom hole pressure constraint after 10 years injection which corresponds to injection of double the target volume (green arrow). However, at that point it would be entirely feasible to add new injectors within the existing pore space to extend the plateau for the required duration of injection; in this illustration the bottom hole pressure constraint is overridden and injection continues to 2040.

Various permutations can be conceived with combinations of rate, time, BHP, well count, and well location for the various geological realizations. However, it is most likely that the Quest project has room for considerable future additional CO_2 volumes.

7.7.4. Offset CO2 Sequestration Schemes

In the event that a mid to high reservoir property realization is confirmed it is possible that offset CO_2 sequestration schemes may be developed in the future. Offset schemes would effectively shrink the pore volume available to quest for pressure relief. The expectation case scenario was run iteratively while shrinking the models boundaries to determine how large of an area we will likely need. Figure 107 illustrates that an area of approximately 1500 km² is required to contain our 27 Mt of CO_2 while not exceeding the designed maximum bottom hole pressure of 28 MPa. With lower reservoir properties a larger area or more wells and or higher injection pressure would be required.

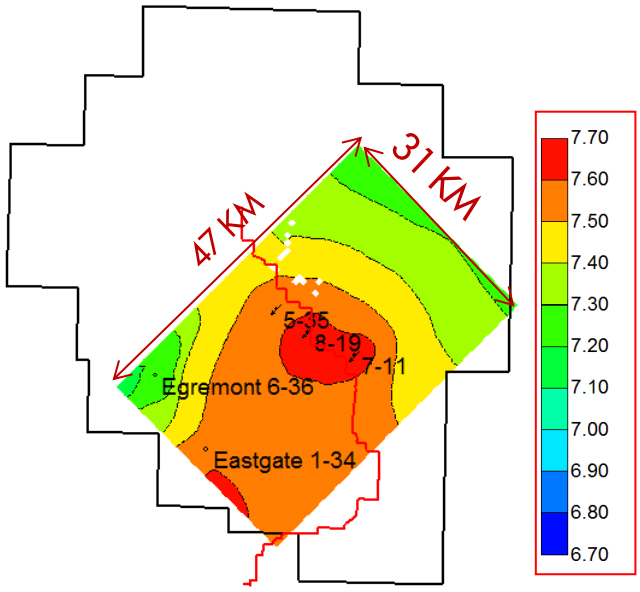

Figure 107: Minimum area required to inject 1.08 Mtpa of CO2 into three wells over 25 years in the mid property and mid connectivity scenario without exceeding 28 MPa FBHP.

7.7.5. Legacy Well Pressures

The four legacy wells in the AOI will encounter pressurized saline brine. Given the BCS reservoir pressure (20,036 kPa) and insitu fluid gradient (11.7 kPa/m) a minimum incremental pressure of 3.3 – 4.5 MPa in the BCS would be required to lift BCS brine into the Base of Ground Water Protection zone (BGWP) through an open hole at hydrostatic conditions (See Table 34. Note that the Westcoast 9-31 legacy well does not penetrate the BCS and therefore was not included in the modeling. However, the Redwater 3-4 project well was included as an observation well.

Table 34: Pore Pressure increase required to lift BCS brine to the Base Groundwater Protection (BGWP)

Well Name	Surface elevation (mBSL)	BGP depth (mBSL)	Hydrostatic pressure at BGP (kPaa)	Extrapolated BCS pressure at BGP (kPaa)	Delta P (kPa)
Imperial Eastgate No. 1-34	-641.3	-401	2,456	996	3,452
Imperial Egremont W 6-36	-627.9	-408	2,259	1,175	3,334
Imperial Darling No. 1	-704.4	-469	2,406	1,795	4,201
Westcoast 9-31	-699	-471	2,338	1,808	4,146
NOTE: mBSL – metres below sea level					

Current dynamic models indicate that the pressure increases expected at the legacy wells will be about half that required to lift BCS brine into the BGWP or to surface (see Figure 108). Note the pressure build is plotted as a negative pressure drop at legacy wells. Furthermore Figure 99 illustrates that in the expectation case the FBHP does not ever exceed the delta pressure required to lift BCS brine to BGWP at the injection wells. Figure 109 illustrates that in the event of a low property and low connectivity case we have 15 years to implement a mitigation strategy.

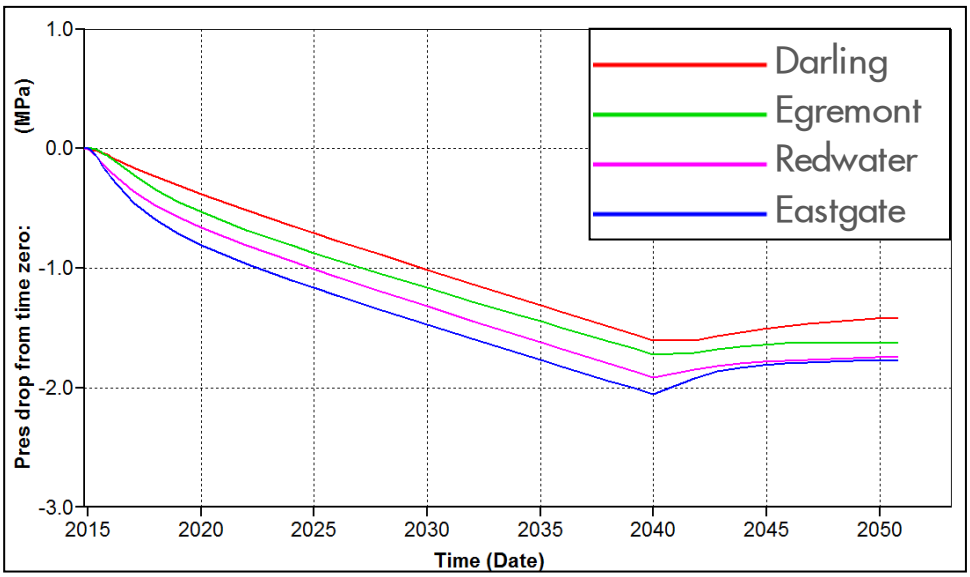

Figure 108: 25 year pressure drop from time zero forecast for the legacy wells using the mid property and mid connectivity scenario.

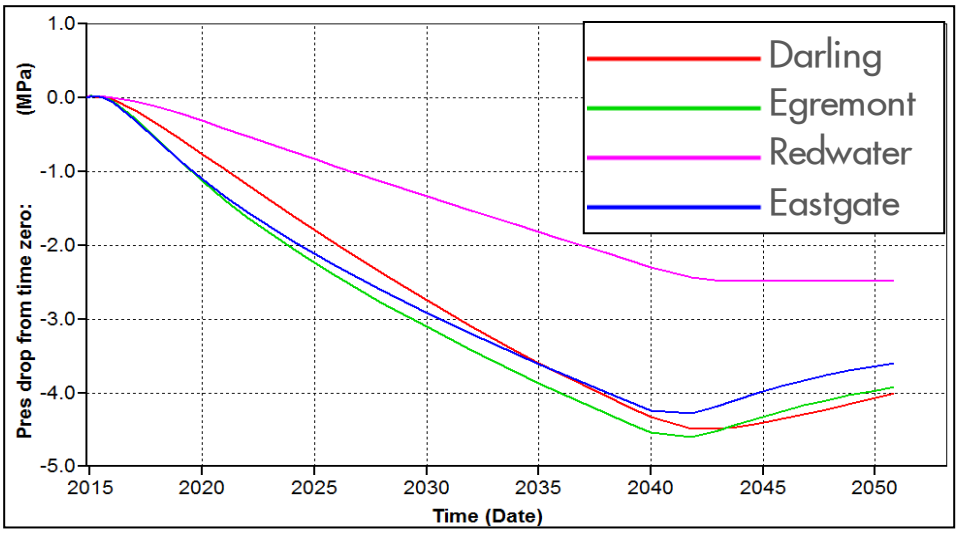

Figure 109: 25 year pressure drop from time zero forecast for the legacy wells using the low property and low connectivity scenario.

However, if one includes the analytical aquifer extension we can see that the pressures at the legacy wells are predicted to be at or below that required to lift BCS brine into the BGWP or to surface (see Figure 110). 10 years into the project it is very reasonable to assume that a combination of well and reservoir management, possibly with infill drilling, could keep the pressures at the legacy wells below the lift threshold. For example, the slope change in 2028 indicates that one of the new wells is in close communication with Egremont and causing it to pressure up faster, injection pressures at this well could be restricted. Figure 111 illustrates that with mid connectivity the Ergemont well does not experience the pressure increase observed in the low connectivity case as the injection is more spread out.

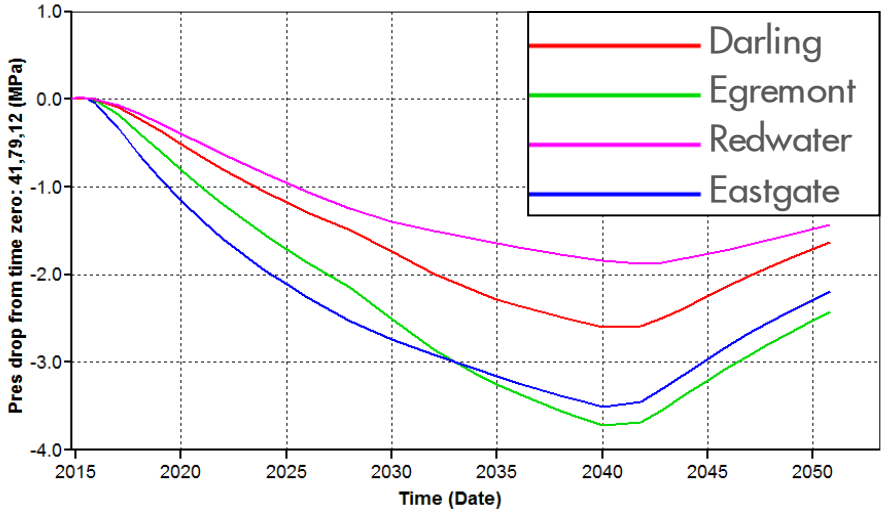

Figure 110: 25 year pressure drop from time zero forecast for the legacy wells using the low property and low connectivity scenario with analytical aquifer extension.

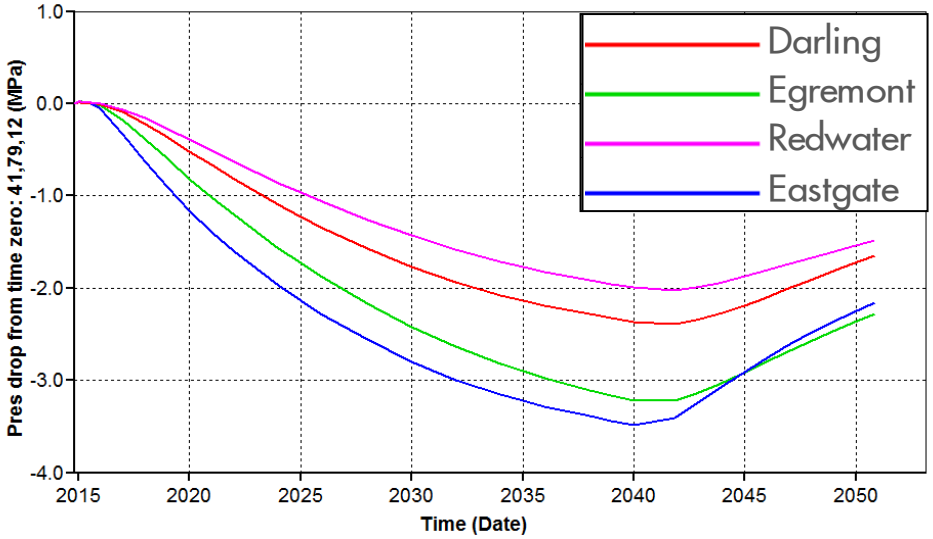

Figure 111: 25 year pressure drop from time zero forecast for the legacy wells using the low property and mid connectivity scenario with analytical aquifer extension.

Alternatively, accepting the leakage risk is a plausible solution as the delta P at the wells is small and for a short duration. Furthermore, the resulting up-hole contamination is expected to be negligible. A 1 km compositional radial well model was constructed from surface to basement for the Dariling-1 legacy well to see what cross flow would look like should it exist. The results are captured in section 0.

8. GEOCHEMISTRY

Geochemical reactive transport modeling can help understand CO_2-brine-rock interactions and provide input for evaluating injectivity, containment, trapping efficiency and geochemical aspects leakage of either CO2 and acidic brine into shallow aquifers. This chapter will cover Gen-4 integrated modeling aspects of the geochemistry study such as:

- halite precipitation and mitigation in a well scale domain using a 2D radial model,
- geochemical processes in the BCS during and after CO_2 injection in near wellbore region using a 2D radial model
- geochemical alteration of the Belly River aquifer due to leakage of CO_2, acidic brine or native BCS brine, and
- vertical migration of CO_2 through hypothetical pathways in a radial 2D model domain including the possible effects of geochemical reactions between the migrating CO_2 and the seal rock using a Cartesian 2D model.

Additional geochemical work has been done, capturing aspects of water compatibility during injection testing of the BCS, the impact on adding KCl during such operations including an geochemical assessment of the effectiveness of a HCl treatment of the formation. These findings are compiled, in addition to the results of the above studies, in the Quest Geochemistry Report (Zhang, 2011).

It should be noted that the formation and fluid properties as used in the geochemical models are consistent with the inputs as used in other Gen-4 activities such as the plume modeling, pressure modeling and well and overburden leak path models.

The models studying the vertical migration of CO_2 and brine through hypothetical pathways (leak pathways) are covered in section 9.5 of the Leak Path Modeling chapter. This also applies to the study of the potential geochemical alteration of the Belly River aquifer since this is a hypothetical leak event as well.

The geochemical models have been performed using TOUGH2/TOUGHREACT software package developed at Lawrence Berkeley National laboratory and licensed to Royal Dutch Shell Inc.

8.1. BCS reservoir mineralogy and brine chemical composition

8.1.1. Mineralogy

The Basal Cambrian Sandstones comprises tidal dune complexes, tidal channels, proximal and distal bay sediment, and thus is a typical aluminosilicate clastic sandstone formation. Based on Radway well data, the BCS is observed between 2040 m -2080 m below the ground surface where temperature is about 60^{o}C and pressure is about 210 bars. Quartz (~65% in average) is the dominant mineral. K-feldspar (~9%), plagioclase (albite/anorthite) (~1.5%), glauconite (<1.5%), carbonates (ankerite/dolomite/siderite) (<1%), anhydrite (<0.5%), clay minerals (<7% in total), zeolite (analcime-Na and analcime-K) (<0.2%) and pyrite (<0.3%)

make up the rest of the mineralogy. This mineralogical composition is slightly different from that found from the Redwater well in which no zeolite is present. Calcite does not occur in any of these wells. Major minerals are summarized in APPENDIX 6.

As the main rock-forming mineral quartz, K-feldspar and albite are original sediments with over-growths. Carbonate minerals such as dolomite, siderite and ankerite are secondary (i.e formed after the BCS has deposited). Calcite was not found and the calculated SI of calcite with respect to the BCS brine is below zero verifying the absence of calcite from the BCS environment. Two zeolitic members, Na-analcime and K-analcime (in trace amount) were observed, a rare occurrence, because these minerals usually form in alkaline environments and at higher temperatures. However, the extremely high concentration of Na in BCS brine (two-three orders of magnitudes higher than normal deposition environments) probably promoted Na-analcime formation under neutral pH. Clay mineral content is low and, especially, swelling clay minerals, e.g. smectite are not found.

8.1.2. BCS brine chemical composition

The BCS brine from the Radway well is a NaCl-dominant brine with NaCl concentrations up to a halite saturation (~6.3 mol) at the reservoir conditions (T>=60^{o}C and P~210 bar). APPENDIX 7 shows the measured brine composition and the aqueous species distribution at room temperature (20^{o}C) and reservoir temperature (60^{o}C), respectively.

The charge imbalance i.e., the ratio of the position-negative charge difference over the total charges is only -2.1%, lower than the generally-accepted criterion (i.e. absolute value <5%). This result indicates that, at least, the accuracy of the measured concentrations of the major ions i.e. Na^{+} and Cl^{-} is good. This is further verified by the calculated saturation index (SI) of halite (very close to zero) which is consistent with the possible presence of halite in the formation implying an equilibrium of BCS brine with respect to halite.

8.2. Modeling halite precipitation and evaluation of mitigation strategies

8.2.1. Cooling Zone and Halite precipitation

A radial TOUGHREACT model was built with the aim to:

1. Calibrate previous work (Gen-3) to the center of the Quest development while incorporating the formation properties and geochemical composition as encountered at the Radway 8-19 well location.
2. To also benchmark the thermal functionality of the radial GEM model (Chapter 4), this TOUGHREACT model was run in thermal mode to estimate the extent of the cooling zone during injection of cold CO_2.

As seen in Figure 112 below, after having injected 1/3 of the Quest CO2 volume in one well, the cooling zone reaches up to a distance of approximately 350m away from the well bore confirming the result of 320m as calculated in the thermal GEM model in Chapter 4, adding confidence that this new GEM functionality delivers reasonable robust results.

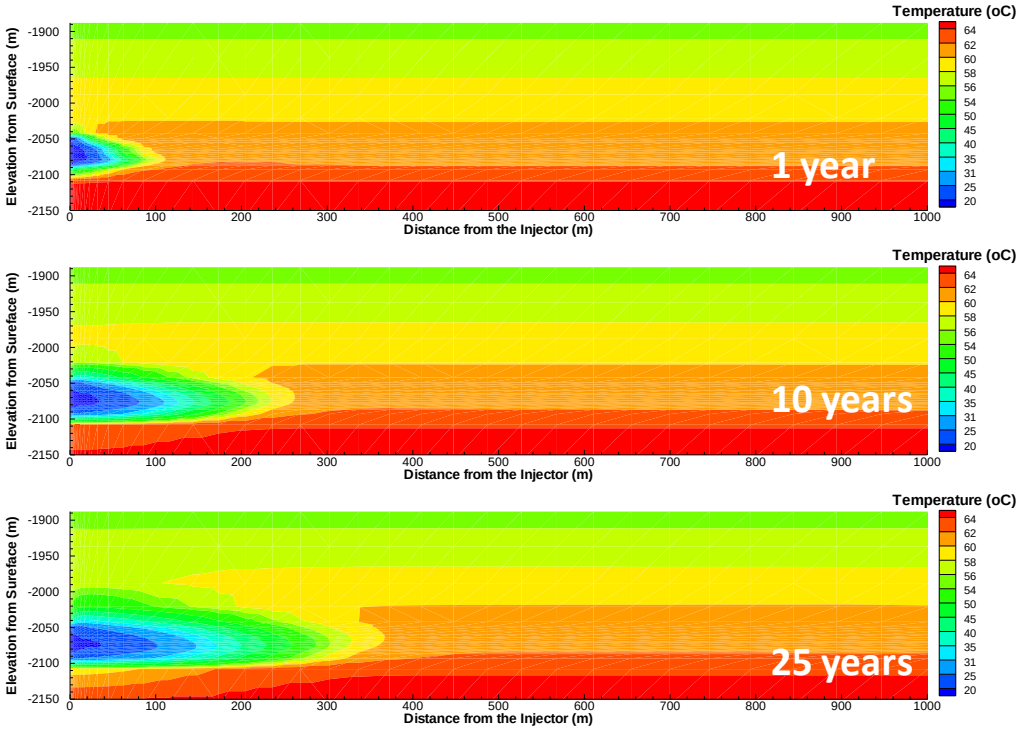

Figure 112: Simulated temperature evolution within the BCS reservoir during CO_2 injection.

As discussed above, BCS brine is halite-saturated at the reservoir conditions.

It is expected that halite will precipitate in the near well bore region due to brine evaporation.

The distribution of the precipitated halite in the BCS is controlled by multiple factors, mainly, CO_2 flow rate, formation heterogeneity, effective permeability and capillarity of the brine.

Assuming a 3-well injection plan (i.e. three injectors, and each injector takes 1/3 of the total injection rate), radial 2D single-well scale simulations were performed.

Initial results of the Gen-3 models based on Redwater well data indicated that the precipitated salt spans a radial zone of up to 60 m. Updating the geochemical models with Radway 8-19 properties and, more importantly, incorporating thermal cooling of the near well bore region as described above reduced the zone of halite precipitation to a radius of only 15m away from the well bore (for comparison see Figure 113).

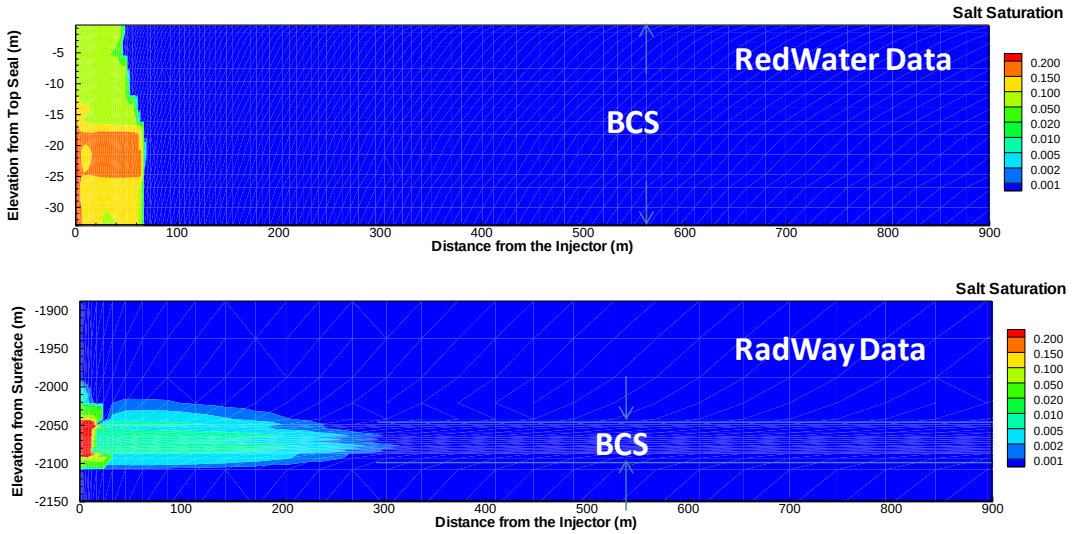

Figure 113: Halite precipitation in the near well bore region, (at the top Redwater well without considering cooling due to injection, below Radway properties and thermal cooling due to injection considered)

It also should be noted that the extent of the cooling zone as calculated in TOUGHREACT shows very good agreement with the results derived using the Thermal radial model as documented in chapter 4, adding confidence in the derived outputs.

8.2.2. Mitigation strategy

While the modeling of precipitation has added geochemical insight on the spatial distribution of halite precipitation and the dynamics of the process. It should be noted that no reports of halite precipitation causing loss of injectivity exists in available literature.

In the unlikely event that this phenomenon creates a challenge for Quest the following mitigation options have been considered and quantified via TOUGHREACT modeling:

- Post-flooding with fresh brine after halite precipitation occurred
- Pre-flooding the near well bore formation with fresh brine as also recommended by K. Pruess and others (Pruess, 2009)
- Co-injection of brine and CO_2 to create water saturated CO_2 (this may not be an option due to material selection)

The listing of above mitigation reflects the ranking with regards to both, efficiency and technical feasibility with the most preferred being post-flooding.

For more detail on the geochemical background of above options refer to the Quest Geochemistry Report (Zhang, 2011)

8.3. Modeling CO_2-water-rock interactions within the reservoir during the injection and flow back

Flow back of acidic brine into the well during injector shut-in, and associated potential corrosion, is of some concern. Estimating the flow back potential of acidic brine especially during the start up phase and early life of the project is of particular interest since the CO_2 front will not extent for from the well bore, hence rapid back flow of acidic brine can be expected.

To guide operational decisions during this phase, a TOUGHREACT screening study of arrival times as a function of "injection time until shut-in" was conducted. These simulations were performed for injection durations (before shut-in) of 1, 10, 30, 60, and 90 days, respectively. An example of a back flow simulation for a 30 day injection resulting in an acidic brine arrival at the well bore after 7 – 30 days is shown below in Figure 114.

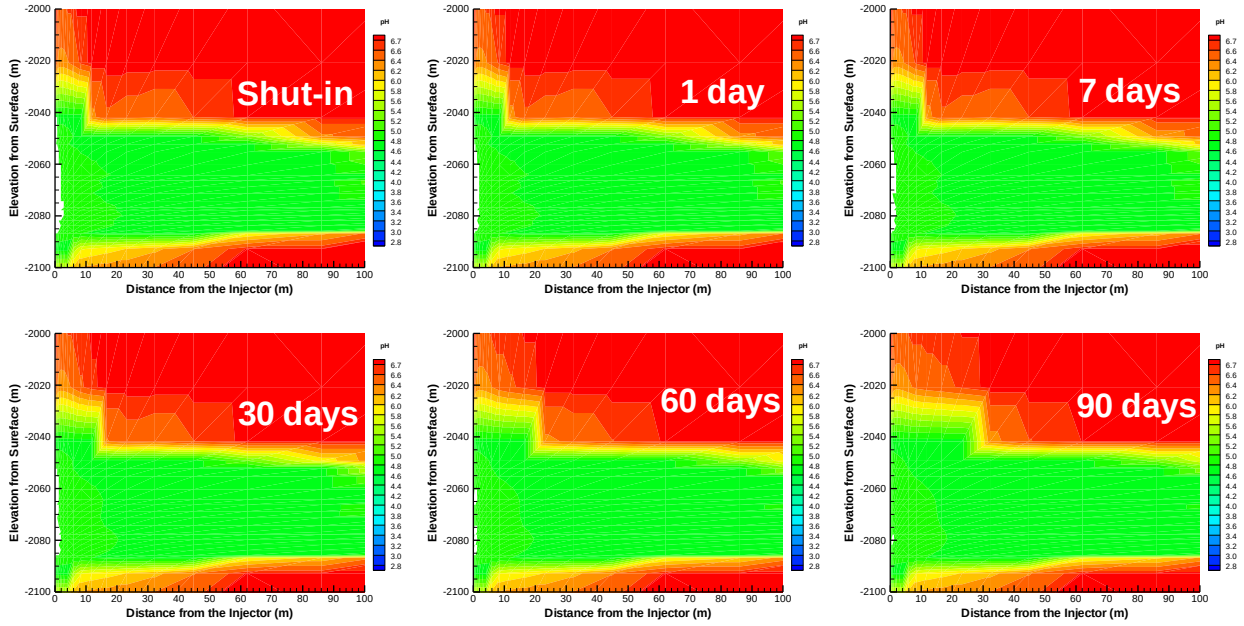

Figure 114: Modeled pH of the flow back of acidic brine after a 30-day injection of CO_2. In this particular case the dry out zone (white space of 1-2m) disappears between 7 to 30 days

In summary, the results indicated that:

- Brine acidification is mainly controlled by CO_2 injection and mineral buffering effects.
- During and after injection, the pH of the Radway brine will decrease to 4.6 with consideration of buffer minerals or 2.9 without mineral buffers. In contrast the pH of Redwater brine would decrease to 3.9 with mineral buffering.

- Mineral buffering depends on the mineral composition and will be highly likely in the BCS under CO_2 injection. Based on the mineralogy, dissolution of carbonates and zeolites will take effect at first and followed by dissolution of feldspars and precipitation of clay minerals.
- In all the scenarios, within 90 days, the backflow reaches the injector wellbore.
- Top and bottom sections of the perforation interval may be constantly in contact with the acidic brine in the top/bottom "seals".

Table 35 below summarizes the acidic brine arrival times, including extent of the dry-out zones, as a function of injection duration prior to injector shut-in.

Table 35: Summarized RTM results after CO2 injection paused at 1, 10, 30, 60 and 90 days, respectively.

Injection Duration (day)	pH-Radway	pH-Radway No buffer	pH-Redwater	Dryout extent (m)	Flowback Time (days after shut-in)
1	4.6	2.9	Not modeled	0	immediate
10	4.6	2.9	Not modeled	1	immediate-7
30	4.6	2.9	Not modeled	1.9	7-30
60	4.6	2.9	3.9	2.3	30-60 (Radway) 7-30 (Redwater)
90	4.6	2.9	Not modeled	4.0	60-90

8.4. Geochemical reactive transport modeling of vertical migration of CO_2

8.4.1. Modeling seal integrity

To assess the long-term-fate of the CO_2 plume within the storage container the interaction of CO_2 and acidic brine was simulated in an TOUGHREACT model using a surface-to-Precambrian 'throughout' radial 2D well-scale model.

Results indicate that:

- The injected CO_2 stays in BCS during the 25-years injection period and the first 100 years after the injection. This is in good agreement with the results of the CMG plume models.
- By 200 years, the plume body will start to invade the LMS (1970-2040m depth) on top of the BCS.
- At 500 years, a significant portion of the injected CO_2 will have entered the LMS.

- By 1000 years, most of the CO_2 will have come into the LMS, and until 2,000 years, the most of the still mobile CO_2 will have arrived in the LMS, and appears stabilized (see Figure 115).

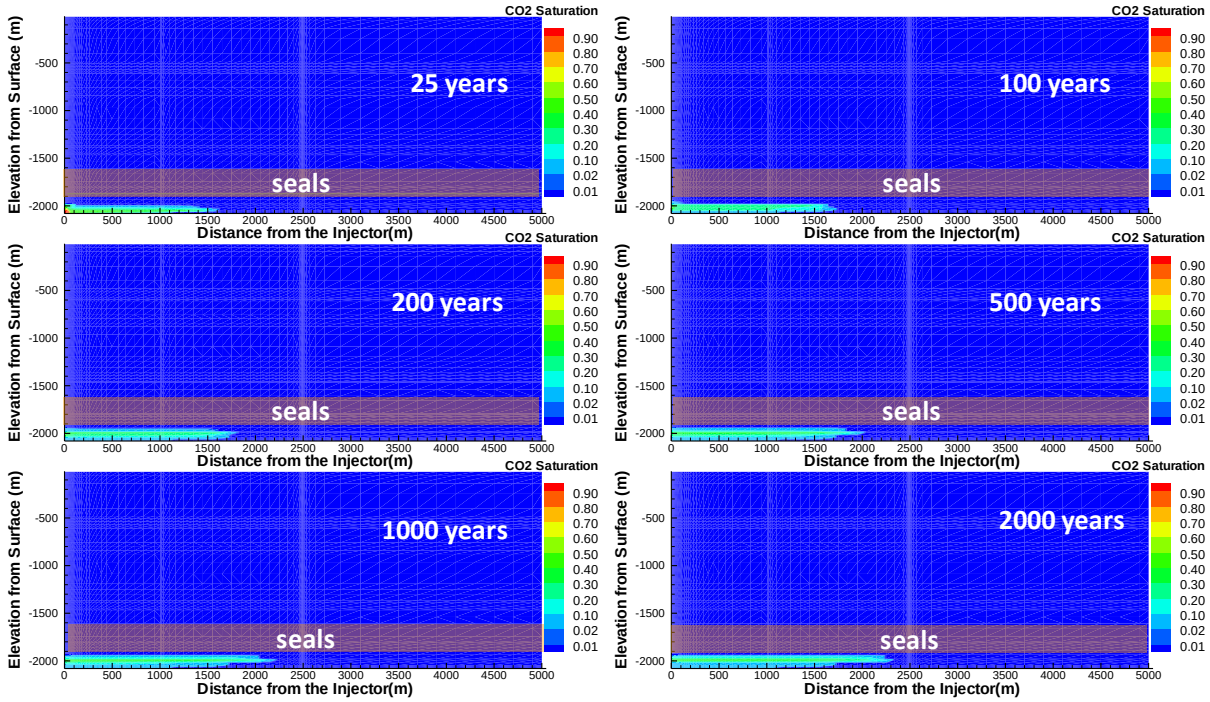

Figure 115: Modeled long-term (up to 2000 years) CO_2 plume migration indicating that CO_2 is restricted in the BCS and LMS formations and cannot break through the seals although most of the still mobile CO_2 stays in LMS (between 1970-2040 m in depths), rather than BCS (between 2040-2080 m in depth) due to the buoyancy effects.

For a detailed breakdown of geochemical reactions between seals and CO_2 and acidic brine refer to the Geochemistry report (Zhang, 2011).

9. LEAK PATH MODELING

9.1. Evidence for BCS Isolation

There is sufficient evidence for seal integrity and hydraulic isolation of the BCS aquifer from all the overlying aquifers within and in close proximity to the Quest AOI. The plotting and interpretation of geochemical data, discussed below, proves that the Basal Cambrian Sand (BCS) is indeed isolated. For additional evidence see the seal integrity report (El Mahdy, 2011).

9.1.1. Geochemical evidence of BCS isolation

Halogen concentrations, plotted on Figure 10-1 illustrate the key geochemical evidence for the Basal Cambrian Sands (BCS) being hydraulically isolated from all overlying aquifers within the area encompassing the Quest AOI and plausibly more regionally. Figure 10-1 is modified from the graphs used in references (Carpenter, 1978), (Hanor, 1994) and (Connolly, 1990) with public and Quest data. The Seawater Evaporation Trajectory (SET), the black line on Figure 10-1, plots a trajectory of evaporating seawater trapped in marine sediments. Along the SET Chloride: Bromide ratio (Cl: Br) is constant until Na:Cl salt saturation is reached. As halite is precipitated Cl is preferentially removed from solution creating a relative excess of Br in solution. Thus, waters that plot to the right of the SET are seawater evaporation brines and relatively enriched in Br.

The BCS data points plot very differently from the remaining formations, which would not be possible if the BCS was not hydraulically isolated from the overlying formations. The BCS brine is very high in chloride (Cl) and relatively depleted in bromide (Br) which is a classic salt dissolution brine composition. This brine received its salinity by dissolving NaCl salts as paleo-meteoric waters passed through evaporate-bearing strata up-dip to the NE of the AOI. (Bachu S. H., 1986), discuss the BCS as part of a basin scale basal aquifer and mapped regional free water levels illustrating a Westward to Eastward flow. The current observed free water level distribution is believed to be a relict of Laramide orogenically induced hydrodynamic drive which at present is slowly equilibrating to its more contemporary basin geometry controlled through a combination of tertiary to present erosion and uplift and Neogene glacial/interglacial subsidence and uplift respectively.

The remaining formations, except for the Belly River Group (BRGP), plot on the Seawater Evaporation Trajectory (SET). The Winnipegosis (WPGS) brine data plot as heavily sub-aerially evaporated seawater brine with minor to no paleo-meteoric influx. The WPGS, like the BCS, plots on its own as evidence of hydraulic isolation from the BCS below and Upper Devonian (UDEV) above. Note that no WPGS samples plotted here are from wells within the AOI. WPGS samples will be endeavored during the Quest baselining campaign.

Post Prairie Evaporite Upper Devonian carbonates (UDEV) contain sub-aerially evaporated seawater brines with major paleo-meteoric influx.

The Mannville Group (MNVL) and Colorado Group (CLRD) clastics contain formation fluids of higher salinity than seawater but are predominantly paleo-meteoric waters where Br may

have been attained in part through dissociation of Br from organics (hydrocarbon charge) ((Connolly, 1990).

The very young meteoric waters of the BRGP plot on their own trajectory and prove isolation from the underlying formations by the Lea Park shale which acts as a regional seal (Connolly, 1990).

The five major hydrostatic units, based on an observed lack of mixing and homogenization, are proposed as follows:

1. The BCS aquifer - sealed by the Middle Cambrian Shales (primary seal), the Lower Devonian Lower Lotsberg Salt (secondary seal) and the Lower Devonian Upper Lotsberg Salt (ultimate seal) which are expected to contain the CO_2 within the BCS storage complex.
2. The WPGS aquifer - sealed by the Middle Devonian Prairie Evaporite. Currently the data labeled WPGS represents the aquifer which is potentially an amalgam of formations found in the upper Elk Point Group which include the Winnipegosis (Keg River), Contact Rapids and where porous, the Ernestina Lake Formation.
3. The UDEV carbonates, and lower Cretaceous MNVL and CLRD Group clastics are sealed ultimately by the regionally extensive Lea Park and therefore cutoff from local surface recharge. The potential for connectivity between these two formations and the UDEV formations is not attempted or discussed here as it is not of primary concern to the BCS formation isolation discussion.
4. BRGP and surficial sediments are in contact with surficial meteoric recharge.

Current data coverage is limited for the BCS and WPGS as detailed in Table 36. Importantly no Br data exists for the WPGS within the AOI. A more comprehensive set of maps illustrating data coverage of all major aquifers can be found in the BCS tracer feasibility report and the BCS brine tracer feasibility report (Pierpont, 2011). Figure 117 below discusses the observed regional congruence of WPGS major ion chemistry, which is currently utilized as a proxy for halogen ratio plotting until high quality WPGS samples from within the Quest AOI are attained.

Both the Radway 8-19 and Redwater 11-32 (Scotford) wells show a significant range in halogen ratio variation that natural variability alone may be difficult to explain (Figure 10-1). The BCS brine Tracer Feasibility Report [5] discusses the potential contamination and sample handling issues. Regardless, all three BCS data plots in Figure 116 show strong evidence of a completely distinct origin and fate of BCS formation fluid from all other aquifers. Natural variability may still be playing a small but as yet undeterminable role in variability.

During future Quest baselining and well operations, multiple formation fluid samples will be attempted and used to further corroborate the current interpretation. Other lines of geochemical evidence are at different stages of understanding and will benefit from higher quality BCS brine samples. Here are examples of other lines of geochemical evidence:

1. Ca concentration vs. Total Dissolved Solids

2. Ca concentration vs. Total Cation concentration
3. Strontium isotopic ratio plots.
4. $\delta^{37}Cl$ and $\delta^{81}Br$ isotope ratio plotting.

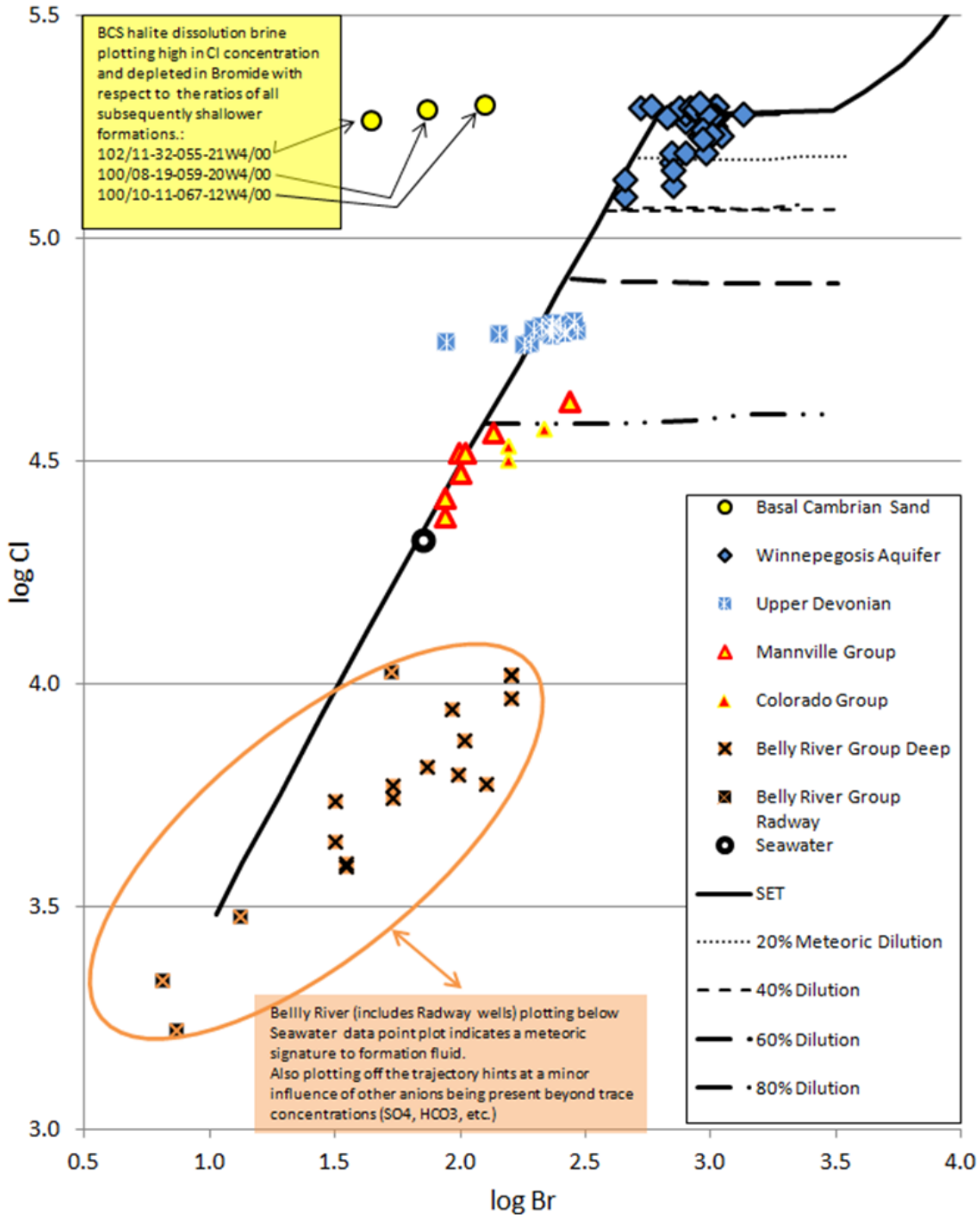

Figure 116: The seawater Cl: Br ratio plotted against the Seawater Evaporation Trajectory (SET).

Table 36: Summary of Data Coverage used for this report. Note Cl data is included in all TDS and Major chemistry data points.

Tracer Tracking Table - Data Currently available				
Please carefully Read L				
MMV Descriptor	Formation	Aquifer System	TDS & Major Ion Chemistry	Bromide (mg/l)
Shallow Groundwater & Base Groundwater Protection	Belly River	Belly River	(*200) / {231^^}	(*14) / {9^^}
As a Group considered a possible barrier to flow. Does contain permeable zones. Viking and Speckled Sst	Colorado Cardium First White Speckled SSt Second White Speckled SSt Viking Joli Fou	Colorado	(415^^) / {1078^^}	(5^^) / {37^^}
3rd Potential Major Mitigative Storage Unit	Grand Rapids Wabiska Mannville McMurray glauconitic sands ellerslie	Mannville	(153^^) / {305^^}	(5^^) / {6^^}
2nd Potential Major Mitigative Storage Unit	Wabamun/Winterburn Cooking Lake/Leduc Beaver Hill Lake	Upper Devonian	(223^^) / {131^^)	(15^^) / {13^^)
1st Potential Major Mitigative Storage Unit	Winnepegosis & Keg River	ElkPoint	(1^^) / {310^^} / [NR]	(0) / {40^^} / [NR]
1st Potential Minor Storage Unit	Ernestina Lake	Ernestina Lake	(0) / {?} / [NR]	(0) / {?} / [NR]
Secondary Strge	Granite Wash	Basal	(0) / {10^^} / [NR]	(0) / {1^^} / [NR]
Secondary Strge Primary Seal/Strge	Basal Red Beds/ Lower Marine Sands		?? ??	?? ??
Primary Storage	Basal Cambrian Sands		(*5) / {32} / [NR]	(2) / {1} / [NR]
	Undifferentiated		??	??

Numbers may be subject to change as more data becomes available and as QA/QC continues.

(8) / {15} / [2] = (Number of data points within AOI) / {Number of data points within Region as defined on Maps in Appendix 2} / [Number of Data Points from Williston Basin] NR-Not Required

Majority of Standard Chemistry from IHS searched data base commissioned by Alessandra Simone, 2009

* - Numbers include Quest obtained Data.

^^Public Data from Geoscout or Accumap

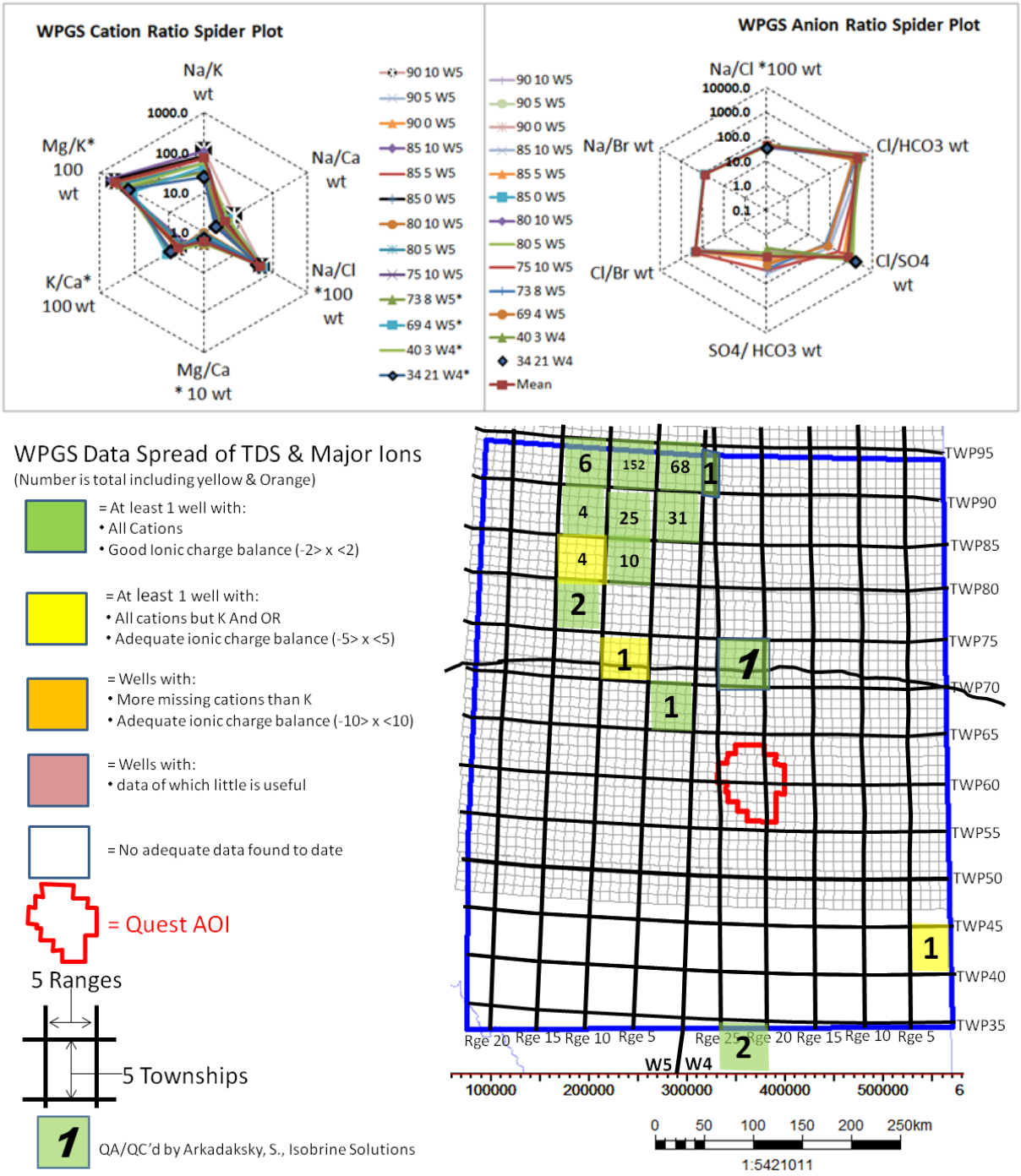

Figure 117: WPGS Major Ion Chemistry: The Graphs above plot mean values of major ion ratios for the WPGS at 5 township x 5 range zones delineated on the map (dark black lines).

9.2. Leak Path Modeling Objectives

There is very strong geochemical evidence for the isolation of the BCS from overlying aquifers suggesting the presence of a competent regional seal that has been acting for millions of years. However, an outcome to the external review held in late 2010 highlighted the need to evaluate a series of both plausible and hypothetical leak paths in greater detail in order to:

- identify any additional risks that have not been recognized to date that may need a more focused work plan moving forward
- create a holistic picture of the entire subsurface to support statements in Government and Public Discussions
- help identify MMV technologies and associated detection thresholds.

As a result, three models were built each serving its specific purpose:

1. Regional Petrel Leak Path Model that goes from surface to basement and covers the entire Sequestration Lease Application area used to help understand the structural/stratigraphic framework of the complete stratigraphic section.
2. Radial Well Model created in GEM to assess the potential leakage of BCS brine up a third party legacy well (i.e. Imperial Darling No. 1). The Radial well model used inputs from surface to basement from the closest available wells to the legacy wells in order to run a series of sensitivities on potential leak paths (See Section 7.7.5 Legacy Well Pressures). Where no information was available, the Radway 8-19 well data was used.
3. Radial 2D Well-Scale Geochemical Reactive Transport Models, of the Radway 8-19 well, built in TOUGHREACT to assess the hypothetical scenarios of leaking CO_2 and acidified brine:
    - creating a stratigraphic leak through the MCS Seal.
    - migration of CO_2 and brine out of the BCS storage complex via an injection well
    - migration of CO_2 and brine out of the BCS storage complex via a hypothetical fault.

Each model evaluated the potential for CO_2 to leak out of the BCS storage complex and above the Base Groundwater Protection Zone (BGWP). The entire stratigraphic section from surface to basement was modeled taking into account the average properties of the various aquifers (Figure 118). The GEM and TOUGHREACT radial well models used properties from the Radway 8-19 well and other offset wells where Radway 8-19 data was not available. The Regional Petrel model used multiple wells as input.

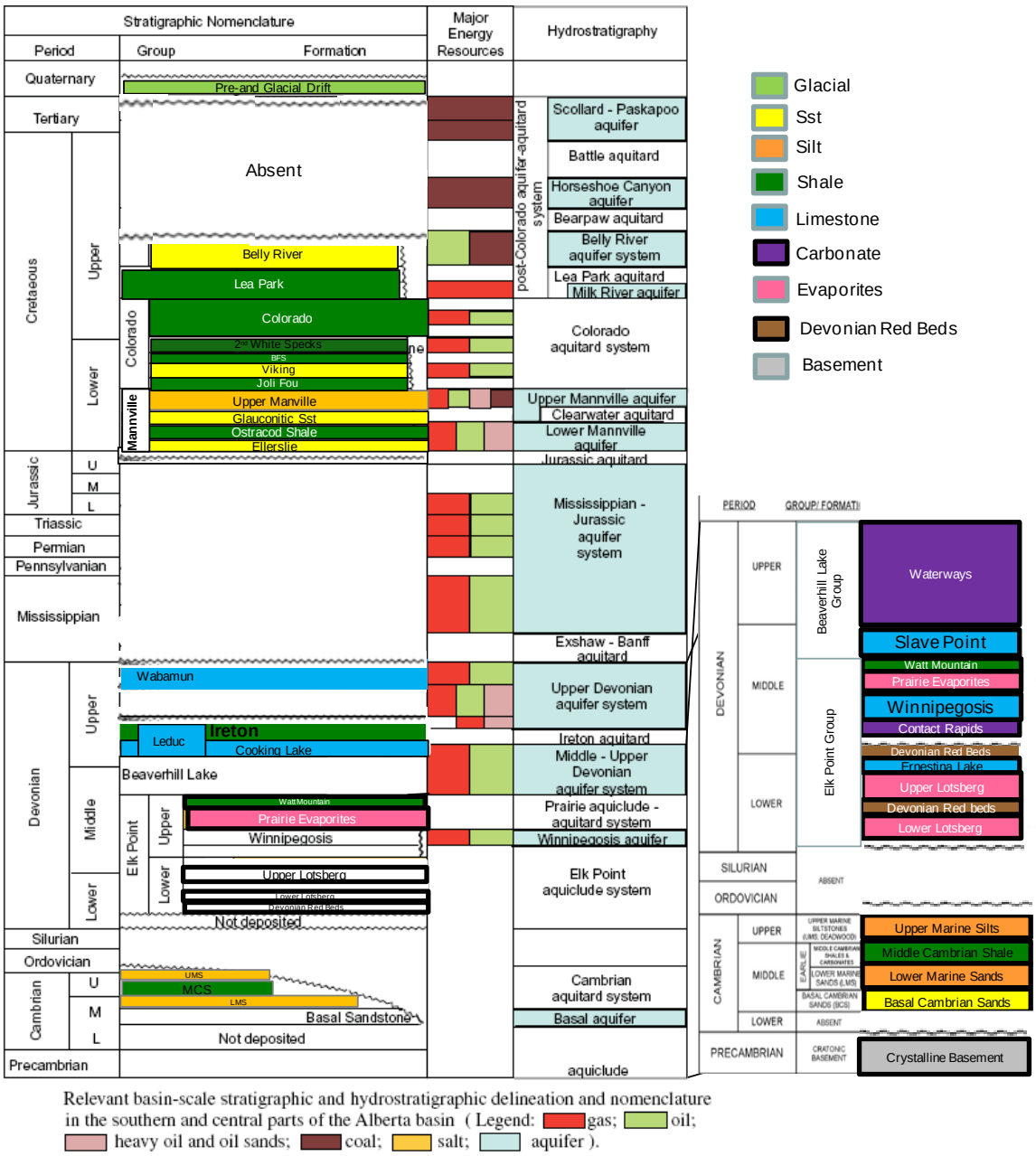

Relevant basin-scale stratigraphic and hydrostratigraphic delineation and nomenclature in the southern and central parts of the Alberta basin (Legend: gas; oil; heavy oil and oil sands; coal; salt; aquifer).

(Bachu, Brulotte, Grobe and Stewart, Earth Sciences Report 2000-11: Suitability of the Alberta Subsurface for Carbon-Dioxide Sequestration in Geological Media, 2000)

Figure 118: Stratigraphic Section from Surface to Basement for Central Alberta.

9.3. Regional Leak Path Model

This was a large scale, screening level model intended to be used as a:

- communication tools for stakeholders
- framework for the regional hydrogeology study that will support the MMV plan moving forward
- framework that will support future more detailed models focused on the shallow aquifers such as the Winnipegosis and Cooking Lake MMV targets.
- means of looking at the regional picture in more detail to ensure that no stratigraphic risks, not previously identified, exist that require further work.

The purpose of this screening model was to verify the existence of potential aquifers for MMV, attain average reservoir properties to assist with MMV technology detection limits and confirm presence of significant regional seals as further evidence of containment.

9.3.1. Data Availability

The model, by definition, is extremely large both in lateral and vertical extent covering 144,400km2 and 2100 of stratigraphy respectively. In addition, there were 45 Formations to interpret and thousands of wells to sort through.

In order to streamline the process, a strategy for data collection was applied. The goal was to attain the highest number of deep well penetrations as possible with a maximum of 14 wells high-graded for petrophysical evaluation. To maximize the value of information the plan was to incorporate:

- the three 3 Quest wells (Redwater 11-32, Scotford 3-4 and Radway 8-19)
- wells strategically placed in the following locations
    - 1 well between Imperial Darling No. 1 legacy well and the Quest injection wells
    - 1 well in the Leduc reef to attain reef properties
    - 1 well between Clyde No.1, Imperial Egremont and the 1st injection well
    - 1 to 2 additional wells to in fill any outstanding data gaps within the AOI.
- 4 regional wells for calibration and QC

As a screening exercise, a query of all wells that penetrated the Lea Park Formation, the Cooking Lake Fm., Beaverhill Lake Group, Upper Lotsberg and the Precambrian were identified in the ACCUMAP public wells database software program. In addition, all wells with more than 10 wireline logs were identified to highlight shallower wells that have a higher likelihood of having sufficient logs for petrophysical evaluation (Figure 119).

Query results were quality checked against wireline logs to ensure they went as deep as indicated by the query results and had basic wireline logs available. A number of the wells identified as deep wells were quality checked to find that they terminate at very shallow depths of approximately 800m .

QC'd wells that appeared to have associated logs were then sent for Petrophysical screening of log availability and quality. In total, 29 wells were high-graded and only eleven wells met

the data quality standards and underwent petrophysical evaluation . Seven of these wells were located within the 3D static model boundary and four were regional wells located outside the model grid and used for quality control purposes (Table 37 and Figure 120).

Each well evaluated all zones penetrated from the Base of the Lower Lotsberg to the base of the Leak Park Formation, which is approximately equal to the Base Groundwater Protection Zone (BGWP). Formations below the Lotsberg salt were included in the BCS modeling program and are covered in the Gen3 and Gen4 modeling reports. Above the Colorado shale the only log data available was that of the Quest 1F1-08-19-059-20W4 shallow water well which was used as the sole data point for formations above the base groundwater protection zone (BGWP).

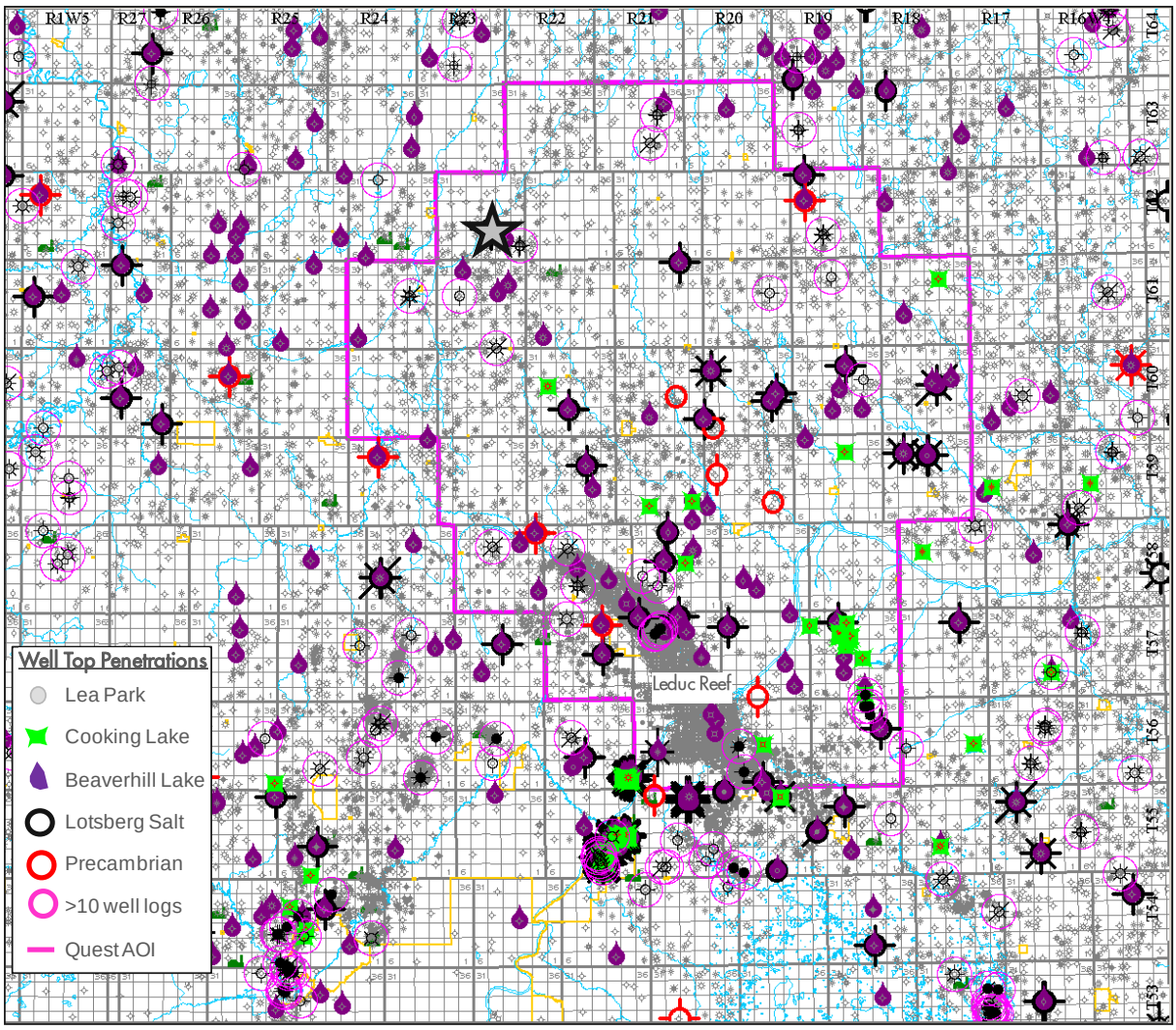

Figure 119: Wells screened in ACCUMAP query. From here wells were quality checked for correct depths of penetration and log availability. Appropriate wells were sent for Petrophysical screening.

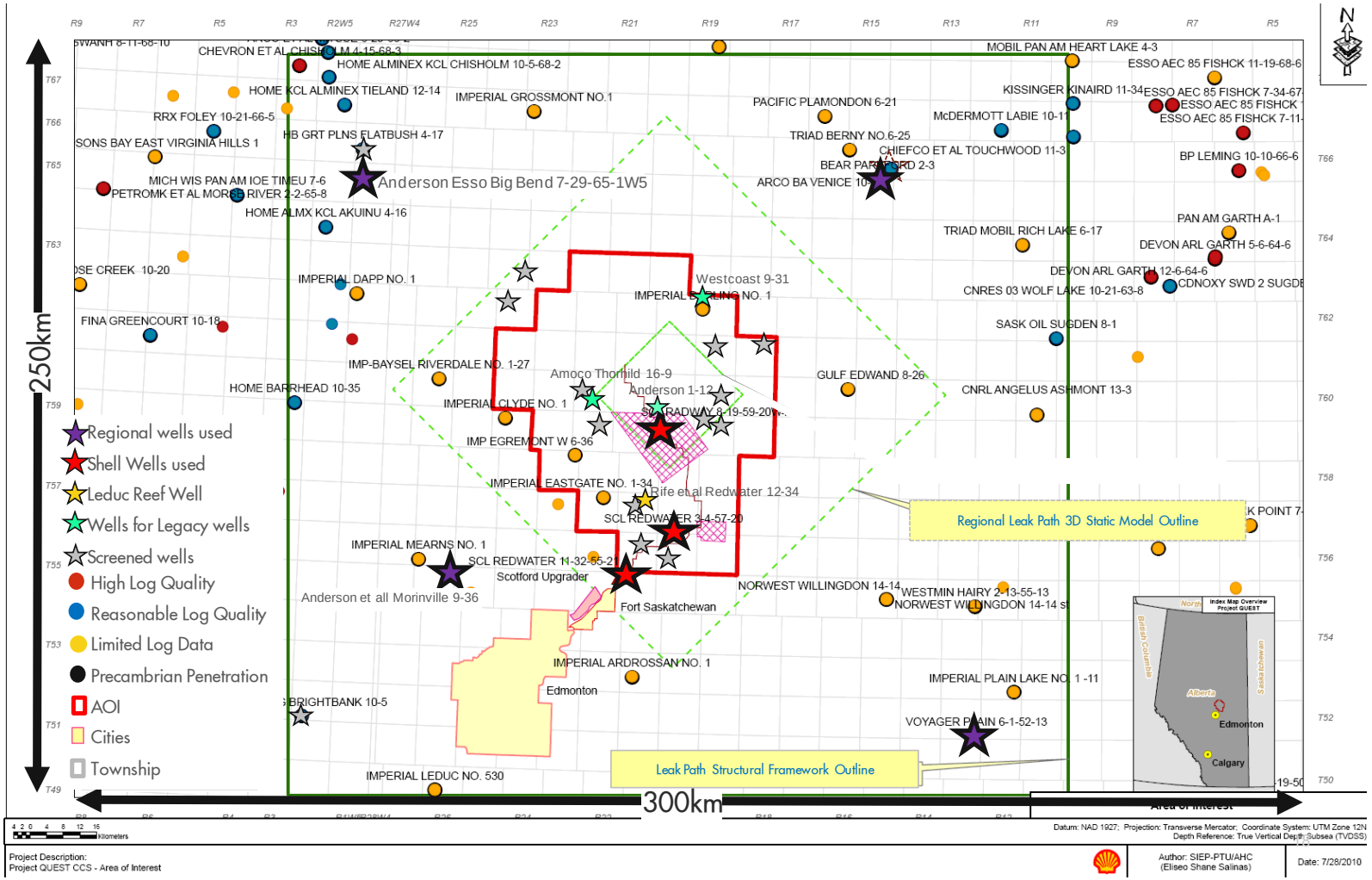

Figure 120: Basemap of outline of wells used to define structural framework for horizons, 3D Static model outline, wells quality checked by the petrophysicist and wells used in petrophysical evaluation. All wells used in petrophysical evaluation were high log quality.

Table 37: Wells used for Petrophysical Evaluation. A complete list of wells used for structural framework, including their location, is presented in APPENDIX 8 and APPENDIX 9.

UWI	Operator Well Name	Short Well Name	Drill TD (m)	Formation TD	Included in Property Model
100030405720W400	SCL REDWATER 3-4-57-20	REDWATER 3-4	2190	PRECAMBRIAN	X
102113205521W400	SCL REDWATER 11-32-55-21	REDWATER 11-32	2243	PRECAMBRIAN	X
100081905920W400	SCL RADWAY 8-19-59-20	RADWAY 8-19	2134	PRECAMBRIAN	X
100093106219W400	WESTCOAST ET AL NEWBROOK 9-31-62-19	WESTCOST 9-31	1923	CAMBRIAN (MCS)	X
100123405721W400	RIFE ET AL REDWATER 12-34-57-21		1547	PRAIRIE EVAPORITE	X
100160906022W400	AMOCO THORHILD 16-9-60-22	AMOCO 16-9	1808	U. LOTSBERG	X
100011206021W400	ANDERSON ET AL THORHILD 1-12-60-21	ANDERSON 1-12	1492	PRAIRIE EVAPORITE	X
100093605526W400	ANDERSON ET AL MORINVILLE 9-36-55-26		1975	PRAIRIE EVAPORITE	
100060105213W400	VOYAGER PLAIN 6-1-52-13	VOYAGER 6-1	2100	PRECAMBRIAN	
102072906501W500	ANDERSON ESSO BIG BEND 7-29-65-1	ANDERSON 2/7-29	2115	CAMBRIAN (LMS)	
100101206615W400	ARCO B.A. VENICE 10-12-66-15	ARCO 10-12	1591	PRECAMBRIAN	

9.3.2. Petrophysical Analysis

Eleven wells were evaluated to determine the net to gross, porosity and permeability of each Formation. Formations that had no net were assumed to have zero porosity and permeability. Figure 121 is an example of the petrophysical evaluation completed for each well.

The wells were then imported into Petrel for further evaluation including correlation and quality control of tops, formation names, upscaling and petrophysical modeling.

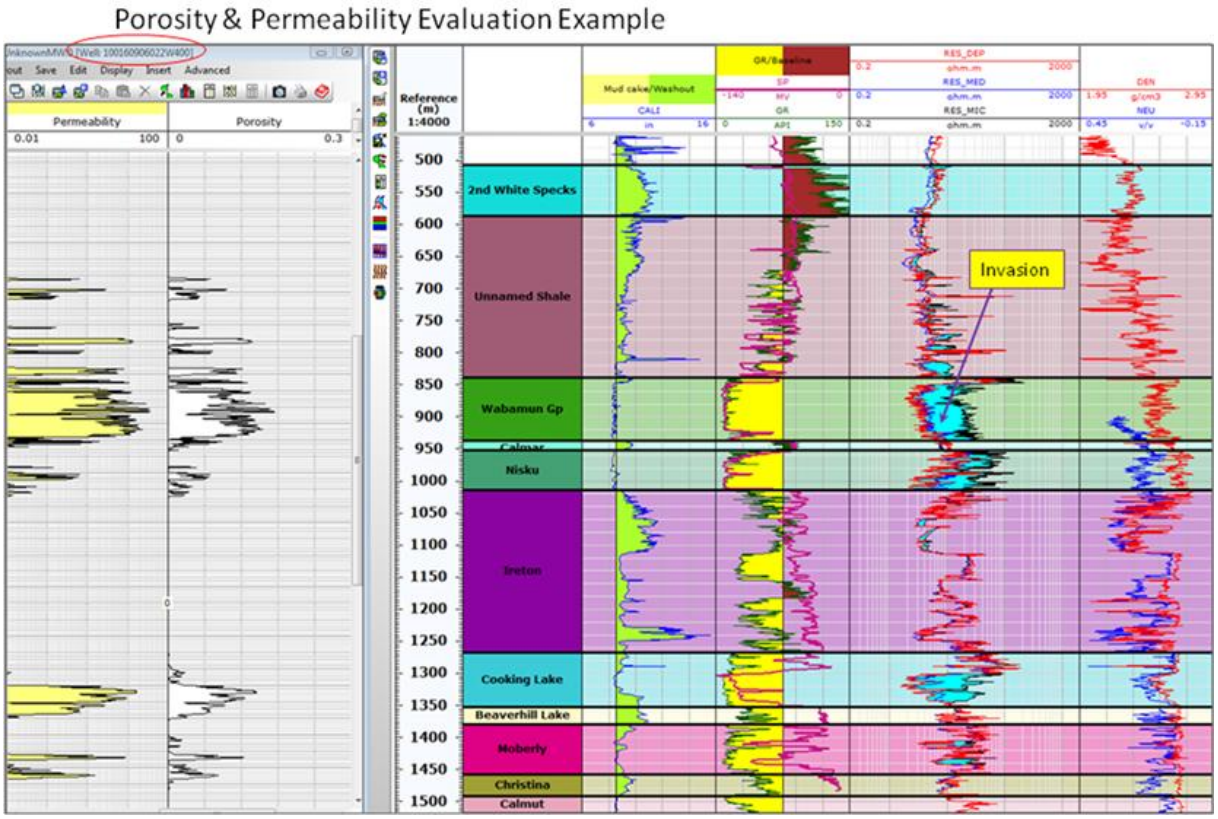

Figure 121: Example of Petrophysical evaluation for Amoco Thorhild 16-9-60-22W4

Post evaluation, an independent petrophysical study of the Cooking Lake and Winnipegosis Formations in the Radway 8-19 well was carried out in SIEP in Houston to support the feasibility work for CO_2 detection limits using Time lapse 3D seismic (07-3-ZG-7180-0025). Through that study, the Contact Rapids/Lower Winnipegosis (Contact Rapids) was identified as an additional formation with significant porosity not identified in the previous evaluation. In addition, this study split the Cooking Lake, Winnipegosis and Contact Rapids into more detailed porous and non-porous intervals further high-grading the reservoirs which was not carried out in the screening level leak path model. The results of the Houston study are shown in Table 38.

Table 38: Petrophysical evaluation 8-19 for Time lapse 3D seismic feasibility study. Note the names Contact Rapids and Lower Winnipegosis are interchangeable

Zones		Top	Bottom	Thickness	DEN	VP	VS	POR	VSH_GR
		[m]	[m]	[m]	[g/ccm]	[m/s]	[m/s]	[m/s]	[frac]
Cooking Lake Tight		1150.8	1180.8	30.0	2.649	5169.1	2733.2	0.048	0.131
Cooking Lake Porous		**1184.6**	**1222.4**	**37.8**	**2.521**	**4952.7**	**2578.6**	**0.117**	**0.010**
Winnipegosis Porous		1602.5	1604.3	1.8	2.610	5699.8	3075.4	0.077	0.029
Winnipegosis Tight		1604.6	1615.4	10.8	2.707	5955.3	3192.7	0.028	0.085
Lower Winnipegosis Dolomitic LS Interval		**1615.4**	**1663.9**	**48.5**	**2.739**	**5485.4**	**2975.5**	**0.074**	**0.422**
Lower Winnipegosis Calacarous / Shaly		1665.0	1684.6	19.7	2.668	4741.0	2554.3	0.061	0.809

Due to absence of information in the Contact Rapids/ Lower Winnipegosis in any other well, the average values determined in this study were used to represent the entire Contact Rapids/Lower Winnipegois Formation in the property model. Furthermore, detail work of high-grading and separating the formations into porous/tight intervals was not completed in this screening study but was captured in the comments portion of Table 39 in the Leak Path Model Results Section of this document. Future models will need to appropriately rectify this issue.

9.3.3. Structural Framework

9.3.3.1. Areal extent and skeletal grid

The 3D static model covers an area of 144,400 km2 and has a total average thickness 2100m. The model was gridded at 500m x 500m resolution with grid oriented with structural dip. The extent of the 3D static model and the model grid orientation are the same as that used in the Gen 3 Dynamic Pressure Model (Figure 120).

9.3.3.2. Zonation

All existing well tops within the leak path model structural framework boundary, equivalent to the Gen3 Static Model Boundary, and above the Base of the Lower Lotsberg Salt were re-

evaluated and subsequently re-picked with a focus on the shallower section (Figure 120 and APPENDIX 8). In addition, tops for a subset of shallower wells located within the AOI were also incorporated for additional structural control.

The well tops are stored under the Well Tops folder in the Petrel project labeled "CHRONOSTRAT Gen 1 Leak Path Model_FOR MODELING". The tops have been arranged in a chrono-stratigraphic hierarchy, see Figure 122. The one exception is the Majeau Lake Formation which is time equivalent to the Cooking Lake and therefore not in chrono-stratigraphic order due to its complex relationship with the Leduc and Cooking Lake Formations (See Section 9.3.3.7). All of the well tops were assigned to an appropriate stratigraphic category, i.e. base, conformable, erosional or discontinuity.

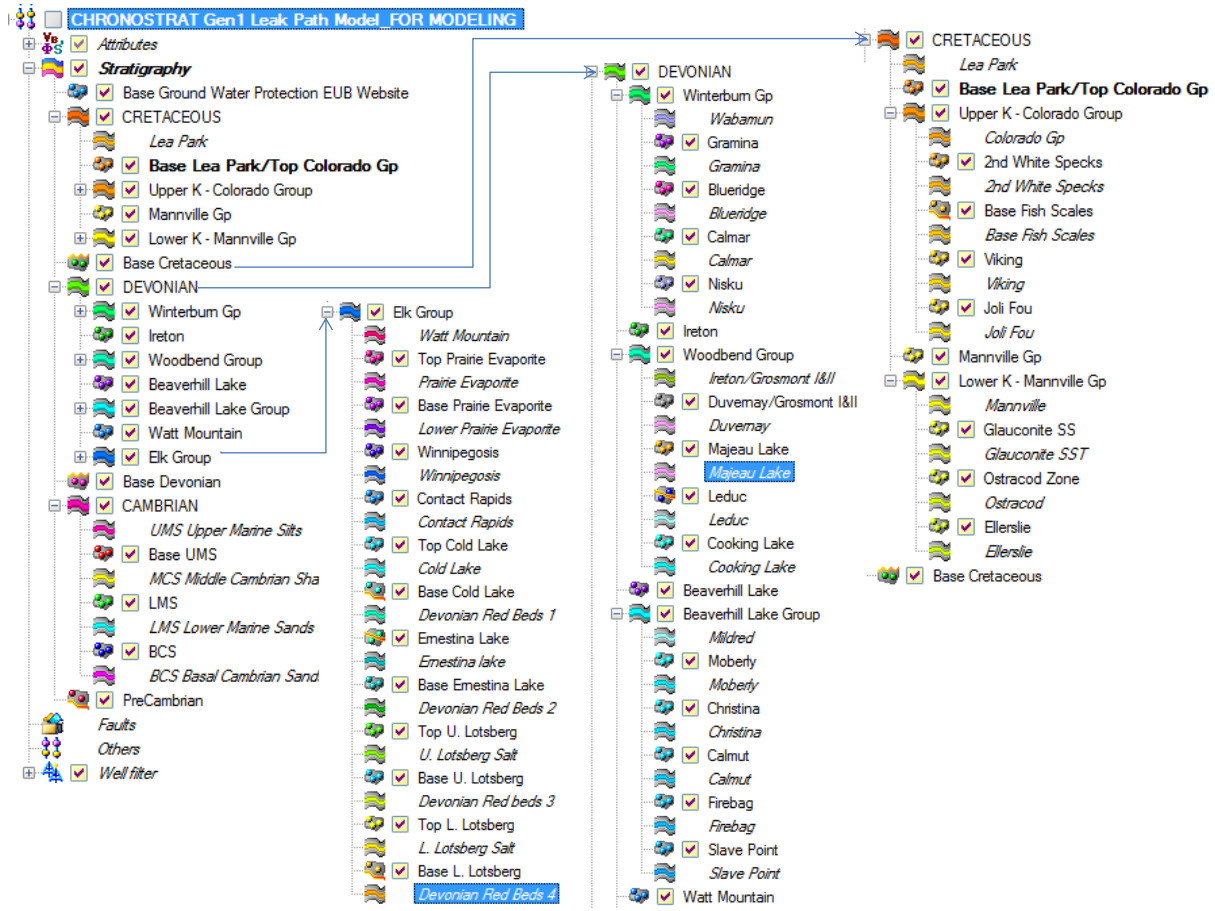

Figure 122: Petrel Well Tops Hierarchy

9.3.3.3. Horizons and Zones

The static model structural framework was constructed to describe stratigraphy from the top of the Precambrian basement to surface within and in close proximity to the Quest AOI.

Nine surfaces representing the bounding and key internal stratigraphy were used as input to the Make Horizons process (from shallow to deep):

- Surface elevation map from Digital Elevation Model (erosional)
  - Quaternary and Zone of groundwater Protection (Upper Cretaceous)
- Base Lea Park/Top Colorado Group (conformable)
  - Lower to Early Upper Cretaceous section
- Top Mannville Group (conformable)
  - Upper and Lower Mannville section of the Lower Cretaceous
- Base Cretaceous (Erosional)
  - Upper Devonian Section
- Top Ireton Formation (Conformable)
  - Includes the Leduc Reefs, Cooking Lake, Duvernay/Majeau Lake Formations
- Top Beaverhill Lake Group (conformable)
  - Waterway Formation Members and Slave Point of Middle to Upper Devonian
- Top Watt Mountain (conformable)
  - Devonian Elk Point Group
- Base Devonian Unconformity (Erosional)
  - Cambrian Section isopachs input from Gen4 model
- Base BCS / Top Pre Cambrian/ (Base)
  - Isopach taken input from Gen4 model

All surfaces were generated by gridding of well tops using Make/Edit Surface in Petrel using the convergent gridding algorithm. See Figure 123 for a cross section showing top level stratigraphic zonation.

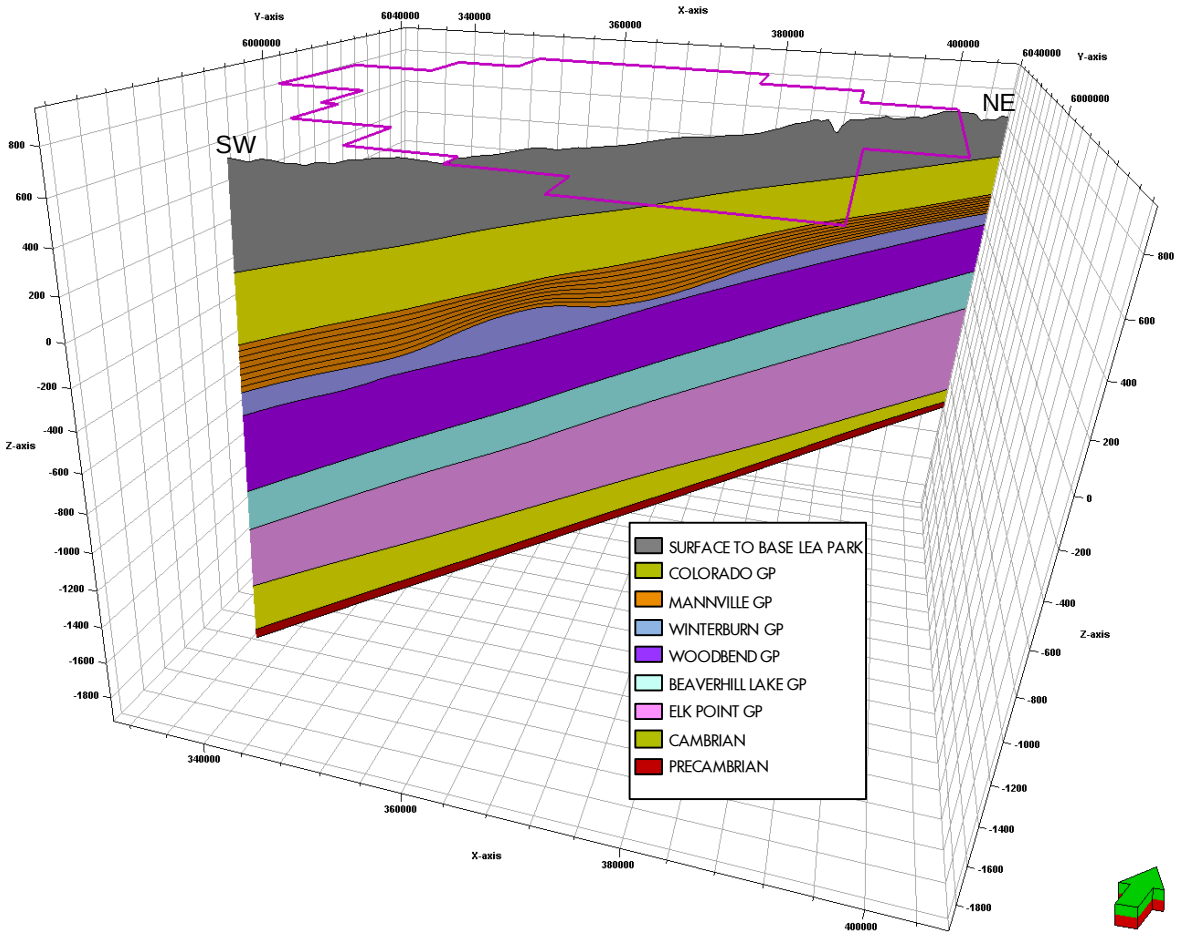

Figure 123: J-intersection running SW-NE across the model showing top-level zones.

Further sub-zonation was achieved using the Make/Edit Zones process. Most zones are generated by simple conformable gridding of well tops within the parent zone defined from the horizon modeling using convergent gridding algorithm. There were some exceptions to this including:

- An isochore was used to constrain the Cold Lake salt which pinches out within the study area.
- Due to the complexity of the Woodbend Group, the Cooking Lake, Leduc Reefs, Duvernay and Ireton Formations were created in a 3D Grid model called 'Part of Working_3D_grid_using_Model_specific_Tops_simplified_Leduc' and imported back into the main model as isochores (Section 9.3.3.7).
- The Cambrian section which was imported as isochores from the Gen4 model for consistency. Not the focus of this model.
- The Precambrian basement was defined using a constant thickness of 50m below top Precambrian.

9.3.3.4. Layering

Layering was predominantly used as a simple method to:

1. correlate and high-grade porous intervals within a thicker unit.
   - Mannville Group (proportional – 8 layers) used to highlight the increased porosity at the base of the section associated with the Ellerslie Formation.
2. Add more detail to the zones with the highest porosities and therefore most likely targets for future more detailed work to support MMV.
   - Nisku (proportional – 3 layers)
   - Leduc Reef (cell thickness – 100) – 3 layers to approximately represent property variations between Lower, Middle and Upper Leduc.
   - Cooking Lake (proportional – 4 layers)
   - Moberly (proportional – 3 layers)
   - Calmut (proportional -2 layers)
3. Distinguish minor localized porosity within a larger section that is predominantly shale.
   - 2nd White Specks (proportional – 5 layers) thick shale except for top few meters of porous sandstone in localized area.
   - Ireton (cell thickness – 75) some porosity associated with the appearance of Grosmont Carbonates to the extreme west of study area situated in the middle to top of the Ireton Shale. For simplicity, the Grosmont was not modeled independently due to its presence only in the extreme E-NE of the 3D static model and its location encased within and near the top of the thick Ireton Shale seal.

No layering was defined for the Cambrian section because it is not the focus of this model and the details are covered in the Gen4 model.

9.3.3.5. Quality Control for Structural Framework

A significant amount of work went into correlation of formation tops consistency/accuracy in determining the appropriate nomenclature of Formations represented within the AOI. The reason being that if the structural framework is correct in this large screening level model, future models can easily pull out a particular zone of interest to evaluate in more detail with facies modeling and detailed petrophysical analysis.

The large number of formations (45 in total) and the vast area covered by the model, forced choices to be made in regards to naming conventions (i.e. Winnipegosis vs. Keg River), lithology (i.e. formations grading laterally from dolomite to shale) and stratigraphic simplification through combining formations for modeling.

The main literature references used for determining type sections, depositional environments, lithology, lateral facies changes, and nomenclature include:

1. The Geologic Atlas of the Western Canadian Sedimentary Basin (Mossop, 1994)
2. The CSPG Western Canada Lexicon 4 (Glass, 2000)

3. Canstrat lithology logs in older Precambrian wells with poor/absent wireline data
4. Lithologic Strip-logs from the drilling of the 3 Quest wells (11-32, 3-4 and 8-19)
5. Reservoir Architecture of the Leduc Reef in Central Alberta (Wendte, 2009)

For obvious reasons, the depositional environments and lithofacies for each formation is not explained in detail in this report. However, determination of top Lea Park used and unconventional approach and is therefore highlighted below. Furthermore, due to the complexity of the Cooking Lake and the Winnipegosis/Contact Rapids aquifers and their importance to MMV they are also explained in greater detail.

9.3.3.6. Lea Park Formation Structural Complexities

The Lea Park Formation is a thick, regional extensive shale deposited during a marine transgression. It is the main sealing formation separating the fresh water aquifers of the Quaternary glacial deposits and Upper Cretaceous Belly River Group from the more saline aquifers below. The top Lea Park and its equivalents elsewhere in the basin, approximate the depth of the Base Groundwater Protection zone (BGWP).

In order to protect the fresh water aquifers, the Government of Alberta has Regulations in-place requiring companies to set surface casing to completely cover the BGWP. As a result, the majority of wireline logging runs only start below the surface casing and do not cover the top Lea park.

To assist companies in defining the top Lea Park to determine surface casing setting depths, the Government created a Base Groundwater Protection Query Tool used to reference the approximate depth to the Top Lea Park based on their large regional database (https://www3.eub.gov.ab.ca/Eub/COM/BGP/UI/BGP-Main.aspx). The database provides an estimated depth to BGWP for each Legal subdivision (LSD) in Alberta. In the absence of tops to define the Lea Park, each well used in the structural model was entered into the query tool and the top Lea Park was assigned based on the result. This is believed to be a close approximation for top Lea Park/Base Groundwater Protection for the AOI.

9.3.3.7. Cooking Lake Formation Structural Complexities

The Cooking Lake formation is part of the Woodbend Group which represents a gradual deepening of the basin and development of thick aggradational succession of carbonates including the Cooking Lake and Leduc Formations . The Cooking Lake is predominantly composed of extensive sheet like shelf carbonates however, the Quest AOI is situated at the apex of 4 different facies. It is predominantly limestone except for directly below the Leduc-Homeglen-Rimbey-Meadowbrook reef chain where it is characteristically dolomite (Figure 124). To the west of the reef chain the Cooking lake is abruptly replaced by the time equivalent Majeau Lake Formation basin filling shale. In the NE of the study area, an Upper Cooking Lake shale exists above the extensive limestone unit, however for simplicity, the

shale was combined with the overlying Duvernay shale in the static model. Likewise, the Majeau Lake Formation shale was also combined with the Duvernay shale.

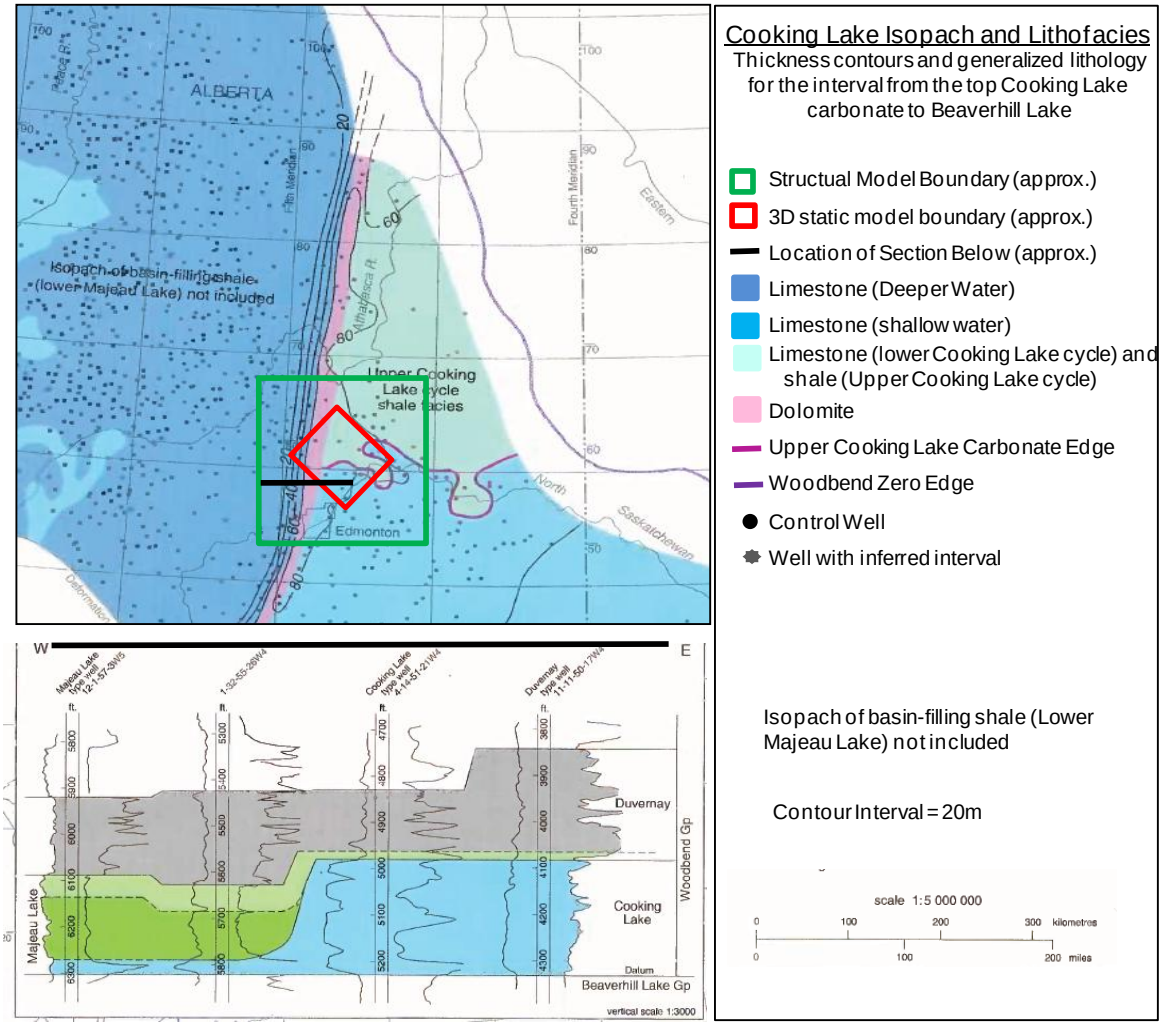

Figure 124: Cooking Lake isopach and lithofacies. Modified from (Switzer, 1994).

Modeling this portion of the Woodbend Group presented some structural modeling difficulties. The Leduc reefs directly overlie and are in communication with the Cooking Lake aquifer. The Majeau Lake is time equivalent to the Cooking Lake. The Duvernay formation shale conformably overlies both the Majeau Lake and the Cooking Lake but only onlaps against the Leduc reefs. Conformably overlying everything is the Ireton shale which represents the top of the Woodbend Group.

In order to handle the complexity in the structural model the following steps were applied:

1. Woodbend Group pulled out of main 3D model by creating a copy of the global grid using the zone filter.

2. The structural envelop of the approximate areal extent and heights of the Leduc reefs were defined from literature and flexed to well tops (Wendte, 2009) and (Switzer, 1994).
3. An isopach of the Cooking Lake defining the abrupt pinch out west of the reef chain was created.
4. The Duvernay and Majeau Lake shale were combined and set to conformably overlie a combined Cooking Lake and Leduc Reef structural horizon flexed to the respective well tops in the Petrel Calculator.
5. Ireton comformably overlies the Duvernay and the Leduc Reef
6. Isopachs were created for each final zone and the zones were re-imported back into the main 3D static model as isopachs.

9.3.3.8. Winnipegosis and Contact Rapids/Lower Winnipegosis Formations Stratigraphic Complexities

The relationship between the Winnipegosis, "Lower Winnipegosis" and Contact Rapids within central Alberta is poorly defined within the vicinity of the AOI. The purpose of this discussion is not to solve this problem but to highlight the effect on correlations and nomenclature. This is especially important because many hydrogeology reports refer to what is known as the Winnipegosis aquifer which in fact includes both the Winnipegosis Formation and the Contact Rapids/Lower Winnipegosis. In addition, if the underlying Ernestina Lake is porous it too may be considered part of the Winnipegosis aquifer system. However the Ernestina Lake appears to be tight in the Quest AOI and is therefore not discussed here.

The Winnipegosis and Contact Rapids were deposited as part of the Elk Point Group within a shallow, restricted, epicontinental seaway that was separated from the open ocean to the north and northwest of the Study area by highlands. Most units in the Elk Point Group have a clastic inshore facies equivalent on the flanks of the basin, or contain coarse siliciclastic interbeds derived from the Peace River Arch ((Meijer – Drees, 1994). For example, the dolomites and dolomitic shale of the Contact Rapids pass laterally into a thick unit of granite wash clastics (far to the west of the AOI). In addition, the shelf carbonates of the Winnipegosis Fm. are commonly interbedded with the siliclastics and pass both vertically and laterally into the silty-sandy dolostone of the Contact Rapids.

The regional depositional environment is well understood however the lithostratigraphic correlation and associated nomenclature remain unclear. The confusion lies with the definition of the Contact Rapids as predominantly red beds and dolomitic shales or contrastingly as a porous dolostone which is also correlated as part of the Lower portion of the Winnipegosis Formation (Lower Winnipegosis) in the literature ((Meijer – Drees, 1994).

In the Type section wells in the Atlas of the Western Canadian Basin, that are in close proximity to each other and the AOI ,the Contact Rapids is shown to be predominantly composed of porous dolostone or dolomitic shale depending on the Well chosen (Figure 125). When the Type section from the 10-13 well is compared to the same well in the regional cross section (Figure 126) the Contact Rapids Formation is contradictorily depicted as part of the Lower portion of the Winnipegosis. The logs on the right side of Figure 125 show the

correlation between the Quest Radway 8-19 well pick and the 1-11-53-12W4 well which is also included in the regional cross section in Figure 126.

In the original petrophysical evaluation, there was no net reservoir in either the Contact Rapids or the Lower Winnipegosis Formation. Therefore, for the purpose of this study the two were combined and the Contact Rapids/Lower Winnipegosis nomenclature was applied.

In the updated petrophysical interpretation created to evaluate the feasibility of time lapse seismic the Lower Winnipegosis/Contact Rapids was determined to have significant porosity. Therefore, going forward, the Lower Winnipegosis is considered the porous dolostone section which grades laterally and vertically downward into the more shaly Contact Rapids. The separation of these two Formations into individual zones will have to be completed in the next generation of modeling.

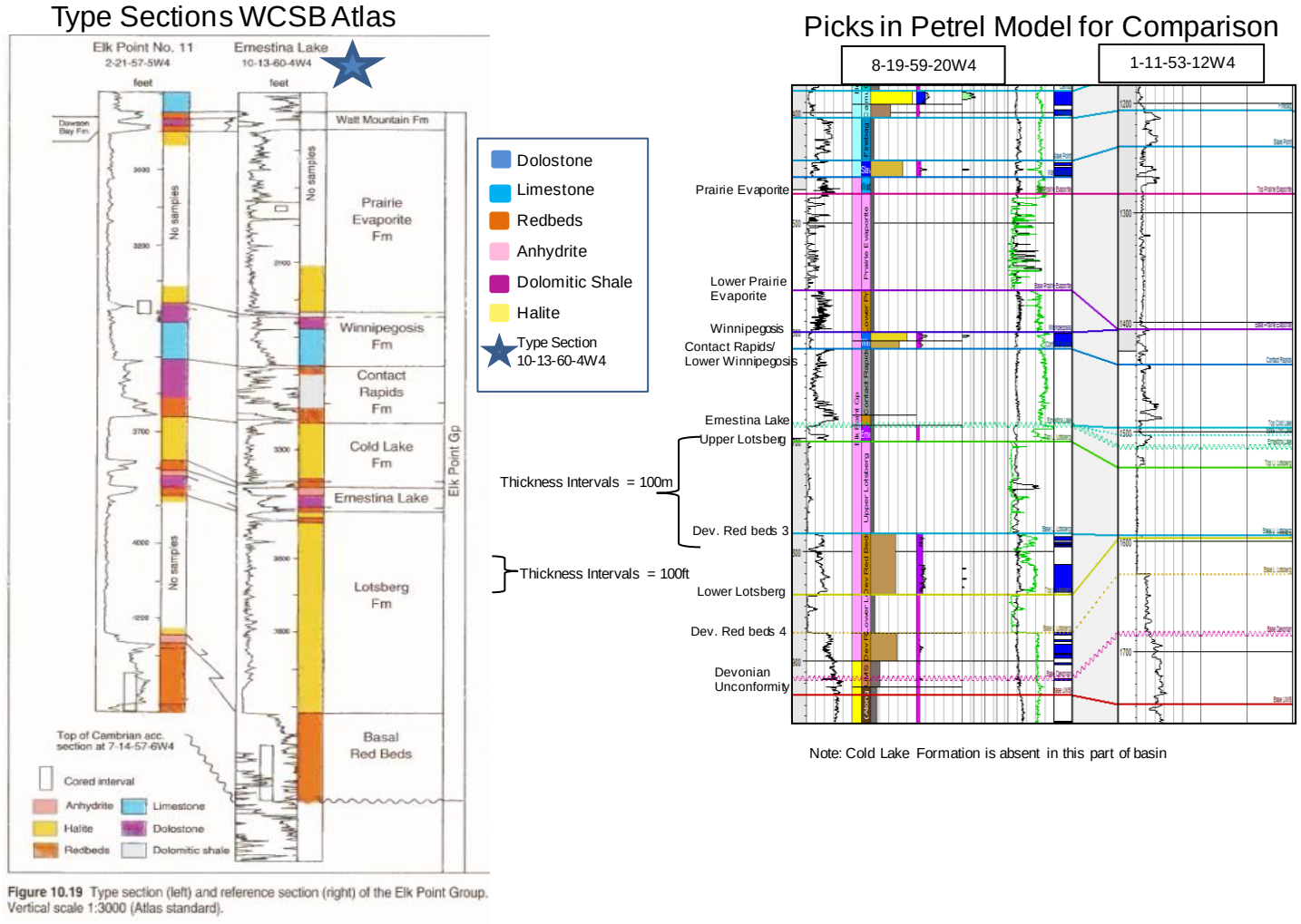

Figure 10.19 Type section (left) and reference section (right) of the Elk Point Group. Vertical scale 1:3000 (Atlas standard).

Figure 125: Left - Type section of the Elk Point Group modified from Meijer-Drees, N.C. 1994 (WCSB Atlas). Right - Correlation of the Elk Point Group in the Quest Radway 8-19 well with Type wells and well 1-11-59-12W4 also shown in the following Figure.

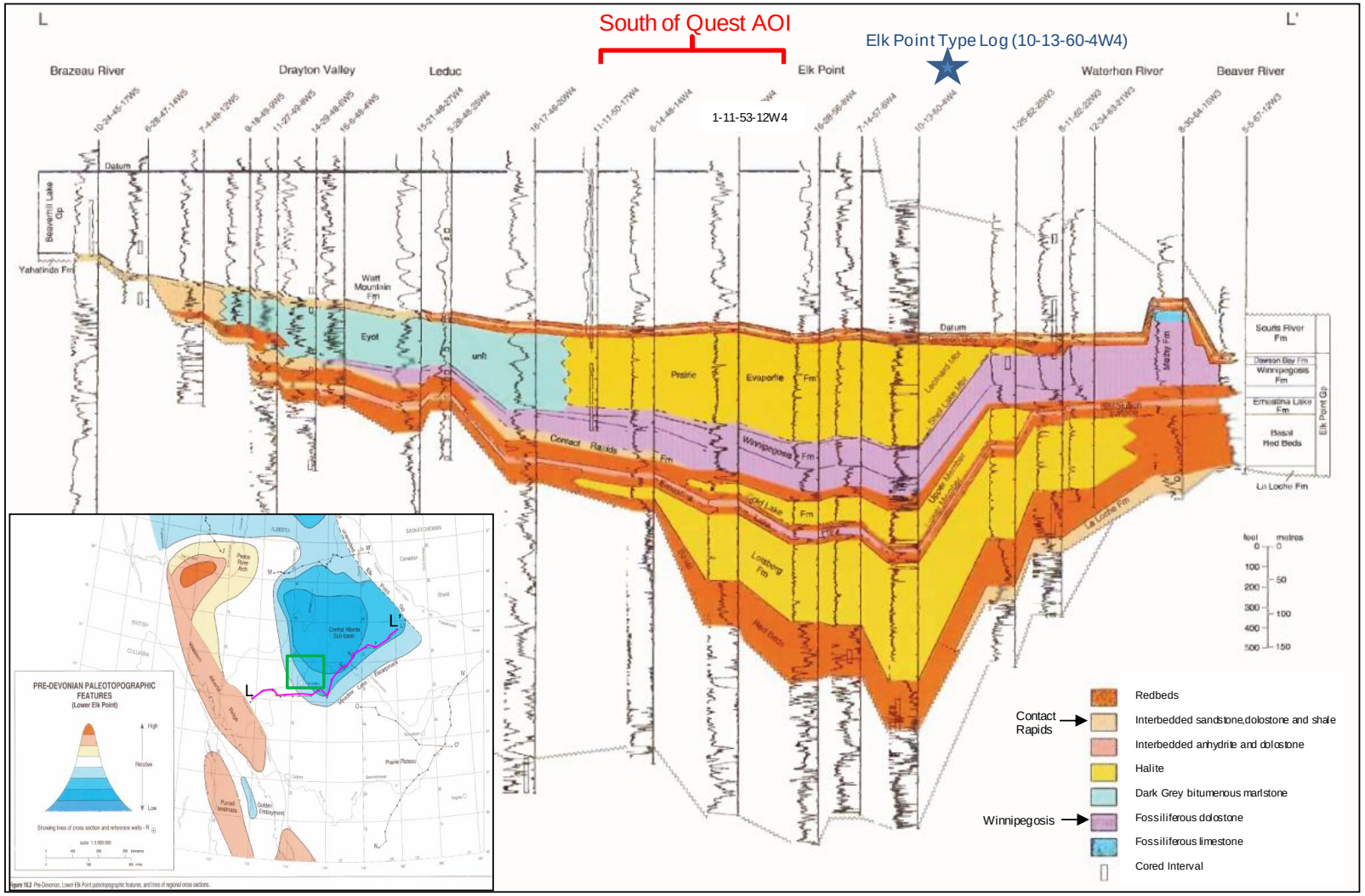

Figure 126: Cross Section L-L' modified from Meijer Drees, N.C. 1994 (WCSB Atlas). Figure in bottom right shows the Pre-Devonian, Lower paleotopogaphic features, approximate location of AOI and line L-L' of regional cross section.

9.3.4. Property Upscaling

The following methods of upscaling were performed on the relevant properties:

- NTG – Arithmetic averaging
- Porosity – Arithmetic averaging, weighted to NTG
- Permeability – not completed in the current study. Permeability should be appropriately incorporated into the more detailed studies of individual aquifers.

9.3.5. Petrophysical Modeling

The data set has large variations in the amount of data available for each interval requiring the use of various petrophysical modeling algorithms depending on the density and type of data available. In this large screening level model, no variograms were used. The three methods used for petrophysical modeling include:

1. Gaussian random functions simulation algorithm – stochastic approach used for zones with enough data to complete a normal score in the transformation window of the Data Analysis Tab. The zones modeled this way include (from shallow to deep):
   - 2nd White Specks, Base Fish Scales, Viking, Mannville Group, Wabamun, Calmar, Nisku, Ireton, Duvernay, Cooking Lake, Moberly, Calmut and Winnipegosis.
2. Kriging algorithm – deterministic approach used for Formations that did not have enough data to reliably perform Data Analysis.
   - Colorado, Joli Fou, Blueridge, Mildred, Christina, Firebag, Slave Point, Watt Mountain, Lower Prairie Evaporite, Ernestina Lake and Devonian Red Beds 4.
3. Assigned Values – zones assigned a constant value
   - Groundwater Protection Zone – given an assigned value based on the average results attained in the shallow 8-19 water well.
   - Leduc Reef – assigned average values for the Lower, Middle and Upper Leduc zones based on Wendte et al, 2009.
   - Contact Rapids/Lower Winnipegosis – average porosity value assigned based on results from the petrophysical evaluation of the 8-19 well completed in Houston for 4D seismic feasibility study.
   - Zones with no net and therefore no porosity were assigned a value of zero including: Graminia, Prairie Evaporite, Cold Lake salt, Devonian Red Beds 1 and 2, Ernestina Lake, Upper Lotsberg salt, Devonian Red Beds 3 and Lower Lotsberg salt.
   - Cambrian section – assigned average values from the mid case results of Gen4.
   - Precambrian basement- assigned a value of zero.

9.3.6. Model Results

Figure 127 through Figure 130 are a series of 3D viewgraphs and cross-sections through the complete leak path model showing the zonation, net to gross, and porosity respectively. In addition, Table 39 provides a summary of all the formation names, their composition and depositional environments, thickness ranges, porosities and associated comments.

The model results suggest that there is no obvious regional stratigraphic leak paths that would result in CO_2 or BCS brine migrating out of the BCS storage complex. Furthermore, the large number of thick regional seals that cover the entire AOI and beyond provide a very strong safeguard against either CO2 or BCS brine reaching the groundwater protection zone via a stratigraphic pathway. In conclusion, no additional risks associated with containment, that have not been identified to date have been discovered through this modeling exercise.

The model successfully screened numerous aquifers that can act as potential targets for deep MMV observation wells. However, more detailed work to incorporate pressure, geochemistry and detailed petrophysics on high-graded intervals needs to be completed. The Model suggest that the zones of interest to date include (deepest to shallowest):

1. Winnipegosis/Contact Rapids carbonates
2. Beaverhill Lake Group carbonates focusing on the Moberly and the Calmut Members
3. Cooking Lake carbonate
4. Nisku Formation carbonate
5. Mannville Group –Ellerslie Formation – fluvial clastic formation at base of Mannville

9.3.7. Recommendations for Future Models

- Petrophysical and structural re-evaluation of the Contact Rapids/Lower Winnipegosis Formation in all wells to properly model the petrophysical properties.
- Incorporation of 2D seismic for increased structural control. For the current study it was advised the structural uncertainty in the 2D seismic was greater than the regional dip adding questionable value to the structural definition. However, using seismic input for the comparison in some of the trouble areas would be beneficial especially in relation to unconformities where the picks are hard to make (i.e. Sub-Cretaceous unconformity and mapping of the Lower Mannville, Ellerslie Formation channels).
- Extract the key horizons and make smaller property models to correlate zone of higher quality over more discrete intervals.

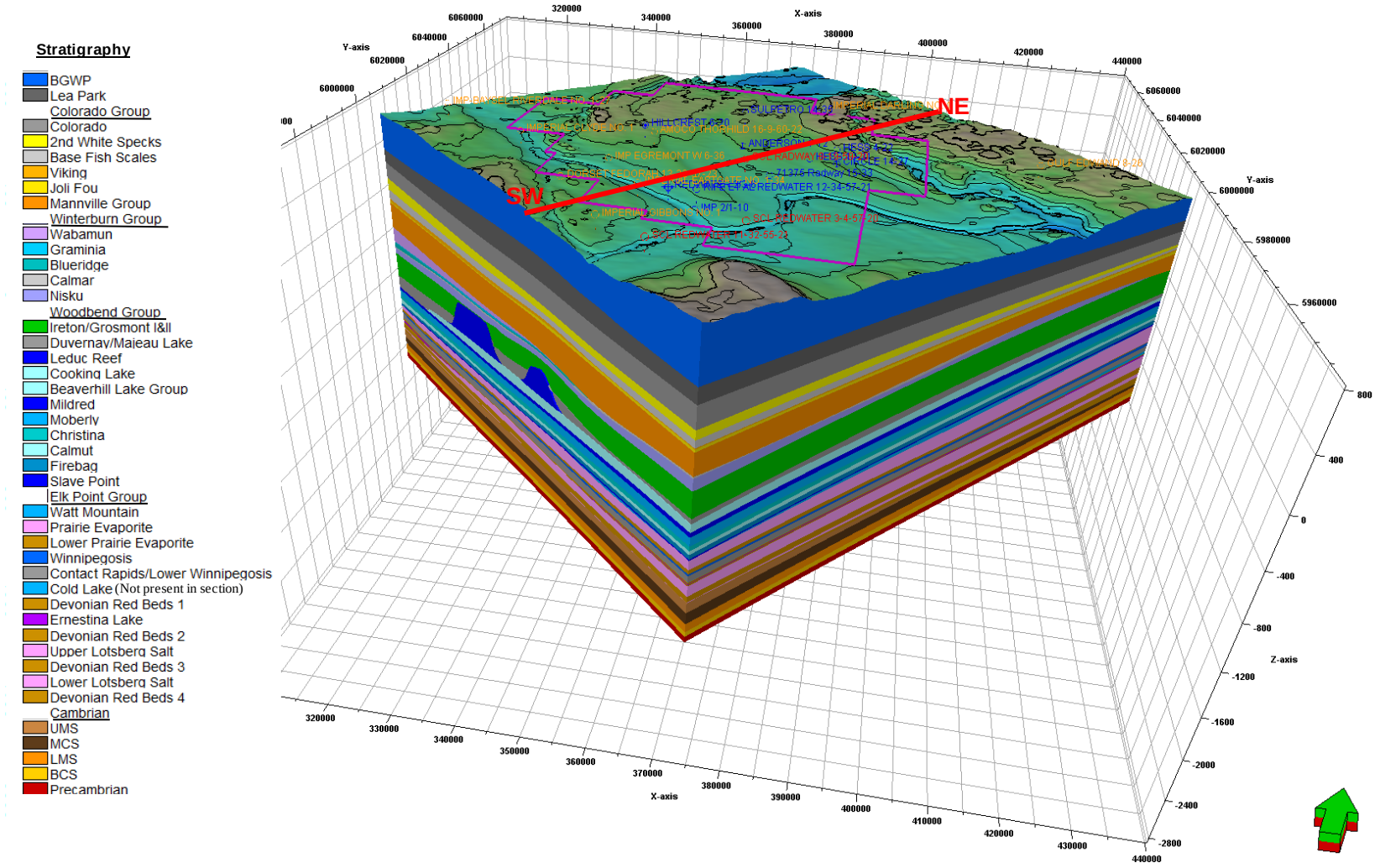

Figure 127: 3D representation of model zonation. Detailed SW-NE Section shown on following Figure.

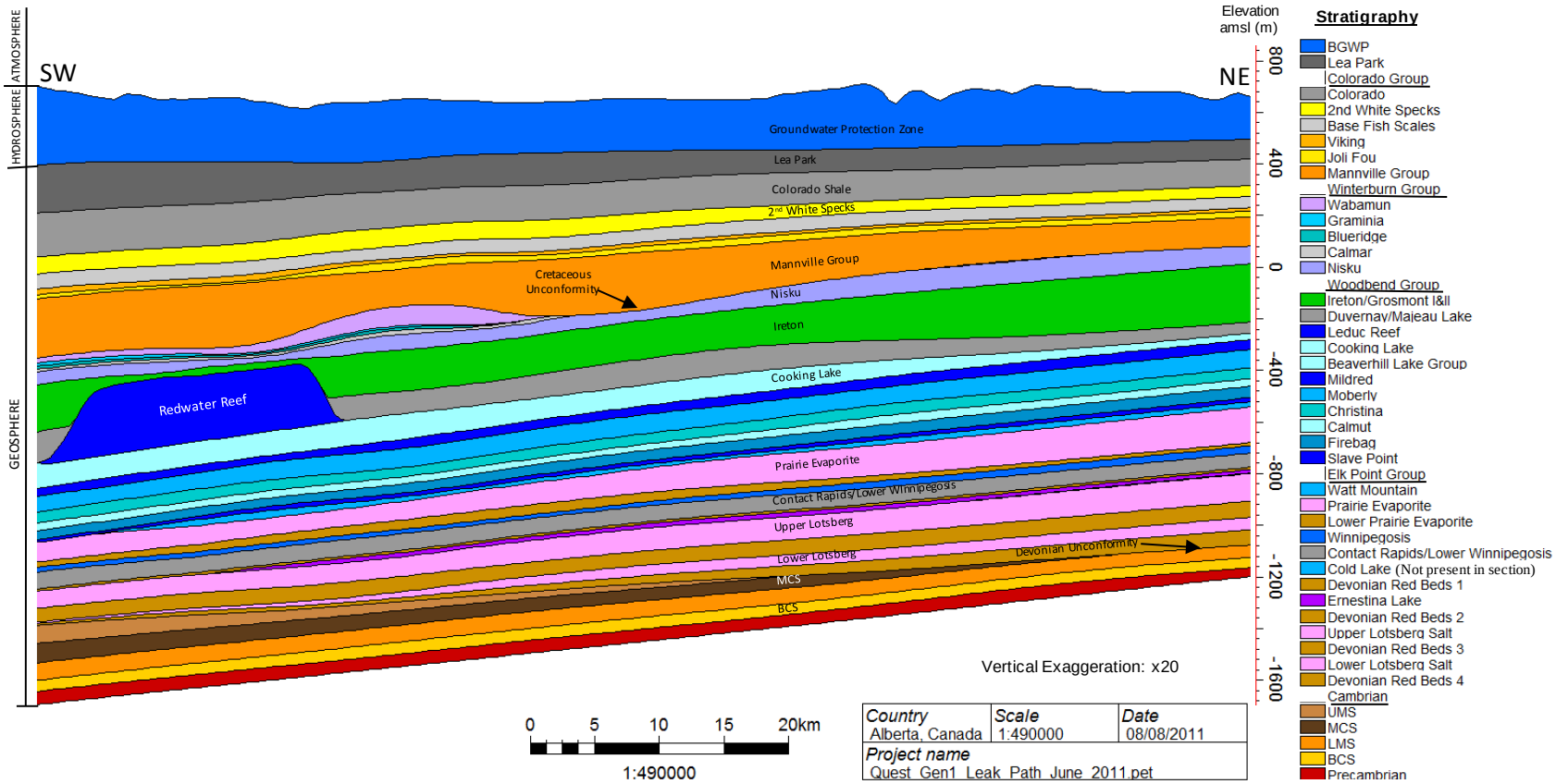

Figure 128: Annotated Cross Section from SW to NE across the center of the 3D Static Model.

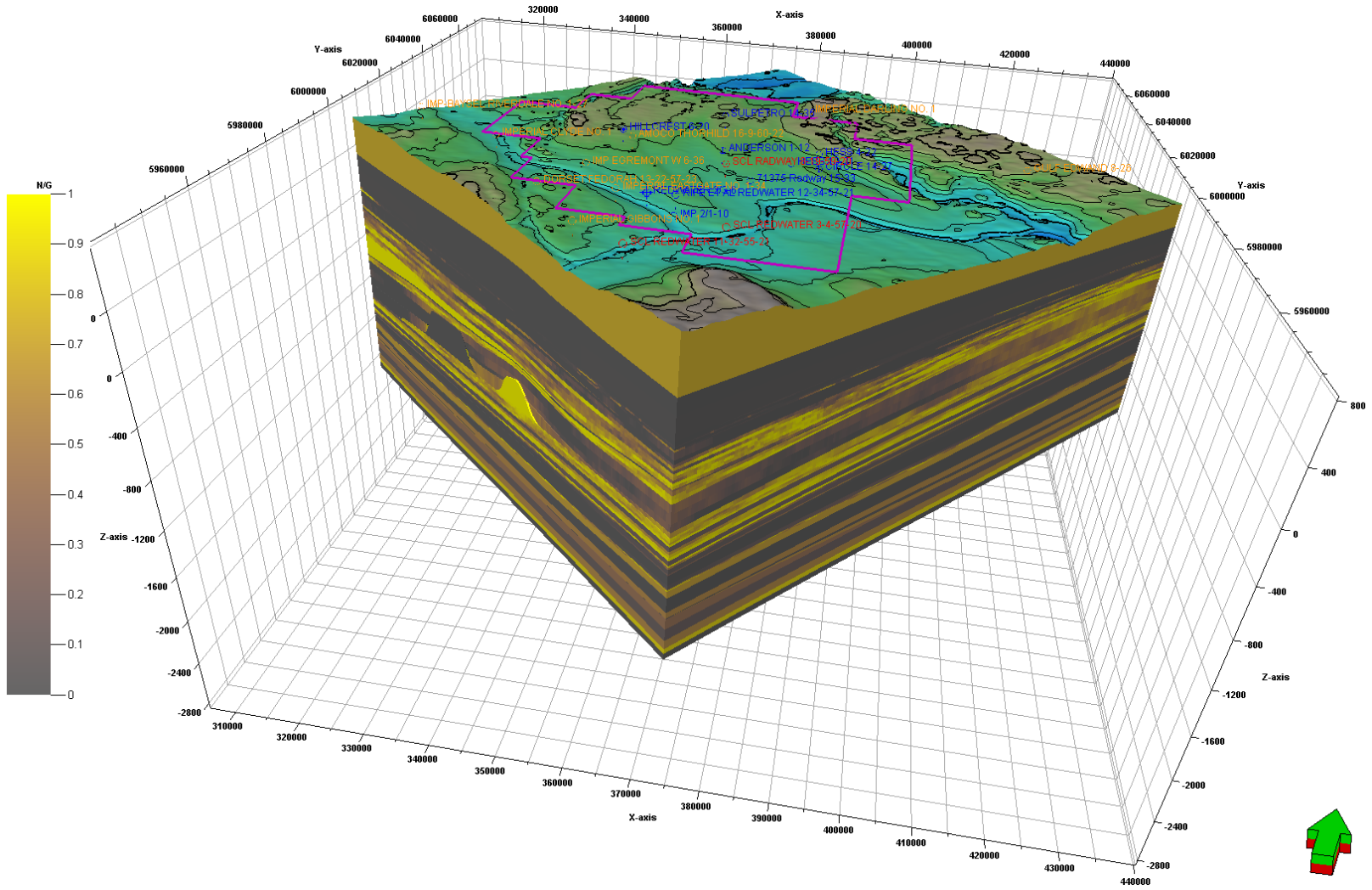

Figure 129: 3D representation of model zonation with net to gross superimposed.

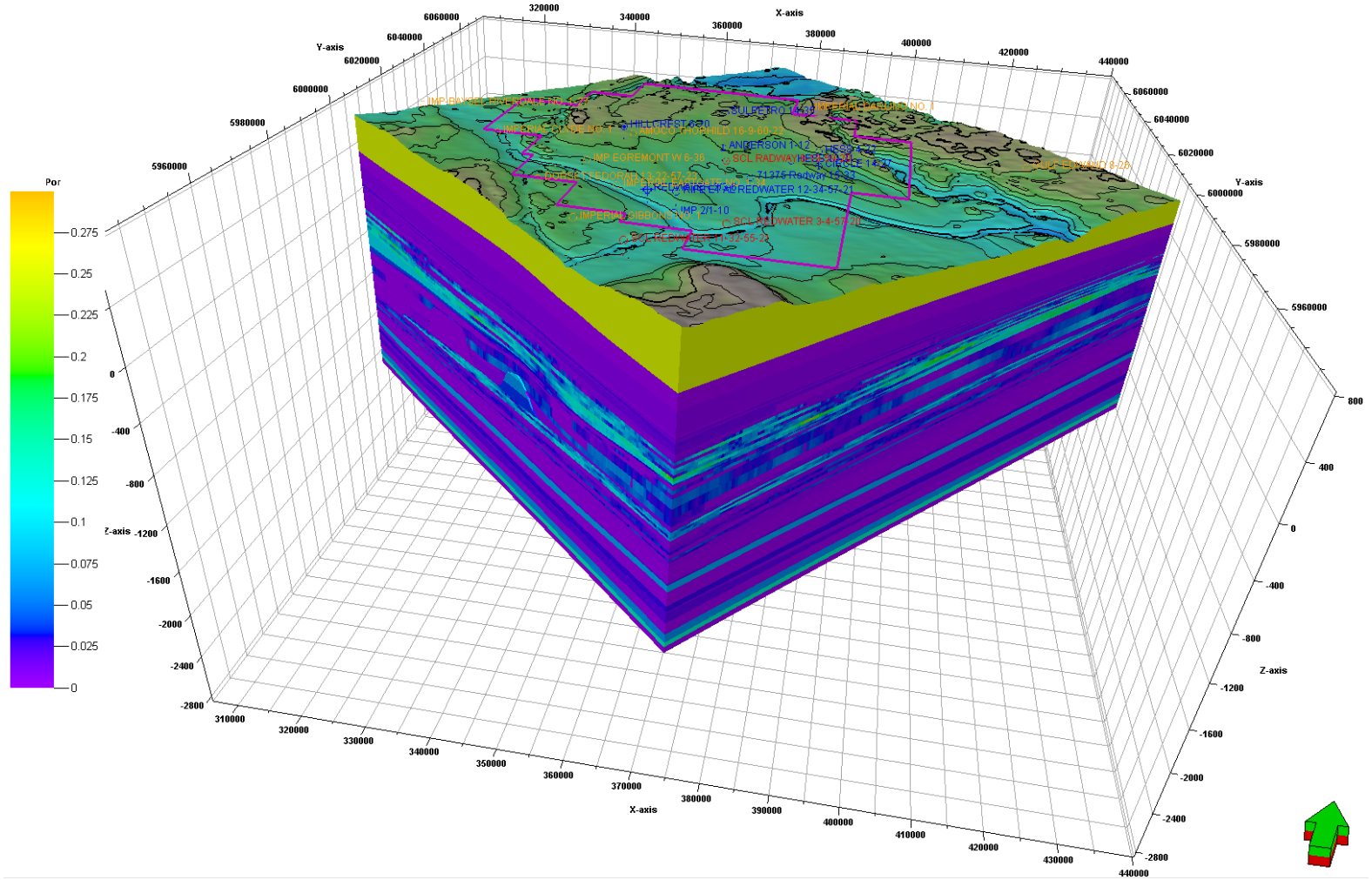

Figure 130: 3D representation of model zonation with porosity superimposed.

Table 39: Geologic descriptions of the formations above the Winnipegosis complex. For the purpose of this Table the AOI is equivalent to the Sequestration Lease Application Area.

	Group/ Formation		Quest Name	Type	Composition and Depositional Environment	Thickness in AOI	Porosity in AOI	Comments
Hydrosphere	Quaternary		Groundwater Protection Zone	Aquifer	Pre-glacial channel fill deposits, glacial drift and other glacially derived sediments deposited above the bedrock surface.	144m to 289m with a mean of 217m. In general it thins towards the N-NE	25% assigned an average value.	Not specifically modeled in the GEN1 leak path model due to lack of information. Thickness determined through isopach of surface elevation map down to well tops for Base Ground Water Protection as specified by Alberta Government base Groundwater Projection Query Tool (https://www3.eub.gov.ab.ca/Eub/COM/BGP/UI/BGP-Main.aspx) for each well. The Glacial deposits are included in this thickness, which are expected to range from 0 to 100m within the AOI. The only log that covers this section is the SCL 1F1-08-19-059-20W400 water well. Properties for the Belly River were taken from this well.
	Belly River Group	Oldman		Aquifer	Belly River Group forms the uppermost bedrock in the region, and hosts aquifers above Base Groundwater Protection (BGWP). The Oldman Formation is composed of continental deposits of interbedded sandstone, siltstone, shale and coal. It subcrops beneath the AOI.			
		Foremost		Aquifer	Marine and continental shale, with sandstone members forming regionally extensive aquifers. Distinctive coal-bearing zones also present (i.e. McKay and Taber coals). The Foremost subcrops beneath portions of the NE and central areas of the AOI.			
	Lea Park			Seal	Medium to dark grey shale with minor amounts of silt deposited during a marine transgression. Based on estimated depth from Top Colorado to BGWP as specified by the Alberta Government in Deep Rights Reversion, the thickness ranges from 92m to 170m thinning towards the NE.	92m to 170m. mean of 120m	0%	
	Colorado Group	Colorado		Seal	Thick, grey regional marine shale present across entire AOI with an average thickness of 134m thinning towards the NE	110m to 168m mean of 134m.	0% to 1.2% with a mean of 0.7%	Within the AOI, the entire Colorado Group ranges in thickness from 233m to 322m with mean of 287m. Thinning towards the NE.
		2nd White Specks		Gas Reservoir & Seal	Calcareous mudstone deposited in a marine setting. The uppermost ~5m of the Second White specks is represented by a thin sandstone layer that is a gas reservoir in the central part of the AOI reaching porosities of up to 8%. The average thickness in the AOI is 67m. thinning towards the E-NE.	42m to 85m with a mean of 67m.	0% to 2.5% mean of 1.2%.	
		Base Fish Scales		Seal	Abundant fish remains within finely laminated, generally non-bioturbated sandstone, siltstone and shale. Within the AOI it is predominantly shale of consistent thickness.	42m to 55m with a mean of 50m	0% to 1.7% mean of 1.1%.	
		Viking		Oil and Gas Reservoir	Derived from Cordilleran erosion in the West. In the AOI it is shallow shelf deposits with dominantly sandstone to the West and shale dominating towards the East. There is Viking Production in the AOI (Oil in the SW corner only) in a thin 2m sandstone at top of section that reaches porosities of 20%. The Viking thins to the NE.	8m to 23m with a mean of 14m	0% to 9.5% with a mean of 3.6%	
		Joli Fou		Seal	Dark grey, non-calcareous marine shale with minor interbedded fine to medium grained sandstone deposited unconformably on top of the Upper Mannville. Major flooding surface that covered most of WCSB averaging a thickness of 21m.	10m to 30m with a mean of 21m	0% to 0.67% mean of 0.65%	
	Upper Mannville	Upper Mannville	Mannville Group	Baffle	Upper Mannville is predominantly shale with grey silt interbedded with fine-grained, moderately sorted, silty , sandstone with local coal seams deposited as part of a prograding deltaic sequence with sediment transport towards the N-NE transitioning upward to be more fluvial in nature. There is porosity within the sandstones portion of this heterogeneous interval. Exists across the entire AOI.	The Upper and Lower Mannville were combined in the Gen1 leak path model due to the heterogeneity of the Mannville. The two are commonly undifferentiated within this area. However, there is an increase in Porosity towards the base of the zone (Ellerslie) which was captured using layers and a vertical porosity trend. Total Thickness of the Mannville is from 127m to 247m with a mean of 180m. It thins towards the NE. The average porosity of the entire Mannville within the AOI ranges from 3% to 12% with a mean of 7%.		See Explanation to the Left
		Glauconitic Sandstone		Gas Reservoir	Interbedded shale, siltstone, and fine-grained sandstones. The sandstones range from glauconitic to salt-and-pepper. Absent in the very N-NE of the AOI as the Wainwright Highlands were finally covered. Gas Production in the AOI, predominantly to the SW half of the AOI.			
	Lower Mannville	Ostracod Zone		Baffle	Interbedded fine clastics and limestone. Predominantly composed of shale, siltstones and lenticular sandstones with locally occurring limestone representing deposition in a low-energy, brackish, subaqueous environment. Minor patchy porosity associated with sand lenses. Absent towards the NE of the AOI along the Wainwright Highlands (Devonian).			
		Ellerslie		Gas Reservoir	Fluvial deposit of fine to medium grained quartz with chert sandstone with fairly good porosity deposited in the Edmonton Valley likely under brackish water conditions. Sediment transport towards the N-NW. Gas Production in AOI. Absent towards the NE of the AOI along the Wainwright Highlands (Devonian). Thickness of the Ellerslie inside the AOI reaches a maximum of 90m. depending on the unconformity and the presence of channel sands.			Based on Wells the avg. thickness of the Ellerslie inside the AOI ranges from 4 to 90m depending on the unconformity and presence/absence of channel sands. Based only on wells used in PP (not modeled individually) the porosity of the Ellerslie within the AOI ranges from 2% to 18% in the channel sands. The average within the sands is ~ 14%. A North-south orientation was given to the layers at the base of the section to better represent the channel architecture and flow direction.
	Winterburn Group	Wabamun		Gas Bearing	Characterized by Dolomite, brown, finely crystalline, porous in part; with subsidiary interbeds of brown, micritic, pelloidal limestone. Only exists in the W-NW half of the AOI due to erosion by the sub-cretaceous unconformity. However, there is some gas production within the AOI. Thickness ranges from 0m to 100m.	0m to 100m.	0% to 10% with a mean of 8%	
		Graminia		Baffle	A silt unit at the top of the Winterburn. Exists predominantly in the W-NW of the AOI. Thin and patchy across the rest of the AOI due to irregularities in the Sub-Cretaceous unconformity.	0m to 18m.	2.8% to 6.7% mean of 4%	
		Blueridge		Gas Bearing	Last widespread carbonate cycle in Western Canada. Exists predominantly in the W-NW of the AOI. Exists predominantly in the W-NW of the AOI. Thin and patchy across the rest of the AOI due to irregularities in the Sub-Cretaceous unconformity. Has some minor porosity within the AOI. Production in the Eastern part of the AOI commonly mislabeled as Wabamun Production.	0m to 40m.	1.7% to 7% mean of 4%	
		Calmar		Baffle	Predominantly silts and clays likely the result of reworking of the underlying lowstand Nisku siliciclastics. Exists predominantly in the W-NW of the AOI. Thin and patchy across the rest of the AOI due to irregularities in the Sub-Cretaceous unconformity.	0m to 24m.	0% to 9.3% mean of 3.5%	minor porosity associated with minor silts
		Nisku		Oil and Gas Reservoir	A mixed carbonate-siliciclastic deposited during a lowstand. Within the AOI the Nisku is a porous light brown to light grey crystalline dolomite with lesser amounts of brownish grey dolomitic siltstones, green shales and anhydrite. It is commonly truncated by the Sub-Cretaceous unconformity. Within the AOI oil production is only above and to the West of the Redwater reef, some minor gas exists in the NE portion of the AOI. The Nisku has a relatively constant thickness of the AOI at 57m. It is absent outside the AOI to the East.	27m to 81m	0% to 14% mean of 7%	Although the porosity in the Nisku is reasonable. The permeability does not appear to be as consistent.
Geosphere above the Winnipegosis Complex	Woodbend Group	Ireton	Ireton/ Grosmont I & II	Seal	Only the Lower Ireton exists in the AOI represented by a cyclic succession of basin filling shales considered to be a regional aquitard. The Lower Ireton is thin on top of the Leduc Reefs (~10m) and thickens to an average of 160m away from the reef. Grosmont Carbonates begin to appear within the Upper part of the Ireton to the East of the AOI.	10m to 209m. Average away from reef is ~160m	0% - 10% with a mean of 2.2%	In the Leak path model, towards the extreme NE the is a Grosmont carbonates that exist within the Ireton that have porosity. They were not pulled out as a separate unit but instead dealt with by using layering and porosity trends. Porosity in this layer is due to contribution from the Grosmont carbonate.
		Duvernay	Duvernay/ Majeau Lake	Seal	Grades from a bituminous rich shale to a shale to a dolomite towards the NE of the Basin. Within the AOI represented by dark brown shale and limestones to the west and as you move towards 8-19 it is predominantly tight argillaceous limestone with shale interbeds. Relatively uniform thickness across basin (~67m) except it is absent over the Leduc Reefs.	0m to 154m. Mean of 67m	0% to 1.9% with a mean of 0.8%	The average thickness is likely less then this. There is some overestimation of thickness near the edges of the reefs. Considered irrelevant as the Duvernay and Ireton above are both seals.
		Leduc	Leduc Reef	Oil Reservoir	Within the AOI is the Redwater Reef and the Morinville Reef trend associated with the Rimbey-Arc. The Morinville reef trend is a tight dolomitic structure except for a localized field just west of the Redwater reef called the fairydell-Bon Accord Field. In contrast, the Redwater pinnacle reef, is a major oil producing limestone and the focus for this study.	0m to 284m	Upper = 9% Middle = 6% Lower = 3.5%	In the Leak path model the Reefs structure was simplified to meet model objectives. The Morinville reef was given a porosity of zero. The Redwater reef was split into 3 equal layers each given different average properties based on simplification of Wendte et al. 2009.
		Majeau Lake	Not modeled	Seal	In the AOI only the Lower Majeau Lake is present. Characterized by greenish grey and dark brown shale that are time equivalent to the Cooking Lake (West of and underlying the reef chain). Only exists to the West of the AOI.	0m. Only exists to the West of AOI	n/a	In the Leak path model the Majeau Lake was combined with the Duvernay for simplicity as they are both shale units.
		Cooking Lake		Intermediate Aquifer	Major regional aquifer made up of extensive sheet like shelf carbonates and an equivalent basin-fill shale (Majeau Lake). Consists of pelloidal and skeletal limestones (bracs, crinoids, stromatoporoids, bryzoans). Unlike most younger Woodbend carbonates it is predominantly undolomitized (except directly under the Leduc-Homeglen-Rimbey-Meadowbrook reef chain). The AOI is at the intersection of three facies. There is a sharp edge to the West of the reef chain where the Cooking lake is non-existent, replaced by Majeau Lake, it is thickest under the reefs and then thins to the NE.	44m to 92m. Thickest under the reefs. Mean of 78m	Total zone modeled: 2.6% to 12%. Mean of 7%	Based on the high-graded porous interval defined in the Time lapse 3D seismic feasibility study, the 8-19 well has an average porosity of 11.7% over a 37.8m interval (Quest Time Lapse Seismic – Radway Well Calibration and Shallow Horizons" 07-3-ZG-7180-0025) .
	Beaverhill Lake Group	Waterways	Mildred	Baffle	The Firebug, Calmut, Christina, Moberly and Mildred Members make up the Waterways Formation deposited during a regressive basin fill phase of the Waterways Basin. The Waterways Formation is composed of a series of shallowing upwards shale-carbonate clinothem cycles deposited in a basin slope depositional setting. Each cycle is composed of a shale base that grades vertically to argillaceous carbonate. The Waterways and Slave Point are combined to form the Beaverhill Lake Group Aquifer System. IN the AOI, the Moberly and Calmut appear to be the only members that have porosity but this might change away from the AOI.	24m to 45m. Mean of 36m. Thins towards NW	0% to 1% mean of 0.46%	
			Moberly	Intermediate Aquifer		62m to 76m. Mean of 69m. Consistent across AOI.	0% to 5.5% mean 2.6%.	Top of interval is tight however, logs show streaks of up to 12% porosity. Based only on average well values inside the AOI (not modeled): the porous interval at the base would have a higher average porosity of 3.9% and the thickness would be decreased to 25m-50m thick.
			Christina	Baffle		30m to 46m. Mean of 38m	0% to 0.7% with a mean of 0.5%	
			Calmut	Intermediate Aquifer		19m to 38m . Mean of 28m	0 to 5% mean 2%	The uppermost ~15m has consistently higher porosity ranging up to 7%. Lower portion of unit is tight. Based on well averages alone (not modeled), the interval of higher porosity has an average of 3.1% porosity with streaks of up to 7%.
			Firebag	Baffle		31m to 44m. Mean of 38m.	0% to 0.9% mean of 0.45%	
		Slave Point		Baffle	The Slave Point Fm. is a distinct, non-contemporaneous event from the Waterways Fm. above, deposited in a transgressive "reefal" phase dominated by restricted to open-marine carbonates. In the AOI Slave Point is a thin, limestone unit that contains some minor porosity. Although represented here as a baffle, on a regional scale it is included in the Beaverhill Lake Group Aquifer System.	9m to 18m. Mean of 13m. Slight thinning to NE	0% to 1.2% with a mean of 0.3%	

Table 40: continued from above: Geologic description of the BCS storage complex, the Winnipegosis Complex and the overlying Geosphere.

	Group/ Formation		Quest Name	Type	Composition and Depositional Environment	Thickness in AOI	Porosity in AOI	Comments
Winnipegosis Complex	Elk Point Group	Watt Mountain		Seal	Top of the Elk Point Group represented by a thin (10m to 40m) green/greyish shale with thinly interbedded limestone units that overlie the sub-watt mountain unconformity. It is absent to the west and North of the study area because it is commonly mapped as part of the Muskeg Fm. which is equivalent to the Prairie Evaporite.	10-40m, mean of 22m	0% to 0.3%	
		Prairie Evaporite		Ultimate Seal WPGS Complex	Regional Seal for the WPGS complex. The Prairie Evaporite is predominantly halite with thin anhydrite layers in middle and at base. There is a marked increase in dolomite and shale laminae near the base of the Formation. Within the AOI, the Prairie Evaporite increases in thickness from 80m to 145m towards the NE and acts as a regional aquiclude. There are no known hydrocarbons below this point within the AOI.	Prairie evaporite: 45-129m mean of 84m. Lower Prairie Evaporite: 17-38m mean of 27m	0%	In the leak path model the Prairie Evaporite(PE) was unofficially split into the Prairie Evaporite and the Lower Prairie evaporite in order to differentiate the upper halite dominant section from the lower more dolomite/shale interval. The Lower Prairie evaporite is an interval between the PE and the underlying WPGS that is predominantly shale with an increasing amount of dolomite beds towards the base. Total thickness of the Prairie Evaporite is 80m to 145m within AOI.
		Winnipeg-osis		Regional Aquifer	Fossiliferous carbonates decreasing in thickness towards the SE grading into the silty/sandy dolostone of the underlying Contact Rapids. The Winnipegosis-Contact Rapids regional aquifer is the first reliable aquifer above the BCS storage complex that can potentially be used for MMV purposes.	15m to 26m mean of 19m	0.38% to 3.4% with a mean of 3.1%	The evaluation of the Winnipegosis was completed on the 8-19 well the Winnipegosis can be separated into a porous interval near the top (~1.8m) and a lower interval that is tight (~10.8m). In 8-19, the upper porous interval has an average porosity of 7.7%. Porosity range taken from average map of Cut_porosity and Cod against well data.
		Contact Rapids	Contact Rapids/ Lower Winnipegosis	Regional Aquifer / Baffle	Correlation between the Contact Rapids and overlying Winnipegosis is poorly defined within the region and are therefore treated as one Regional aquifer. Within the heart of the AOI Contact Rapids is characterized by porous dolostone that transitions towards the basin edges to a grey to green, argillaceous dolomite and dolomitic shale, and towards the base of the section it grades to red shale. The porous intervals are referred to here as the Lower Winnipegosis. In the AOI there is good porosity within this zone as it is predominantly dolomite.	54-76m mean of 63m. Thins towards the East	7%	The reservoir properties were not modeled in the Gen1 leak path model. Should be incorporated in future Generations of modeling. Average porosity determined from 8-19-59-20W4 well only. Average of 6.1% porosity in more calcareous/shaly portion at base (20m) and 7.4% in Dolomitic Limestone interval near top (49m)
		Cold Lake		Seal	Eastern thickening wedge of halite represented in the far eastern portion of the Quest Static Model Boundary where it reaches a thickness of 48m. There is no Cold Lake salt within the Sequestration Lease AOI. Where it exists, it acts as an additional seal. In central Alberta it grades westward into red, dolomitic shale overlying the Ernestina Lake Formation which for this study were included in the Contact Rapids Formation.	0m	0%	
		Red Beds	Devonian Red Beds 1	Baffle	Devonian Red Beds confined to the Central Alberta Sub-Basin characterized by a thin 10m red dolomitic shale that merges at the basin margins with the other Devonian Red Beds. Commonly stratigraphically described as the part of the Cold Lake Salts.	9m to 11m across AOI.	0%	No net or associated porosity found in this interval
		Ernestina Lake		Baffle	Anhydrite, light grey at top, underlain by light grey-brown, crypto-to-micro-grained limestone, locally anhydritic with salt plugged porosity. Ernestina Lake is present only in lows in underlying Lotsberg and is absent in the SW section of the AOI.	0m to 23m. Mean of 14m.	0%	No net or associated porosity found in this interval
		Red Beds	Devonian Red Beds 2	Baffle	Devonian Red Beds confined to the Central Alberta Sub-Basin characterized by a thin, maximum 11m red dolomitic shale that merges at the basin margins with the other Devonian Red Beds. Only occurs in the lows of the underlying Lotsberg Salt. Equivalent to Elk Point Group, Member 6 in the CSPG Western Canadian Lexicon.	0m to 11m. Only present in the lows around the underlying Lotsberg salt. Mean of 2m. Absent over most of AOI.	0%	No net or associated porosity found in this interval
		Lotsberg	Upper Lotsberg Salt	Ultimate Seal to BCS Storage Complex.	Over 90% pure halite that acts as an aquiclude, ranging in thickness from 53m to 94m across the AOI and thickening to 150m up-dip, NE of the AOI in the Central Alberta Sub-Basin.	53m to 94m mean of 83m	0%	The thickness of the Upper Lotsberg increased from the D65 submission because of the information attained in Westcoast 9-31 that confirms 94m of Lower Lotsberg. Previous thickness was based on Canstrat data. Salt permeability is typically less than $10^{-19}m^2$.
		Red Beds	Devonian Red Beds 3	Baffle	Devonian Basal Red Beds confined to the Central Alberta Sub-Basin. Basal Red Bed intervals exist between and below the Lotsberg Salts, merging at the basin margins together with the Devonian Red beds above. Brick red dolomitic or calcareous silty shale that grade downwards through to red sandy shale into greenish fine to coarse grained quartzose sandstone. Consistent thickness across AOI	47m to 62m mean of 57m.	0 to 2.7%	Only one porosity data point so opted to assign a value corresponding to maximum porosity seen in upscaled logs to be conservative.
		Lotsberg	Lower Lotsberg Salt	2nd Major Seal	Over 90% pure halite that acts as a regional aquiclude, ranging in thickness from 9m to 41 across the AOI and thickening to 60m up-dip, NE of the AOI in the Central Alberta Sub-Basin.	9m to 41m mean of 30m	0%	The thickness of the Lower Lotsberg increased from the D65 submission because of the wireline data from the Westcoast 9-31 well that confirms 41m of Lower Lotsberg. Previous thickness was based on seismic isochron data. Salt permeability is typically less than $10^{-19}m^2$.
		Red Beds	Devonian Red Beds 4	Baffle	Devonian Basal Red Beds confined to the Central Alberta Sub-Basin. Basal Red Bed intervals exist between and below the Lotsberg Salts, merging at the basin margins together with younger Devonian Red beds above. Brick red dolomitic or calcareous silty shale that grade downwards through to red sandy shale into greenish fine to coarse grained quartzose sandstone.	5m to 51m mean of 28m thickening towards the NE	0.5%	
BCS Storage Complex	Upper Deadwood		Upper Marine Silts	Baffle	Flow baffle composed of greenish shale and minor silty and sandy interludes deposited in the offshore shelf in response to either an increase in sediment supply or a relative sea level fall. Absent in the Eastern part of the AOI due to the Sub-Cretaceous unconformity.	0m to 63m with a mean of 44m	2%	See Gen4 static modeling report for details.
	Lower Deadwood		Middle Cambrian Shale	1st Major Seal	The first major seal composed of shale deposited in an offshore shelf environment associated with continued flooding of the basin. Present across the entire AOI ranging in thickness from 21m to 75m tinning towards the NE. The MCS is absent due the Sub-Cretaceous unconformity just to the NE of the AOI.	21m to 75m with a mean of 50m.	0%	For details see Gen4 Static Modeling Report.
	Earlie		Lower Marine Sands	Baffle	Regional flow baffle created by these transgressive, heterogeneous subtidal clastics representative of transition from marginal marine sediments of the BCS to the more distal environment of the MCS above. Present across the entire AOI.	50m to 68m with a mean of 61m	6%	In Gen3 net to gross ranges from 0.35 to 0.57. Used 0.57 in order to represent worst case scenario. Likewise, assigned a value of 6% porosity. See Gen4 Modeling Report.
	Basal Sandstone		Basal Cambrian Sands	CO2 injection zone	The BCS is transgressive sheet sand, deposited in a tide dominated bay margin, that acts as a basin-scale saline aquifer. Existing data internal and external to Shell indicates the BCS saline aquifer has suitable injectivity, capacity, and containment for CO2. The BCS is the primary target for the potential CO2 storage operation.	40m to 48m with a mean of 44m	Mid Case average 14%	Thickness based on structural model constructed by well tops in absence of structural constraint. For Details on thickness associated with structural uncertainty see Gen4 Static Modeling Report. Porosity based on Gen4 mid case averages. Incorporation of the basement high the thickness decreases to 29.7, 30.9 and 32.7m in the low, mid and high cases respectively. Net to Gross of 0.9.
	Precambrian Basement			Basal Bounding Fm	Cratonic basement on which the BCS unconformably lies on top of. Considered an aquiclude.			

9.4. Radial Well Leak Path Model using GEM

9.4.1. Legacy Well Pressures

The legacy well pressures within the BCS, as used in any of the leak path models to drive leakage of brine out of the BCS, are direct outputs of the full field pressure models. For a detailed discussion on inputs, uncertainties and dynamic outputs refer to the discussion in section 7.7.5 of the pressure modeling chapter.

9.4.2. Model description and results

A 1 km compositional radial well model was constructed from surface to basement for the Darling-1 legacy well to see what cross flow would look like should it exist. 10 000 MD was applied to the first cell surrounding the well to generate a vertical flow path. Each of the 50 discriminate layers was initialized with its own permeability, porosity, initial pressure, and salinity. For details of the model inputs see Table 41. The BCS was initialized with an 8 MPa delta pressure (28 MPa) with an infinite aquifer attached.

The resulting invasion profile seen in Figure 131 is underwhelming. As most of these layers have tight permeability they do not readily receive water injection. In reality some of the layers may fracture under the pressure and have more impressive invasion profiles. It should be noted that the Cooking Lake is under pressured and no scenario ran had brine move higher than the Cooking Lake as it is a pressure sink.

Table 41: Darling Legacy Well leakage Model Inputs

Formation	top	Porosity	Perm	kv/kh	Salinity	Datum pressure	Datum depth
	m		mD		g/l	kPa	mTVD
TBD	0	0.02	0.001	0.1		**GWPZ**	
TBD	49	0.3	500	0.1			
TBD	98	0.02	0.001	0.1			
TBD	147	0.02	0.001	0.1			
TBD	196	0.02	0.001	0.1	1	200	10
TBD	245	0.02	0.001	0.1			
TBD	294	0.02	0.001	0.1			
Lea Park	343	0.02	0.001	0.1		**Viking**	
Colorado	392	0.02	0.001	0.1			
2nd White Specks	442	0.02	0.001	0.1			
Base Fish Scales	492	0.01	0.001	0.1			
Viking	544	0.03	0.1	0.1	42	0	544
Joli Fou	556	0.02	0.01	0.1			
Mannville Gp	579	0.07	1	0.1		**Mannville**	
Mannville Gp	626	0.07	1	0.1	42	0	579
Mannville Gp	673	0.07	1	0.1			
Blueridge	721			0.1			
Calmar	751	0.01	0.001	0.1			
Nisku	760	0.06	1	0.1			
Ireton	815	0.02	0.001	0.1		**Cooking Lake**	
Ireton	867	0.02	0.001	0.1			
Ireton	919	0.02	0.001	0.1			
Ireton	971	0.02	0.001	0.1			
Ireton	1023	0.02	0.001	0.1			
Duvernay	1075	0.03	0.1	0.1			
Cooking Lake	**1120**	**0.12**	**15**	**0.2**	**65**	**9369**	**1186.6**
Beaverhill Lake	1156	0.02	0.001	0.1			
Moberly	1187	0.02	0.001	0.1			
Christina	1255	0.02	0.001	0.1			
Calmut	1299	0.02	0.001	0.1			
Firebag	1338	0.02	0.001	0.1			
Slave Point	1380	0.02	0.001	0.1			
Watt Mountain	1393	0.02	0.001	0.1			
Prairie Evap	1409	0.01	0.00001	0.1		**WPGS**	
Prairie Evap	1452	0.01	0.00001	0.1			
Prairie Evap	1496	0.01	0.00001	0.1			
WPGS	**1540**	**0.1**	**10**	**0.15**	**270**	**15228**	**1602.7**
Contact rapids	1567	0.02	0.001	0.1			
Ernestina Lake	**1625**	**0.08**	**6**	**0.1**			
Upper Lotsberg	1653	0.01	0.000001	0.1		**BCS**	
Upper Lotsberg	1698	0.01	0.000001	0.1			
Dev. Mudtsone	1744	0.04	0.1	0.1			
Dev. Mudtsone	1777	0.04	0.1	0.1			
Lower Lotsberg	1810	0.01	0.000001	0.1			
Red Beds	1847	0.03	0.01	0.1			
MCS	1892	0.04	0.1	0.1			
LMS	1912	0.09	4	0.2			
LMS	1940	0.09	4	0.2			
BCS	1969	0.16	150	0.7	311	**28036**	2041.3
Precambrian	2007	0.02	0.1	1000?	1181		

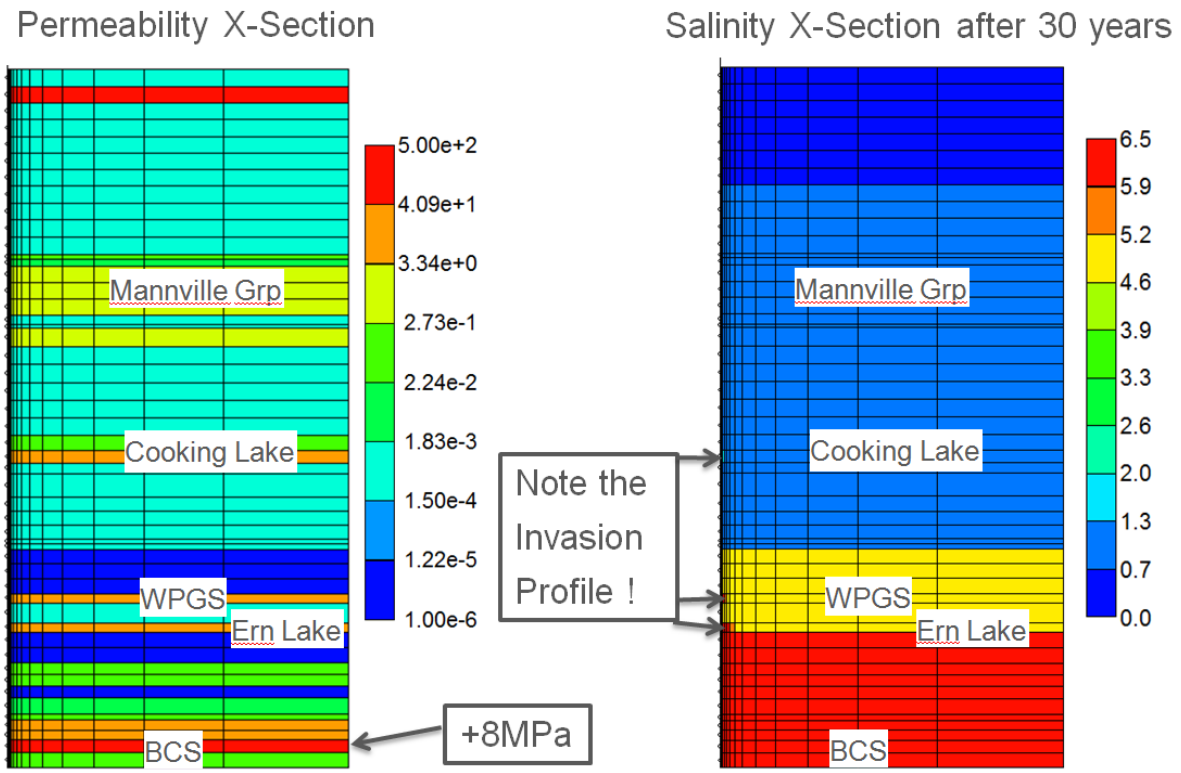

Figure 131: Initial permeability X-Section and 30 year forecast of the invasion profile as depicted in the Salinity X-section.

The Legacy well pressures will be a more probable concern in the event of the growth scenarios. The extended injection of 1.08 Mtpa will cut off in about 50 years resulting in a total injection of 54 Mts of CO_2 storage. Alternatively, if the rate were to be ramped up as in Figure 106 then the pressure rise quickly resulting in pressure exceeding what could displace BCS brine up legacy wells as soon as 7 years; resulting in only about 40 Mt's of CO_2 storage.

9.5. Radial Well Leak Path Model using TOUGHREACT

Vertical migration of CO_2 from the BCS reservoir through a potential migration-path crossing the overlaying seals into the near-surface environment is considered as a risk. Potential migration-paths consist of (1) injector wells, (2) monitor wells, (3) legacy wells, and (4) geological structures, i.e. faults/fractures.

It should be noted that:

1. No known legacy wells are expected to be exposed to CO_2 or acidic brine.
2. No seismically detectable faults have been identified in legacy and recent seismic surveys over the area of interest.

3. Taking this into account the performed vertical leak path modeling was conducted as a sensitivity study to qualitatively describe the impact of a "what if" scenario.

The assumption of a leaking injector well (100mD effective permeability) should serve as one example to illustrate the approach and reflect on some of the key findings. Figure 132 below shows the vertical migration of CO_2 from the BCS along such leak path into the overburden formations.

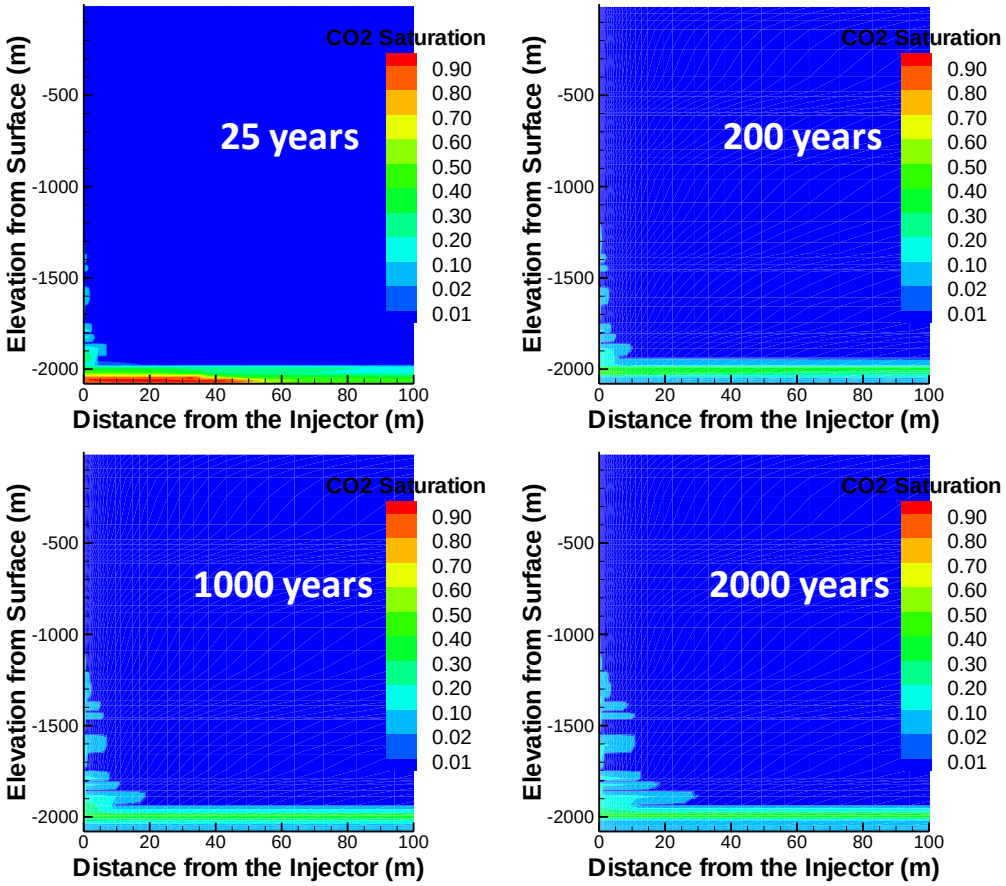

Figure 132: Modeled vertical migration of CO_2 from the BCS into overlaying layers though an injector well assumed permeable (100mD).

Such vertical migration through a permeable injector wellbore can reach 700m above the BCS at 25 years (the end of the injection), 800m above BCS at 200 years, 900m above BCS at 1000 years and stays there until the simulation ends at 2000 years.

In overburden formations, the CO_2 can reach horizontally about 30 meters away from the injector wellbore into the formations above BCS. These results are in very good qualitative agreement with the invasion calculations as performed using the radial well leak path model in GEM, as described in section 9.4 above. Even with the cases significantly different, such as CO_2 leakage along an injector versus brine leakage at the closest legacy well in the later, the

invasion of leaking fluids into the overburden will remain a very localized event of very slow dynamics.

9.5.1.1. Modeling vertical migration through a hypothetical fault with 1 mD permeability

A hypothetical scenario of a leaking fault of 1mD effective permeability 1,000 m away from an injection well should serve as a second example to illustrate aspects of leak path sensitivities (Figure 133). Results show that vertical migration starts at about 200 years after the injection and reaches 800 m above the BCS at 2000 years. The migration rate is declining and reduces down to about 10 kg/m^2/year at 2000 years. Horizontally the CO_2 can reach up to 250 m away from the fault.

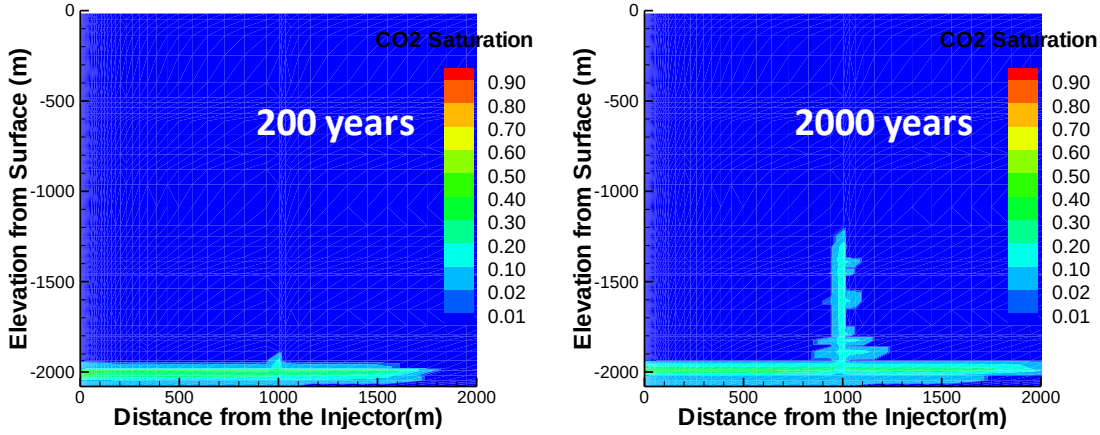

Figure 133: Modeled CO_2 vertical migration through a hypothetical fault with 1 mD permeability 1000 meter away from the injector. Note that this is a hypothetical scenario conducted to calculate the possible vertical migration rates of a hypothetical fault passing by an injector 1000m away

9.6. Geochemical alteration of the Belly River Formation through leakage

A radial 2D TOUGHREACT grid has been developed covering the sandstones within the 150m – 162m of the deep Belly River aquifer. The model accounts for aqueous component species including major ions and trace elements, aqueous complexes, redox, minerals, surface complexes, and cation exchanges. Leaking fluids have been assumed to be either CO2, acidic brine or native BCS brine. The increase of contaminants concentrations such as As, Pb and Fe was modeled as a propagation as a function of time and leak rate. Initial results show the highest concentration increase of As (10^{-6} mol/kg$_{H2O}$), Pb ($2*10^{-5}$ mol/kg$_{H2O}$) and Fe ($2*10^{-3}$ mol/kg$_{H2O}$) during leakage of CO_2 rather than leakage of acidic brine or native brine.

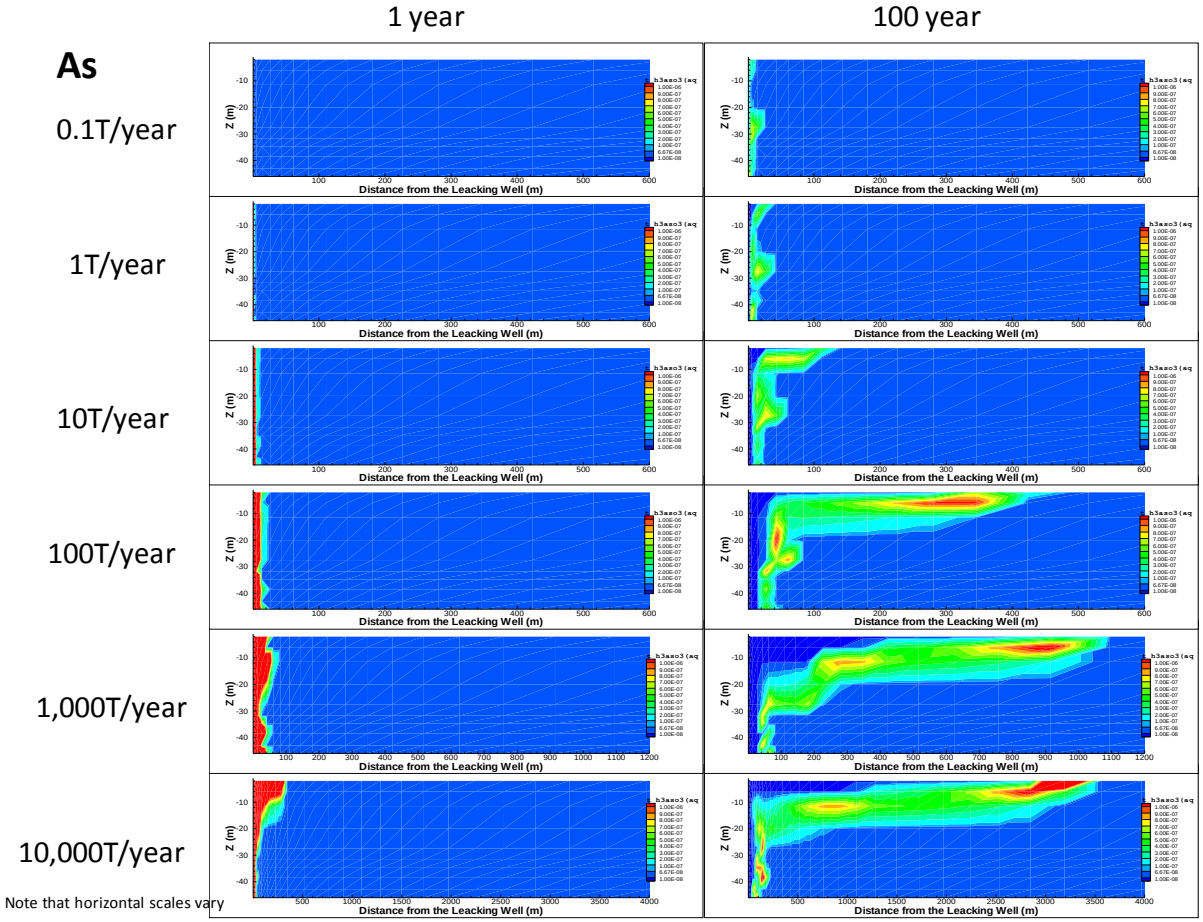

Figure 134: CO_2 leakage along an injector into overburden aquifer, arsenic (As) contamination front as a function of leak rate and duration.

Figure 134 above illustrates an example of such contamination calculation. All runs, no matter if CO_2, acidic brine or native brine was assumed leaking, exhibited similar patterns as shown above with contamination fronts extending only several tens of meters away from the wellbore (except at unrealistic high leak rates and in combination with very prolonged leak duration that would trigger corrective actions). To inform the MMV plan regarding the expected location of an hypothetical contamination front, all model results have been compiled as shown in Figure 135.

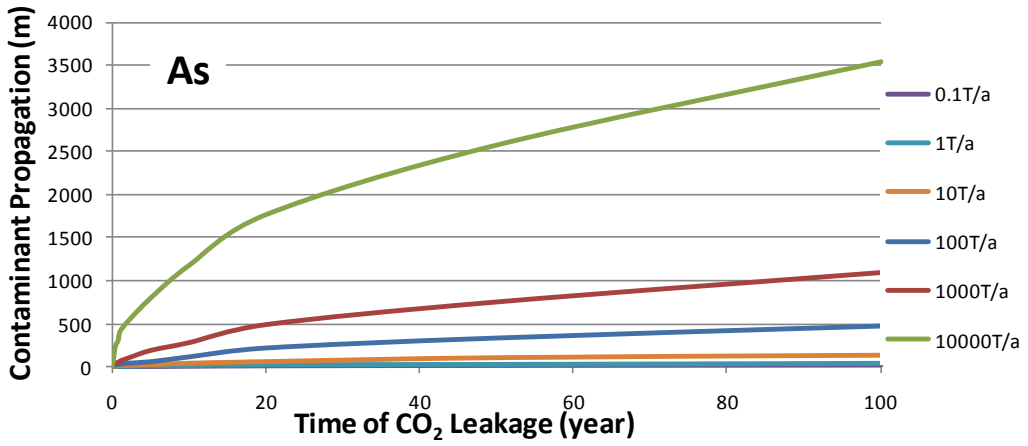

Figure 135: Distance of the contamination front as a function of leak rate and leak time (it should be noted that excessive leak rates at prolonged leak times are unexpected and would trigger corrective measures)

Additional calibration of the reactive transport modeling coefficients as used in the contamination modeling software is ongoing while performing Belly River core flooding experiments at Shell's Bellaire Technology Center.

For more detail on the geochemical modeling of induced contamination in the Belly River aquifer refer to the Gen-4 Geochemistry Report (Zhang, 2011).

10. IMPACT ON MMV

10.1. 4D Seismic Feasibility Confirmation

10.1.1. Sensitivity study of seismic CO2 detection in the BCS

Model time-lapse seismic data have been calculated to test the sensitivity of 4D to the presence of CO2 sequestered in the Basal Cambrian Sandstone ('BCS') at around 2050m depth within the Quest Project area. To create model seismic data, a multilayered structural model was built up using Shell's in house 'XStream' software, based on horizon interpretation of the 3D seismic data around the Radway well.

For modeling purposes, the 40-50m thick BCS was broken down into 24 layers, which is similar to the sub-division used in the current GEN4 reservoir model. Acoustic rock property calculations within the model followed a process similar to previous Quest 4D feasibility studies, using updated petrophysical trend analysis inclusive of new log data from the Radway 8-19 well. In keeping with previous work, acoustic impedance was regarded as primarily sensitive to saturation change and pressure effects on the relatively stiff rock frame were taken as negligible. However, an adjustment was made for changes in CO_2 properties in high pressure areas adjacent to an active injection well. Brine case compressional and shear velocities and density within the model were checked back layer by layer against the Radway well logs which tied to the center-point of the model (Figure 136).

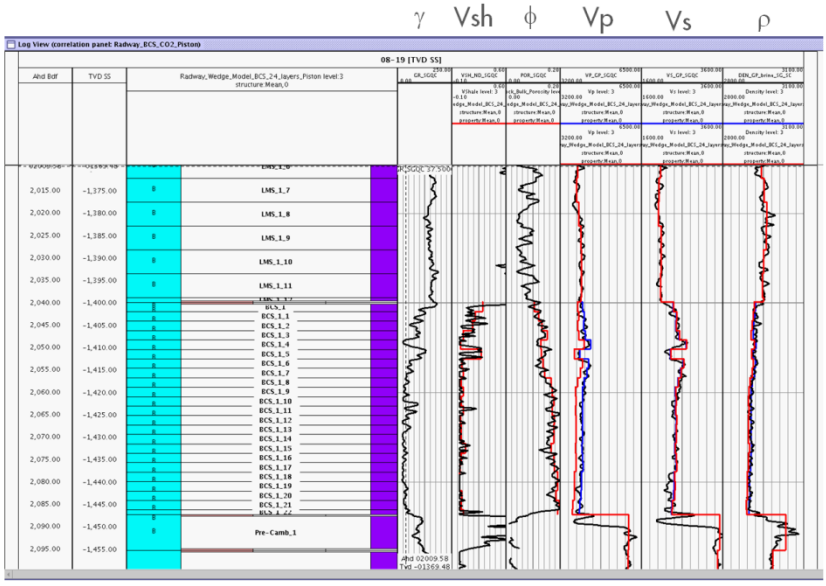

Figure 136: Model acoustic properties (CO2 case in red, brine case in blue, plotted against corresponding well logs from the Radway well. Well logs are in black, model brine charge values are in blue and CO2 charge in red.

A range of CO_2 plumes of different sizes were introduced into the model and the calculated 4D difference seismic data tested against noise levels ranging from 5 to 50% NRMS. The high net:gross and good porosities seen in the BCS, particularly in the lower two thirds of the interval, mean that, for CO_2 saturations approaching 70%, acoustic impedance changes reach 10%. The resulting 4D signal is predicted to be robust to noise levels in excess of the 15% NRMS (or equivalently RRR) achieved in the recent Geophysical Field Trial of DAS at Quest (Figure 137).

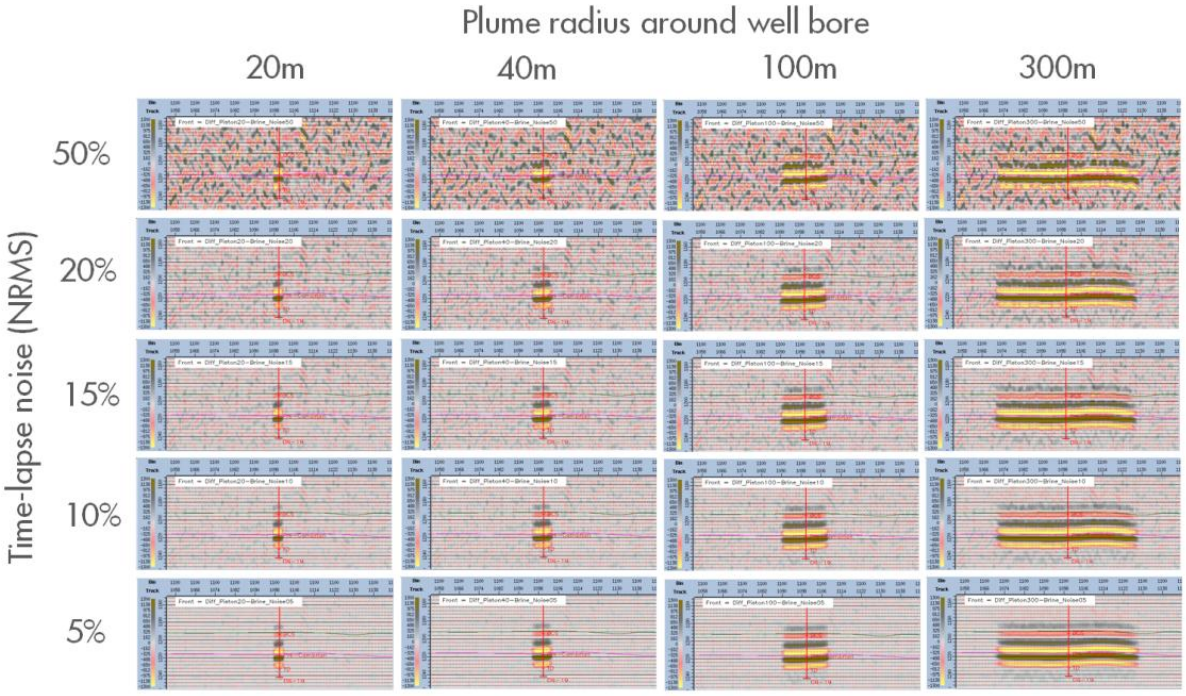

Figure 137: Model 4D difference signatures (monitor survey – baseline survey) for a range of CO2 plume sizes and noise levels.

Changes in 4D signature associated with different plume cross-sections were also modeled. A 'piston' case, in which the plume radius was constant throughout the BCS was compared to a 'gravity segregated case' in which plume diameter was largest at the top and a 'complex' case in which plume size was varied according to reservoir quality, therefore tending to favor the lower part of the BCS. (Figure 138). The 4D signatures are measurably different at expectation noise levels, indicating there may be scope to invert the time-lapse data for plume shape, although it would have to be recognized that in the real data situation, variability in subsurface properties may also have an impact.

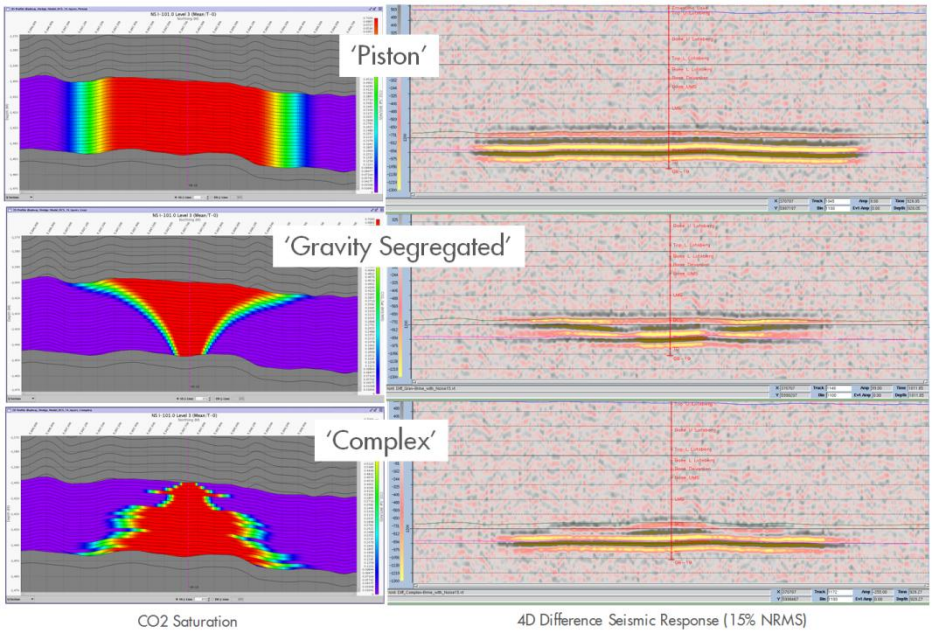

Figure 138: Model 4D difference signatures in response to differences in plume cross-section.

In summary, modeling updated to incorporate the results from the Radway well and linked to the 3D seismic data in the area, confirms previous results that a measurable time-lapse response can be expected related to CO_2 sequestered in the Basal Cambrian Sandstone in the Quest Project area. The response is robust to expected noise levels as seen in recent field trials of DAS. Indications are that it may be possible to draw some conclusion from 4D seismic as to the outline in cross-section of the plume as well as its mapped outline.

10.1.2. Seismic CO2 plume detection within the BCS

Time-lapse response modeling at BCS level was extended to include work on the Gen-4 reservoir model. An example run (expectation CO_2 plume case) containing a history of CO_2 injection in annual time-steps beginning in 2015 was imported via Petrel into the XStream software (Figure 139). As imported, the model focused solely on the BCS which was broken down into 24 layers. It was structurally smoother than the '3D Based' model already discussed but included more realistic variability in reservoir properties. As a consequence the outline of the developing plume was more complex.

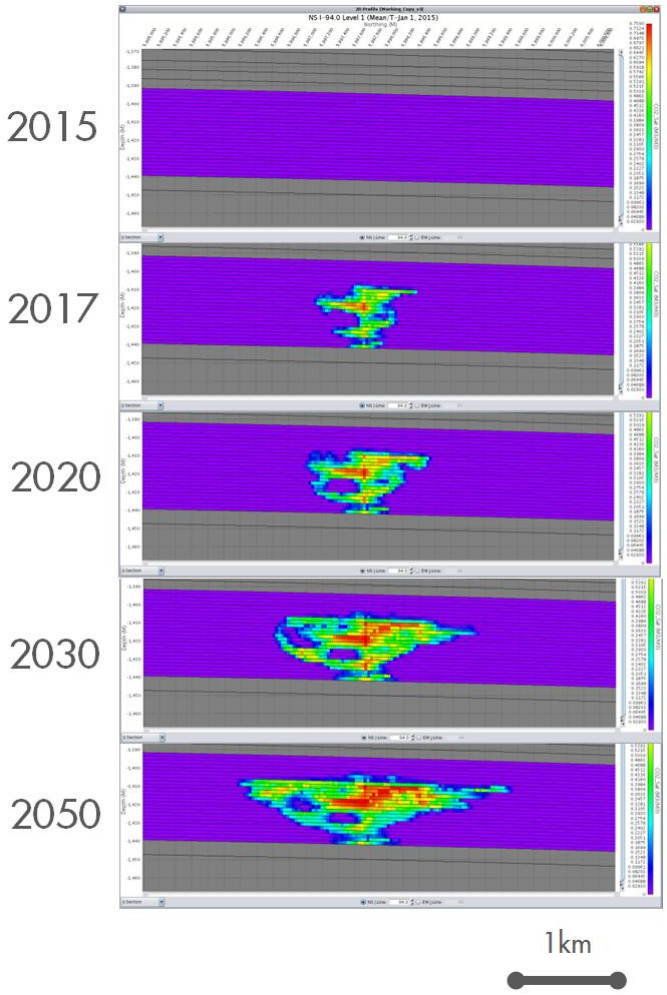

Figure 139: Development through time of a CO_2 plume injected into the BCS as represented in an example run (expectation case of the CO_2 plume model) of the GEN4 reservoir model.

Using the XStream software package, the imported GEN4 model was adapted for time-lapse seismic modeling by the addition of under and over-burden layers and incorporation of an acoustic rock model into the BCS interval. The under and over-burden was copied from the layering used in the '3D seismic' model, the associated properties being based on logs from the Radway well. The acoustic rock model in the BCS was also an adaptation; reading in porosity, net:gross and CO2 saturation from the imported GEN4 data in order to calculate Vp, Vs and Density. Resulting Acoustic Impedance signatures are shown in Figure 140 to match the CO_2 outlines shown in Figure 139.

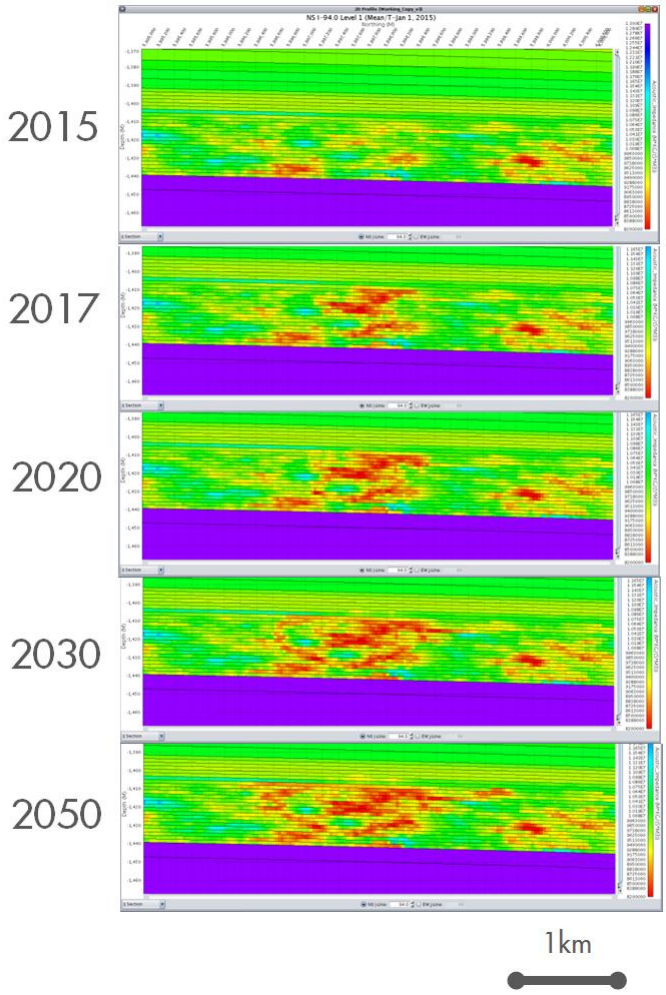

Figure 140: Development through time of a CO2 plume from the GEN4 model, translated into acoustic impedance.

4D seismic signatures were then calculated for each time-step in the injection history (Figure 139). In keeping with the DAS field results, these were calculated with the expectation 15% level of NRMS noise. The modeled time-lapse signatures show a good correlation with the lateral extent of the plume. At a more detailed level, 4D changes are quite complex with a mixture of brightening and dimming along individual horizons, combined with a time delay of some 2ms at Top Basement level within the plume area.

10.1.3. Seismic CO2 detection in reservoirs above the Upper Lotsberg Salt

Model time-lapse seismic data have been calculated to test the sensitivity of 4D to CO_2 leakage into the shallow overburden in the Quest Project area. The study focused on two intervals, the predominantly limestone Cooking Lake (~1200ft depth) and the Winnipegosis

(~1600ft depth), consisting primarily of dolomites, highlighted as candidate zones that might accumulate CO_2 in the case of leakage above the Upper Lotsberg Salt, perceived to be the ultimate Top Seal to sequestered CO_2.

To create model seismic data, a multilayered structural model was built up using Shell's in house 'XStream' software, based on horizon interpretation of the 3D seismic data around the Radway well. Acoustic rock models were established for layers in the Cooking Lake and Winnipegosis using petrophysical trend analysis of logs from the Quest Project appraisal wells. Brine case compressional and shear velocities and density within the model were checked back layer by layer against the Radway well logs which tied to the center-point of the model (Figure 141). CO_2 plumes were then introduced and the associated acoustic property changes calculated using Gassmann's equation.

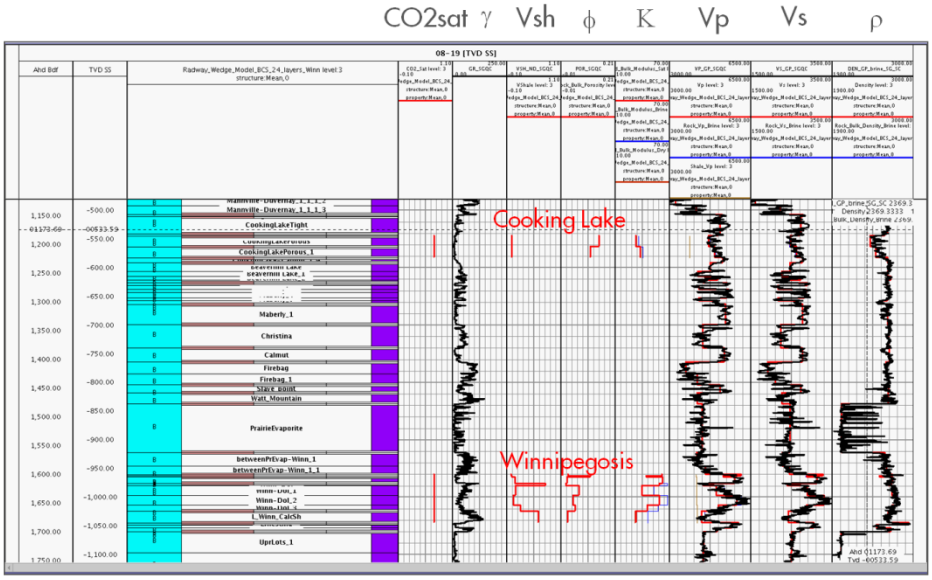

Figure 141: Model acoustic properties (CO_2 case in red, brine case in blue, plotted against corresponding well logs from the Radway well.

4D sensitivity to CO_2 presence is predicted to be relatively weak, likely due to generally low porosities (2-12%). At 70% CO_2 saturation, acoustic impedance changes within the Cooking Lake are not calculated to exceed 4% , but do reach about 7% locally within the Winnipegosis (Figure 142). As a consequence, 4D seismic difference data are not immediately perceived as robust against even modest noise levels (NRMS 10%, Figure 143). However, particularly in the Winnipegosis, coherent CO_2 related anomalies centered round the well bore (or other vertical fracture in real life) may be still be picked out when scanning through, for example, time-slices on an RMS difference data cube (Figure 144).

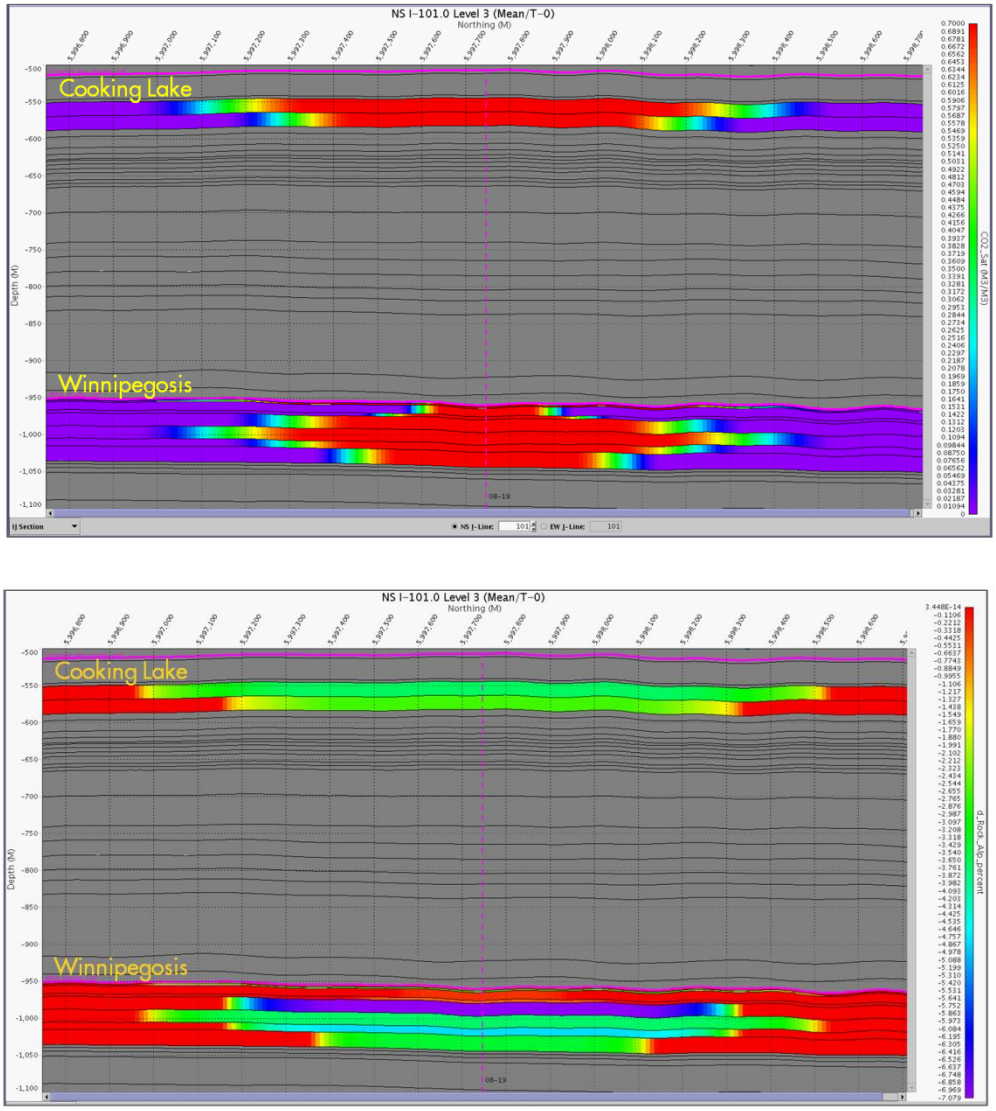

Figure 142: Model CO_2 saturations (above) and corresponding induced change in acoustic impedance (expressed in %) for the Cooking Lake and Winnipegosis.

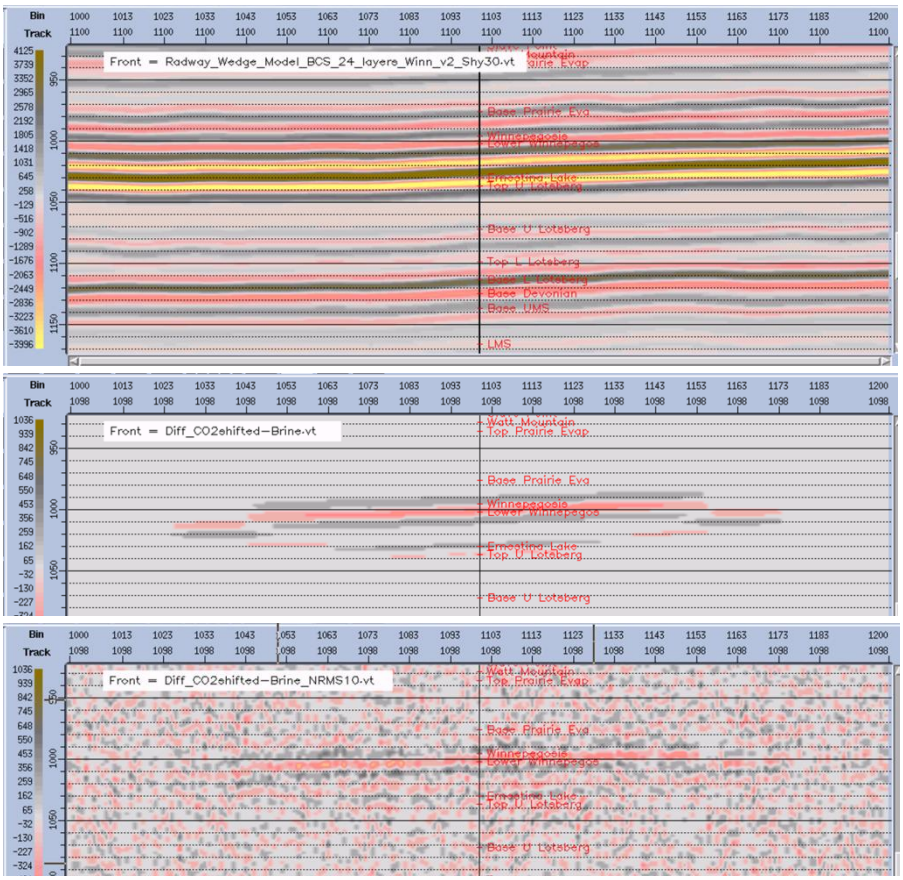

Figure 143: Model baseline seismic (top), 4D difference after time-alignment of base and monitor (middle) and 4D difference with 10% NRMS noise (bottom) for the Winnipegosis. The relatively weak 4D signal appears almost swamped in the presence of noise.

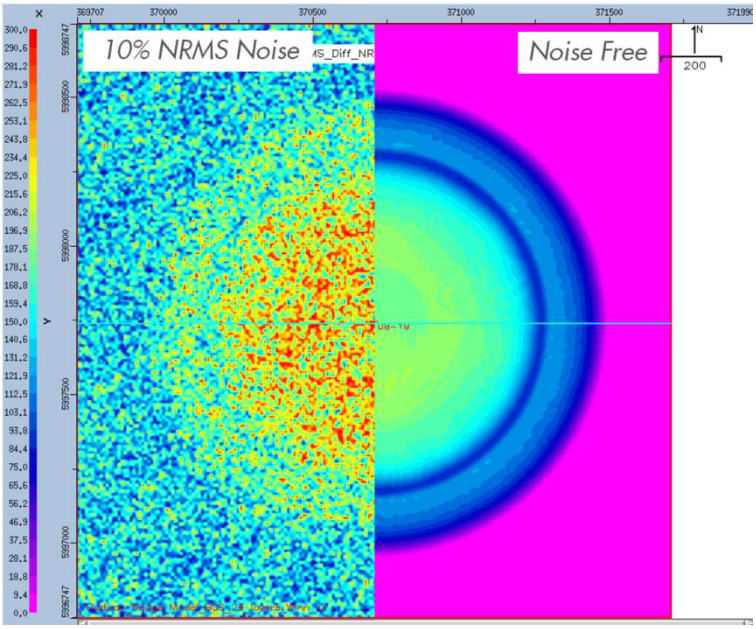

Figure 144: Mapped RMS 4D difference for the Winnipegosis; noise free case on the right, with 10% NRMS noise on the left. Despite the weak 4D response, the CO_2 plume outline is still detectable in the presence of noise.

4D time-delays due to velocity slow down accumulate progressively through the shallow CO_2 charged layers and so seismic two-way shifts mapped at the Top Upper Lotsberg Salt level are a potential indication of leakage. As modeled, these are only of the order of 1ms but, though this is a small difference, the Top Upper Lotsberg horizon is a relatively strong reflection and indications are that even small time-lapse time-shifts can be mapped reliably, even in the presence of noise (Figure 145).

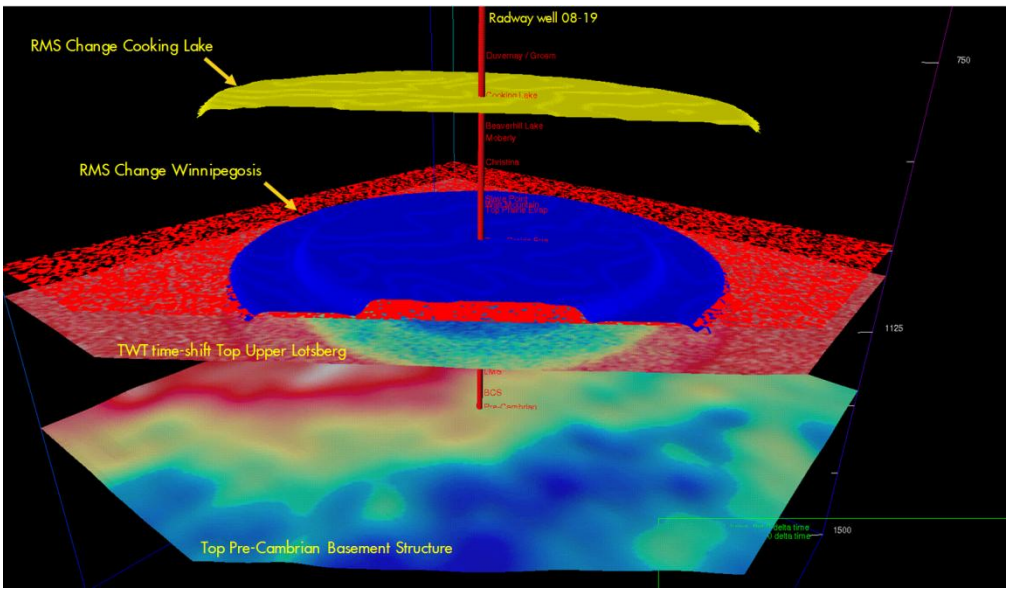

Figure 145: 3D view summarizing interpretation of model 4D seismic data. CO_2 charged zones in the Cooking Lake (yellow) and Winnipegosis (blue) are highlighted by body-checking an RMS difference data cube (requires low-noise). Mapped time-shift at Top Upper Lotsberg Salt, though small (max 1ms in blue towards the well at the center of the model, areas of no change in red), appears robust to random noise.

In summary, modeled seismic 4D responses to CO_2 charge in the shallow Cooking Lake and Winnipegosis are relatively weak. However, although the immediate perception is that the 4D signal will be swamped by even modest noise levels, the coherent shape of the CO_2 plumes (if migration through overburden formations occurs coherent) in map view vs. random noise, and the integral effect on time shifts of potentially having a number of vertical stacked plumes could still render time-lapse seismic data a useful tool to confirm CO_2 containment.

It was recommend that a Quantitative Interpretation project is initiated with the Shell Canada Geophysics team to investigate further reservoir characterization using the latest data processing products. This project could help predict reservoir thickness and quality distribution across the 3D seismic area. This prediction would be calibrated with the information from the next 2 wells and could be quickly updated at that time.

10.2. Minimum Formation Stress Reduction

To obtain input for the Geomechanical modeling, a rock property model and an insitu stress model developed in the previous FEM modeling work were used. These models were constructed using field data collected from two pilot appraisal wells (Scotford 11-32) and Redwater 3-4). The collected field data include well logs, MDT, LOT/FIT, mini fracs, and FMI image/Caliper. The rock property models were further calibrated with log data and core measurements obtained from the Radway 8-19 well. The boundary conditions and geometry

data are consisted with the parameters as used in all other Quest Gen-4 models. The increase in reservoir pressures corresponding to latest Gen-4 models were provided by the reservoir modeling group in the Shell Quest team. Far-field temperature and pressure changes were obtained from the radial well model as described in section 4 of this report. This note provides a brief summary of the results and the detailed description of the model and results are included in the final report.

Minimum Stress Reduction

As CO_2 is injected at temperatures lower than the virgin temperatures of the BCS formation, the formation is cooled and the temperature front advances into the formation. At the same time the injection results in an increase in the reservoir pressure. The reduction in formation temperatures results in a decrease in the minimum horizontal stress due to the thermoelastic effect. On the other hand, the increase in the pore pressure increases the minimum horizontal stress due to the poroelastic effect. A 2D axisymmetric finite element model has been setup which takes temperature input from the radial injection model and computes the associated reduction in the stresses. The impact of the pore pressure increase and the associated poroelastic effect is incorporated considering a horizontal stress arching factor. The radial injection model considers various sub-layers within the main BCS reservoir where different temperature profiles are computed depending on their injectivity, permeability and thermal parameters. The base case mechanical properties obtained from core calibrated measurements are E=18 GPa and v= 0.18. Stress reduction profiles are obtained for the two layers with the minimum and maximum temperature change are shown in Figure 146 and Figure 147, respectively. As the temperature front advances the region where the minimum stress reduces grows which extends about 275 m into the formation. Results shown here are after a 25 year injection period and show that minimum stress reduces to 27 – 30 MPa.

Some key observations from these models are:

- Impact of thermal cooling on minimum stress is limited to ~300m
- The impact of the stress reduction is limited to the BCS and does not impact the integrity of the seals
- The impact of the thermal stress reduction to 27-30 Mpa is covered by the range of BHP limitations evaluated in the project which are:
    - 32 MPa as the maximum allowable BHP and what has been requested in the Regulatory submission
    - 28 MPa has been used for all modeling scenario’s except the growth options
    - 26 MPa is the low case BHP limitation although no case was run with this scenario as the base case reservoir model never reached this value.

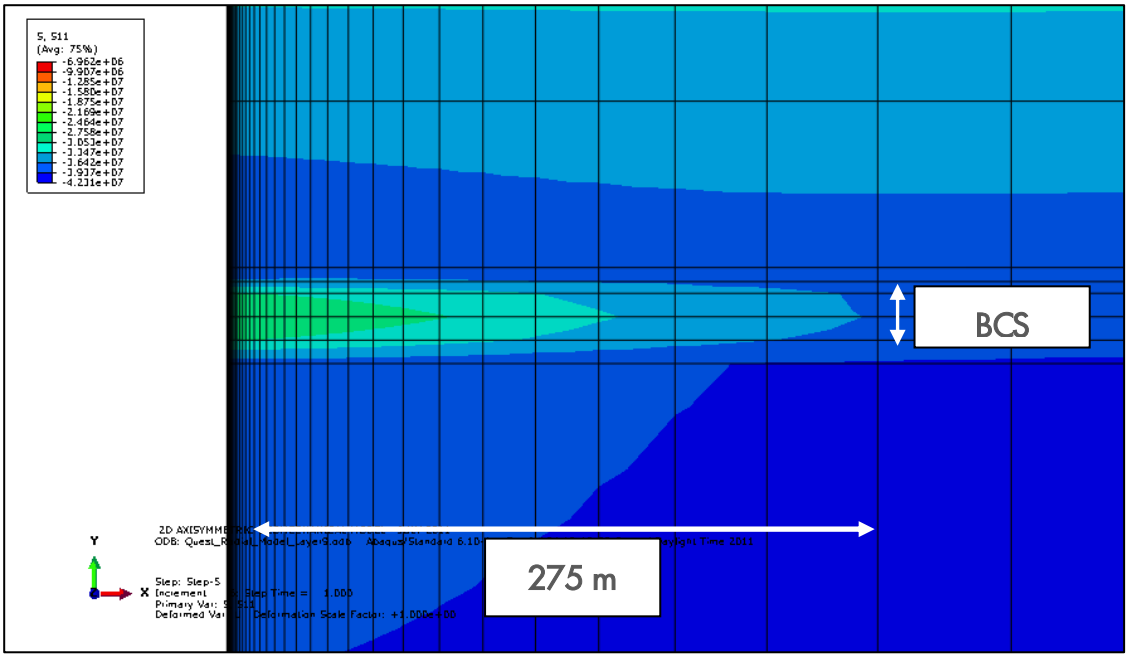

Figure 146: Minimum stress profile obtained for the case with least temperature change in the BCS interval.

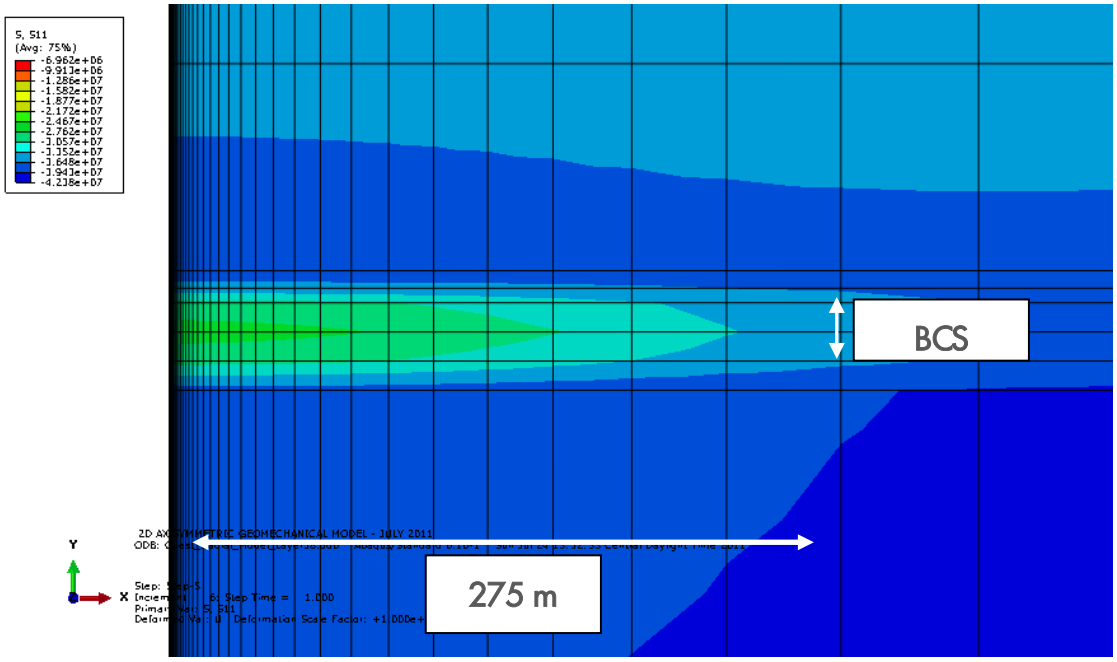

Figure 147: Minimum stress profile obtained for the case with largest temperature change in the BCS interval.

11. WORKS CITED

Bachu, S. H. (1986). *Preliminary Analysis of Transport Processes in the Basal Cambrian Aquifer of South-Central Alberta.* Third Canadian/American Conference on Hydrogeology.

Bachu, S. (2009). *Identification of a Storage Site for CO2 Emissions from Statoil's Oil Sands Operation in North Eastern Alberta.* Alberta Research Council.

Begg, S. H. (1985). *A Simple Statistical method for Calculating the Effective Vertical Permeability of a Reservoir Containing Discontinuous Shales.* Society of Petroleum Engineers Paper No. 14271.

Carpenter, A. B. (1978). *Origin and chemical evolution of brines in sedimentary basins.* Oklahoma Geologicsal Survey Circular .

Chafetz, H. (1978). *A throug cross-stratified glaucarenite: A Cambrian tidal inlet accumulation.* Sedimentology.

Clark, C. (2010). *Quest IPSM Compressor Design Modeling Report.* 07-3-ZG-7180-0004.

Connolly, C. W. (1990). *Origin and evolution of formation waters, Alberta Basin: I, Chemistry.* Applied Geochemistry 5.

Crouch, S. (2011). *Quest Storage Development Plan.* 07-0-AA-5726-0001.

Dalrymple, R. W. (2007). *Morphologic and facies trends through the fluvial-marine transition in tide-dominated depositional systems: A schematic framework for environmental and sequence-stratigraphic interpretation.* Journal of Earth-Science Reviews.

Doe, P. Z. (2011). *Quest CCS Gen4 - Capillary Pressure & Relative Permeability Modeling and Uncertainties.* 07-3-ZG-7180-0029.

El Mahdy, R. (2011). *Seal Integrity and Fracture Pressures.* 07-3-ZG-718-0012.

Glass, D. (2000). *Canadian Society of Petroleum Geologists Lexicon of Canadian Stratigraphy.* Volume 4 - Western Canada.

Hanor, J. (1994). *Origin of saline fluids in sedimentary basins. In Geofluids: origin, migration, and evolution of fluids in sedimentary basins.* . Geological Society Special Publication (London) .

Howell, B. F. (1944). *Correlation of the Cambrian formations of North America.* Geological Society of America Bulletin.

Hugonet, V. (2011). *Quest Wells Conceptual Completion Design Document.* 07-3-ZW-7180-0003.

Kestin, J. (1981). *Tables of Dynamic and Kinematic Viscosity of Aqueous KCL Solutions in the Temperature Range 25-150C and the Pressure Range 0.1-35 MPa.* J. Phys. Chem. Ref. Data.

Lonergan, L. (1994). *Default Rock Properties for Thermal Modeling.* Report RKGR94.139.

Meijer – Drees, N. (1994). *Devonian Elk Point Group of the Western Canadian Sedimentary Basin. In: Geological Atlas of the Western Canadian Sedimentary Basin. G.D. Mossop, I. Shetsen (comps.).* . Canadian Society of Petroleum Geologists and Alberta Research Council.

Mossop, G. S. (1994). *Geological Atlas of the Western Sedimentary Basin.* Canadian Society of Petroleum Geologists and Alberta Research Council.

Ojakangas, R. W. (1963). *Petrology and sedimentation of the Upper Cambrian Lamotte Sandstone in Missouri.* Journal of Sedimentary Petrology.

Otvos, E. G. (1966). *Sedimentary structures and depositional environments, Potsdam Formation, Upper Cambrian.* American Association of Petroleum Geologists Bulletin.

Pierpont, R. (2011). *BCS Brine Tracer Feasibility Report.* 07-3-ZG-718-0027.

Pruess, K. (2009). *Formation dry-out from CO2 Injection into Saline Aquifers.* Water Resour. Res. 45, W03402.

Rowe, A. J. (1970). *Pressure-Volume-Temperature-Concentration Relation of Aqueouse Sodium Chloride Solutions.* J. Chem. Eng. Data.

Runkel, A. C. (2007). *High-resolution sequence Stratigraphy of lower Paleozoic sheet sandstones in central North America: The role of special conditions of cratonic interiors in development of cratonic interiors in debvelopment of stratal architecture.* Geological Society of America Bulletin.

Runkel, A. C. (1998). *Origin of a classic cratonic sheet sandstone: Stratigraphy across the Sauk II – Sauk III boundary in the Upper Mississippi Valley.* Geological Society of America Bulletin.

Simone, A. (2011). *Quest Generation-4 Petrophysical Evaluation and Integration with Sedimentary Petrology.* Report 07-3-ZG-7180-0022.

Switzer, S. H. (1994). *Devonian Woodbend-Winterburn Strat of the Western Canada Sedimentary Basin.* Canadian Society of Petroleum Geologists and Alberta Research Council.

Tare, U. (2011). *Quest Geochemical Calibration - Radway 8-19 Well Input.* Report 07-3-ZG-7180-0024.

Wendte, J. S. (2009). *Reservoir Architecture of the Redwater Leduc Reef, Central Alberta* . Alberta Research Council. Stoakes Consulting Groups (SCG).

Willis, M. (1994). *Thermal Conductivity of Rock Materials.* Report RKGR94.111.

Winkler, M. (2010). *Quest CCS Project - Technical Feasibility and Forward Plans to FID.* EP 2010-3099.

Winkler, M. (2010). *Quest Generation-3 Integrated Reservoir Modeling Report.* Report 07-3-AA-8211-0001.

Wood, L. J. (2004). *Predicting tidal sand reservoir architecture using data from modern and ancient depositional systems; in Integration of outcrop and modern analogs in reservoir modeling.* American Association of Petroleum Geologists Memoir.

Zhang, G. (2011). *Quest Geochemical Study - Radway Well Calibration and Shallow Horizons.* Report 07-3-ZG-7180-0026.

12. NOMENCLATURE

2D	Two-Dimensional
3D	Three-Dimensional
4D	Four-Dimensional
AOI	Area of Interest
BCS	Basal Cambrian Sand
BGWP	Base of Ground Water Protection zone
BHP	Bottom Hole Pressure
BRGP	Belly River Group
CCS	Carbon Capture and Storage
CDF	Cumulative Density Function
CLRD	Colorado Group
cm	Centimeter
CMG	Computer Modeling Group
CO2	Carbon Dioxide
cp	Centipoise
D	Non-Darcy skin factor
D65	Directive 65 of the ERCB
DB	Distal Bay
EoD	Environment of Deposition
ERCB	Energy Resources Conservation Board
FBHP	Formation Bottom Hole Pressure
FID	Final Investment Decision
FIT	Formation Integrity Test
FMI	Formation Imager
ft	foot
GEM	Generalized Equation of state Model reservoir simulator
Gen-1	Generation-1 Integrated Subsurface
Gen-2	Generation-2 Integrated Subsurface
Gen-3	Generation-3 Integrated Subsurface
Gen-4	Generation-4 Integrated Subsurface
HED	High Energy Dune
HRAM	High Resolution Aero Magnetics
IPM	Integrated Production Modeling

k	Permeability (mD)
kg	Kilogram
Kh	Horizontal Permeability
km	Kilometer
kPa	Kilopascal
kPa	Kilopascal
Kv	Vertical Permeability
LGR	Local Grid Refinement
LMS	Lower Marine Sand
LOT	Leak Off Test
LSD	Legal Subdivision
MCS	Middle Cambrian Shale
mD	Millidarcy
MDT	Modular Formation Dynamics Tester
mg	Milligram
MMV	Measuring Monitoring and Verification
MNVL	Manville Group
MPa	Mega Pascal
Mtpa	Million Tone per annum
NE	North-East
NTG	Net-to-Gross
P10	10% probability
P50	50% probability
P90	90% probability
PB	Proximal Bay
PLD	Plume Length Dashboard
ppm	Parts per Million
PVD	Plume Volume Dashboard
QC	Quality Control
RDL	Red Deer Lineament
S	Well Bore Skin
SET	Seawater Evaporation Trajectory
SIEP	Shell International Exploration and Production
STZ	Snowbird Tectonic Zone
SW	South-West
T	Temperature in degrees Centigrade

TDBM	Tide Dominated Bay Margin
TGSwT	Truncated Gaussian Simulation with Trends
TMI	Total Magnetic Intensity
TS	Thomas – Stieber
UDEV	Upper Devonian
UMS	Upper Marine Siltstone
Vp	Compressional Sonic Velocity
Vs	Shear Sonic Velocity
Vsand	Sand Volume Fraction
WCSB	Western Canadian Sedimentary Basin
WPGS	Winnipegosis

APPENDIX 1. QUEST ITERATIVE MODELING STRATEGY

Quest Subsurface Modelling Strategy

	Type/Description	Topic	Inputs	Variables	Outputs	Learnings
Generation 1	**Gen1 Full Field Models**	**Project Screening, FPP Submission** and planning of 1st appraisal campaign	**Regional formation properties** (105 wells in BCS, 88 used for structural, 49 for PP input)	Reservoir quality, BHP constrained injection	Pressure contours, CO2 footprint, # of injector wells	Base case of 5 injector wells is sufficient
Generation 2	**Gen2 Full Field Models**	Project feasibility assessment and **Exploration Tenure**	As above and updated by **SF, RW** appraisal well results.	Reservoir quality, BHP constrained injection	Pressure contours, CO2 footprint, # of injector wells	Low case of 1 injector well feasible, base case of 3 wells confirmed, high case of 7 wells
	Gen2 Sector Model	**Exploration Tenure**, sensitivity assessment of plume migration and trapping mechanisms	As above with the addition of connectivity updated by **RW 3D seismic mini-survey**	Formation connectivity, reservoir quality, BHP constrained injection, injected volume down-scaled to model size	Pressure contours, detailed CO2 footprint, # of injector wells	Key sensitivities driving plume migration and trapping are permeability, and relative permeability.
	Gen2 Interference	**Exploration Tenure**, Urban planning assessment while including "competing" inection projects at pore space boundary.	As Gen2 Full Field model with the addition of compeating schemes at NE and SW pore space boundaries (each 1.2 Mtpa for 25 years)	Base case Gen2 models with varying total injection rates	Pressure contours, CO2 footprint, # of injector wells and inhibited well rates at inteference between the schemes.	Competing "Quest like" injection schemes right at the tenure boundary would inhibit Quest injectivity by 2025.
	Gen2PLus Full Field Models	**Funding Agreement**, Low Connectivity case to de-risk feasibility assessment	As above with the addition of connectivity updated by **RW 3D seismic mini-survey**	Formation connectivity and reservoir quality, BHP constrained injection	Pressure contours, CO2 footprint, # of injector wells	A 7 well development is feasible to mitigate this low case scenario.
	Gen2 radial TOUGHREACT Model in BCS	Geochemical alteration of BCS formation and brine, halite precipitation CO2 path ways	Gen2 base case formation properties, layered perm model as per Scotford appraisal well	Single injector of a 3 well development with down-scaled injected volume (1/3), kv/kh of high perm layer as variable	Halite dry-out zone, pressure profile,CO2 pume reach and dynamics of trapped volume fractions	Dry out zone of 60-70m estimated.

	Type/Description	Topic	Inputs	Variables	Outputs	Key Learnings
Generation 3	**Gen3 Full Field Models**	**Regulatory Submission**, Storage Complex	Regional formation properties, updated by **SF, RW** appraisal wells, **2D & 3D seismic results and HRAM**	Formation connectivity, reservoir quality and facie distribution, BHP constrained injection	pressure contours, CO2 footprint, # of injector wells	Confirmed the project description and well count between 3 to 10 injector wells
	Gen3 Full Field Model + High Perm Basal Layer	**Regulatory Submission**, Storage Complex, High Permeability Thieve Zone	As above plus 8m high permeability layer at BCS/Precambrian	Base layer 10-20D perm, 8m thickness, variable kv/kh of BCS, BHP constrained injection	Pressure distribution and CO2 plume geometry	While a high perm basal layer certainly acts as a pressure sink, CO2 will quickly migrate back into the BCS due to buoyancy.
	IPSM Study	Compressor Selection and Pipeline Size	Generation 3 range of injector well count and BHP constrains.	Number of injection wells, pipeline length and size, length of laterals, seasonal variations in ground temperature, compressor discharge temperature	Required discharge pressure to drive the integrated system.	A compressor discharge pressure of 14.5 Mpa under discharge temperature control and a pipeline size of 12" provides a robust development concept.
	Surface Heave Models	InSaR Feasibility and input to well bore stability models	Gen3, 3 well and 7 well pressure field (worst case for localized pressure effect)	Elastic formation properties	Surface heave and stress field near well bore	A surface vertical uplift of approx. 40 mm was estimated for the reference case after 25 years of injection.
	Radial TOUGHREACT model in BCS+LMS+MCS	Geochemistry in Storage Complex	Brine and matrix composition(s)	Permeability profile & kv/kh	"Trapped volume count", halite dry out zone, alteration of primary seal	BCS is geochemically inert, adding reactive transport modeling will have no impact on filed development decisions (plume size, pressure front), on average 3.7% of the CO2 is dissolved in brine, no mineral trapping until 100's of years post injection
	Radial TOUGHREACT model in Wapiti Formation	Shallow Aquifer Contamination (MMV)	Wapiti and BCS brine composition, GeoChem of Wapiti formation, BCS Pressure from Base Case Gen3 dynamic model	1. Leakage at Injector, 2. Leakage at MMV well (1 km), 3. Leakage at closest legacy well (20 km).	Concentration Maps around leaking well, changes in rock and fluid chemistry including potential release of unwanted compounds.	Small amounts of As, Pb and Fe may be mobilized due to leakage of CO2 or CO2 saturated brine into shallow aquifers. Contamination front will only reach a few 100's of meters from leak point.

	Type/Description	Topic	Inputs	Variables	Outputs	Key Learnings
Generation 4	Radial Sector Models	Detailed SDP, Thermal Cooling and Well Start-up behavior	Radway well results (core calibrated).	Thermal conductivity of formation, CO2 injection temperature, grid size of model(s)	Formation temperature as function of distance from wellbore and time. Grid size around wells to avoid boundary effects	Cooling front reaches approx. 350m into formation (3 well development at 25 years). Formation takes a long time to re-equilibrate.
	Gen4 Full Field Pressure Models	Detailed SDP, Storage Complex, full-field pressure distribution	As Gen 3, updated with Radway results, both well and geophysical data plus 1B seismic results.	Reservoir quality, Formation connectivity and reservoir quality, BHP constrained injection	pressure contours, confirm # of injector wells, pressure at legacy wells.	Confirmed the range of required injector well count to be between 3 to 8 vertical injectors.
	Gen4 Plume Sector Model	Detailed SDP, CO2 plume migration, conformance and detailed MMV planning	As Gen 3, updated with Radway results and Radway 3D interpretation,	Reservoir quality, 3D reservoir heterogeneity, well interference, static and dynamic reservoir properties, CO2 injection volume.	Plume radius probability distribution, trapping efficiency, storage volume utilization	Sensitivity to Rel Perms. Conformance may drive final well count.
	Flow Assurance Models	Integrated System, standard operation and upset conditions, down-turn options	14.5 Mpa compresion system, 12" pipeline, pipeline topography	Rates, temperature, CO2 composition	Operating envelop, hydrate formation risk, condensation.	Confirmed robust operating envelop without encountering hydrate issues.
	Surface Heave Model	MMV Plan, InSaR local calibration	Core calibrated Radway properties, formation temperature distribution, base case pressure distribution	Formation compressibility ranges, formation pressure	Surface heave and near wellbore stress field - reduction in fracture pressure	
	Overburden Leak Path Models	Assessment of hypothetical leak paths and rates into shallow aquifers	Legacy well properties and Quest well properties at regional scale	Leak features (legacy wells, own injector wells or faults) pressure and plum distribution, leak path properties (porosity, perm)	Arrival times, leak rates and gechemical reactions in formationa above the storage complex.	
	Analytical Point Source Model	BCS leakage into Winnepegosis (MMV)	Winnepegosis formation properties	DTS Sensitivity	Detectable leakage rate and radial concentration decay	
	Time Laps Seismic Modeling Study	Feasibility was confirmed in Gen3, additional modeling for conformance benchmarking.	Radway calibrated geophysical properties, CO2 plumes from sector model study	CO2 saturation as function of time	Seismic detection thresholds as function of CO2 net-thickness and noise level	
	Well Bore Stability Models	Stress field change and impact on completion, cement integrity and wellbore stability.	Radway formation properties, temperature distribution	Thermal expansion coefficient, BHP	Stress field change and associated fracture pressure reduction	Estimated reduction in BHP constraint (28 MPa) with a low case of 24 MPa due to reservoir cooling.

APPENDIX 2. CAPILLARY PRESSURE FUNCTIONS

Low case, base case and high case capillary pressure functions were derived based on fitting the Quest primary drainage capillary pressure experiment data. Those functions and parameters are summarized below.

Brooks Corey Equation $S_{wi} = S_{wi} + (1 - S_{wi})\left(\frac{PC_e}{PC_{IFT1}}\right)^{1/n}$

$$PC_{IFT1} = \frac{PC}{IFT_{lab}.\cos(\theta)_{lab}} = \frac{PC_{lab}}{480*0.76}$$

$$PC_{res} = \frac{PC_{lab}*IFT_{res}*\cos(\theta)_{res}}{IFT_{lab}.\cos(\theta)_{lab}} = PC_{IFT1} * IFT_{res} * \cos(\theta)_{res}$$

$$HAFWL = \frac{PC_{res}}{g*(\rho_{brine}-\rho_{HC})}$$

	Low Case	Base Case	High Case
Swi	$Swi = 0.192 - 0.063 * LOG\sqrt{\frac{K}{Phi}}$	$Swi = 0.18723 - 0.0792 * LOG\sqrt{\frac{K}{Phi}}$	$Swi = 0.187 - 0.095 * LOG\sqrt{\frac{K}{Phi}}$
PCe	$PCe = 0.009 * K^{-0.3}$	$PCe = 0.007488 * K^{-0.4038}$	$PCe = 0.0048 * K^{-0.46}$
N	$N = 2.1 * K^{-0.02}$	$N = 1.93397 * K^{-0.021916}$	$N = 1.8 * K^{-0.035}$

Where PC is in [bars], HAFWL in [meters], IFT in [dynn/cm] and $\theta$is in [degrees]. The IFT of 27.7 dynn/cm and wettability angle of 180 degrees were assumed between the supercritical CO_2 phase and brine.

APPENDIX 3. COREY MODEL PARAMETERS

The relative permeability Corey model is an empirical model. For an Oil-Water (or Supercritical CO_2 – brine) system, the Corey functions for the drainage cycle (inject CO_2 to displace reservoir brine) can be expressed as:

$$Kro_{\_drain} = Kroi * (S^*_{o\_drain})^{n_{o\_drain}}$$

$$Krw_{\_drain} = Krwi_{\_drain} * (S^*_{w\_drain})^{n_w}$$

$$S^*_{w\_drain} = \frac{S_w - S_{wirr}}{1 - S_{wirr}}$$

$$S^*_{o\_drain} = 1 - S^*_{w\_drain}$$

The Corey functions for the imbibition cycle (re-imbibition of brine) are:

$$Kro_{\_imb} = Kroi * (S^*_{o\_imb})^{n_{o\_imb}}$$

$$Krw_{\_imb} = Krwi_{\_imb} * (S^*_{w\_imb})^{n_w}$$

$$S^*_{w\_imb} = \frac{S_w - S_{wirr}}{1 - S_{wirr} - S_{or}}$$

$$S^*_{o\_imb} = 1 - S^*_{w\_imb}$$

Combining the low, mid, high cases of relative permeability Corey models together with the low, mid, high cases of the capillary pressure models, results in total of nine permutations for the relative permeability and capillary pressure inputs. The tables below summarizing those relative permeability Corey model parameters accordingly.

	LM	MM	HM	ML	MH	LL	HH	LH	HL
Rel.Perm	Low	Mid	High	Mid	Mid	Low	High	Low	High
Cap.Pre	Mid	Mid	Mid	Low	High	Low	High	High	Low

Table 42 (LM) Low Case Rel. Perm. Corey Model with Mid Case Capillary Pressure

Rel. Perm Case	Cap. Pres. Case	Perm Class	$Krwi_{\_drain}$	n_{o_drain}	n_w	Swirr	Kroi	Sor
Low	Mid	<3 mD	1	3.751	3.878	0.17	1.643	0.50
		3~10 mD				0.14	1.57	0.514
		10 ~36 mD				0.12	1.472	0.526
		36 ~128 mD				0.09	1.345	0.538
		128 ~ 446 mD				0.07	1.197	0.549
		>446 mD				0.05	1.032	0.559

Table 43: (MM) Base Case Rel. Perm. Corey Model with Mid Case Capillary Pressure

Rel. Perm Case	Cap. Pres. Case	Perm Class	$Krwi_{\_drain}$	n_{o_drain}	n_w	Swirr	Kroi	Sor
Mid	Mid	<3 mD	1	2.625	4.804	0.17	2.378	0.345
		3~10 mD				0.14	2.273	0.352
		10 ~36 mD				0.12	2.130	0.358
		36 ~128 mD				0.09	1.946	0.364
		128 ~ 446 mD				0.07	1.732	0.369
		>446 mD				0.05	1.493	0.373

Table 44: (HM) High Case Rel. Perm. Corey Model with Mid Case Capillary Pressure

Rel. Perm Case	Cap. Pres. Case	Perm Class	$Krwi_{\_drain}$	n_{o_drain}	n_w	Swirr	Kroi	Sor
High	Mid	<3 mD	1	1.731	5.284	0.17	3.577	0.274
		3~10 mD				0.14	3.418	0.278
		10 ~36 mD				0.12	3.204	0.281
		36 ~128 mD				0.09	2.928	0.284
		128 ~ 446 mD				0.07	2.605	0.286
		>446 mD				0.05	2.245	0.288

Table 45: (ML) Mid Case Rel. Perm. Corey Model with Low Case Capillary Pressure

Rel. Perm Case	Cap. Pres. Case	Perm Class	$Krwi_{\_drain}$	n_{o_drain}	n_w	Swirr	Kroi	Sor
Mid	Low	<3 mD	1	2.625	4.804	0.20	2.224	0.338
		3~10 mD				0.17	2.114	0.345
		10 ~36 mD				0.15	1.974	0.350
		36 ~128 mD				0.13	1.797	0.352
		128 ~ 446 mD				0.11	1.594	0.360
		>446 mD				0.09	1.370	0.364

Table 46: (MH) Mid Case Rel. Perm. Corey Model with High Case Capillary Pressure

Rel. Perm Case	Cap. Pres. Case	Perm Class	$Krwi_{\_drain}$	n_{o_drain}	n_w	Swirr	Kroi	Sor
Mid	High	<3 mD	1	2.625	4.804	0.15	2.506	0.351
		3~10 mD				0.12	2.400	0.358
		10 ~36 mD				0.09	2.255	0.364
		36 ~128 mD				0.06	2.064	0.370
		128 ~ 446 mD				0.04	1.842	0.375
		>446 mD				0.01	1.592	0.380

Table 47: (LL) Low Case Rel. Perm. Corey Model with Low Case Capillary Pressure

Rel. Perm Case	Cap. Pres. Case	Perm Class	$Krwi_{\_drain}$	n_{o_drain}	n_w	Swirr	Kroi	Sor
Low	Low	<3 mD	1	3.751	3.878	0.20	1.537	0.490
		3~10 mD				0.17	1.461	0.501
		10 ~36 mD				0.15	1.364	0.512
		36 ~128 mD				0.13	1.242	0.522
		128 ~ 446 mD				0.11	1.102	0.531
		>446 mD				0.09	0.947	0.540

Table 48: (HH) High Case Rel. Perm. Corey Model with High Case Capillary Pressure

Rel. Perm Case	Cap. Pres. Case	Perm Class	$Krwi_{\_drain}$	n_{o_drain}	n_w	Swirr	Kroi	Sor
High	High	<3 mD	1	1.731	5.284	0.15	3.769	0.277
		3~10 mD				0.12	3.610	0.281
		10 ~36 mD				0.09	3.391	0.284
		36 ~128 mD				0.06	3.105	0.286
		128 ~ 446 mD				0.04	2.770	0.288
		>446 mD				0.01	2.395	0.291

Table 49: (LH) Low Case Rel. Perm. Corey Model with High Case Capillary Pressure

Rel. Perm Case	Cap. Pres. Case	Perm Class	$Krwi_{\_drain}$	n_{o_drain}	n_w	Swirr	Kroi	Sor
Low	High	<3 mD	1	3.751	3.878	0.15	1.732	0.512
		3~10 mD				0.12	1.659	0.526
		10 ~36 mD				0.09	1.558	0.539
		36 ~128 mD				0.06	1.427	0.551
		128 ~ 446 mD				0.04	1.273	0.563
		>446 mD				0.01	1.101	0.574

Table 50: (HL) High Case Rel. Perm. Corey Model with Low Case Capillary Pressure

Rel. Perm Case	Cap. Pres. Case	Perm Class	$Krwi_{\_drain}$	n_{o_drain}	n_w	Swirr	Kroi	Sor
High	Low	<3 mD	1	1.731	5.284	0.20	3.345	0.271
		3~10 mD				0.17	3.179	0.274
		10 ~36 mD				0.15	2.968	0.277
		36 ~128 mD				0.13	2.703	0.279
		128 ~ 446 mD				0.11	2.398	0.282
		>446 mD				0.09	2.061	0.284

The Kroi and $Krwi_{\_drain}$ values in the Corey models (Tables above) must be scaled down because GEM reservoir simulator requires a normalization of the relative permeability end point (Kroi or Krwi) to a value of 1. Corey exponents, Swirr and Sor in those tables are not affected by the scaling process. The table below summarizes the scaling factors and the resulting Kroi and $Krwi_{\_drain}$ for the relative permeability Corey models as finally applied in GEM.

Table 51 Scaled Relative Permeability Corey Model Parameters for GEM Inputs

	LM	MM	HM	ML	MH	LL	HH	LH	HL
Rel.Perm. Case	Low	Mid	High	Mid	Mid	Low	High	Low	High
Cap.Pres. Case	Mid	Mid	Mid	Low	High	Low	High	High	Low
Scaling factor	1.643	2.378	3.577	2.224	2.506	1.537	3.769	1.732	3.345
$Krwi_{\_drain}$	0.61 (=1/1.643)	0.42 (=1/2.378)	0.28 (=1/3.577)	0.45 (=1/2.224)	0.40 (=1/2.506)	0.65 (=1/1.537)	0.27 (=1/3.769)	0.58 (=1/1.732)	0.30 (=1/3.345)
Kroi, <3 mD	1.0	1.0	1.0	1.0	1.0	1.0	1.0	1.0	1.0
Kroi 3~10 mD	0.956	0.956	0.956	0.950	0.958	0.950	0.958	0.958	0.950
Kroi 10 ~36 mD	0.896	0.896	0.896	0.887	0.900	0.887	0.900	0.900	0.887
Kroi 36 ~128 mD	0.818	0.818	0.818	0.808	0.824	0.808	0.824	0.824	0.808
Kroi 128 ~ 446 mD	0.728	0.728	0.728	0.717	0.735	0.717	0.735	0.735	0.717
Kroi >446 mD	0.628	0.628	0.628	0.616	0.636	0.616	0.636	0.636	0.616

APPENDIX 4. RADIAL THERMAL MODEL – LAYER PROPERTIES

The following table are the Radway well data including depth, porosity, permeability as well as environment of deposition (EOD), model zone and Rock Type as incorporated into the radial thermal model. The data is given by every meter interval for the radial well thermal modelling purpose. The perforation interval for injection was selected to be the Tide Dominated Bay Margin (TDBM) except the bottom two layers, consistent with the general field development strategy.

The average permeability for the entire model is 682 mD, with 894 mD for the TDBM interval and 955 mD for the perforation interval. The RTYPE column in the table is added for information on assigning relative permeability curves.

Layer properties (porosity, permeability) from the Radway well logs

Well	Cell Base (MD)	Cell Top (MD)	Cell Mid Point (MD)	Porosity (v/v)	Permeability (mD)	RTYPE	Environment of Deposition	Model Zor
Radway	2046.265	2045.265	2045.765	0.128	38.2918	3	Distal Bay	LMS
Radway	2047.265	2046.265	2046.765	0.135	59.7694	3	Distal Bay	LMS
Radway	2048.265	2047.265	2047.765	0.135	59.6069	3	Proximal Bay	BCS
Radway	2049.265	2048.265	2048.765	0.148	140.3804	4	Proximal Bay	BCS
Radway	2050.265	2049.265	2049.765	0.144	109.8148	4	Proximal Bay	BCS
Radway	2051.265	2050.265	2050.765	0.156	230.0752	4	Proximal Bay	BCS
Radway	2052.265	2051.265	2051.765	0.135	59.7658	3	Proximal Bay	BCS
Radway	2053.265	2052.265	2052.765	0.121	22.8845	2	Proximal Bay	BCS
Radway	2054.265	2053.265	2053.765	0.148	139.6791	3	Proximal Bay	BCS
Radway	2055.265	2054.265	2054.765	0.141	90.1433	4	Proximal Bay	BCS
Radway	2056.265	2055.265	2055.765	0.163	341.5923	5	Proximal Bay	BCS
Radway	2057.265	2056.265	2056.765	0.163	337.0177	5	Proximal Bay	BCS
Radway	2058.265	2057.265	2057.765	0.179	775.8865	5	Tide Dominated Bay Margin	BCS
Radway	2059.265	2058.265	2058.765	0.165	364.6759	5	Tide Dominated Bay Margin	BCS
Radway	2060.265	2059.265	2059.765	0.168	436.5730	5	Tide Dominated Bay Margin	BCS
Radway	2061.265	2060.265	2060.765	0.182	890.4587	5	Tide Dominated Bay Margin	BCS
Radway	2062.265	2061.265	2061.765	0.180	829.4240	5	Tide Dominated Bay Margin	BCS
Radway	2063.265	2062.265	2062.765	0.168	434.6166	5	Tide Dominated Bay Margin	BCS
Radway	2064.265	2063.265	2063.765	0.192	1474.8290	6	Tide Dominated Bay Margin	BCS
Radway	2065.265	2064.265	2064.765	0.188	1200.0760	6	Tide Dominated Bay Margin	BCS
Radway	2066.265	2065.265	2065.765	0.164	344.5233	5	Tide Dominated Bay Margin	BCS
Radway	2067.265	2066.265	2066.765	0.172	549.1040	5	Tide Dominated Bay Margin	BCS
Radway	2068.265	2067.265	2067.765	0.184	962.2947	5	Tide Dominated Bay Margin	BCS
Radway	2069.265	2068.265	2068.765	0.182	887.3230	5	Tide Dominated Bay Margin	BCS
Radway	2070.265	2069.265	2069.765	0.181	883.4431	5	Tide Dominated Bay Margin	BCS
Radway	2071.265	2070.265	2070.765	0.164	356.8278	5	Tide Dominated Bay Margin	BCS
Radway	2072.265	2071.265	2071.765	0.166	387.9522	5	Tide Dominated Bay Margin	BCS
Radway	2073.265	2072.265	2072.765	0.179	767.2469	5	Tide Dominated Bay Margin	BCS
Radway	2074.265	2073.265	2073.765	0.184	979.6937	5	Tide Dominated Bay Margin	BCS
Radway	2075.265	2074.265	2074.765	0.182	911.7840	5	Tide Dominated Bay Margin	BCS
Radway	2076.265	2075.265	2075.765	0.180	800.7246	5	Tide Dominated Bay Margin	BCS
Radway	2077.265	2076.265	2076.765	0.197	1883.7800	6	Tide Dominated Bay Margin	BCS
Radway	2078.265	2077.265	2077.765	0.178	746.0875	5	Tide Dominated Bay Margin	BCS
Radway	2079.265	2078.265	2078.765	0.200	2092.7080	6	Tide Dominated Bay Margin	BCS
Radway	2080.265	2079.265	2079.765	0.197	1805.0280	6	Tide Dominated Bay Margin	BCS
Radway	2081.265	2080.265	2080.765	0.190	1316.3000	6	Tide Dominated Bay Margin	BCS
Radway	2082.265	2081.265	2081.765	0.179	773.5377	5	Tide Dominated Bay Margin	BCS
Radway	2083.265	2082.265	2082.765	0.190	1327.0680	6	Tide Dominated Bay Margin	BCS
Radway	2084.265	2083.265	2083.765	0.190	1324.8180	6	Tide Dominated Bay Margin	BCS
Radway	2085.265	2084.265	2084.765	0.192	1443.3300	6	Tide Dominated Bay Margin	BCS
Radway	2086.265	2085.265	2085.765	0.180	739.7865	5	Tide Dominated Bay Margin	BCS
Radway	2087.265	2086.265	2086.765	0.114	12.3892	2	Tide Dominated Bay Margin	BCS
Radway	2088.265	2087.265	2087.765	0.032	0.0001	1	Tide Dominated Bay Margin	BCS
Average	2067.265	2066.265	2066.765	0.165	682.124	4.651		
BCS	2068.265	2067.265	2067.765	0.167	713.006	4.732		
TDBM	2073.265	2072.265	2072.765	0.174	893.622	5.065		
Perf	2072.265	2071.265	2071.765	0.181	954.824	5.310		

The relative permeability and capillary pressure table that best fits the Radway 8-19 permeability range (279 mD – 1036 mD) is attached in the format of the CMG GEM input deck.

```
RPT 1
 ***use table 5 (from Gen 3) for k 760mD (in range 279 - 1036)

 ***RPT 5
 SWT
 **$       Sw          krw         krow      Pcow
 ***       0.000           0        0.703  1.14E+03
         0.099           0        0.703  1.14E+03
       0.155313  7.35771e-007      0.520405  1.24E+02
       0.211625  2.03552e-005      0.377323  5.86E+01
       0.267938   0.000141956      0.267136  3.69E+01
        0.32425   0.000563132      0.183967  2.63E+01
       0.380563    0.00163987      0.122644  2.02E+01
       0.436875    0.00392724     0.0786604  1.63E+01
       0.493188    0.00821792     0.0481422  1.35E+01
         0.5495     0.0155791     0.0278071  1.15E+01
       0.605812     0.0273882      0.014925  9.98E+00
       0.662125     0.0453673    0.00727681  8.78E+00
       0.718437     0.0716166    0.0031114  7.82E+00
        0.77475      0.108648    0.00109991  7.04E+00
       0.831063      0.159416   0.000287833  6.38E+00
       0.887375       0.22735  4.35067e-005  5.83E+00
       0.943688      0.316388   1.7209e-006  5.36E+00
              1         0.431           0        0
 SLT
 **$       Sl          krg         krog      Pcog
 ***       0.000         0.703           0  1.14E+03
         0.099         0.703           0  1.14E+03
       0.155312      0.520405  1.20011e-006  1.24E+02
       0.211625      0.377323  3.32012e-005  5.86E+01
       0.267937      0.267136   0.000231543  3.69E+01
        0.32425      0.183967   0.000918519  2.63E+01
```

```
0.380563     0.122644    0.00267477  2.02E+01
0.436875    0.0786604    0.00640568  1.63E+01
0.493188    0.0481422     0.0134042  1.35E+01
  0.5495    0.0278071      0.025411  1.15E+01
0.605812     0.014925     0.0446727  9.98E+00
0.662125   0.00727681     0.0739981  8.78E+00
0.718438    0.0031114      0.116813  7.82E+00
 0.77475   0.00109991      0.177214  7.04E+00
0.831063  0.000287833      0.260022  6.38E+00
0.887375 4.35067e-005      0.370829  5.83E+00
0.943688  1.7209e-006      0.516057  5.36E+00
       1            0         0.703         0
HYSKRG 0.362
```

Table 4. Reservoir rock and over/under burden thermal properties

LMS (overburden) -siltstone	Dependency	Base Case	Low	high	Equation	Reference
Heat Capacity, J/(Kg*K)	dependent on lithology and some variation with T	900	875	925	England and Schatz & Simmons, and Figure 3a-f	Shell report from Deniz (94.139); See tab "Extra"
Density, Kg/m3	dependent on T	2648	2628	2668	$\rho_T = \rho_0 (1-\alpha T)$; ρ_0 – density at 0°C, α– thermal expansion coefficient, T - temperature	Shell Report from Deniz (94.139), SD=20 for siltstone
Thermal Expansion Coeff. (1/K)		3.3E-5 or negligible	2.8E-5; or negligible	3.4E-5 or negligible		Shell Report from Deniz (94.139) for geodynamic modeling
Thermal Conductivity, W/(m*K)	dependent on lithology and some variation with T	1.8	1.2	2.4	Somerton function	Shell report from Deniz - 94.111
BCS (target formation) -quartz sand	**Dependency**	**Base Case**	**Low**	**high**	**Equation**	**Reference**
Heat Capacity, J/(Kg*K)		890	865	915		web
Density, Kg/m3		2650	2633	2667		
Thermal Expansion Coeff. (1/K)		3.3E-5 or negligible	2.8E-5; or negligible	3.4E-5 or negligible		Ohio River analog - 5.4E-6 1/K; Shell Report from Deniz (94.139) for geodynamic modeling
Thermal Conductivity, W/(m*K)		6.0	3.2	8.8		Shell Report from Deniz (94.111). See tab "Extra".
BCS (target formation) -sandstone	**Dependency**	**Base Case**	**Low**	**high**	**Equation**	**Reference**
Heat Capacity, J/(Kg*K)	dependent on lithology and some variation with T	834	809	859	England and Schatz & Simmons, and Figure 3a-f	Shell report from Deniz (94.139) ; See tab "Extra"; Ohio River analog - 900
Density, Kg/m3	dependent on T	2650	2633	2667		Alessandra, BCS core measurement +-10; Shell Report from Deniz (94.139), SD=17
Thermal Expansion Coeff. (1/K)		3.3E-5 or negligible	2.8E-5; or negligible	3.4E-5 or negligible		Ohio River analog - 5.4E-6 1/K; Shell Report from Deniz (94.139) for geodynamic modeling
Thermal Conductivity, W/(m*K)	dependent on lithology and some variation with T	3.175	1.075	5.275	Somerton function	Shell Report from Deniz (94.139, 94.111).Ohio River analog 2.34 W/mK
Precanbrian basement (underburden)	**Dependency**	**Base Case**	**Low**	**high**	**Equation**	**Reference**
Heat Capacity, J/(Kg*K)	dependent on lithology and some variation with T	805	765	845	England and Schatz & Simmons, and Figure 3g-j	Shell report from Deniz (94.139); See tab "Extra"
Density, Kg/m3	dependent on T	2800	2740	2860		Shell Report from Deniz (94.139), SD=60 for Crust (crystalline basement)
Thermal Expansion Coeff. (1/K)		3.3E-5 or negligible	2.8E-5; or negligible	3.4E-5 or negligible		Shell Report from Deniz (94.139) for geodynamic modeling
Thermal Conductivity, W/(m*K)	dependent on lithology and some variation with T	2.82	1.32	4.32	Figure6 - Granite temp. curve:	Shell Report from Deniz (94.111). See tab "Extra".

GEM Thermal Functionality (I)

The energy balance calculation includes heat conduction and convection within the reservoir rock and fluids as well as heat loss to the surrounding. The following is a direct quote from the GEM 2010.10 technical manual.

Energy Balance Equation

To calculate the temperature distribution for the thermal cases, the following energy balance equation is added to the equation set.

$$\begin{aligned}\Psi_I \equiv\ & \Delta T_o^m H_o^m \left(\Delta p_o^{n+1} - \tilde{\rho}_o^m g \Delta D\right) + \Delta T_g^m H_g^m \left(\Delta p_o^{n+1} + \Delta P_{cog}^m - \tilde{\rho}_g^m g \Delta D\right) + \\ & \Delta T_w^m H_w^m \left(\Delta p_o^{n+1} - \Delta P_{cwo}^m - \tilde{\rho}_w^m g \Delta D\right) + \Delta t_c^m \Delta T^{n+1} + Q_{loss} + \sum_j H_j^{n+1} q_j^{n+1} - \\ & \frac{V}{\Delta t}\left[\phi^{n+1}\left(\sum_j \rho_j^{n+1} S_j^{n+1} U_j^{n+1}\right) - \phi^n \left(\sum_j \rho_j^n S_j^n U_j^n\right)\right] - \\ & \frac{V}{\Delta t}\left[\left(1-\phi^{n+1}\right) c_R \tilde{\rho}_R \left(T^{n+1} - T_R^0\right) - \left(1-\phi^n\right) c_R \tilde{\rho}_R \left(T^n - T_R^0\right)\right] = 0, \quad k = o, g, w\end{aligned} \tag{F.1}$$

where

c_R	=	heat capacity of rock
H_k	=	molar enthalpy of Phase k (k = o, g, w)
S_k	=	saturation of Phase k (k = o, g, w)
Q_{loss}	=	heat loss rate to the (over/underburden) surroundings
T	=	temperature
T^0	=	reference temperature (= 0 K)
U_k	=	$H_k - p/\rho_k$; molar internal energy of Phase k
$\tilde{\rho}_R$	=	rock mass density
T_c	=	total thermal conductivity of rock and fluids

Equation (F.1) is an energy balance equation involving convection, conduction and heat losses to the surroundings.

GEM Thermal Functionality (II)

The heat loss to the over- and under-burden is calculated heat diffusivity model by Vinsome and Westerveld, which is also quoted from the GEM2010.10 manual below for easy reference.

Heat Loss Calculation

The heat loss to the overburden and underburden is calculated using the method of Vinsome and Westerveld (1980). They assumed a temperature profile in the overburden and underburden of the form:

$$T(t,z) = \left(\theta - \theta^0 + b_1 z + b_2 z^2\right)\exp(-z/d) + \theta^0 \quad \text{(F.12)}$$

where

$T(t,z)$	=	over/underburden temperature at time t at a distance z from the reservoir boundary
b_1, b_2	=	time-dependent parameters
d	=	thermal diffusion length
θ	=	temperature in the boundary gridblock
θ^0	=	initial temperature in boundary gridblock

The diffusion length is taken as:

$$d = \frac{\sqrt{\eta t}}{2} \quad \text{(F.13)}$$

where η is the thermal diffusivity

$$\eta = \frac{\kappa_R}{c_R \widetilde{\rho}_R} \quad \text{(F.14)}$$

and where

c_R	=	rock heat capacity
$\widetilde{\rho}_R$	=	mass density of rock
κ_R	=	rock thermal conductivity

Vinsome and Westerveld (1980) derived the following expression for b_1 and b_2 and the heat loss rate:

$$b_1^{n+1} = \frac{\dfrac{\eta\,\Delta t\left(\theta^{n+1} - \theta^0\right)}{d^{n+1}} + \xi^n - \dfrac{\left(d^{n+1}\right)^3\left(\theta^{n+1} - \theta^n\right)}{\eta\,\Delta t}}{3\left(d^{n+1}\right)^2 + \eta\,\Delta t} \quad \text{(F.15)}$$

$$b_2^{n+1} = \frac{2b_1^{n+1}\left(d^{n+1}\right) - \left(\theta^{n+1} - \theta^0\right) + \dfrac{\left(d^{n+1}\right)^2\left(\theta^{n+1} - \theta^n\right)}{\eta\,\Delta t}}{2\left(d^{n+1}\right)^2} \quad \text{(F.16)}$$

$$\xi^n = \left[\left(\theta - \theta^0\right)d + b_1 d^2 + 2b_2 d^3\right]^n \quad (17)$$

$$Q_{loss} = \kappa_R A\left[\frac{\left(\theta^{n+1} - \theta^0\right)}{d^{n+1}} - b_1^{n+1}\right] \quad \text{(F.18)}$$

where A is the cross-sectional area for heat loss to the overburden/underburden.

APPENDIX 5. ANALYTICAL ESTIMATE OF BHP REDUCTION

The net change in stress level are dictated by the balance between the increased pore pressure (yielding a higher stress) and the decreased temperature (yielding a lower stress). Though the temperature effects will be dominating, the overall change in the total stress is obtained by adding the individual changes to temperature reduction and pore pressure increase. The effects due to each can be summarized into the following two equations:

Poro-elastic: $\Delta\sigma_h = A_p\Delta p$, where $A_p = (1-\beta)*(1-2\nu)/(1-\nu)$

Thermo-elastic: $\Delta\sigma_h = A_T\Delta T$, where $A_T = \alpha*E/(1-\nu)$

Δp = increase (inflation) of reservoir pressure
β = ratio of rock grain compressibility to rock matrix compressibility
ν = Poisson's ratio
ΔT = decrease in temperature in the cooled reservoir zone
α = Thermal expansion / contraction coefficient ($°C^{-1}$)
E = Young's modulus

The poro-elastic constant A_p and the thermo-elastic constant A_T can be measured on core samples.

'Typical' values for A_p are in the following ranges:

- Soft rocks: A_p = 0.55-0.70 ('Soft': E in the range below ca. 10 GPa)
- Hard rocks: A_p = 0.35-0.60 ('Hard": E in the range above ca. 10 GPa)
- Solid rock (i.e. no pore space): $A_p = 0$

If no measurements are available, a recommended value is 0.6.

A typical value of A_T for a typical 'medium tight' sandstone (E in the order of 10 GPa) is 0.1 MPa / °C.

Note that the thermo-elastic constant A_T is proportional to E. Therefore, for the same thermal expansion coefficient α, a stiffer rock will develop more thermo-elastic stresses as a result of cooling than a softer rock. This appears to be generally in line with field observations.

Though the E numbers of the BCS have all been above 10 GPa (> 1.45e6 psi), using the above rule of thumb yields a stress reduction of up to 4.5 MPa assuming worst case temperature (~0degC at wellhead).

APPENDIX 6. MINERAL COMPOSITION OF THE BCS

BCS minerals composition based on Radway well data

Mineral	**Content (v%)**
halite	detected*
albite/anothite	~1.00
k-feldspar	~9.00
calcite	0.00
dolomite/ankerite/siderite	<1.00
anhydrite	<0.5
analcime	<0.2
glauconite	<1.5
quartz	~65.00
mica (muscovite, biotite)	~2.5
illite	<2.00
kaolinite	<0.50
clay undiff. and other rock segments	~3.5%
pyrite	<0.10
porosity	~12.00
Sum	100.00

APPENDIX 7. CHEMICAL COMPOSITION OF BCS BRINE

Measured BCS brine composition from Radway well and distribution of major aqueous species calculated at room temperature (20°C) and reservoir temperature (60°C), respectively

Species	Measured Total Aqueous Concentration	Species Concentration at 20°C	Species Concentration at 60°C
unit	molality	molality	molality
H_2O	5.55E+01	5.55E+01	5.55E+01
H^+	-7.62E-12	2.17E-08	5.68E-08
Ba^{+2}	4.08E-06	4.08E-06	4.08E-06
Ca^{+2}	5.61E-02	5.56E-02	5.56E-02
Mg^{+2}	4.27E-02	4.19E-02	4.19E-02
Na^+	5.54E+00	5.54E+00	5.54E+00
K^+	3.46E-02	3.46E-02	3.46E-02
Fe^{+2}	5.88E-05	5.88E-05	5.88E-05
Cl-	6.28E+00	6.28E+00	6.28E+00
HCO_3^-	1.35E-03	5.03E-04	5.26E-04
SO_4^{-2}	2.20E-03	1.79E-03	1.86E-03
$^1AlO_2^-$	5.00E-08	5.00E-08	5.00E-08
$^1SiO_{2(aq)}$	5.85E-05	5.82E-05	5.80E-05
$^1O_{2(aq)}$	5.85E-70	5.85E-70	5.85E-70
OH^-		8.85E-08	6.84E-07
CO_3^{-2}		5.82E-06	8.52E-06
$CaCO_{3(aq)}$		1.04E-05	1.61E-05
$CaOH^+$		1.55E-07	1.35E-06
$CaSO_{4(aq)}$		4.06E-04	3.40E-04
$CaCl^+$		3.54E-05	1.42E-04
$CaCl_{2(aq)}$		2.04E-17	1.14E-12
$CO_{2(aq)}$		2.51E-05	4.63E-05

HSO_4^-		5.26E-10	3.85E-09
$HSiO_3^-$		2.90E-07	5.18E-07
$MgCO_{3(aq)}$		6.72E-06	6.95E-06
$MgHCO_3^+$		8.03E-04	7.50E-04
$MgOH^+$		1.75E-06	1.23E-05
Al^{+3}		1.05E-13	4.31E-16
pH		6.903	6.658
Ionic Strength		6.12	6.123
Charge Inbalance:		-2.1%	-2.1%

[1] Concentration was not measured, numbers in the table are estimations that will be later validated during brine reconciliation by assuming an equilibrium with respect to a dominant mineral.

APPENDIX 8. WELL LIST FOR LEAK PATH 3D STATIC MODEL

List of Project Wells used for the Leak Path Structural Framework and 3D Static Modeling

UWI	Petrel Well Name	X	Y	KB m	TD (MD) m	Spud Date	TD Formation	Petrophysical Evaluation
100153305820W400	71375 Radway 15-33	375149.4762	5991790.6563	632	1168	10/9/1976	COOKING LAKE	
100043005922W400	ACL 4-30	350167.8167	5999738.9195	653	889	7/10/1995	BASE CRETACEOUS	
100040905921W400	ACL 4-9	363185.2625	5994090.0114	655	1345	29/12/1997	COOKING LAKE	
100052005922W400	ACL 5-20	351422.2065	5998504.9279	649	849	24/01/1998	BASE CRETACEOUS	
100160906022W400	AMOCO THORHILD 16-9-60-22	354506.0000	6005428.6000	670	1808		U. LOTSBERG	YES
100011206021W400	ANDERSON 1-12	369321.5119	6003773.9468	652	1492	3/11/1980	PRAIRIE EVAPORITE	YES
102072906501W500	ANDERSON ESSO BIG BEND 7-29-65-1	299135.4000	6060250.6000	645	2115		CAMBRIAN (LMS)	YES
100093605526W400	ANDERSON ET AL MORINVILLE 9-36-55-26	320652.7215	5964112.2000	715	1975		PRAIRIE EVAPORITE	YES
100101206615W400	ARCO BA VENICE 10-12	427084.9000	6061574.6000	579	1591		PRECAMBRIAN	YES
103073405521W400	ATCO-LPG-STORAGE 7-34	365881.6000	5962482.1000	634	1860		U. LOTSBERG	
102081005522W400	BRINE DISPOSAL 8-10	356670.6000	5956222.9000	633	1974		DEVONIAN RED BEDS 4	
100041506803W500	CHEVRON ET AL CHISHOLM 4-15-68-3	283355.4000	6086704.0000	604	2100		PRECAMBRIAN	
100142705919W400	CIRCLE 14-27	384749.1262	5999628.6280	653	1099	13/09/1998	COOKING LAKE	
100113006222W400	CONOCO 11-30	351264.4168	6029696.4504	689	884	3/1/1996	GLAUCONTIC SANDS	
100132205723W400	DORSET FEDORAH 13-22-57-23	346202.1000	5979965.7000	660	1981		DEVONIAN RED BEDS 1	
100082606016W400	GULF EDWAND 8-26	416644.3000	6008000.6000	682	1905		PRECAMBRIAN	
100103105919W400	HESS 10-31	380392.6031	6001077.3979	649	1406	18/07/1980	WATT MOUNTAIN	
100042206019W400	HESS 4-22	384320.3995	6006504.9669	661	1390	30/09/1980	PRAIRIE EVAPORITE	
100062006022W400	HILLCREST 6-20	352400.5150	6008073.9043	675	1345	20/07/2000	COOKING LAKE	
100100506802W500	HOME ALMINEX KCL CHISHOLM 10-5-68-2	290481.3000	6083840.2000	603	2079		PRECAMBRIAN	
100103505903W500	HOME BARRHEAD 10-35	282151.5000	6004761.9000	668	2514		PRECAMBRIAN	
100103506202W500	HOME CDN-SUP GRIDGELK 10-35	293272.5000	6033435.7000	642	2145		CAMBRIAN (MCS)	
100100505202W500	HOME CPOG BRIGHTBANK 10-5	283858.2000	5928527.9000	744	2920		PRECAMBRIAN	
100121406702W500	HOME KCL ALMINEX TIELAND 12-14	294255.3000	6077164.5000	619	2079		PRECAMBRIAN	
102011005721W400	IMP 2/1-10	366753.7429	5974871.4867	611	982	20/07/1978	LEDUC	
100063605823W400	IMP EGREMONT W 6-36	350266.0000	5991966.9000	632	2242		PRECAMBRIAN	
100012706026W400	IMP-BAYSEL RIVERDALE NO. 1-27	317236.7000	6010541.1000	650	2292		PRECAMBRIAN	
100081705321W400	IMPERIAL ARDROSSAN NO. 1	364123.5000	5938055.4000	725	2378		BCS	
100092905924W400	IMPERIAL CLYDE NO. 1	333313.7347	6001013.2610	629	2294		PRECAMBRIAN	
100052906201W500	IMPERIAL DAPP NO. 1	297257.2000	6031257.1000	636	2309		PRECAMBRIAN	
100161906219W400	IMPERIAL DARLING NO. 1	381275.3000	6027383.6000	708	2013		PRECAMBRIAN	
100013405722W400	IMPERIAL EASTGATE NO. 1-34	357203.1000	5981630.7000	646	2206		PRECAMBRIAN	
100021605622W400	IMPERIAL GIBBONS NO. 1	354723.5000	5967152.6000	654	2024		CAMBRIAN (UMS)	
100131706723W400	IMPERIAL GROSSMONT NO.1	340320.3040	6075567.6170	630	1953		PRECAMBRIAN	
103081705026W400	IMPERIAL LEDUC NO. 530	316203.2543	5910504.7400	723	2742		PRECAMBRIAN	
100150605626W400	IMPERIAL MEARNS NO. 1	312284.6000	5966650.4000	700	2535		PRECAMBRIAN	
100021605525W400	IMPERIAL VOLMER NO. 1	325017.4000	5958479.2000	701	2217		CAMBRIAN (UMS)	
100101106712W400	McDERMOTT LABIE 10-11	453839.0000	6071004.9000	598	1481		PRECAMBRIAN	
100103505720W400	MELAND 10-35	378012.5379	5981909.3056	625	1254	21/09/1977	BEAVERHILL LAKE	
100060906021W400	MICH 6-9	363397.4892	6004293.1689	653	1280	11/3/1973	BEAVERHILL LAKE	
100162205922W400	MOSAIC THORH 16-22-59-22	356203.8000	5999173.6000	648	1845		U. LOTSBERG	
100141405515W400	NORWEST WILLINGDON 14-14	425930.4000	5956843.6000	633	1992		PRECAMBRIAN	
100100205922W400	NYTIS 10-2	357282.1044	5993768.0851	646	1251	7/11/1970	COOKING LAKE	
102030605821W400	REDWATER 2/3-6	361399.1989	5983023.6185	617	1189	10/8/1974	LEDUC	
100123405721W400	RIFE ET AL REDWATER 12-34-57-21	365717.5162	5982236.8000	635	1547		PRAIRIE EVAPORITE	YES
100080106211W400	SASK OIL SUGDEN 8-1	467260.0000	6020338.2000	630	1635		PRECAMBRIAN	
100081905920W400	SCL RADWAY 8-19-59-20	370705.4800	5997747.3900	647	3500		PRECAMBRIAN	YES
102113205521W400	SCL REDWATER 11-32-55-21	362440.3000	5962787.3200	628	2233		PRECAMBRIAN	YES
100030405720W400	SCL REDWATER 3-4-57-20	374208.3000	5973110.4000	614	2206		PRECAMBRIAN	YES
100101305522W400	STANDING 10-13	359299.2000	5958252.1000	637	1937		BASE DEVONIAN	
100143506121W400	SULPETRO 14-35	367315.7632	6021153.5598	683	778	3/7/1983	GLAUCONTIC SANDS	
100070305719W400	TALISMAN 7-3	385952.5724	5972951.9115	637	1184	21/10/1999	COOKING LAKE	
100060105213W400	VOYAGER PLAIN 6-1-52-13	447785.2000	5923646.0000	691	2100		PRECAMBRIAN	YES
100093106219W400	WESTCOAST 9-31	381261.6927	6030218.9313	702	1923	25/02/1978	CAMBRIAN (MCS)	YES
100021305513W400	WESTMIN HAIRY 2-13-55-13	447453.7153	5955168.412	619	1745		PRECAMBRIAN	

APPENDIX 9. WELL LOCATIONS IN THE LEAK PATH STATIC MODEL